Local and Global Neural Mechanisms Underlying the Robust Velocity Coding of Natural Images

Paul Barnett

Discipline of Physiology

School of Molecular and Biomedical Science

The University of Adelaide

October 2009

A thesis submitted for the degree of Doctor of Philosophy

Thesis Abstract

Interpreting motion in the natural world presents a major challenge for visual systems. Natural scenes vary enormously in structure, luminance and contrast, all parameters known to modulate the response of biological motion detectors. Nevertheless, many animals overcome this challenge and adopt visually guided behaviour for which the accurate estimation of self-motion and image velocity is required.

It is generally accepted that Reichardt correlator-like computations underlie local motion detection in insects. Reichardt correlators, however, generate ambiguous estimates of velocity, because they are sensitive to several additional image parameters, such as those mentioned above. How does the visual system generate accurate estimates of apparent image velocity when the elements underlying local motion detection produce ambiguous velocity signals?

This thesis investigates the neural processing of image velocity. I performed sharp electrode intracellular recordings from identified motion sensitive neurons in the lobula plate of the hoverfly, *Eristalis tenax*. A series of natural and artificial images were used to investigate the processing of a vast range of scenes.

I show that the horizontal system (HS) neurons have a remarkable capacity to estimate image velocity reliably for vastly different natural scenes. This property is at odds with the HS neurons' responses to experimenter-defined stimuli. I reveal several activity dependent features of the neural response that may reconcile the ability to accurately encode the velocity of natural images with the mechanisms underlying motion processing. Images that were initially weak neural drivers have long latencies, with responses continuing to increase in magnitude over several hundred milliseconds. Images that were initially strong neural drivers, reached peak responses more rapidly followed by significant reductions in response over longer time scales. Despite being different in sign and time course, these two activity dependent changes in response act as near-ideal normalisers for images that would otherwise produce highly variable response magnitudes.

By analysing the time course of neural response and manipulating image contrast, I show that this property is likely to emerge from a combination of static and dynamic non-linarities. When image contrast is reduced, thus reducing the range of input signals to local motion detectors, the essential non-linearity of the Reichardt correlator model provides a good prediction of global responses. Thus, suggesting an important role for non-linear mechanisms being recruited by high contrast local features in the robust encoding of natural scenes.

Finally, I use an experimental paradigm that reduces the influence of spatial integration and thus enables the analysis of responses equivalent to the outputs of individual local motion sensitive elements presynaptic to the HS neuron. I show evidence for an adaptive gain reduction that affects the sensitivity of individual motion detector responses to subsequent features. This gain reduction is facilitated by local neighbouring motion stimulation and is thus, well suited to take advantage of the predictable nature of natural scenes.

Declaration

This work contains no material which has been accepted for the award of any other degree or diploma in any university or other tertiary institution and, to the best of my knowledge and belief, contains no material previously published or written by another person, except where due reference has been made in the text.

I give consent to this copy of my thesis when deposited in the University Library, being made available for loan and photocopying, subject to the provisions of the Copyright Act 1968.

The author acknowledges that copyright of published works contained within this thesis (as listed below*) resides with the copyright holder(s) of those works.

I also give permission for the digital version of my thesis to be made available on the web, via the University's digital research repository, the Library catalogue, the Australasian Digital Theses Program (ADTP) and also through web search engines, unless permission has been granted by the University to restrict access for a period of time.

1. Nordström, K. Barnett, PD., Moyer de Miguel, IM., Brinkworth, RSA. and O'Carroll, DC. (2008) Sexual dimorphism in the hoverfly motion vision pathway. Current Biology 18: 661–667. DOI 10.1016 DOI 10.1016/j.cub.2008.03.061

2. Barnett, PD., Nordström, K. and O'Carroll, DC. (2009). Motion adaptation and the velocity coding of natural scenes, Submitted to Current Biology, MS Current-Biology-D-09-00354

3. Barnett, PD. and O'Carroll, DC. (2009) Receptive fields of fly motion detecting neurons integrate local features within natural scenes unpredictably.

4. Barnett, PD., Nordström, K. and O'Carroll, DC. (2009) Local motion detection: temporal and spatial modulation of gain and transient responses to features

Acknowledgments

First and foremost I owe a great deal of thanks for the ongoing support and help I received from my three supervisors, David O'Carroll, Karin Nordström, and Russell Brinkworth. I received more help and support throughout the duration of my candidature than I could have ever expected, thank you dearly.

Thanks to all the members of the O'Carroll lab who have been present at one stage or another and helped me throughout my candidature, Irene Moyer de Miguel, Adam Kane, Joanne Wilkins, Yun Leung (Esther), Bart Geurten, Marcel Mertes, Jodi Gray, Sharn Perry, Melissa Walker, Lachlan Dowd.

Special thanks to Steve Weiderman and Douglas Bolzon who not only continually provided constructive and critical conversations but also friendship and support in the lab at all times.

Outside of the lab I must also thank my friends: El Geko, Sprat Cat, Lukozade, Stefan, Bergs, Moff, Bod, Gerry, Puff, Lara, Stevey D, and Bryant for housing me and maintaining my sanity, albeit marginally on occasions, throughout the whole PhD.

Finally, a big thanks to Mum, Dad and the Sister.

Statement of Contributions to Jointly Authored Works

The following states the contribution of the authors to the following published works

1. Nordström, K., Barnett, PD., Moyer de Miguel, IM., Brinkworth, RSA. and O'Carroll, DC. (2008) Sexual dimorphism in the hoverfly motion vision pathway. Current Biology 18: 661–667. DOI 10.1016/j.cub.2008.03.061

Conceptualization: Receptive field mapping and analysis techniques were developed by David O'Carroll. The primary observation resulted from collection of various receptive fields from motion sensitive neurons collected during electrophysiological experiments (see below). The interpretation of these results was shared amongst all the coauthors.

Realization: Electrophysiological recordings were conducted by Karin Nordström, Paul Barnett, and Irene Moyer de Miguel. Anatomy was done by Paul Barnett. Stimulus movies were collected and modified by Russell Brinkworth. Data collection and analysis was primarily done by Karin Nordström.

Documentation: Karin Nordström and David O'Carroll were primary writers of the paper, with contributions from Paul Barnett and Russell Brinkworth. Figures were made by Karin Nordström, except for the anatomy where Paul Barnett developed the images and movies.

2. Barnett, PD., Nordström, K. and O'Carroll, DC. (2009) Motion adaptation and the velocity coding of natural scenes. Submitted to Current Biology, MS Current-Biology-D-09-00354

Conceptualization: All the coauthors were involved in the conceptualization and development of ideas included throughout the paper.

Realization: Electrophysiological recordings were conducted by Paul Barnett and Karin Nordström. Data analysis was done by Paul Barnett.

Documentation: Paul Barnett, Karin Nordström and David O'Carroll were all involved in writing the paper. Figures were made by Paul Barnett.

3. Barnett, PD. and O'Carroll, DC. (2009) Receptive fields of fly motion detecting neurons integrate local features within natural scenes unpredictably.

Conceptualization: Both authors were involved in the conceptualization and development of ideas included throughout the paper.

Realization: Electrophysiological recordings were conducted by Paul Barnett. Analysis was done by Paul Barnett.

Documentation: Paul Barnett and David O'Carroll wrote the paper. Paul Barnett made the figures.

4. Barnett, PD., Nordström, K. and O'Carroll, DC. (2009) Local detector analysis reveals a locally mediated mechanism of motion adaptation.

Conceptualization: Paul Barnett and David O'Carroll conceived the experiments. Paul Barnett, Karin Nordström and David O'Carroll all contributed to the development of ideas.

Realization: Electrophysiological recordings were conducted by Paul Barnett. Analysis was done by Paul Barnett.

Documentation: Paul Barnett primarily wrote the paper. Karin Nordström and David O'Carroll provided significant written contributions and editing. Paul Barnett made the figures.

I agree with the above statements of contributions and give permission for the papers to be included in this thesis.

Paul Barnett:

Karin Nordström:

Irene Moyer de Miguel:

Russell Brinkworth:

David O'Carroll:

Author's Comments

All publications within this thesis are in the exact form of the original articles as published or as submitted in cases where the article are not yet in press, with the following exceptions:

Typesetting has been altered so that there is a consistent format throughout the entire thesis.

The figures have been inserted into the text at appropriate places, which may differ from the final published version of the papers.

Figures are referenced throughout the text as they are in the published or submitted versions of the papers, but are captioned based on their chapter and figure number, e.g. Figure 1 in Chapter 2 is captioned as Figure 2.1.

Table of contents

Chapter 3: Motion adaptation and the velocity coding of natural scenes.....101

Chapter 1:
Introduction

1.1 Motion vision and velocity estimation

While numerous animals have visual systems that do not permit the analysis of colour, or depth through binocular vision, the ability to compute movement is ubiquitous. After the most basic visual task of detecting changes in light intensity, the computation of motion may represent one of the most fundamental capabilities of biological visual systems (reviewed in Nakayama, 1985). Motion of the entire visual scene, arising from self-motion, or object motion relative to the viewer, are not explicitly represented at the level of the retina, however. Rather, the brain has to compute motion based on local changes in light intensity across space and through time (Reichardt, 1961).

The detection and analysis of visual motion can provide an animal with a wealth of information about its surrounds. For example, motion cues are essential for tracking the trajectory of moving objects, avoiding obstacles, and for interpreting the orientation of self-motion (Collett & Land, 1978, Srinivasan, Zhang, Lehrer & Collett, 1996). Furthermore, parallax induced by self-motion relative to the scene can provide important cues for gathering three-dimensional information about the surrounding environment (Koenderink & Van Doorn, 1976, Nakayama & Loomis, 1974) (see section 1.2 below – *Optic-flow processing and the optomotor response*).

While motion detection *per se* is an important cue to gather information about the environment, the velocity of visual motion, at least as a crude estimate of relative speed and direction, is essential for many tasks. It comes as little surprise then that there is a great deal of evidence suggesting that animals exploit apparent retinal velocities to control behaviour. Honeybees, for example, balance the apparent velocity in the left and right visual hemispheres to pass centrally between obstacles

or along corridors (Srinivasan et al., 1996), while fruit flies use similar cues to control their ground speed when flying through tunnels (David, 1982). In addition, both honeybees and ants integrate apparent retinal velocity over time to estimate total distances travelled to or from food sources (Esch & Burns, 1996, Ronacher & Wehner, 1995, Srinivasan, Lehrer, Kirchner & Zhang, 1991, Srinivasan et al., 1996). These observations are not limited to insects: human subjects also integrate image velocity over time to estimate distance travelled (Bremmer & Lappe, 1999, McKee, Silverman & Nakayama, 1986)

Computing motion, and particularly velocity, within the natural environment is a challenging task. Natural scenes vary tremendously in brightness, contrast, and spatial structure (Ruderman, 1994, Ruderman & Bialek, 1994, Torralba & Oliva, 2003). For example, in one instance the visual system might have to interpret motion above a lake or in the desert where the visual panorama is sparse, homogenous, and bright, and yet in another, a densely wooded forest where the panorama is otherwise dark cluttered. How does the visual system overcome the problems associated with computing motion in an enormously variable natural world?

These problems seem to be solved with apparent ease by even the simple visual system of the fly. For example, a hoverfly may in an instance switch from precisely controlled stationary hovering to zip off through the foliage and chase a conspecific in an aerobatic courtship display where they engage in turns at up to 3000°/s (Collett & Land, 1975, Land & Collett, 1974). The precision and speed when flying in their natural environment is enough to impress even the most reserved viewer. Although small in absolute terms, the fly visual system is often huge with respect to overall body size and is organised in a highly structured manner. In fact, much of the fly's brain is devoted to the task of processing vision. For example, in the housefly, minus the retina, the visual neuropils make up 50% of the volume of the entire brain and the first two optic neuropils are 20 and 10 times more densely packed than equivalent areas in the primate visual system (Strausfeld, 1976).

The fly's optic lobes and particularly, the motion processing ganglia are amenable to electrophysiological recordings and individual neurons can be easily identified from one animal to the next. The modern conceptual understanding of motion detection

arose from experiments using insects in the 1950's and over the subsequent decades, insects, and the fly particularly, have remained dominant models for investigating the neural processing of motion.

In this thesis the hoverfly, *Eristalis tenax*, has been used as an experimental model to investigate the neural mechanisms of natural image processing. *Eristalis* is a master of exquisite flight control in multiple flight modalities. In the subsequent sections of this chapter, I will review some of the most relevant literature pertaining to the processing of motion in the flies visual system.

1.2 Optic flow and the optomotor response

Animals will encounter: either motion of the entire visual field generated by self-motion; object motion relative to the visual field; or a combination of both wide-field and object motion (Hausen & Egelhaaf, 1989). For self-motion, translation and/or rotation about different body axes result in characteristic patterns of velocity vectors, known as optic flow fields (Figure 1.1) (Koenderink & van Doorn, 1987, Nakayama & Loomis, 1974). For example, forward translation generates a flow field with a pole of expansion in the direction of heading with the velocity of the scene moving past the eyes more rapidly lateral to the direction of heading (Figure 1.1B) (Franz & Krapp, 2000, Krapp, Hengstenberg & Hengstenberg, 1998, Krapp & Hengstenberg, 1996). Roll rotation, on the other hand generates a different flow-field whereby local velocities run in concentric rings converging around poles of singularity frontally and caudally (see Figure 1.1C). Optic flow fields generated by self-motion provide useful feedback to the animal about how it is moving relative to its surrounds (Gibson, 1958, Koenderink, 1986, Lee & Kalmus, 1980, Warren & Hannon, 1988). Many animals ranging from insects to fish, reptiles, birds, and primates have all been shown to rely on optic flow cues to gather information about their own motion within the environment (Lappe, Bremmer & van den Berg, 1999, Reichardt & Poggio, 1976, Srinivasan, Poteser & Kral, 1999).

In tethered insects, image motion produces a robust syn-directional motor response that stabilizes the image on the retina, a reflex known as the optomotor response (Buchner, 1984, Pflugfelder & Heisenberg, 1995, Poggio & Reichardt, 1976). In

flies, optic flow fields simulating different types of self-motion generate different motor responses matched to the optic flow field. For example, tethered flies respond to purely rotating stimulus with turning responses in the same direction as the image motion (Blondeau & Heisenberg, 1982, Götz, 1968), whereas an expanding optic flow field, simulating back to front motion, results in the animal producing forward thrust (Götz, 1968). Optic flow fields do not just generate changes in heading from tethered flies, though. When presented with expanding optic flow fields or dimming ambient light levels, flies have been shown to initiate landing responses (Borst & Bahde, 1986, Braitenberg & Taddei-Ferretti, 1966, Wagner, 1982). Recent experiments using tethered *Drosophila* in a flight arena have challenged the basic premise that flies respond to rotating flow-fields, instead suggesting that the optomotor response is generated by image expansion at different locations in the visual field (Tammero, Frye & Dickinson, 2004). These results suggest that the visual system is responding to translational movements, such as side-slip, to control stable flight, rather than rotational flow-fields (Tammero et al., 2004). This is yet to be confirmed in other fly species, though.

Optic flow does not only provide useful information about the animal's self-motion. It can also provide important information about the three-dimensional layout of scenes. Translational optic flow causes closer objects to generate faster retinal velocities than those that are farther away, thus enabling the animal to ascertain relative distance information based on relative retinal velocity cues (Koenderink, 1986, Koenderink & Van Doorn, 1976, Nakayama & Loomis, 1974). For example, locusts and praying mantids display characteristic peering behavior, swaying in a controlled way to induce lateral translational shifts in the scene, to gather information about the distance of objects in their frontal visual field (Horridge, 1986, Kral, 1998, Kral, 2003, Sobel, 1990). Self-induced optic flow has also been suggested to be important for figure-ground discrimination and the tracking response of flies (Reichardt & Poggio, 1979, Virsik & Reichardt, 1976).

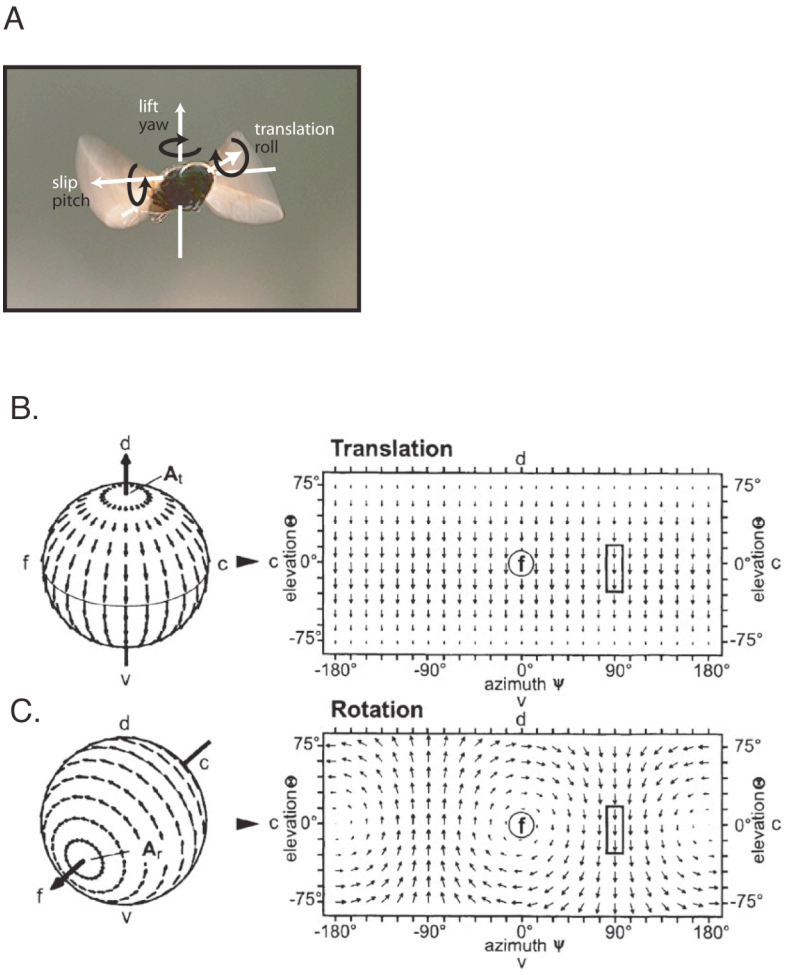

Figure 1.1 Optic flow

An animal's movement through the environment can be thought of as either rotation or translation about different body axes (A). Different self-movements generate different patterns of local velocity vectors across the eye, known as optic flow fields. Optic flow field resulting from translation along the vertical axis (lift), B, and rotation around the horizontal axis (roll), C. The distribution of velocity vectors depends on the momentary self-motion. Generally, there is no motion at the flow field singularities (A_t for translation and A_r for rotation). The Mercator plots show optic flow across the whole visual field. Positions are specified by angles of azimuth ψ and elevation Θ, where ψ<0 represents the left visual hemisphere and ψ>0 the right. f, denotes frontal; c, caudal; d, dorsal; v, ventral. Although globally different, locally, different optic flow fields can produce undistinguishable motion signals. Boxes at ψ=90° shows a region of local similarity between the two flow fields. Adapted from Krapp and Hengstenberg (1996).

1.2 The motion-processing pathway in flies

1.2.1 Optics and photoreception

The compound eyes of insects are fundamentally different from those of vertebrates. Vertebrates have camera-type eyes, where a single lens focuses light onto arrays of receptors each with different receptive fields. Insects, on the other hand, have compound eyes, which sample the visual panorama with thousands of tiny lenses, or facets (Figure 1.2A; Land, 1981, Land, 1989). Each facet points in a different direction and focuses light from a narrow angle onto a waveguide structure containing a set of (typically) eight photoreceptors (R1-8). Collectively, this optical cartridge is known as an ommatidium (Figure 1.2B; Nilsson, 1989, Strausfeld, 1989).

There are two basic variants of the compound eye: apposition and superposition eyes. For apposition compound eyes, the photoreceptors behind each facet are optically isolated from one another, only accepting light from the lens in its own ommatidium (Figure 1.2C). The photoreceptors of superposition eyes are separated from the facet by a clear zone, enabling many neighbouring facets to act in unison as a single optical device (Figure 1.2C; Land, 1981, Land, 1989). Apposition compound eyes however, are the stereotypical eye design for day active insects as they enable maximum spatial resolution (but see Warrant 2008), while the superposition compound eyes enable greater light capture at the expense of spatial resolution and thus, are typically found in nocturnal insects (Land, 1981, Land, 1989).

Flies utilize a variant of the apposition eye design, the neural-superposition eye (Figure 1.2C). In the neural superposition eye, photoreceptors within one ommatidium are optically separated from each other and accept light from different optical axes. Each photoreceptor shares a parallel optical axis with six other photoreceptors from the six neighbouring ommatidia. Photoreceptors orientated along the same optical axis from neighbouring ommatidia cross over in the first optic chiasm and converge onto a common neural column in the following neuropil, thus generating a topographic representation of visual scene (Figure 1.2C). Neural pooling of signals in this manner results in greatly enhanced light capture without any sacrifice in visual acuity (Land, 1981, Land, 1989, Nilsson, 1990).

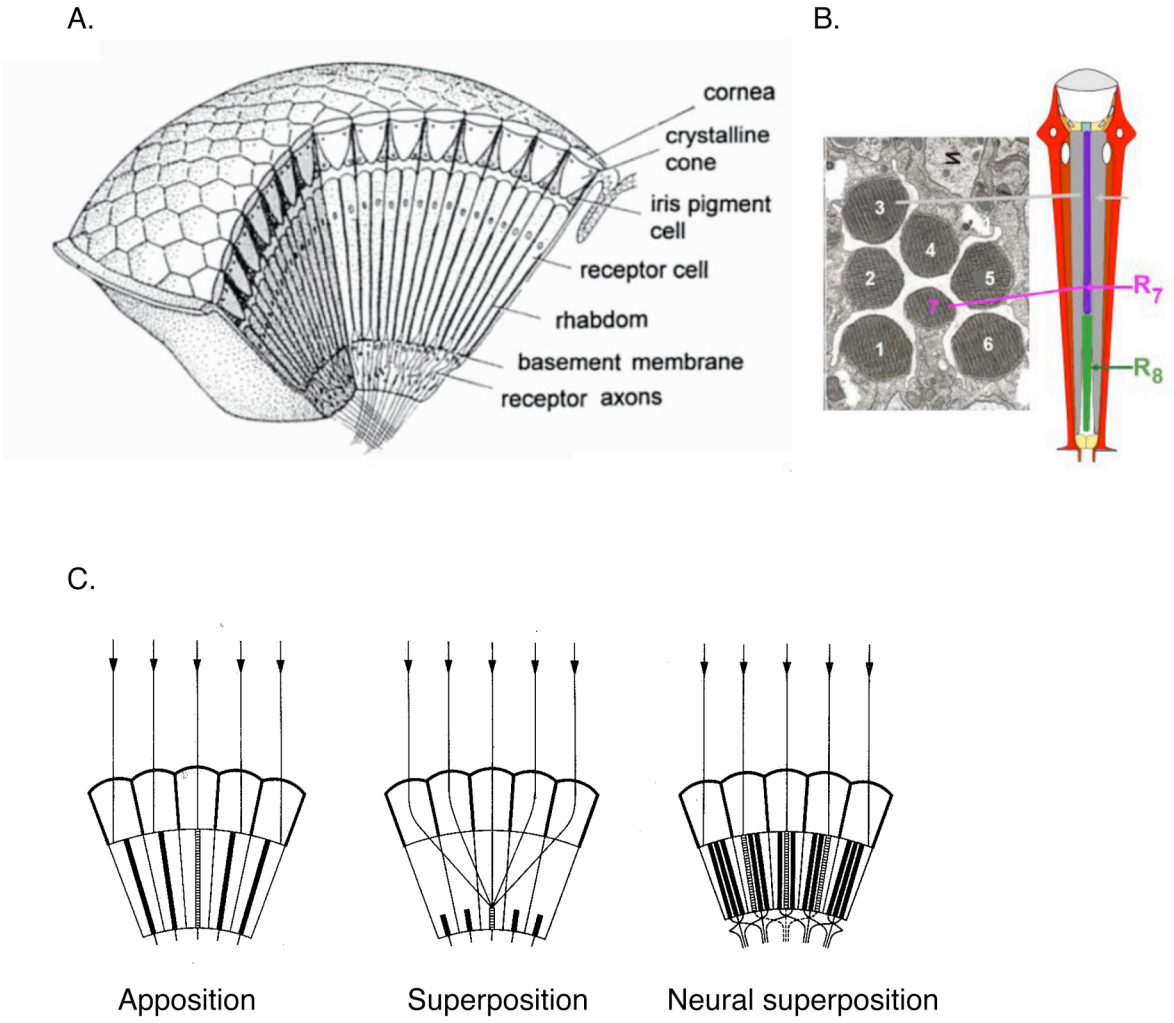

Figure 1.2 The compound eye

A. Diagram of a compound eye. B. A single ommatidium from lens to basement membrane. Each ommatidium has 8 photoreceptors, R1-8. Their arrangement is shown on the inset to the left. C. The two main types of compound eye: apposition and superposition compound eyes. Photoreceptors of apposition eyes are optically isolated from neighbouring ommatidium, whereas the photoreceptors of superposition eyes are separated from the facet by a clear zone, enabling many neighbouring facets to act in unison as a single optical device. Far right, the neural superposition eye is a form of apposition eye. Photoreceptors within one ommatidium are optically separated from each other and accept light from different optical axes. Each photoreceptor shares a parallel optical axis with six other photoreceptors from the six neighbouring ommatidia. Photoreceptors orientated along the same optical axis from neighbouring ommatidia cross over in the first optic chiasm and converge onto a common neural column. A. Adapted from (Land & Nilsson, 2002). C. Adapted from (Kirschfeld, 1867)

Although the front end of the fly's visual system is substantially different from that of vertebrates, it still results in light being focussed onto an array of receptors representing visual space. Thus in that sense, the initial neural representation is similar. However, the quality of the image represented at the retinal level does differ substantially between flies and vertebrates. The fruitfly, *Drosophila,* for example has just 700 facets per eye with an interommatidial angle of 4.6°, resulting in a very blurry field of view that covers almost 180° of visual space (Land, 1981). In stark contrast, the human fovea has roughly 60,000 cones in about 2° of visual space with an interreceptor angle of approximately 0.01° (Land, 1981). Thus, between fruitflies and humans, as an extreme example, there is an enormous difference in the spatial quality of the image represented at the level of the photoreceptors (approx. 500-fold). Many larger flies species do not suffer from quite as low resolution as the fruitfly. For example, the spatial resolution in blowflies is about 1-2° (Land, 1997) and large hoverflies and dragonflies can carry even larger compound eyes, improving their spatial resolution further (Land, 1981, Land, 1997). However, even in these eyes the spatial resolution is still far lower than the resolution of most vertebrate eyes.

As each facet has its own receptor cartridge, improvements in spatial resolution require an increase in the total number of ommatidia and consequently, an increase in eye size. For flying insects particularly, there is a huge trade-off associated with increased spatial resolution and the energy burden of having to fly around with large, heavy, and cumbersome compound eyes. The importance of having a visual system with relatively high spatial resolution is not more apparent than in many fly species, which have evolved enormous optical apparatus covering their entire head and in some cases amounting to roughly 30% of their entire body weight (O'Carroll, Niven, and Laughlin, in preparation). To reduce the overall increase in eye size required to improve spatial resolution, many species have improved spatial resolution in specialized regions of the eye (acute zones), similar to the fovea in vertebrates (Land & Eckert, 1985). Other species have similar specialized regions but where facet size is increased (bright zones) allowing greater light capture and thus, contrast sensitivity, as opposed to increased resolution (Straw, Warrant & O'Carroll, 2006, van Hateren, Hardie, Rudolph, Laughlin & Stavenga, 1989). The amount of blurring

induced by the optics of the eye is the first stage of image processing and has important consequences for motion processing at later stages of the visual system (Dror, O'Carroll & Laughlin, 2001; Brinkworth and O'Carroll, 2009).

1.2.2 Early visual processing

The six off-axis photoreceptors in each ommatidium, R1-6, are achromatic and send projections onto the first optic ganglion, the lamina, whereas the two central photoreceptors, R7 and R8, are chromatic sending their projections further to the second optic ganglion, the medulla (Figure 1.2). Studies in *Drosophila* have verified that only the achromatic photoreceptors R1-R6 are involved in motion processing (Heisenberg & Buchner, 1977, Yarnaguchi, Wolf, Desplan & Heisenberg, 2008). Logarithmic encoding of luminance combined with dynamic adaptive mechanisms enable these photoreceptors to operate across the enormous range of light intensities encountered in the natural environment, despite having a limited coding range (Laughlin, 1994, van Hateren & Snippe, 2001, van Hateren & Snippe, 2006).

Photoreceptors R1-6 form histaminergic synapses with the Large Monopolar Cells (LMC) of the lamina (Laughlin, Howard & Blakeslee, 1987). Each retinotopic column in the lamina contains five principal LMCs, L1-5, an amacrine cell and a basket T1 cell. The amacrine cells spread laterally across the visual columns of the lamina and are thought to play a role in lateral spatial inhibition (Strausfeld, 1976). The basket neuron, T1, is proposed to receive input from photoreceptors R1-6 indirectly via the amacrine neurons. It projects to the medulla where its outputs mix with the L2 terminals. The response properties of the LMCs have been extensively studied and can be well approximated with high-pass filtering in space and time (James, 1990, Laughlin, 1981, Srinivasan, Laughlin & Dubs, 1982). This has been shown to be effective for removing redundant information in the visual input and enhancing edge-like boundaries (Srinivasan et al., 1982, Srinivasan, Pinter & Osorio, 1990). Of the LMCs, only L1 and L2 are necessary for generating the optomotor response to visual motion (Rister, Pauls, Schnell, Ting, Lee, Sinakevitch, Morante, Strausfeld, Ito & Heisenberg, 2007). The LMCs project their axons to the second optic ganglion, the medulla.

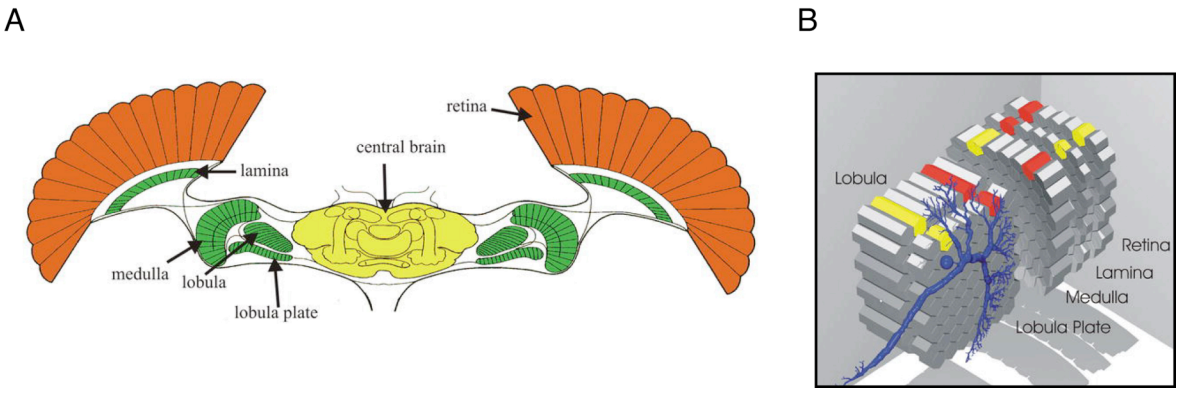

Figure 1.3 Anatomy of the fly's brain

A. Dorsal view of the fly's brain showing the retina and four main optic neuropils: lamina, medulla, lobula and lobula plate. B. Three-dimensional schematic of the successive optic ganglia from the retina to the lobula plate. Each of the main optic neuropils retains a retinotopic organization, however the orientation of these neuropils change from one to the next (B). Colored columns show the orientation of visual space at each successive ganglion. Adapted from Borst and Haag (2002).

Recordings from neurons in the following optic ganglion, the medulla, show some evidence for direction selectivity (DeVoe, 1980, Douglass & Strausfeld, 1995, Douglass & Strausfeld, 1996). Activity dependent labelling in *Drosophila,* shows that different layers of the medulla are excited when motion is presented as opposed to full field flicker with the same temporal frequency, suggesting the medulla is likely to be the first location of the emergence of direction selectivity (Bausenwein & Fischbach, 1992, Buchner, Buchner & Bülthoff, 1984). These layers contain ramifications of the T4 neuron, which has been shown to form chemical synapses with the motion sensitive neurons of the lobula plate (Strausfeld & Lee, 1991). Motion sensitive neurons in the medulla are small and notoriously difficult to record from (Douglass & Strausfeld, 1995, Douglass & Strausfeld, 1996, Douglass & Strausfeld, 2003, Strausfeld, 1976), hence the precise neural elements involved in the early detection of motion have largely remained elusive.

The third optic ganglion, or the lobula complex, is split into two separate interconnected ganglia, the lobula and the lobula plate, the latter of which contains a

range of identified motion sensitive neurons (Borst & Haag, 2002, Egelhaaf & Borst, 1993, Nordström & O'Carroll, 2009). Different identified neural classes give complex response properties, which parse the processing of different types of motion (Borst & Haag, 2002, Egelhaaf & Borst, 1993, Nordström & O'Carroll, 2009).

1.2.3 Feature and target motion detection

Several neural classes have been identified that respond exclusively to the motion of features or objects. The Feature Detecting (FD) and Contralateral Inhibited (CI) neurons respond optimally to the motion of grating patterns far smaller than the size of their receptive fields, e.g. less than 10° (Egelhaaf, 1985, Gauck & Borst, 1999). They are hypothesised to be involved in the detection of features and in figure-ground discrimination. Using photo-ablation techniques, the size tuning of the FD neurons was shown to arise from inhibitory feedback from the GABA-ergic wide-field centrifugal horizontal (CH) neurons (Egelhaaf, Borst, Warzecha, Flecks & Wildemann, 1993, Warzecha, Egelhaaf & Borst, 1993). However, their optimal responses are still to relatively large features (Egelhaaf, 1985, Gauck & Borst, 1999b; Nordström and O'Carroll, 2009a).

Small Target Motion Detectors (STMDs), have been identified and characterized in the lobula of hoverfly and dragonfly visual systems with exquisite sensitivity for the motion of small objects (Barnett, Nordström & O'Carroll, 2007, Collett, 1971, Nordström & O'Carroll, 2009a, Nordström & O'Carroll, 2006, Nordström, Barnett & O'Carroll, 2006, O'Carroll, 1993). STMDs show optimal sensitivity for the motion of very small features, 1.6-3.2°, close to the size of individual ommatidia. Olberg identified pre-motor descending neurons in the ventral nerve cord of dragonflies with similar response properties (Olberg, 1981, Olberg, 1986). The response properties of many STMDs have also been shown to be robust against the presence of background motion, suggesting that the likely mechanisms underlying their small target selectivity are different from that described for the FD neurons (Barnett et al., 2007, Nordström et al., 2006). They have been suggested to have a role in the detection and tracking of small moving targets during prey capture or courtship behaviour (reviewed in Nordström & O'Carroll, 2009a).

1.2.4 Wide-field motion detection: The lobula plate tangential cells

While the study of neurons sensitive to smaller features is still in its infancy, wide-field motion processing in the lobula has been extensively studied. There is a suit of roughly 60 giant motion-sensitive interneurons known as the lobula plate tangential cells (LPTCs), which have formed the basis for the study of motion processing in the fly (Borst & Haag, 2002, Egelhaaf & Borst, 1993, Strausfeld, 1976) (Figure 1.4). The LPTCs spatially pool local motion inputs across their receptive fields, responding optimally to wide-field motion. Their input dendrites span across many thousands of input columns in the peripheral layers of the lobula plate corresponding to their extensive receptive fields (Borst & Haag, 2002, Egelhaaf & Borst, 1993, Strausfeld, 1976).

Numerous studies have revealed that LPTCs are crucial elements in the processing pathway from visual stimulation to motor output (Borst & Bahde, 1988, Geiger & Nässel, 1981, Hausen & Wehrhahn, 1983, Heisenberg, Wonneberger & Wolf, 1978). The response properties of LPTC show spatio-temporal frequency tuning and sensitivity to pattern contrast with remarkable resemblance to torque responses produced by tethered flies (Hausen, 1982b, Hausen & Wehrhahn, 1989, Hengstenberg, 1982). The ablation of some LPTCs in larval houseflies results in reduced optomotor responses (Geiger & Nässel, 1981) and *Drosophila* mutants that are missing the entire lobula plate do not display optomotor responses at all whilst walking (Blondeau & Heisenberg, 1982, Heisenberg et al., 1978). Additionally, microsurgical lesions that sever LPTC projections to central brain areas (protocerebrum) result in altered optomotor responses in the blowfly (Hausen & Wehrhahn, 1983, Hausen & Wehrhahn, 1990), providing further evidence that the LPTCs are a necessary link in the visuo-motor pathway for the animal to generate optomotor responses. Furthermore, activation of LPTCs via extracellular field potentials can produce turning and landing responses from flies in the absence of visual stimuli, suggesting that activation of these neurons alone may be enough to initiate certain responses (Blondeau & Heisenberg, 1982).

Unlike the optic ganglia preceding the lobula complex, where neurons show remarkable similarity not just across dipteran species but also arthropods (Osorio,

Averof & Bacon, 1995, Strausfeld, 2005), species differences in the lobula plate appear to be far more pronounced (Buschbeck & Strausfeld, 1997). Nevertheless, the LPTCs can be grouped into two prominent subclasses based on their global direction selectivity: the vertical system (VS), and the horizontal system (HS). Although VS and HS neurons are conserved as groups across taxa, the number and structure of neurons differs from species to species (Buschbeck & Strausfeld, 1997).

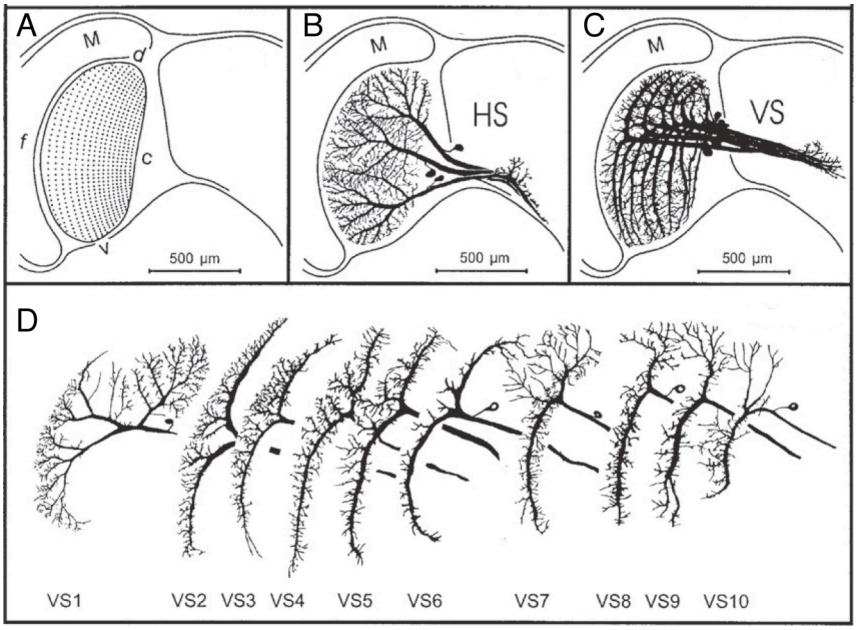

Figure 1.4 Lobula plate tangential cells

A. Retinotopic organization of the lobula plate in the left visual hemisphere, f, frontal; c, caudal; d, dorsal; v, ventral. B. The three horizontal system (HS) neurons in the blowfly. C. The 10 vertical system neurons (VS) in the blowfly. Both the VS and HS neurons cover the whole neuropil. D. The 10 VS neurons separated to more clearly show their dendritic arbors. Modified from Krapp et al. (1998). A. Originally adapted from Hausen, (1993); B originally adapted from Hausen (1982a); C and D originally adapted from Hengstenberg et al. (1982).

1.2.5 Horizontal System (HS) neurons

Neurons of the Horizontal System (HS) are sensitive to horizontal image motion. In blowflies, and many other flies, there are three HS neurons in each visual hemisphere (Hausen, 1982a, Strausfeld, 1976). The HS neurons have semi-overlapping receptive fields, which are centred at different locations along the dorso-ventral axis of the visual field (Figure 1.4B). They are named based on the location of their receptive fields on the dorsal to ventral axis: north, equatorial, and south (HSN, HSE, and HSS respectively Hausen, 1982a, Hausen, 1982b, Krapp, Hengstenberg & Egelhaaf, 2001). Their receptive fields stretch from the visual midline and far (~100 degrees) into the ipsilateral visual field (Hausen, 1982a, Hausen, 1982b). Whereas most fly species have three HS neurons in each visual hemisphere, hoverflies have four HS. The HSNE, north-equatorial, neuron's receptive field lies between that of HSN and HSE on the dorsal-ventral axis (Buschbeck & Strausfeld, 1997, Nordström, Barnett, Moyer de Miguel, Brinkworth & O'Carroll, 2008, O'Carroll, Laughlin, Bidwell & Harris, 1997).

The HS neurons receive their inputs from the distal layers of the lobula plate and send stout axons and output dendrites into areas of the sub-oesophageal ganglion associated with pre-motor descending neurons (Hausen, 1982a, Strausfeld, 1976). HS neurons respond to visual motion in the ipsilateral visual field with characteristic graded shifts in membrane potential either depolarisation for preferred direction stimulation or hyperpolarization for motion in the opposite direction (Haag & Borst, 1996, Haag, Vermeulen & Borst, 1999, Hausen, 1982a, Nordström & O'Carroll, 2009). In blowflies, motion in the contralateral visual field produces spikelets, which coincide in a one-to-one fashion with extracellularly recorded spikes presumed to be from the heterolateral H2 neuron (Haag et al., 1999). The fast irregular HS spikelets have been suggested to enhance specificity to rotational optic flow (Horstmann, Egelhaaf & Warzecha, 2000) and arise from fast-activating sodium currents (Haag & Borst, 1996, Haag, Theunissen & Borst, 1997).

Other neurons sensitive to horizontal image motion include two additional centrifugal horizontal neurons (CH) in each hemisphere (Eckert & Dvorak, 1983, Gauck, Egelhaaf & Borst, 1997, Strausfeld, 1976). Unlike the HS neurons, the CH neurons receive their inputs from areas in the midbrain and have their output dendrites in the distal layers of the lobula pate. They also make post-synaptic connections in the distal layers of the lobula plate. They are GABA-ergic neurons and amongst other things play an important role in size selectivity of the FD neurons (Egelhaaf, 1985, Egelhaaf et al., 1993, Warzecha et al., 1993). Several other neurons sensitive to horizontal image motion have been identified that send output projections to the contralateral hemisphere, for example the H1-4 neurons (Borst & Haag, 2001, Eckert, 1980).

1.2.6 Vertical System (HS) neurons

The VS neurons are primarily sensitive to vertical image motion. There are 10 VS neurons whose receptive fields are elongated vertically (Hengstenberg, 1982, Hengstenberg, Hausen & Hengstenberg, 1982, Krapp & Hengstenberg, 1996) (Figure 1.4C and D). Each VS neuron has a receptive field that spreads the dorsal-ventral axis of the visual field, but unlike the HS neurons they have limited spread laterally. In the blowfly, the VS neurons are numbered 1-10 based on their location around the azimuth, with VS1 having a frontally orientated receptive field around to VS10 which has a receptive field towards the posterior visual field (Hengstenberg, 1982, Hengstenberg et al., 1982). Like the HS neurons, the VS neurons also respond to image motion with graded shifts in membrane potential superimposed with spikelets of irregular amplitude.

1.2.7 Local motion sensitivity

The naming convention for vertical (VS) and horizontal (HS) system neurons reflects the global direction preferences of LPTCs. However, the LPTC are not just sensitive to motion in one direction, but rather pool their inputs from local motion sensitive elements with different local preferred directions (Franz & Krapp, 2000, Karmeier, Krapp & Egelhaaf, 2003, Krapp et al., 1998, Krapp & Hengstenberg, 1996, Krapp & Hengstenberg, 1997, Krapp et al., 2001). A key observation that has been thoroughly investigated in all the HS and VS neurons is that their local preferred directions share remarkable similarities to optic flow fields generated by self-rotation (Franz & Krapp, 2000, Krapp et al., 1998, Krapp & Hengstenberg, 1996) (Figure 1.5). These observations have led to the proposal that many of the LPTCs act as matched filters for specific optic flow fields generated from self-motion about different body axes (Figure 1.5). Similar observations have also been made for motion sensitive neurons in primates (for review see Lappe et al., 1999). Nevertheless, despite the 'matched filter' nature of their receptive fields it is still unclear how these neurons are able to deal with the enormous variability inherent within natural images.

One mechanism for overcoming locally variable responses is to integrate these over a large region of space. Owing to the retinotopic organization of the lobula plate the LPTCs should have receptive fields that are matched to the extent of their dendritic arbours. However, intracellularly recorded receptive fields of VS neurons are 3-4 times larger than that predicted by spread of their input dendrites (Farrow, Borst & Haag, 2005, Krapp et al., 1998, Krapp & Hengstenberg, 1996). Several recent studies have revealed that this increase in receptive field size is the direct result of lateral gap-junctions between the VS neurons, thus blurring their receptive fields with those of their neighbours (Elyada, Haag & Borst, 2009, Farrow et al., 2005, Haag & Borst, 2004, Haag & Borst, 2005). This cross-communication of retinotopic inputs has been suggested to lead to more robust representation of specific optic flow fields in natural image conditions (Cuntz, Haag, Forstner, Segev & Borst, 2007).

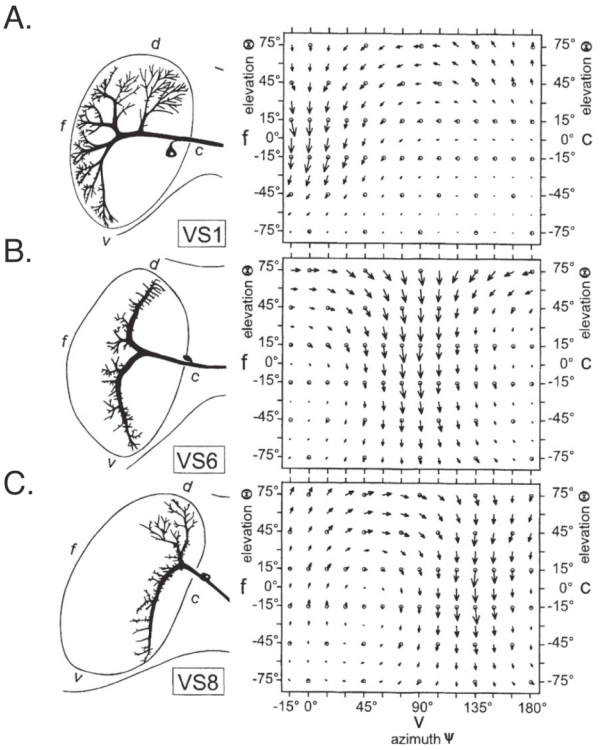

Figure 1.5 Local preferred directions

A-C shows the anatomy and response fields for VS1, VS6, and VS8. Local motion sensitivities are shown as Mercator maps as in Figure 1.1. The direction of the arrows show local preferred direction and arrow length shows local sensitivity (response strength). The response fields of all VS neurons show similarity to rotatory optic flow fields. Each VS neuron, however, matches rotation around a different body angle. Adapted from Krapp and Hengstenberg (1996).

1.2.8 Descending and pre-motor neurons

The output dendrites of HS and VS neurons project to central areas in the mid-brain, which are associated with pre-motor descending neurons involved in the control of neck and flight muscles (Gronenberg & Strausfeld, 1990, Strausfeld & Bassemir, 1985a, Strausfeld & Bassemir, 1985b). The descending neurons of the ocellar and vertical system (DNOVS) integrate the outputs of different combinations of VS neurons, most likely via both chemical and direct electrical connections (Haag, Wertz & Borst, 2007, Wertz, Borst & Haag, 2008). The extra spatial pooling of motion signals is suggested to further improve the DNOVS neurons selectivity for specific rotational optic flow fields (Haag et al., 2007, Wertz et al., 2008).

In a hierarchical manner the neck motor neurons (NMNs), receive direct input directly from LPTCs and indirectly via the descending neurons (Grönenberg, Milde & Strausfeld, 1995, Huston & Krapp, 2008, Strausfeld & Seyan, 1985). The neck motor neurons synapse directly on muscles that control head rotations and have receptive fields that extend substantially into each visual hemisphere, far beyond the

extent of any individual LPTCs or DNOVS neurons (Huston & Krapp, 2008). Like the DNOVS neurons, the NMNs pool their inputs to enhance their selectivity for specific optic flow fields (Huston & Krapp, 2008). Thus, a direct chain from photoreception at the level of the retina to the muscles that control head rotations might include as few as five serial synapses (Hausen & Egelhaaf, 1989).

The control of the wing steering muscles is slightly more sophisticated though. Evidence suggests that steering muscles do not receive direct input from motion sensitive descending neurons but rather indirectly via the mechano-sensory hind wings, the halteres (Chan, Prete & Dickinson, 1998). The halteres mediate corrective reflexes during flight by detecting coriolis forces that result from angular rotations of the animal and presumably combining this with visual feedback from the direction selective descending neurons (Frye & Dickinson, 2001).

1.3 Mechanisms of visual motion detection

How is motion computed locally prior to the integration by the LPTC receptive fields? Computer scientists and engineers have developed several different schemes for computing image motion, each with its own pros and cons. These models can be grouped into three major schemes: The feature tracking schemes; the gradient detectors; and the family of correlation-based motion detection models, which include the popular motion energy models.

1.3.1 Feature-based tracking schemes

The feature-based tracking schemes rely on identifying particular features, or derivatives of features, within a scene and then comparing their positions at different points in time. By calculating the displacement of an object over a known amount of time, the velocity of motion can easily be derived (Smith & Brady, 1997). These models are highly popular with computer scientists and engineers, but require the challenging task of identifying and locating the same feature through multiple time points. Consequently, they require large amounts of computing power.

1.3.2 Gradient schemes

The family of gradient detector models has emerged as one of the best-known approaches for reliably detecting the velocity of image motion (Limb & Murphy, 1975, Srinivasan, 1990). Gradient detectors measure local light intensity gradients at multiple locations in space (Figure 1.6B). A major advantage of this family of movement detectors is that they are able to accurately calculate image velocity under a wide range of conditions. The gradient detector calculates motion by dividing the temporal luminance gradient taken from one receptor by the spatial luminance gradient measured across at least two different points in space. Consequently, if the spatial derivative is small, noise in the temporal derivate gets amplified and furthermore, if the spatial derivative is equal to zero, then the velocity is undefined (Limb & Murphy, 1975, Srinivasan, 1990). Subsequently, at low light levels the gradient detector has a poor signal to noise ratio (Borst, 2007, Srinivasan, 1990). Although these models have gained momentum in the areas of machine vision and image processing, there has been little reciprocity in biology, where neurobiological evidence has directly contradicted the implementation of such mechanisms underlying motion detection in flies (Haag, et al, 2004).

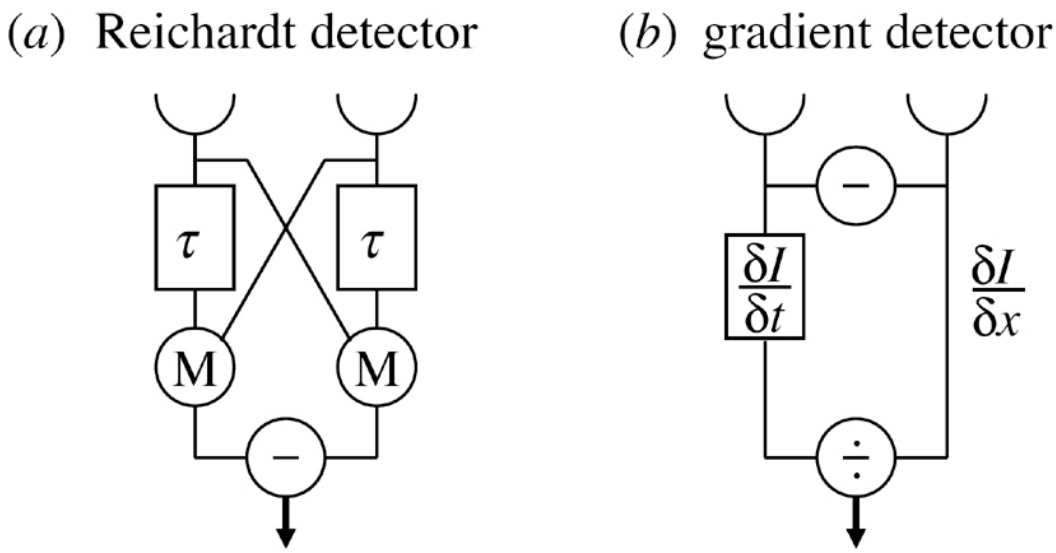

Figure 1.6 Motion detector models

Two popular models for motion detection in the insect visual system. (a) The Hassenstein-Reichardt detector consists of two mirror symmetrical subunits whose outputs are subtracted. Each subunit receives luminance inputs from two adjacent points in space and correlates them (M) after one has been delayed by a low-pass filter (τ). Correlation (M) is often modeled as multiplication. (b) The gradient detector divides the temporal luminance gradient from one point in space ($\delta I/\delta t$) by the spatial luminance gradient across two points in space ($\delta I/\delta x$). Adapted from Borst (2007).

1.3.3 The Hassenstein-Reichardt correlator and motion energy models

More than half a century ago, in an elegant suit of experiments using the robust optomotor response of the beetle *Chlorophanus,* Hassentstein and Reichardt characterized behavioural responses to different visual stimuli. These experiments led to the proposal of a delay and correlate model for motion detection, commonly known as the 'Hassenstein – Reichardt correlator' or 'Reichardt correlator' (Figure 1.6A) (Hassenstein & Reichardt, 1956, Reichardt, 1961). Over the past 50 years or so, this model has received widespread acclaim and is now one of the most enduring models in visual neuroscience (Borst & Egelhaaf, 1989, Clifford & Ibbotson, 2002, Egelhaaf & Borst, 1993).

Broken down into its principal components the Reichardt correlator computes the direction of image motion by correlating luminance at one point in space with the temporally delayed luminance at a neighbouring, or spatially offset, point in space (Hassenstein & Reichardt, 1956, Reichardt, 1961). In the implementation of the Reichardt detector, the correlation is typically modelled as a supra-linear interaction, such as multiplication (Figure 1.6A). The above description produces a model whose output is greater for motion in one direction than the other. It is sensitive to absolute changes in brightness, i.e. if the stimulus becomes brighter without the presence of any motion, model output also increases confounding the two parameters. By subtracting the output of two such subunits with mirror symmetry, a model whose output is sensitive to the direction of image motion is generated. The response is positive in one direction, negative in the oppsite direction, and is also largely insensitive to changes of non-motion related stimuli, such as absolute changes in brightness (Figure 1.6A).

Hassenstein and Reichardt's original description of the model was far more complicated than described above. In order to accurately predict the behavioural responses of the beetle used in their experiments, they had to include several linear filtering stages (Hassenstein & Reichardt, 1956, Reichardt, 1961). They represented the delay as a first-order low-pass filter (Figure 1.6A) as opposed to the more simple, pure temporal delay. This enables the model to detect motion across a range of speeds, as opposed to a pure temporal delay that would result in sensitivity at only one speed, defined by the duration of the delay (Buchner, 1984, Reichardt, 1961, Reichardt, 1987).

Since its inception, various elaborations and changes have been made to match the Reichardt correlator to the properties of motion detection in many additional animal species. For example in humans (Vansanten & Sperling, 1985), primates (Emerson, 1992), birds (Crowder, Dawson & Wylie, 2003, Wolf-Oberhollenzer & Kirschfeld, 1994), and marsupials (Ibbotson, Mark & Maddess, 1994; for reviews see Borst & Egelhaaf, 1989, Clifford & Ibbotson, 2002, Srinivasan et al. 1999). In some cases, the problem has been approached from a different angle only to arrive at a solution

that despite starting with different internal structures, produces outputs that are mathematically similar to the Reichardt correlator model (Adelson & Bergen, 1985).

Other studies have developed alternative schemes where some of the response properties are otherwise in opposition to the predictions of the Reichardt correlator, for example, the delayed inhibitory mechanisms (or veto mechanisms) underlying the direction selective responses in DS ganglion neurons of the rabbit and turtle retinas (Ariel & Adolph, 1985, Barlow & Levick, 1965). Nevertheless, while the specific implementation of such motion detecting mechanisms may vary, they are all qualitatively similar to the Reichardt correlator in terms of their input/output relationship.

1.3.4 Response characteristics of the Reichardt correlator

The Reichardt correlators fixed spatial inputs with simple delay and multiplication operation, generate several nontrivial predictions about responses to motion stimuli.

1. Response increases with the square of image contrast (changes in luminance) due to the multiplicative non-linearity at the correlation stage (Figure 1.6 and 1.7B).

2. Response does not increase monotonically with stimulus velocity, but rather increases up to an optimum, based on the characteristics of the delay filter, and then falls away again for faster stimulus velocities (Figure 1.7).

3. Any imperfection in the subtraction stage causes the response to a sinusoidal grating to modulate at double the temporal frequency of the grating, i.e. it responds to both polarities of the sinusoid (increasing and decreasing luminance changes). Such imbalance is a likely consequence of any biological implementation of subtraction via, for example, excitatory versus inhibitory interactions mediated by different neurotransmitters, and has been observed in locally measured motion responses (Egelhaaf, Borst & Reichardt, 1989a).

4. The fixed spatial separation results in the response being sensitive to the spatial frequency of the stimulus, with an optimum which depends on the angle of the separation of the inputs, $\Delta\phi$, by $f_{s,opt} = \frac{1}{4\Delta\phi}$ (Figure 1.7A).

5. Consequently, the response is sensitivity to the spatial and temporal frequency of the stimulus as opposed to velocity *per se,* whereby $Velocity = \frac{Tf}{Sf}$, where Tf is the temporal frequency of the stimulus and Sf is the spatial frequency.

6. The correlator also produces response reversals (spatial aliasing) for sinusoidal gratings with spatial frequencies between $\frac{1}{2\Delta\phi}$ and $\frac{1}{\Delta\phi}$, although these are damped by the gaussian blur introduced by the optics of the eye (Buchner, 1984).

1.3.5 Behavioural evidence for the Hassenstein - Reichardt correlator underlying motion detection in insect

While the underlying structure of the Reichardt correlator was originally proposed from behavioural experiments on beetles, a great deal of subsequent work and development has been based on tethered flies (Götz, 1975, Poggio & Reichardt, 1976, Virsik & Reichardt, 1976). By attaching a rod dorsally to the flies torso and measuring the magnitude of the optomotor response, Reichardt and his colleagues were able to confirm many of the predictions of the correlator model (Buchner, 1976, Buchner, 1984). I briefly list some of these below in the same order as described above.

1. At lower pattern contrasts, the torque response increased quadratically with stimulus contrast. Similar behavioural result were also obtained from both walking and flying fruitflies, *Drosophila* (Buchner, 1984).

2. Torque responses varied with the temporal frequency of the stimulus: increasing to an optimum then decreasing for higher frequencies.

3. By limiting the stimulus to a vertically elongated slit, Reichardt and Egelhaaf (Reichardt & Egelhaaf, 1988) were able to remove much of the influence of spatial integration and record optomotor responses that approximated the outputs of local detectors. They showed that consistent with predictions of the correlator model, optomotor responses in flies were modulated by the spatial phase of the stimulus pattern. These responses fluctuated tremendously and periodically signalled motion in the opposite direction (Reichardt & Egelhaaf, 1988).

4. Torque responses of the fly depended on the spatial frequency of the stimulus in the same way as that predicted by the Reichardt correlator, with an optimal spatial frequency related to the inter-ommatidial angle, $\Delta\phi$, by $f_{s,opt} = \frac{1}{4\Delta\phi}$.

   Behavioural work in light adapted animals showed that 70% of the optomotor response could be explained by nearest neighbour interactions (Buchner, 1976).

5. Responses are sensitive to spatial and temporal frequency, as opposed to velocity per se.

6. Torque responses produced negative response for spatial frequencies between $\frac{1}{2\Delta\phi}$ and $\frac{1}{\Delta\phi}$ (Buchner, 1984).

1.3.6 Neurophysiological evidence for the Hassenstein-Reichardt correlator underlying motion detection in insects

Electrophysiological recordings from fly LPTCs have also provided a great deal of support for Reichardt correlator at the cellular level. Some of the key observations are listed below again in the same order as above (for reviews see Borst & Egelhaaf, 1989, Clifford & Ibbotson, 2002, Egelhaaf & Borst, 1993).

1. At low stimulus contrasts, LPTCs show a quadratic response relationship with contrast. However, at higher stimulus contrasts the response saturates, consistent with the optomotor responses (Egelhaaf & Borst, 1993, Egelhaaf,

Borst & Reichardt, 1989b, Harris, O'Carroll & Laughlin, 2000, Hausen, 1982b, Srinivasan & Dvorak, 1980).

2. The response of HS neurons are temporal frequency tuned, rising to a maximum and then declining for higher temporal frequencies (Haag et al., 2004, Hausen & Egelhaaf, 1989, O'Carroll et al., 1997, O'Carroll, Bidwell, Laughlin & Warrant, 1996, Straw et al., 2006).

3. Egelhaaf et al. (1989a) extended the slit paradigm used in the behavioural experiments mentioned above to characterize local motion detector responses. They showed that HS neuron responses fluctuated at double the temporal frequency of the stimulus grating.

4. The spatial frequency tuning of HS neurons rises to an optimum, which is proportional to spatial sampling baseline of the ommatidial lattice, before falling away at higher spatial frequencies (Eckert, 1980, Egelhaaf & Borst, 1989, Egelhaaf et al., 1989a, Haag et al., 2004, Haag, Egelhaaf & Borst, 1992, O'Carroll et al., 1997, O'Carroll et al., 1996, Srinivasan & Dvorak, 1980, Straw et al., 2006). Apparent motion flashes showed that LPTCs responded to motion over only neighbouring ommatidia. This indicates that the spatial baseline of motion computation is primarily on the order of individual ommatidia, consistent with the behavioural observation (Franceschini, Riehle & Le Nestour, 1989, Schuling, Mastebroek, Bult & Lenting, 1989).

5. In addition, Srinivasan and Dvorak (1980) showed in H1 recordings that there is an inversion of the response at high spatial frequencies as a result of spatial aliasing, as predicted by the correlator.

Many additional investigations have further verified the response properties of the LPTCs. For example, showing the transient oscillating responses properties of HS neurons can be accounted for by intrinsic properties of the Reichardt correlator (Egelhaaf & Borst, 1989). Furthermore, even some of the adaptive rescaling responses of the H1 neuron can be explained as a consequence of the non-linearity

inherent within motion detectors of the correlation type (Borst, Flanagin & Sompolinsky, 2005). Finally, Egelhaaf et al. (1989b) showed that the correlation of the Reichardt detector is well approximated with a pure multiplication and that the underlying motion detectors were not perfectly anti-symmetrical, but rather allowed some transfer of non-motion stimuli.

The Reichardt correlator makes some clear predictions about the type of neural elements that might be involved in motion detection. However, few studies have been successful in recording from areas of the brain (i.e. the medulla) that are likely to contain these elements and as such, to date their anatomical and physiological identity remain elusive. Douglass and Strausfeld (1995) recorded from a number of small-field elements in the medulla, lobula, and lobula plate, where they found motion-sensitive interneurons whose anatomical location may suggest that they could serve a putative role in the elementary computation of motion. However, the physiological response properties of these elements, the so-called Tm1 and T5 interneurons, are still inconclusive (Douglass & Strausfeld, 1995).

1.3.7 Velocity estimation

The above evidence supports the Reichardt correlator or similar mechanism underlying local motion detection in biological vision. Although, such a mechanism is sufficient to compute local 2-D velocity fields in controlled circumstances (Reichardt & Egelhaaf, 1989), it produces local responses that are sensitive to many stimulus parameters and thus, are enormously variable in natural environments (Reichardt, 1987). However, behavioural observations show conclusively that animals can accurately calculate retinal velocities (Srinivasan et al., 1996). This has led to the proposal of many alternative mechanisms for computing motion. For example, some authors have suggested that the biological system might employ two schemes for motion detection, a gradient like detector in high luminance conditions and then switch to Reichardt correlator like mechanisms under low light conditions. This would enable velocity estimation at both high light levels, and with high signal to noise ratio in low light conditions (Potters & Bialek, 1994). However, subsequent studies from blowfly LPTCs have revealed that, in these neurons at least, this is not the case, with responses consistent with a Reichardt correlator-like mechanism

persisting to very high luminance conditions (Borst, 2007, Haag et al., 2004). Other species, such as crabs, appear to have solved this problem by having multiple parallel EMD channels tuned to different temporal frequencies (Nalbach, 1989).

Natural scenes

Much of the earlier, *characterizational,* research on biological motion detectors took advantage of their predictable responses to experimenter defined stimuli, such as sinusiodally modulated contrast gratings, bars, spots, or square-wave gratings. These stimuli have proven to be powerful tools for revealing many of the fundamental processes underlying motion detection (Borst & Egelhaaf, 1989, Egelhaaf & Borst, 1993). However, they share little similarity with the kinds of scenes that biological visual systems have adapted to encode. It is generally assumed that visual systems are specifically tuned to the statistics of natural images on both developmental and evolutionary time scales (Carandini, Demb, Mante, Tolhurst, Dan, Olshausen, Gallant & Rust, 2005, Simoncelli & Olshausen, 2001).

Although natural scenes appear complex and enormously variable, there is a remarkable degree of predictability from one scene to the next and as such, natural scenes only occupy a small niche within the parameter space of all potential images (Balboa & Grzywacz, 2003, Field, 1987, Ruderman & Bialek, 1994, Simoncelli & Olshausen, 2001, Tadmor & Tolhurst, 1993, Tolhurst, Tadmor & Chao, 1992). Importantly, for correlation-based motion processing, natural images have a characteristic spatial frequency amplitude spectrum with the following relationship, $amplitude \propto Sf^{-1\,0+n}$, where n has been shown to vary between ~ -0.25 to 0.25 (Sf =spatial frequency) (Field, 1987, Tolhurst et al., 1992). This property of natural scenes alone negates the spatial frequency sensitivity of Reichardt correlators, because the fixed spatial sampling baselines produces the same velocity optimum across enormously different natural scenes (Figure 1.7B and C; Dror et al., 2001). Note that the small variation in n has little qualitative effect on the shape of the predicted velocity tuning (Figure 1.7C; Dror et al., 2001).

Natural scenes however, vary enormously in contrast (average amplitude) and because the response of correlation-based models increases with the square of image contrast, absolute model responses are highly variable from one scene to the next (Figure 1.7B; Dror et al., 2001, Straw, Rainsford & O'Carroll, 2008 see also Chapters 3 Figure S1C). This presents a fundamental problem for velocity analysis.

Recently, Straw et al. (2008) recorded the responses of hoverfly HS neurons to the motion of natural images. Across a large range of velocities, they showed that the responses of HS neurons had the same optimal velocity for all the natural images used, consistent with the predictions of the Reichardt correlator mentioned above (Straw et al., 2008). Interestingly though, although the images spanned a large range of contrasts, the magnitude of the responses were relatively consistent across the image set and accurately represented image velocity with membrane potential (Straw et al., 2008). This observation is in direct contradiction to the response properties of HS neurons to experimenter-defined stimuli, such as sinusoidal gratings. Straw et al. (2008) showed that this same set of images produced a near 10-fold range in responses from a Reichardt correlator model, which had many elaborations matched to motion processing in the hoverfly.

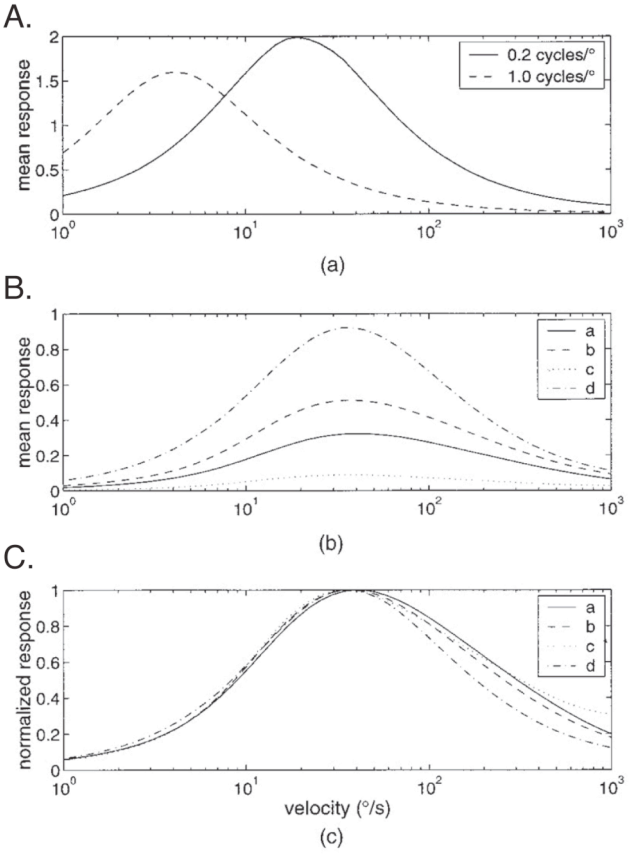

Figure 1.7 Responses of a Reichardt correlator as a function of velocity

A. Response to a sinusoidal grating at two different spatial frequencies, 0.2 cycles/° and 1.0 cycles/°, shows that velocity is confounded with spatial frequency. B. Responses to four natural images and C. same four curves as B but normalized to their maximum shows that different natural images result in correlator responses peaking at the same velocity. Adapted from Dror et al. (2001).

1.4 Naturalistic motion

Beyond the statistics of natural images, the dynamics of naturalistic motion are also critical for understanding how the visual system is processing motion and negotiating the natural environment (for a brief review see Zeil, Boeddeker & Hemmi, 2008). In naturally occurring behaviour the visual system is under closed loop, i.e. it is sensing changes in visual input and combining them with other sensory signals, such as those from olfactory and inertial sensors, and initiating motor responses appropriately (Frye & Dickinson, 2004, Zeil et al., 2008). Thus, the patterns of optic flow and feedback from other sensory modalities experienced by the visual system during flight are not going to be random, but rather well orchestrated sequences matched to specific behaviours that may well simplify a lot of the problems associated with motion estimation.

In free flight, flies adopt a characteristic flight behaviour, whereby periods of forward translation are interspersed with rapid alterations of flight direction, called saccades (Schilstra & Van Hateren, 1999). This stereotypical saccadic flight mode greatly defines the optic flow experienced by the animal. For example, the animal compresses rotational optic flow fields into brief high velocity turns, of 90° over ~50 ms with peak rotational velocities of >1000°/s (Schilstra & Van Hateren, 1999, Tammero & Dickinson, 2002b). During inter-saccadic periods of flight, the animal minimizes rotational optic flow with precisely controlled flight and head orientation so it only experiences optic flow fields matched to translation (Kern, van Hateren, Michaelis, Lindemann & Egelhaaf, 2005, Van Hateren & Schilstra, 1999). Separating different flow-fields into different parts of flight might greatly simplify the task of having to interpret self-motion and thus, enable the visual system to extract information about the spatial layout of the environment (Lindemann & Egelhaaf, 2005). More recently, studies in *Drosophila* have suggested that these saccadic turns are initiated by lateral image expansion, i.e. by optic flow fields generated from sideslip translation or approaching objects (Tammero & Dickinson, 2002a, Tammero & Dickinson, 2002b).

Recording neural activity during naturally occurring flight behaviour is not feasible with current technology. Nevertheless, research has begun to explore the response properties of motion sensitive neurons to naturalistic image motion reconstructed from optic flow experienced by freely flying or walking flies. Although some authors endeavoured to reconstruct optic flow experience in outdoor environments, they were not able to account for the head position during flight (Boeddeker, Lindemann, Egelhaaf & Zeil, 2005). Subsequent studies revealed the importance of taking into consideration the animal's head position before reliable interpretations of neural response could be made (Kern, van Hateren & Egelhaaf, 2006, Kern et al., 2005). During saccades the fly's head turns faster than the body thereby increasing the retinal velocities experienced as well as shortening the duration of the saccade. During periods of inter-saccadic flight, head orientation counteracts roll and sideslip, further stabilizing image motion and limiting optic flow fields experienced to translation (Schilstra & Van Hateren, 1999).

When presented with optic flow reconstructed from freely walking flies where the head orientation could be resolved, HS neurons were shown to encode turning responses relatively independent of translation experienced by the animal (Kern, Petereit & Egelhaaf, 2001). However, when optic flow was reconstructed from animals flying freely inside a confined space, the HS neurons were now shown to respond to both image rotation and translation, because of the higher translational velocities experienced (Karmeier, van Hateren, Kern & Egelhaaf, 2006, Kern et al., 2005). On the other hand, the H1 neuron, which is also sensitive to horizontal image motion, only produced responses during saccades and was suppressed during periods of forward translation (van Hateren, Kern, Schwerdtfeger & Egelhaaf, 2005). Subsequently, it has been suggested that once one considers the responses of populations of VS and HS neurons it is possible to parse optic flow generated by either rotation or translation (Karmeier et al., 2006). Separating these two types of flow fields might enable the animal to take advantage of motion parallax induced by translatory motion and gather three-dimensional information about the structural layout of the scene.

Although these endeavours are generating interesting conclusions about the functional roles of LPTCs, they are still very different from simulating the conditions experienced during naturally occurring flight. For example, on the occasions where head orientation was taken into account during flight, the arena was small (0.4 x 0.4 m) and had flat walls with no three-dimensional information (Schilstra & Van Hateren, 1999, Van Hateren & Schilstra, 1999). This could have promoted a collision avoidance low-speed flight mode in which objects were fixated followed by regular saccades to a new path. The blowflies never reached forward speeds above 0.4 m/s in this scenario (Schilstra & Van Hateren, 1999, Van Hateren & Schilstra, 1999) compared with those observed in more natural habitats (up to 2 m/s, see Boeddeker et al., 2005), let alone during hoverfly conspecific pursuit (up to 10 m/s, see Collett & Land, 1978). Furthermore, these conditions still have the system in open-loop, consequently, although the visual neurons are 'seeing' the stimulus they are not controlling it or receiving feedback from motor areas or other sensory modalities, all likely to be active during free flight.

1.5 Additional Neural Processes

Although the flight patterns adopted by flies will likely simplify many of the problems associated with analysing optic flow, i.e. separating rotatory and translatory motion, they still need to accurately interpret visual motion to coordinate flight. For example, in order to precisely control head positions during inter-saccadic flight periods the animals must be continually updating retinal image motion to account for unintentional shifts in self-motion, such as sideslip. Furthermore, the evidence that animals are able to make accurate estimates of image velocity is impossible to reconcile with accepted models for motion processing, which show a dependence on image contrast amongst other parameters. Thus, it still remains unclear how the visual system accurately computes motion within the natural environment.

Simple computational models for motion detection, such as the Hassensten–Reichardt correlator, often seek to represent as much of the experimental observations as possible with as few computational elements as possible. In the visual systems of animals though, the neural networks that make these kinds of computations are undoubtedly far more complex. The question beckons, how might additional neural processes be influencing the generation of local motion signals? The response properties of LPTCs show several characteristics additional to those typically included in motion processing models, yet their role in natural image processing remains poorly understood.

1.5.1 Static nonlinearities

The expansive non-linearity resulting from the multiplication stage in the correlator could only operate over a limited range in any biological implementation due to the biophysical limitation of signal transmission. Although the LPTC response increases as a function of the square of stimulus contrasts for sinusoids at very low contrast, as the contrast of the stimulus increases further the response becomes saturated, so that high stimulus contrasts are no longer accompanied by increases in response (Dvorak, Srinivasan & French, 1980, Egelhaaf & Borst, 1989). Subsequently, several authors have investigated the effects of including saturating elements in computational

models of motion detection in the insect visual system (Rajesh, Rainsford, Brinkworth, Abbott & O'Carroll, 2007, Rajesh, Straw, O'Carroll & Abbott, 2005, Rivera-Alvidrez & Higgins, 2005, Shoemaker, O'Carroll & Straw, 2005).

Dror and colleagues (Dror et al., 2001) showed that the inclusion of a saturating nonlinearity prior to motion correlation on the input arms of a Reichardt correlator improved the accuracy with which the model encoded the velocity of different natural images by reducing the amount of variability from one image to the next. In a subsequent modelling study using an elaborated Reichardt correlator, Shoemaker et al. (Shoemaker et al., 2005) included saturation in both early visual processing and after motion correlation. They showed that inclusion of compressive non-linearities at both these levels, in the form of response saturation, improved the performance of a correlator in terms of the response strength for one scene compared to another. Although the inclusion of these elaborations provided a degree of contrast invariance for natural scenes, no single elaboration, or combination of elaborations, has been shown to match the invariance observed for the HS neurons in the recent experiments (Straw et al., 2008; see also Chapter 3).

The spatial integration properties of LPTC have been studied thoroughly (Borst, Egelhaaf & Haag, 1995, Gauck & Borst, 1999a, Haag et al., 1992, Hausen, 1982b, Single, Haag & Borst, 1997). The responses of LPTCs saturate significantly as stimulus size increases. Interestingly, when the pattern is displayed at different velocities, the LPTC response saturates at different levels (Single et al., 1997). Single et al. (1997) showed that this could be predicted by a compartment model of the LPTC if the opponent operation from Reichardt correlator type local motion elements occurs on its dendrites, because motion in one direction jointly activates both excitatory and inhibitory conductances with a ratio that depends on pattern velocity (Single et al., 1997). They verified this experimentally by blocking inhibitory inputs in LPTCs with picrotoxin, which abolished the velocity dependence of the response saturation and increased the level of the excitatory response (Single et al., 1997). Gain control in spatial integration like this has been proposed to have important consequences for the processing of image velocity in natural environments (Borst et al., 1995), but how it is recruited in natural conditions remains unknown.

1.5.2 Dynamic nonlinearity: motion adaptation

Adaptation in sensory systems is ubiquitous and the motion-processing pathway is no exception. Motion adaptation manifests in a very salient visual illusion and was first reported in the scientific literature nearly two centuries ago by Robert Addams (1834). He noted after staring at a particular part of a waterfall for several seconds, that when he shifted his gaze to the stationary rock-face adjacent to the fall, he saw the rocky surface in motion upwards, i.e. in the opposite direction that the water was travelling. This impressive after-affect induced by staring at a continually moving surface, coined 'the waterfall effect' or 'motion after effect' (MAE) has subsequently attracted enormous attention, particularly in the psychophysical literature (Wade, 1994).

Recently, there has been an explosion of research focussing on the function and basis of motion adaptation (Fairhall, Lewen, Bialek & van Steveninck, 2001, Harris & O'Carroll, 2002, Harris, O'Carroll & Laughlin, 1999, Harris et al., 2000, Kalb, Egelhaaf & Kurtz, 2008, Maddess, 1986, Maddess & Laughlin, 1985, Nordström & O'Carroll, 2009, Reisenman, Haag & Borst, 2003, Safran, Flanagin, Borst & Sompolinsky, 2007, Sanchez-Vives, Nowak & McCormick, 2000a, Sanchez-Vives, Nowak & McCormick, 2000b). Such motion adaptation may allow motion responses to remain sensitive to subtle changes in velocity at low speeds whilst rescaling it from saturation at high velocities, thus increasing the coding range of the system. Yet, despite thorough investigation our understanding of the mechanisms and reasons for motion adaptation are still limited (Anstis, Verstraten & Mather, 1998).

As in other animals, the visual system of flies also reveals substantial adaptive properties at all levels from photoreception to higher-order neurons. At the level of the LPTCs motion adaptation manifests as a reduction in membrane potential, or spike frequency, over several seconds as a grating is moved at constant velocity (Maddess & Laughlin, 1985). In early experiments, Maddess and Laughlin (1985) showed that if they suddenly switched a grating to a new location in the receptive field of the H1 neuron, the response immediately returned to its original level. Thus, they concluded that motion adaptation was occurring in the retinotopically organized columnar elements presynaptic to the H1 neuron. More recently, studies on HS

neurons have shown that some components of motion adaptation are local while other components are able to transfer to previously unstimulated areas of the receptive field (Neri & Laughlin, 2005, Nordström & O'Carroll, 2009).

Brenner et al. (2000) showed that, not only did the amplitude of the H1 neuron's response change after adaptation with constant velocity stimulus, but also that its dynamics changed with changing stimulus history. When they increased the dynamic range of the input signal, in this case a white noise modulated velocity signal, the input/output relationship of the neuron adjusted to maximize its coding range and thus, match the dynamic range of the input signal (Brenner et al., 2000). For example, when the stimulus incorporated only a narrow range of velocities, the H1 neuron showed high sensitivity to changes in stimulus velocity and reached saturation at relatively low velocities. However, when the velocity of the stimulus varied over a large range, the H1 neuron showed a low sensitivity to changes in stimulus velocity and saturated only at higher velocities. This change in sensitivity incorporated several regimes and operates over timescales ranging from tens of milliseconds to minutes (Fairhall et al., 2001). The timing of individual spikes or brief spike patterns may encode individual stimulus features, whereas the statistics of the interspike intervals may encode the stimulus ensemble on slightly longer timescales. Furthermore, the spike rate itself could provide information about the changing stimulus ensemble on even longer timescales.

Adaptation with prior motion has been shown to change the contrast sensitivity of HS neurons (Harris et al., 2000, Nordström & O'Carroll, 2009) (Figure 1.8). By stimulating the neuron with a high contrast adapting probe and then recording responses to subsequent stimuli of varying contrast Harris et al. (2000) showed that HS neurons were far less sensitive to stimulus contrast following constant velocity adaptation. Harris et al. (2000) revealed that three separable adaptive components contributed to the reduction in sensitivity (Figure 1.8). Subsequenlty, Nordström and O'Carroll (2009) highlighted a fourth adaptive component that contributes to gain reduction by altering the spikelet generation mechanism (AC component of adaptation). These four different consequences of motion adaptation have been thoroughly characterized and are recruited differently (Figure 1.8):

1. Hyperpolarizing antagonistic after-potential, or motion after effect (MAE)

2. Contrast gain reduction, seen as a rightward shift in the contrast response function

3. Reduction in the output range of the neuron, causing it to saturate at a lower response level

4. Direction-selective boost in spikelet probability that is independent of membrane potential (AC component)

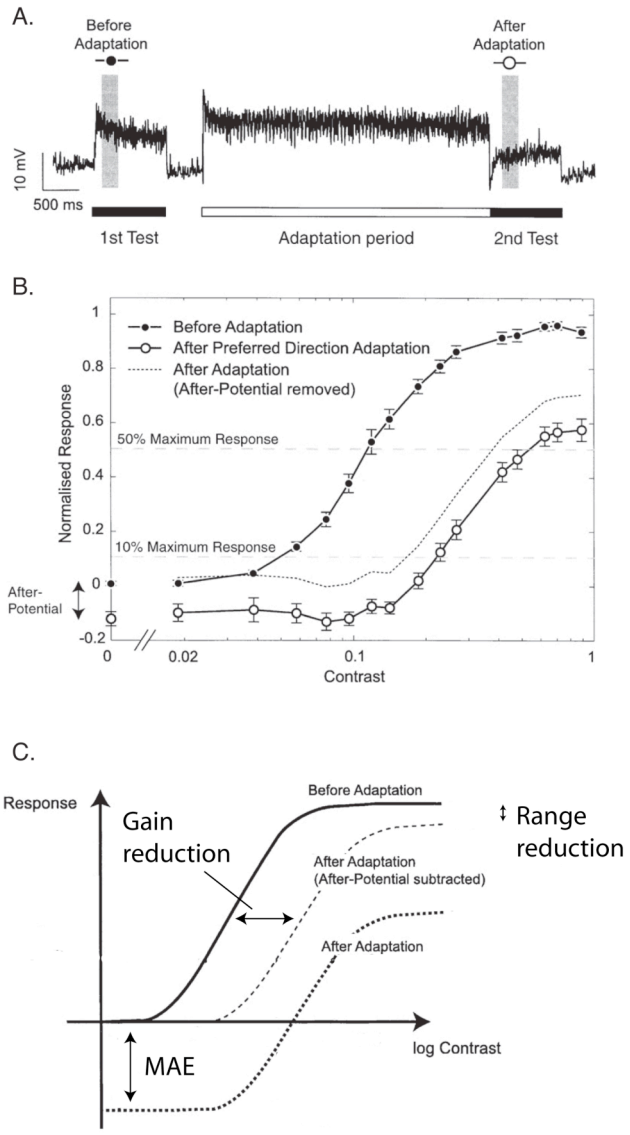

Figure 1.8 Motion adaptation

A. Data from an HS neuron using a test-adapt-test protocol to evaluate adaptation to sinusoidal gratings. The response to the 2nd test, immediately after stimulation with a high contrast constant velocity grating, is weaker than the 1st test response. B. By changing the test contrasts Harris et al. (2000) could evaluate the effect of adaptation on the contrast response function. C. Shows the different components of adaptation: 1 antagonistic after-potential (MAE), 2 contrast gain reduction, and 3 output range reduction. From Harris et al. (2000).

The hyperpolarizing antagonistic after-potential (1; Figure 1.8C) is direction selective and is recruited by preferred direction stimuli that maximally excite the HS neuron (Harris et al., 2000, Nordström & O'Carroll, 2009). Stimuli that depolarise the neuron cause the neuron to be more hyperpolarized relative to resting membrane potential following the cessation of motion. Studies using calcium imaging have shown that the MAE is associated with an accumulation of dendritic calcium and it has been suggested to be generated within the HS neurons itself (Durr & Egelhaaf, 1999, Kurtz, 2007, Kurtz, Durr & Egelhaaf, 2000). The MAE is able to transfer to previously unadapted regions in the receptive field and thus, while the antagonistic after potential may still be generated locally it exerts its influence globally (Nordström & O'Carroll, 2009).

The contrast gain reduction (2; Figure 1.8C) is direction insensitive: motion in any direction, even orthogonal motion that produces no response from the neuron, strongly reduces the contrast gain of the neuron. Unlike the MAE it does not transfer to unadapted regions in the receptive field. Thus, the contrast gain reduction is locally generated and local in its influence, and, most likely associated with decreased gain at the synaptic inputs to the HS neurons (Harris et al., 2000, Nordström & O'Carroll, 2009).

The reduction in output range (4; maximum response; Figure 1.8C) is recruited by either preferred or anti-preferred direction stimulation but not by orthogonal motion. It is generated locally and acts locally and is either generated in local pre-synaptic elements or the dendrites of the HS neuron itself (Nordström & O'Carroll, 2009).

Finally, the most recently identified component of motion adaptation, the AC component, results in an increase in the generation of spikelets following prior motion stimulation (Nordström & O'Carroll, 2009). It is recruited by motion in the anti-preferred direction (opposite to that of the MAE), but like the MAE it is globally acting even though it may be recruited locally (Nordström & O'Carroll, 2009).

Shoemaker et al. (2005) implemented a form of locally generated contrast gain reduction in an elaborated Reichardt correlator model, inspired from the aforementioned experiments, and investigated its performance to natural images. They showed that although such an elaboration improved the performance of the model as a velocity estimator, output was still far more variable than the observed neural responses (Shoemaker et al., 2005). This held true even when they included several adaptive and saturating non-linearities (Shoemaker et al., 2005).

1.6 Approach and aims of this thesis

Insects manage to control their visually guided behaviour using underlying motion computations that are sensitive to several image parameters and thus, generate ambiguous estimates of pattern velocity. However, when confronted with natural stimuli (Straw et al., 2008) or when moving around freely (Baird, Srinivasan, Zhang & Cowling, 2005, Srinivasan et al., 1996) they seem to be able to overcome many of these problems. The question beckons: How do they get away with using ambiguous local motion information to control their behaviour with precision?

In this thesis, I use a combination of natural and artificial images as stimuli to explore the response properties of the HS neurons in the hoverfly, *Eristalis tenax*. In Chapter 2 we characterize the two most dorsal HS neurons and uncover an interesting sexually dimorphic receptive field adaptation, which is hard to reconcile with a role in optic flow processing. We go on to explore the response properties of these neurons to a dynamic broadband stimulus collected from natural fly habitats. In Chapters 3 and 4 we investigate the time-averaged and time-varying response characteristics to a large and diverse range of natural panoramic images. We reveal several activity dependent processes that act as a powerful normaliser of neural responses, reducing variability across otherwise vastly different natural scenes. Finally, in Chapter 5 we investigate the recruitment of local changes in response gain associated with motion adaptation using artificial stimuli. The results show that there are interactions between features beyond those predicted by the Reichardt correlator. There are changes in gain that are rapid in their activation and which greatly alter the response of subsequent features. The recruitment of the local adaptive changes in response gain seem to be mediated by simultaneous activity of neighbouring motion sensitive elements. Recent studies suggest that a locally mediated gain control, such as the one described, may be ideally suited to take advantage of the statistics of natural signals (Schwartz & Simoncelli, 2001).

1.7 References

1. Adelson, E.H., & Bergen, J.R. (1985). Spatiotemporal energy models for the perception of motion. *Journal of the Optical Society of America a-Optics Image Science and Vision, 2* (2), 284-299.

2. Anstis, S., Verstraten, F.A.J., & Mather, G. (1998). The motion aftereffect. *Trends in Cognitive Sciences, 2* (3), 111-117.

3. Ariel, M., & Adolph, A.R. (1985). Neurotransmitter inputs to directionally selective turtle retinal ganglion-cells. *Journal of Neurophysiology, 54* (5), 1123-1143.

4. Baird, E., Srinivasan, M.V., Zhang, S.W., & Cowling, A. (2005). Visual control of flight speed in honeybees. *Journal of Experimental Biology, 208*, 3895-3905.

5. Balboa, R.M., & Grzywacz, N.M. (2003). Power spectra and distribution of contrasts of natural images from different habitats. *Vision Research, 43* (24), 2527-2537.

6. Barlow, H.B., & Levick, W.R. (1965). The mechanisms of directionally selective units in rabit's retina. *Journal of Physiology, 178* (3), 477-504.

7. Barnett, P.D., Nordström, K., & O'Carroll, D.C. (2007). Retinotopic organization of small-field-target-detecting neurons in the insect visual system. *Current Biology, 17* (7), 569-578.

8. Bausenwein, B., & Fischbach, K.F. (1992). Activity labeling patterns in the medulla of drosophila-melanogaster caused by motion stimuli. *Cell and Tissue Research, 270* (1), 25-35.

9. Blondeau, J., & Heisenberg, M. (1982). The 3-dimentional optomotor torque system of Drosophila-melanogaster - studies on wildtype and the mutant optomotor-blind H31. *Journal of Comparative Physiology, 145* (3), 321-329.

10. Boeddeker, N., Lindemann, J.P., Egelhaaf, M., & Zeil, J. (2005). Responses of blowfly motion-sensitive neurons to reconstructed optic flow along outdoor flight paths. *Journal of Comparative Physiology a-Neuroethology Sensory Neural and Behavioral Physiology, 191* (12), 1143-1155.

11. Borst, A. (2007). Correlation versus gradient type motion detectors: the pros and cons. *Philosophical Transactions of the Royal Society B-Biological Sciences, 362* (1479), 369-374.

12. Borst, A., & Bahde, S. (1986). What kind of movement detector is triggering the landing response of the housefly. *Biological Cybernetics, 55* (1), 59-69.

13. Borst, A., & Bahde, S. (1988). Visual information-processing in the flys landing system *Journal of Comparative Physiology a-Sensory Neural and Behavioral Physiology, 163* (2), 167-173.

14. Borst, A., & Egelhaaf, M. (1989). Principles of Visual-Motion Detection. *Trends in Neurosciences, 12* (8), 297-306.

15. Borst, A., Egelhaaf, M., & Haag, J. (1995). Mechanisms of Dendritic Integration Underlying Gain-Control in Fly Motion-Sensitive Interneurons. *Journal of Computational Neuroscience, 2* (1), 5-18.

16. Borst, A., Flanagin, V.L., & Sompolinsky, H. (2005). Adaptation without parameter change: Dynamic gain control in motion detection. *Proceedings of the National Academy of Sciences of the United States of America, 102* (17), 6172-6176.

17. Borst, A., & Haag, J. (2001). Effects of mean firing on neural information rate. *Journal of Computational Neuroscience, 10* (2), 213-221.

18. Borst, A., & Haag, J. (2002). Neural networks in the cockpit of the fly. *Journal of Comparative Physiology a-Neuroethology Sensory Neural and Behavioral Physiology, 188* (6), 419-437.

19. Braitenberg, V., & Taddei-Ferretti, C. (1966). Landing reaction of musca domestica induced by visual stimuli. . *Naturwissenschaften, 53*, 155-156.

20. Bremmer, F., & Lappe, M. (1999). The use of optical velocities for distance discrimination and reproduction during visually simulated self motion. *Experimental Brain Research, 127* (1), 33-42.

21. Brenner, N., Bialek, W., & van Steveninck, R.D. (2000). Adaptive rescaling maximizes information transmission. *Neuron, 26* (3), 695-702.

22. Brinkworth, R.S.A. & O'Carroll, D.C. (2009). Robust models for optic flow coding in natural scenes inspired by insect biology. *PLoS Computational Biology 5*.

23. Buchner, E. (1976). Elementary Movement Detectors in an Insect Visual-System. *Biological Cybernetics, 24* (2), 85-101.

24. Buchner, E. (1984). Behavioral analysis of spatial vision in insects. In: M.A. Ali (Ed.) *Photoreception and vision in invertebrates* 561-621. New York: Plenum.

25. Buchner, E., Buchner, S., & Bülthoff, I. (1984). Deoxyglucose mapping of the nervous activity induced in Drosophila brain by visual movement. *Journal of Comparative Physiology A, 155*, 471-483.

26. Buschbeck, E.K., & Strausfeld, N.J. (1997). The relevance of neural architecture to visual performance: Phylogenetic conservation and variation in dipteran visual systems. *Journal of Comparative Neurology, 383* (3), 282-304.

27. Carandini, M., Demb, J.B., Mante, V., Tolhurst, D.J., Dan, Y., Olshausen, B.A., Gallant, J.L., & Rust, N.C. (2005). Do we know what the early visual system does? *Journal of Neuroscience, 25* (46), 10577-10597.

28. Chan, W.P., Prete, F., & Dickinson, M.H. (1998). Visual input to the efferent control system of a fly's "gyroscope". *Science, 280* (5361), 289-292.

29. Clifford, C.W.G., & Ibbotson, M.R. (2002). Fundamental mechanisms of visual motion detection: models, cells and functions. *Progress in Neurobiology, 68* (6), 409-437.

30. Collett, T.S. (1971). Visual neurons for tracking moving targets. *Nature, 232* (127-130)

31. Collett, T.S., & Land, M.F. (1975). Visual Control of Flight Behavior in Hoverfly, Syritta-Pipiens L. *Journal of Comparative Physiology, 99* (1), 1-66.

32. Collett, T.S., & Land, M.F. (1978). How Hoverflies Compute Interception Courses. *Journal of Comparative Physiology, 125* (3), 191-204.

33. Crowder, N.A., Dawson, M.R.W., & Wylie, D.R.W. (2003). Temporal frequency and velocity-like tuning in the pigeon accessory optic system. *Journal of Neurophysiology, 90* (3), 1829-1841.

34. Cuntz, H., Haag, J., Forstner, F., Segev, I., & Borst, A. (2007). Robust coding of flow-field parameters by axo-axonal gap junctions between fly visual interneurons. *Proceedings of the National Academy of Sciences of the United States of America, 104* (24), 10229-10233.

35. David, C.T. (1982). Compensation for height in the control of ground speed by Drosophila in a new, barbers pole wind-tunnel. *Journal of Comparative Physiology, 147* (4), 485-493.

36. DeVoe, R.D. (1980). Movement sensitivities of cells in the fly's medulla. *Journal of Comparative Physiology A, 138*, 93-119.

37. Douglass, J.K., & Strausfeld, N.J. (1995). Visual-Motion Detection Circuits in Flies - Peripheral Motion Computation by Identified Small-Field Retinotopic Neurons. *Journal of Neuroscience, 15* (8), 5596-5611.

38. Douglass, J.K., & Strausfeld, N.J. (1996). Visual motion-detection circuits in flies: Parallel direction- and non-direction-sensitive pathways between the medulla and lobula plate. *Journal of Neuroscience, 16* (15), 4551-4562.

39. Douglass, J.K., & Strausfeld, N.J. (2003). Retinotopic pathways providing motion-selective information to the lobula from peripheral elementary motion-detecting circuits. *Journal of Comparative Neurology, 457* (4), 326-344.

40. Dror, R.O., O'Carroll, D.C., & Laughlin, S.B. (2001). Accuracy of velocity estimation by Reichardt correlators. *Journal of the Optical Society of America a-Optics Image Science and Vision, 18* (2), 241-252.

41. Durr, V., & Egelhaaf, M. (1999). In vivo calcium accumulation in presynaptic and postsynaptic dendrites of visual interneurons. *Journal of Neurophysiology, 82* (6), 3327-3338.

42. Dvorak, D., Srinivasan, M., & French, A. (1980). The contrast sensitivity of fly movement-detecting neurons. *Vision Research, 20*, 397-407.

43. Eckert, H. (1980). Functional properties of the H1-neurone in the third optic ganglion of the blowfliy, Phaenicia. *Journal of Comparative Physiology A, 135*, 29-39.

44. Eckert, H., & Dvorak, D.R. (1983). The centrifugal horizontal cells in the lobula plate of the blowfly, Phaeicia sericata *Journal of Insect Physiology, 29* (7), 547-560.

45. Egelhaaf, M. (1985). On the neuronal basis of figure-ground discrimination by relative motion in the visual system of the fly. 2. Figure-detecting cells, a new class of visual interneurons. *Biological Cybernetics, 52* (3), 195-209.

46. Egelhaaf, M., & Borst, A. (1989). Transient and steady-state response properties of movement detectors *Journal of the Optical Society of America a-Optics Image Science and Vision, 6* (1), 116-127.

47. Egelhaaf, M., & Borst, A. (1993). A Look into the Cockpit of the Fly - Visual Orientation, Algorithms, and Identified Neurons. *Journal of Neuroscience, 13* (11), 4563-4574.

48. Egelhaaf, M., Borst, A., & Reichardt, W. (1989a). Computational structure of a biological motion-detecting system as revealed by local detector analysis in the flys nervous-system. *Journal of the Optical Society of America a-Optics Image Science and Vision, 6* (7), 1070-1087.

49. Egelhaaf, M., Borst, A., & Reichardt, W. (1989b). The nonlinear mechanisms of direction selectivity in the fly motion detection system. *Naturwissenschaften, 76* (1), 32-35.

50. Egelhaaf, M., Borst, A., Warzecha, A.K., Flecks, S., & Wildemann, A. (1993). Neural circuits tuning fly visual neurons to motion of small objects. 2. input organization of inhibitory circuit elements revealed by electrophysiological and optical recording techniques. *Journal of Neurophysiology, 69* (2), 340-351.

51. Elyada, Y.M., Haag, J., & Borst, A. (2009). Different receptive fields in axons and dendrites underlie robust coding in motion-sensitive neurons. *Nature Neuroscience, 12* (3), 327-332.

52. Emerson, R.C. (1992). Do direction selective simple cells use motion-energy subunits. *Investigative Ophthalmology & Visual Science, 33* (4), 953-953.

53. Esch, H.E., & Burns, J.E. (1996). Distance estimation by foraging honeybees. *Journal of Experimental Biology, 199* (1), 155-162.

54. Fairhall, A.L., Lewen, G.D., Bialek, W., & van Steveninck, R.R.D. (2001). Efficiency and ambiguity in an adaptive neural code. *Nature, 412* (6849), 787-792.

55. Farrow, K., Borst, A., & Haag, J. (2005). Sharing receptive fields with your neighbors: Tuning the vertical system cells to wide field motion. *Journal of Neuroscience, 25* (15), 3985-3993.

56. Field, D.J. (1987). Relations between the statistics of natural images and the response properties of cotical cells. *Journal of the Optical Society of America a-Optics Image Science and Vision, 4* (12), 2379-2394.

57. Franceschini, N., Riehle, A., & Le Nestour, A. (1989). Directionally selective motion detection by insect neurons. In: D.G. Stavenga, & R.C. Hardie (Eds.), *Facets of vision* (pp. 360-390). Berlin Heidelberg New York: Springer.

58. Franz, M.O., & Krapp, H.G. (2000). Wide-field, motion-sensitive neurons and matched filters for optic flow fields. *Biological Cybernetics, 83* (3), 185-197.

59. Frye, M.A., & Dickinson, M.H. (2001). Fly flight: A model for the neural control of complex behavior. *Neuron, 32* (3), 385-388.

60. Frye, M.A., & Dickinson, M.H. (2004). Closing the loop between neurobiology and flight behavior in Drosophila. *Current Opinion in Neurobiology, 14* (6), 729-736.

61. Gauck, V., & Borst, A. (1999a). Spatial response properties of contralateral inhibited lobula plate tangential cells in the fly visual system. *Journal of Comparative Neurology, 406* (1), 51-71.

62. Gauck, V., & Borst, A. (1999b). Spatial response properties of contralateral inhibited lobula plate tangential cells in the fly visual system. *Journal of Comparative Neurology, 406* (1), 51-71.

63. Gauck, V., Egelhaaf, M., & Borst, A. (1997). Synapse distribution on VCH, an inhibitory, motion-sensitive interneuron in the fly visual system. *Journal of Comparative Neurology, 381* (4), 489-499.

64. Geiger, G., & Nässel, D.R. (1981). Visual orientation behaviour of flies after selective laser beam ablation of interneurones. *Nature, 293*, 398-399.

65. Gibson, J.J. (1958). Visually controlled locomotion and visual orientation in animals. *British journal of Pyschology, 49*, 182-194.

66. Götz, K.G. (1968). Flight control in drosophila by visual perception of motion. *Kybernetik (Biological Cybernetics), 2*, 77-92.

67. Götz, K.G. (1975). Optomotor equilibrium of Drosophila navigation system. Journal of Comparative Physiology *99*, 187-210.

68. Gronenberg, W., Milde, J.J., & Strausfeld, N.J. (1995). Oculomotor control in calliphorid flies - organization of descending neurons to the neck motor - responding to visual stimuli. *Journal of Comparative Neurology, 361* (2), 267-284.

69. Gronenberg, W., & Strausfeld, N.J. (1990). Descending neurons supplying the neck and flight motor of diptera - physiology and anatomical characteristics. *Journal of Comparative Neurology, 302* (4), 973-991.

70. Haag, J., & Borst, A. (1996). Amplification of high-frequency synaptic inputs by active dendritic membrane processes. *Nature, 379* (6566), 639-641.

71. Haag, J., & Borst, A. (2004). Neural mechanism underlying complex receptive field properties of motion-sensitive interneurons. *Nature Neuroscience, 7* (6), 628-634.

72. Haag, J., & Borst, A. (2005). Dye-coupling visualizes networks of large-field motion-sensitive neurons in the fly. *Journal of Comparative Physiology a-Neuroethology Sensory Neural and Behavioral Physiology, 191* (5), 445-454.

73. Haag, J., Denk, W., & Borst, A. (2004). Fly motion vision is based on Reichardt detectors regardless of the signal-to-noise ratio. *Proceedings of the National Academy of Sciences of the United States of America, 101* (46), 16333-16338.

74. Haag, J., Egelhaaf, M., & Borst, A. (1992). Dendritic Integration of Motion Information in Visual Interneurons of the Blowfly. *Neuroscience Letters, 140* (2), 173-176.

75. Haag, J., Theunissen, F., & Borst, A. (1997). The intrinsic electrophysiological characteristics of fly lobula plate tangential cells .2. Active membrane properties. *Journal of Computational Neuroscience, 4* (4), 349-369.

76. Haag, J., Vermeulen, A., & Borst, A. (1999). The intrinsic electrophysiological characteristics of fly lobula plate tangential cells: III. Visual response properties. *Journal of Computational Neuroscience, 7* (3), 213-234.

77. Haag, J., Wertz, A., & Borst, A. (2007). Integration of lobula plate output signals by DNOVS1, an identified premotor descending neuron. *Journal of Neuroscience, 27* (8), 1992-2000.

78. Harris, R.A., & O'Carroll, D.C. (2002). Afterimages in fly motion vision. *Vision Research, 42* (14), 1701-1714.

79. Harris, R.A., O'Carroll, D.C., & Laughlin, S.B. (1999). Adaptation and the temporal delay filter of fly motion detectors. *Vision Research, 39* (16), 2603-2613.

80. Harris, R.A., O'Carroll, D.C., & Laughlin, S.B. (2000). Contrast gain reduction in fly motion adaptation. *Neuron, 28* (1,22), 595-606.

81. Hassenstein, B., & Reichardt, W. (1956). Systemtheoretische Analyse Der Zeit, Reihenfolgen Und Vorzeichenauswertung Bei Der Bewegungsperzeption Des Russelkafers Chlorophanus. *Zeitschrift Fur Naturforschung Part B-Chemie Biochemie Biophysik Biologie Und Verwandten Gebiete, 11* (9-10), 513-524.

82. Hausen, K. (1982a). Motion Sensitive Interneurons in the Optomotor System of the Fly .1. The Horizontal Cells - Structure and Signals. *Biological Cybernetics, 45* (2), 143-156.

83. Hausen, K. (1982b). Motion Sensitive Interneurons in the Optomotor System of the Fly .2. The Horizontal Cells - Receptive-Field Organization and Response Characteristics. *Biological Cybernetics, 46* (1), 67-79.

84. Hausen, K., & Egelhaaf, M. (1989). Neural mechanisms of visual course control in insects. In: D.G. Stavenga, & R.C. Hardie (Eds.), *Facets of vision* 391-424. Berlin Heidelberg New York: Springer.

85. Hausen, K., & Wehrhahn, C. (1983). Microsurgical Lesion of Horizontal Cells Changes Optomotor Yaw Responses in the Blowfly Calliphora-Erythrocephala. *Proceedings of the Royal Society of London Series B-Biological Sciences, 219* (1215), 211-216.

86. Hausen, K., & Wehrhahn, C. (1989). Neural Circuits Mediating Visual Flight Control in Flies .1. Quantitative Comparison of Neural and Behavioral-Response Characteristics. *Journal of Neuroscience, 9* (11), 3828-3836.

87. Hausen, K., & Wehrhahn, C. (1990). Neural Circuits Mediating Visual Flight Control in Flies .2. Separation of 2 Control-Systems by Microsurgical Brain-Lesions. *Journal of Neuroscience, 10* (1), 351-360.

88. Heisenberg, M., & Buchner, E. (1977). The role of retinula cell types in visual behavior of Drosophila malanogaster. *Journal of Comparative Physiology A, 117* (2), 127-162.

89. Heisenberg, M., Wonneberger, R., & Wolf, R. (1978). Optomotor-blind H31 - a drosophila mutant of the lobula giant neurons. *Journal of Comparative Physiology A, 124*, 287-296.

90. Hengstenberg, R. (1982). Common visual response properties of giant vertical cells in the lobula plate of the blowfly calliphora. *Journal of Comparative Physiology, 149* (2), 179-193.

91. Hengstenberg, R., Hausen, K., & Hengstenberg, B. (1982). The number and structure of giant vertical cells (VS) in the lobula plate of the blowfly Calliphora-erythrocephala. *Journal of Comparative Physiology, 149* (2), 163-177.

92. Horridge, G.A. (1986). A theory of insect vision - Velocity paralax. *Proceedings of the Royal Society B-Biological Sciences, 229*, 13-27.

93. Horstmann, W., Egelhaaf, M., and Warzecha, A.K. (2000). Synaptic interactions increase optic flow specificity. *European Journal of Neuroscience 12*, 2157-2165.

94. Huston, S.J., & Krapp, H.G. (2008). Visuomotor transformation in the fly gaze stabilization system. *Plos Biology, 6* (7), 1468-1478.

95. Ibbotson, M.R., Mark, R.F., & Maddess, T.L. (1994). Spatiotemporal Response Properties of Direction-Selective Neurons in the Nucleus of the Optic Tract and Dorsal Terminal Nucleus of the Wallaby, Macropus-Eugenii. *Journal of Neurophysiology, 72* (6), 2927-2943.

96. James, A.C. (1990). White-noise studies in the fly Lamina. PhD (Canberra: Australian National University.

97. Kalb, J., Egelhaaf, M., & Kurtz, R. (2008). Adaptation changes directional sensitivity in a visual motion-sensitive neuron of the fly. *Vision Research, 48* (16), 1735-1742.

98. Karmeier, K., Krapp, H.G., & Egelhaaf, M. (2003). Robustness of the tuning of fly visual interneurons to rotatory optic flow. *Journal of Neurophysiology, 90* (3), 1626-1634.

99. Karmeier, K., van Hateren, J.H., Kern, R., & Egelhaaf, M. (2006). Encoding of naturalistic optic flow by a population of blowfly motion-sensitive neurons. *Journal of Neurophysiology, 96* (3), 1602-1614.

100. Kern, R., Petereit, C., & Egelhaaf, M. (2001). Neural processing of naturalistic optic flow. *Journal of Neuroscience, 21* (8), art. no.-RC139.

101. Kern, R., van Hateren, J.H., & Egelhaaf, M. (2006). Representation of behaviourally relevant information by blowfly motion-sensitive visual interneurons requires precise compensatory head movements. *Journal of Experimental Biology, 209* (7), 1251-1260.

102. Kern, R., van Hateren, J.H., Michaelis, C., Lindemann, J.P., & Egelhaaf, M. (2005). Function of a fly motion-sensitive neuron matches eye movements during free flight. *Plos Biology, 3* (6), 1130-1138.

103. Kirschfeld, K. (1867). The resolution of lens and compound eyes. In: F. Zettler, & R. Weiler (Eds.), *Neural Principles in Vision* 354-370. Berlin-Heidelberg-New York: Springer.

104. Koenderink, J.J. (1986). Optic flow. *Vision Research, 26* (1), 161-179.

105. Koenderink, J.J., & Van Doorn, A.J. (1976). Local structure of movement paralax of the plane. *Journal of the Optical Society of America a-Optics Image Science and Vision, 66*, 717-723.

106. Koenderink, J.J., & van Doorn, A.J. (1987). Facts on optic flow. *Biological Cybernetics, 56* (4), 247-254.

107. Kral, K. (1998). Side-to-side head movements to obtain motion depth cues: A short review of research on the praying mantis. *Behavioural Processes, 43*, 71-77.

108. Kral, K. (2003). Behavioural-analytical studies of the role of head movements in depth perception in insects, birds and mammals *Behavioural Processes, 64*, 1-12.

109. Krapp, H.G., Hengstenberg, B., & Hengstenberg, R. (1998). Dendritic structure and receptive-field organization of optic flow processing interneurons in the fly. *Journal of Neurophysiology, 79* (4), 1902-1917.

110. Krapp, H.G., & Hengstenberg, R. (1996). Estimation of self-motion by optic flow processing in single visual interneurons. *Nature, 384* (6608), 463-466.

111. Krapp, H.G., & Hengstenberg, R. (1997). A fast stimulus procedure to determine local receptive field properties of motion-sensitive visual interneurons. *Vision Research, 37* (2), 225-234.

112. Krapp, H.G., Hengstenberg, R., & Egelhaaf, M. (2001). Binocular contributions to optic flow processing in the fly visual system. *Journal of Neurophysiology, 85* (2), 724-734.

113. Kurtz, R. (2007). Direction-selective adaptation in fly visual motion-sensitive neurons is generated by an intrinsic conductanc based mechanism. *Neuroscience, 146*, 573-583.

114. Kurtz, R., Durr, V., & Egelhaaf, M. (2000). Dendritic calcium accumulation associated with direction-selective adaptation in visual motion-sensitive neurons in vivo. *Journal of Neurophysiology, 84* (4), 1914-1923.

115. Land, M.F. (1981). Optics and vision in invertebrates. In: H. Autrum (Ed.) *Handbook of sensory physiology,* VII/6B 472-592. Berlin: Springer.

116. Land, M.F. (1989). Variations in the structure and design of compound eyes. In: D.G. Stavenga, & R.C. Hardie (Eds.), *Facets of Vision* Berlin: Springer-Verlag.

117. Land, M.F. (1997). Visual acuity in insects. *Annual Review of Entomology, 42*, 147-177.

118. Land, M.F., & Collett, T.S. (1974). Chasing Behavior of Houseflies (Fannia-Canicularis) - Description and Analysis. *Journal of Comparative Physiology, 89* (4), 331-357.

119. Land, M.F., & Eckert, H.M. (1985). Maps of the acute zones of fly eyes. *Journal of Comparative Physiology A, 156*, 525-538.

120. Land, M.F., & Nilsson, D.E. (2002). Apposition compound eyes. In: *Animal eyes* 125-155. New-York: Oxford University Press.

121. Lappe, M., Bremmer, F., & van den Berg, A.V. (1999). Perception of self-motion from visual flow. *Trends in Cognitive Sciences, 3* (9), 329-336.

122. Laughlin, S.B. (1981). Neural principles in the peripheral visual system of invertebrates. In: H. Autrum (Ed.) *Handbook of Sensory Physiology* (Berlin: Springer.

123. Laughlin, S.B. (1994). Matching coding, circuits, cells, and molecules to signals - general principles of retinal design in the flys eye. *Progress in Retinal and Eye Research, 13* (1), 165-196.

124. Laughlin, S.B., Howard, J., & Blakeslee, B. (1987). Synaptic limitations to contrast coding in the retina of the blowfly Calliphora. *Proceedings of the Royal Society of London Series B-Biological Sciences, 231* (1265), 437-467.

125. Lee, D.N., & Kalmus, H. (1980). The optic flow field - the foundation of vision. *Philosophical Transactions of the Royal Society B-Biological Sciences, 290* (1038), 169-179.

126. Limb, J.O., & Murphy, J.A. (1975). Estimating the velocity of moving objects in television signals. *Computer graphics and image processing, 4*, 311-327.

127. Lindemann, J.P., Kern, R., van Hateren, J.H., Ritter, H., and Egelhaaf, M. (2005). On the computations analyzing natural optic flow: Quantitative model analysis of the blowfly motion vision pathway. *Journal of Neuroscience 25*, 6435-6448.

128. Maddess, T. (1986). Afterimage-like effects in the motion-sensitive neuron H1. *Proceedings of the Royal Society of London Series B-Biological Sciences, 228* (1253), 433-459.

129. Maddess, T., & Laughlin, S.B. (1985). Adaptation of the Motion-Sensitive Neuron H-1 Is Generated Locally and Governed by Contrast Frequency. *Proceedings of the Royal Society of London Series B-Biological Sciences, 225* (1239), 251-275.

130. McKee, S.P., Silverman, G.H., & Nakayama, K. (1986). Precise velocity discrimination despite random variations in temporal frequency and contrast. *Vision Research, 26* (4), 609-619.

131. Nakayama, K. (1985). Biological image processing - a review. *Vision Research, 25* (5), 625-660.

132. Nakayama, K., & Loomis, J.M. (1974). Optical velocity patterns, velocity-sensitive neurons, and space perception: a hypothesis. *Perception, 3*, 63-80.

133. Nalbach, H.O. (1989). Three temporal frequency channels constitute the dynamics of the optokinetic system of the crab, Carcinus-maenas (L). *Biological Cybernetics 61*, 59-70.

134. Neri, P., & Laughlin, S.B. (2005). Global versus local adaptation in fly motion-sensitive neurons. *Proceedings of the Royal Society B-Biological Sciences, 272* (1578), 2243-2249.

135. Nilsson, D.E. (1989). Optics and evolution of the compound eye. In: D.G. Stavenga, & R.C. Hardie (Eds.), *Facets of Vision* (Berlin: Springer-Verlag.

136. Nilsson, D.E. (1990). From cornea to retinal image in invertebrate eyes. *Trends in Neurosciences, 13* (2), 55-64.

137. Nordström, K., & O'Carroll, D.C. (2009a). Feature detection and the hypercomplex property in insects. *Trends in Neurosciences, 32* (7), 383-391.

138. Nordström, K., & O'Carroll, D.C. (2006). Small object detection neurons in female hoverflies. *Proceedings of the Royal Society B-Biological Sciences, 273* (1591), 1211-1216.

139. Nordström, K., & O'Carroll, D.C. (2009b). The motion after-effect: local and global contributions to contrast sensitivity. *Proceedings of the Royal Society B-Biological Sciences, 276* (1662), 1545-1554.

140. Nordström, N., Barnett, P.D., Moyer de Miguel, I.M., Brinkworth, R.S.A., & O'Carroll, D.C. (2008). Sexual dimorphism in the hoverfly motion vision pathway. *Current Biology, 18*, 661-667.

141. Nordström, N., Barnett, P.D., & O'Carroll, D.C. (2006). Insect detection of small targets moving in visual clutter. *Plos Biology, 4* (3), 378-386.

142. O'Carroll, D. (1993). Feature-detecting neurons in dragonflies. *Nature, 362*, 541-543.

143. O'Carroll, D.C., Laughlin, S.B., Bidwell, N.J., & Harris, R.A. (1997). Spatio-temporal properties of motion detectors matched to low image velocities in hovering insects. *Vision Research, 37* (23), 3427-3439.

144. O'Carroll, D.C., Bidwell, N.J., Laughlin, S.B., & Warrant, E.J. (1996). Insect motion detectors matched to visual ecology. *Nature, 382* (6586), 63-66.

145. Olberg, R.M. (1981). Object-movement and self-movement detectors in the ventral nerve cord of the dragonfly. *Journal of Comparative Physiology, 141* (3), 327-334.

146. Olberg, R.M. (1986). Identified target-selective visual interneurons descending from the dragonfly brain *Journal of Comparative Physiology a-Sensory Neural and Behavioral Physiology, 159* (6), 827-840.

147. Osorio, D., Averof, M., & Bacon, J.P. (1995). Arthropod evolution: great brains, beautiful bodies. *Trends in Ecology and Evolution, 10* (11), 449-454.

148. Pflugfelder, G.O., & Heisenberg, M. (1995). Optomotor-blind of drosophila-melanogaster - a neurogenic approach to optic lobe development and optomotor behavior. *Comparative Biochemistry and Physiology a-Physiology, 110* (3), 185-202.

149. Poggio, T., & Reichardt, W. (1976). Visual control of orientation behaviour in the fly II. Towards the underlying neural interactions. *Quart Rev Biophys, 9*, 377-438.

150. Potters, M., & Bialek, W. (1994). Statistical-mechanics and visual signal-processing. *Journal De Physique I, 4* (11), 1755-1775.

151. Rajesh, S., Rainsford, T., Brinkworth, R.S.A., Abbott, D., & O'Carroll, D. (2007). Implementation of saturation for a modelling pattern noise using naturalistic stimuli. *Smart structures, devises, and systems III,* 6414 (pp. 24-39).

152. Rajesh, S., Straw, A., O'Carroll, D.C., & Abbott, D. (2005). Effects of compressive nonlinearity on insect-based motion detection. *Smart Structures, Devices, and Systems II,* 5649 (pp. 798-810): SPIE.

153. Reichardt, W. (1961). Autocorrelation, a principle for the evaluation of sensory information by the central nervous system. In: W.A. Rosenblith (Ed.) *Sensory communication* (pp. 377-390). New York: MIT Press/Wiley.

154. Reichardt, W. (1987). Evaluation of optical motion information by movement detectors. *Journal of Comparative Physiology a-Sensory Neural and Behavioral Physiology, 161* (4), 533-547.

155. Reichardt, W., & Egelhaaf, M. (1988). Properties of individual movement detectors as derived from behavioral experiments on the visual system of the fly. *Biological Cybernetics, 58* (5), 287-294.

156. Reichardt, W., & Egelhaaf, M. (1989). Movement detectors provide sufficient information for local computation of 2-D velocity field. *Naturwissenschaften, 75*, 313-315.

157. Reichardt, W., & Poggio, T. (1976). Visual Control of Orientation Behavior in Fly .1. Quantitative-Analysis .2. Towards Underlying Neural Interactions. *Quarterly Reviews of Biophysics, 9* (3), 311-&.

158. Reichardt, W., & Poggio, T. (1979). Figure-ground discrimination by relative movement in the visual system of the fly. Part I: Experimental results. *Biol Cybern, 35*, 81-100.

159. Reisenman, C., Haag, J., & Borst, A. (2003). Adaptation of response transients in fly motion vision. I: Experiments. *Vision Research, 43* (11), 1293-1309.

160. Rister, J., Pauls, D., Schnell, B., Ting, C.Y., Lee, C.H., Sinakevitch, I., Morante, J., Strausfeld, N.J., Ito, K., & Heisenberg, M. (2007). Dissection of the peripheral motion channel in the visual system of Drosophila melanogaster. *Neuron, 56* (1), 155-170.

161. Rivera-Alvidrez, Z., & Higgins, C.M. (2005). Contrast saturation in a neuronally-based model of elementary motion detection. *Neurocomputing, 65*, 173-179.

162. Ronacher, B., & Wehner, R. (1995). Desert ants Cataglyphis-fortis use self-induced optic flow to measure distances travelled. *Journal of Comparative Physiology a-Sensory Neural and Behavioral Physiology, 177* (1), 21-27.

163. Ruderman, D.L. (1994). The statistics of natural images. *Network-Computation in Neural Systems, 5*, 517-548.

164. Ruderman, D.L., & Bialek, W. (1994). Statistics of natural images - scaling in the woods. *Physical Review Letters, 73* (6), 814-817.

165. Safran, M.N., Flanagin, V.L., Borst, A., & Sompolinsky, H. (2007). Adaptation and Information Transmission in Fly Motion Detection. *Journal of Neurophysiology, 98* (6), 3309-3320.

166. Sanchez-Vives, M.V., Nowak, L.G., & McCormick, D.A. (2000a). Cellular mechanisms of long-lasting adaptation in visual cortical neurons in vitro. *Journal of Neuroscience, 20* (11), 4286-4299.

167. Sanchez-Vives, M.V., Nowak, L.G., & McCormick, D.A. (2000b). Membrane mechanisms underlying contrast adaptation in cat area 17 in vivo. *Journal of Neuroscience, 20* (11), 4267-4285.

168. Schilstra, C., & Van Hateren, J.H. (1999). Blowfly flight and optic flow I. Thorax kinematics and flight dynamics. *Journal of Experimental Biology, 202* (11), 1481-1490.

169. Schuling, F.H., Mastebroek, H.A.K., Bult, R., and Lenting, B.P.M. (1989). Properties of elementary movement detectors in the fly Calliphora-erythrocephala. *Journal of Comparative Physiology a-Sensory Neural and Behavioral Physiology 165*, 179-192.

170. Schwartz, O., & Simoncelli, E. (2001). Natural signal statistics and sensory gain control. *Nature Neuroscience, 4* (8), 819-825.

171. Shoemaker, P.A., O'Carroll, D.C., & Straw, A.D. (2005). Velocity constancy and models for wide-field visual motion detection in insects. *Biological Cybernetics, 93* (1,24), 275-287.

172. Simoncelli, E.P., & Olshausen, B.A. (2001). Natural image statistics and neural representation. *Annual Review of Neuroscience, 24*, 1193-1216.

173. Single, S., Haag, J., & Borst, A. (1997). Dendritic computation of direction selectivity and gain control in visual interneurons. *Journal of Neuroscience, 17* (16), 6023-6030.

174. Smith, S.M., & Brady, J.M. (1997). SUSAN - A new approach to low level image processing. *International Journal of Computer Vision, 23* (1), 45-78.

175. Sobel, E.C. (1990). The locust's use of motion parallax to measure distance. *Journal of Comparative Physiology a-Neuroethology Sensory Neural and Behavioral Physiology, 167*, 579-588.

176. Srinivasan, M.V. (1990). Generalized gradient shemes for the measurement of 2-dimentional image motion. *Biological Cybernetics, 63* (6), 421-431.

177. Srinivasan, M.V., & Dvorak, D.R. (1980). Spatial processing of visual information in the movement-detecting pathway of the fly - characteristics and functional significance. *Journal of Comparative Physiology, 140* (1), 1-23.

178. Srinivasan, M.V., Laughlin, S.B., & Dubs, A. (1982). Predictive coding - a fresh view of inhibition in the retina. *Proceedings of the Royal Society of London Series B-Biological Sciences, 216* (1205), 427-459.

179. Srinivasan, M.V., Lehrer, M., Kirchner, W.H., & Zhang, S.W. (1991). Range perception through apparent image speed in freely flying honeybees. *Visual Neuroscience, 6* (5), 519-535.

180. Srinivasan, M.V., Pinter, R.B., & Osorio, D. (1990). Matched filtering in the visual system of the fly - large monopolar cells of the lamina are optomized to detect moving edges and blobs. *Proceedings of the Royal Society of London Series B-Biological Sciences, 240* (1298), 279-293.

181. Srinivasan, M.V., Poteser, M., & Kral, K. (1999). Motion detection in insect orientation and navigation. *Vision Research, 39* (16), 2749-2766.

182. Srinivasan, M.V., Zhang, S.W., Lehrer, M., & Collett, T.S. (1996). Honeybee navigation en route to the goal: Visual flight control and odometry. *Journal of Experimental Biology, 199* (1), 237-244.

183. Strausfeld, N.J. (1976). Atlas of an Insect brain. Berlin: Springer.

184. Strausfeld, N.J. (1989). Beneath the compound eye: neuroanatomical analysis and physiological correlates in the study of insect vision In: D.G. Stavenga, & R.C. Hardie (Eds.), *Facet of Vision* Berlin: Springer-Verlag.

185. Strausfeld, N.J. (2005). The evolution of crustacean and insect optic lobes and the origins of chiasmata. *Arthropod Structure & Development, 34* (3), 235-256.

186. Strausfeld, N.J., & Bassemir, U.K. (1985a). Lobula plate and ocellar interneruons converge onto a cluster of decending neurons leading to the neck and leg motor neuropil in Calliphora-erythrocephala *Cell and Tissue Research, 240* (3), 617-640.

187. Strausfeld, N.J., & Bassemir, U.K. (1985b). The organization of giant horizontal-motion-sensitive neurons and their synaptic relationships in the lateral deutocerebrum of Calliphora-erythrocephala and Musca-domestica. *Cell and Tissue Research, 242* (3), 531-550.

188. Strausfeld, N.J., & Lee, J.K. (1991). Neuronal Basis for Parallel Visual Processing in the Fly. *Visual Neuroscience, 7* (1-2), 13-33.

189. Strausfeld, N.J., & Seyan, H.S. (1985). Convergence of visual, haltere, and prosternal inputs at the neck motor neurons of calliphora-erythrocephala. *Cell and Tissue Research, 240* (3), 601-615.

190. Straw, A.D., Rainsford, T., & O'Carroll, D.C. (2008). Contrast sensitivity of insect motion detectors to natural images. *Journal of Vision, 8(3):32*, 1-9.

191. Straw, A.D., Warrant, E.J., & O'Carroll, D.C. (2006). A 'bright zone' in male hoverfly (*Eristalis tenax*) eyes and associated faster motion detection and increased contrast sensitivity. *Journal of Experimental Biology, 209*, 4339-4354.

192. Tadmor, Y., & Tolhurst, D.J. (1993). Both the phase and amplitude spectrum may determine the appearance of natural images. *Vision Research, 33* (1), 141-145.

193. Tammero, L.F., & Dickinson, M.H. (2002a). Collision-avoidance and landing responses are mediated by separate pathways in the fruit fly, Drosophila melanogaster. *Journal of Experimental Biology, 205* (18), 2785-2798.

194. Tammero, L.F., & Dickinson, M.H. (2002b). The influence of visual landscape on the free flight behavior of the fruit fly Drosophila melanogaster. *Journal of Experimental Biology, 205* (3), 327-343.

195. Tammero, L.F., Frye, M.A., & Dickinson, M.H. (2004). Spatial organization of visuomotor reflexes in Drosophila. *Journal of Experimental Biology, 207* (1), 113-122.

196. Tolhurst, D.J., Tadmor, Y., & Chao, T. (1992). Amplitude spectra of natural images. *Ophthalmic and Physiological Optics, 12* (2), 229-232.

197. Torralba, A., & Oliva, A. (2003). Statistics of natural image categories. *Network-Computation in Neural Systems, 14* (3), 391-412.

198. van Hateren, J.H., Hardie, R.C., Rudolph, A., Laughlin, S.B., & Stavenga, D.G. (1989). The bright zone, a specialized dorsal eye region in the male blowfly Chrysomyia megacephala. *Journal of Comparative Physiology A, 164*, 297-308.

199. van Hateren, J.H., Kern, R., Schwerdtfeger, G., & Egelhaaf, M. (2005). Function and coding in the blowfly H1 neuron during naturalistic optic flow. *Journal of Neuroscience, 25* (17), 4343-4352.

200. Van Hateren, J.H., & Schilstra, C. (1999). Blowfly flight and optic flow II. Head movements during flight. *Journal of Experimental Biology, 202* (11), 1491-1500.

201. van Hateren, J.H., & Snippe, H.P. (2001). Information theoretical evaluation of parametric models of gain control in blowfly photoreceptor cells. *Vision Research, 41* (14), 1851-1865.

202. van Hateren, J.H., & Snippe, H.P. (2006). Phototransduction in primate cones and blowfly photoreceptors: different mechanisms, different algorithms, similar response. *Journal of Comparative Physiology a-Neuroethology Sensory Neural and Behavioral Physiology, 192* (2), 187-197.

203. Vansanten, J.P.H., & Sperling, G. (1985). Elaborated Reichardt Detectors. *Journal of the Optical Society of America a-Optics Image Science and Vision, 2* (2), 300-321.

204. Virsik, R.P., & Reichardt, W. (1976). Detection and Tracking of Moving-Objects by Fly Musca-Domestica. *Biological Cybernetics, 23* (2), 83-98.

205. Wade, N.J. (1994). A selective history of the study of visual motion aftereffects. *Perception, 23*, 1111-1134.

206. Wagner, H. (1982). Flow-field variables trigger landing in flies. *Nature, 297*, 147-148.

207. Warrant, E.J. (2008). Seeing in the dark: vision and visual behaviour in nocturnal bees and wasps. *Journal of Experimental Biology 211*, 1737-1746.

208. Warren, W.H., & Hannon, D.J. (1988). Direction of self-motion is perceived from optical-flow. *Nature, 336* (6195), 162-163.

209. Warzecha, A.K., Egelhaaf, M., & Borst, A. (1993). Neural circuits tuning fly visual interneuons to motion of small objects. 1. Dissection of the circuit by pharmacalogical and photoinactivation techniques *Journal of Neurophysiology, 69* (2), 329-339.

210. Wertz, A., Borst, A., & Haag, J. (2008). Nonlinear integration of binocular optic flow by DNOVS2, a descending neuron of the fly. *Journal of Neuroscience, 28* (12), 3131-3140.

211. Wolf-Oberhollenzer, F., & Kirschfeld, K. (1994). Motion sensitivity in the nucleus of the basal optic root of the pigeon. *Journal of Neurophysiology, 71*, 1559-1573.

212. Yarnaguchi, S., Wolf, R., Desplan, C., & Heisenberg, M. (2008). Motion vision is independent of color in Drosophila. *Proceedings of the National Academy of Sciences of the United States of America, 105* (12), 4910-4915.

213. Zeil, J., Boeddeker, N., & Hemmi, J.M. (2008). Vision and the organization of behaviour. *Current Biology, 18* (8), R320-R323.

Chapter 2:
Sexual Dimorphism in the Hoverfly Motion Vision Pathway

2.1 Context

My original thesis aims focussed on both local and global encoding of natural image motion and adaptation. I used both physiological and computational approaches to understand global integration of local cues. It was thus essential to obtain detailed information about the receptive field organization of the neurons that form the basis of my experiments and modelling. In the process collecting detailed morphological and receptive field data, we discovered and interesting difference in the horizontal system neurons (HS) between the two sexes that was in many respects in contradiction of the requirements for optic flow detection – the role the HS neurons are proposed to subserve. This sexual dimorphism has not been observed in other fly species, we therefore elaborated my initial data into an extensive comparison.

In this paper, we characterize the receptive field properties and morphology of the two most dorsal HS neurons in the hoverfly, *Eristalis tenax.* We also describe a new technique for rapidly characterizing the receptive field properties of these neurons, a method used throughout subsequent chapters to identify HS neurons and distinguish one from another. We go on to investigate HS neurons response properties under more naturalistic and test whether the sexually dimorphic male HSN may have an alternative role in the hoverfly visual system.

Supplemental data published online with the paper is included at the end of the chapter with its own set of references, as published.

Sexual dimorphism in the hoverfly motion vision pathway

Karin Nordström, Paul D. Barnett, Irene M. Moyer de Miguel, Russell S.A. Brinkworth, and David C. O'Carroll*

Discipline of Physiology,

School of Molecular and Biomedical Science,

The University of Adelaide, SA 5005, Australia

**To whom correspondence should be addressed: karin.nordstrom@adelaide.edu.au, +61-8-8303 8067.*

Keywords: morphology, LPTC, target responses, rotation, translation, optic flow, matched filter, receptive field, HS

Abbreviations: horizontal system (HS), horizontal system equatorial (HSE), horizontal system north (HSN), horizontal system north equatorial (HSNE), horizontal system south (HSS), lobula plate tangential cell (LPTC), local preferred direction (LPD), male lobula giant 1 (MLG1)

2.2 Summary

Many insects perform high-speed aerial maneuvers where they navigate through visually complex surrounds. Among insects, hoverflies stand out with males switching from stationary hovering to high-speed pursuit at extreme angular velocities [1]. In dipterans 50-60 large interneurons, the lobula plate tangential cells (LPTCs), detect changes in optic flow experienced during flight [2-5]. It has been predicted that large LPTC receptive fields are required of accurate 'matched filters' of optic flow [6]. While many fly taxa have 3 horizontal system ('HS') LPTC neurons in each hemisphere, hoverflies have 4 [7], possibly reflecting the more sophisticated flight behavior. We here show that the most dorsal hoverfly neuron (HSN) is sexually dimorphic, with the male receptive field substantially smaller than in females or in either sex of blowflies. The (hoverfly specific) HSNE is, however, sexually isomorphic. Using complex optic flow, we show that HSN codes yaw velocity as well as HSNE, despite its smaller receptive field. Responses to a target moving against a plain or textured background suggest that the male HSN could potentially play a role in target pursuit under some conditions.

2.3 Results and Discussion

2.3.1 Receptive field analysis

The 3 HS neurons in the blowfly lobula plate view the dorsal (HSN - north), medial (HSE - equatorial), and ventral (HSS - south) visual field respectively [8]. Hoverflies have, however, been shown anatomically to have 4 HS neurons [7]. To characterize the physiological receptive fields of the 2 most dorsal of these, we mounted *Eristalis tenax* in front of a monitor on which we moved a small high-contrast bar (1.6 x 3.9º) in 4 directions at 50º/s with the bar oriented perpendicular to its direction of motion. This stimulus elicits a non-saturating membrane potential change that, because of its limited angular extent, primarily reflects the location of the stimulus, as evident from near perfect mirror symmetry of responses in preferred and anti-preferred directions (Figure 2.1A-C). We recorded intracellular responses at 21 elevations and azimuths (Figure 2.1C), allowing reconstruction of the 2-dimensional receptive field for 4 directions of motion (Figure 2.1A, B, D, E). Compared with earlier methods [8-10] our technique permits very fine resolution of subtle receptive field details. For example, small irregularities appear in responses to all 4 scan directions, and thus also in the resulting receptive field (Figure 2.1).

Exploiting the near-sinusoidal direction tuning of these neurons [11], we fitted the responses to the 4 directions of motion with a sinusoid (Figure 2.1F), to determine the local preferred direction (LPD) and the response amplitude for each point in space. We used the LPD and response amplitude for the 21 x 21 matrix to plot vectors for a receptive field map representing the whole visual display, illustrated as a gnomonic azimuthal projection to account for distortions introduced by the flat stimulus screen (Figure 2.1G).

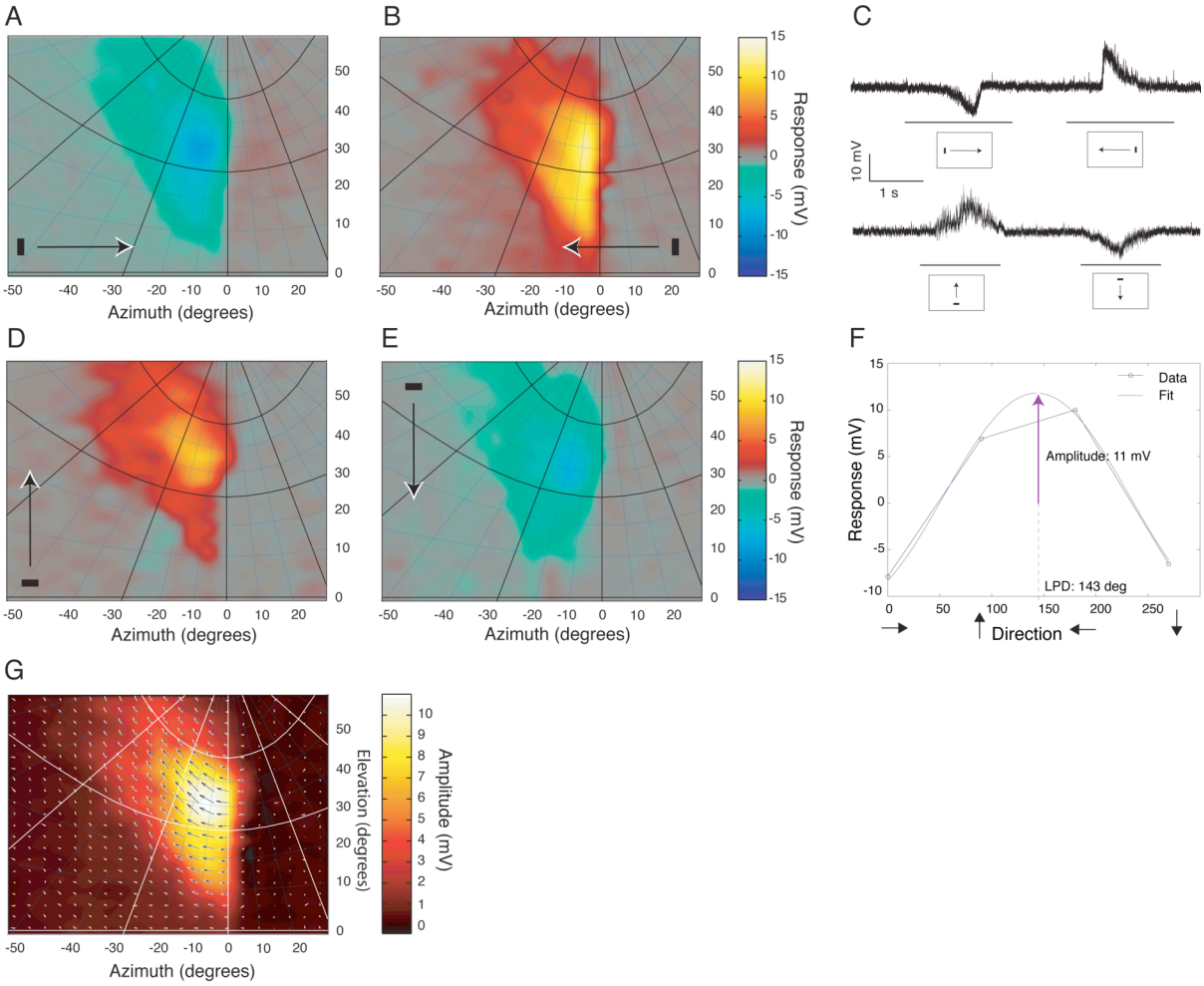

Figure 2.1 Receptive field acquisition

A) Response of a male HSN to horizontal rightward motion of a 1.6 x 3.9º high-contrast bar moving at 50º/s across a bright visual display (shown as a gnomonic azimuthal projection). The interpolated response is color-coded to show hyperpolarizing events compared to pre-stimulus membrane potential (grey). B) The same neuron of the left lobula plate is depolarized by horizontal leftward motion. C) Intracellular response to the target moving across the centre of the screen (top trace), with lines indicating peri-stimulus duration as the bar moved right and then left. Response to vertical motion as the target moved up and then down across the middle of the monitor (lower trace). D) The same neuron is depolarized by upward motion in the fronto-dorsal visual field. E) The neuron is hyperpolarized by downward motion. F) The mean response to 4 directions of motion (black circles) for each point in space was fitted with a sine wave, to estimate the local preferred direction (LPD, 143º) and response amplitude (11 mV), as indicated by the arrow. G) The LPD and response amplitude for the entire 21 x 21 matrix with the length of the arrows normalized to their maximum and projected onto the interpolated response amplitude.

2.3.2 Sexual dimorphism of HSN

We determined complete receptive fields as described above for 16 female and 39 male hoverfly HSN neurons (Figure 2.2). The receptive field of female HSN is asymmetric with maximum sensitivity in the fronto-dorsal visual field and a broad peak in sensitivity between 30 and 60º above the equator (see 4 mV contour, Figure 2.2B). Although the asymmetry makes estimation of a true 'center' for the receptive field difficult, we can quantify its size and shape across multiple individuals by measuring the maximum width and height at a contour representing 75% response amplitude (Figure 2.2A). The intersection of these two measures (the 'centroid', Figure 2.2B) provides a useful basis for comparison of the location of the receptive field. The centroids show individual variation, perhaps reflecting differences in the distribution of synaptic inputs from local motion detectors, as was previously found morphologically in blowfly HS neurons [12].

As the representation of azimuthal angles decreases with increasing elevation to finally become infinitely small at the pole, we need to account for the fact that body-centered coordinates do not represent angular size when we compare receptive field *size* and *shape* between neurons. Hence, we express receptive field dimensions in terms of absolute angular size (i.e. angular subtense at the eye, independent of orientation), and receptive field *location* based on body coordinates (azimuth and elevation). In female HSN (Figure 2.2A), receptive field width at 75% response amplitude is 19 ± 7.1º and the height is 31 ± 6.2º (mean ± SD). The receptive field of male HSN (Figure 2.2D) is 40% narrower (11 ± 2.2º, $p < 0.001$) and 45% shorter (17 ± 5.1º, $p < 0.001$) than the female HSN. To compare the neurons' motion sensitivity across the entire visual display we subtracted the average male from the average female receptive field (using both LPD and response amplitude) and found the two to be significantly different ($p < 0.001$, Figure 2.2A, D).

Both male and female HSN receive input from photoreceptors from a small region of binocular overlap (approximately 20º, [10]) in the fronto-dorsal visual field (Figure 2.2A, D). The female HSN centroid is located at an elevation of 52 ± 7.1º and an azimuth of -16 ± 10º (Figure 2.2B). The male HSN receptive field centroid is located at a similar elevation (47 ± 7.5º, no significant difference), and closer to the midline (-5.0 ± 6.4º, $p < 0.001$, Figure 2.2E). However, as the female receptive field is larger than the male, and we determine the centroid utilizing width and height at 75% maximum, the actual maximal

sensitivity in individual recordings may be similarly frontal to those in males (Figure 2.2A, D).

Lucifer Yellow fills of HSN in females (Figure 2.2C, and see [13]) and males (Figure 2.2F, filled 3 times) show input dendrites confined to the dorsal lobula plate. The input dendrites display pronounced anterior-posterior flattening (Supplementary Movie 1), but cover a smaller part of the dorsal lobula plate than their Calliphorid counterparts [8, 12, 14]. The greater lateral extension of the female receptive field (Figure 2.2B) corresponds to more proximal input dendrites in the medio-ventral lobula plate (arrowheads and inset, Figure 2.2C). These dendrites are absent in male HSN, where most input dendrites terminate in the distal limits of the lobula plate (Figure 2.2F), consistent with a frontally confined receptive field (Figure 2.2E).

Previous work on blowfly HSN neurons [8, 12, 15] suggests that their receptive fields extend more laterally than those of *Eristalis* although the methods used differ and most data are for female flies. To permit more direct comparison we also characterized a male *Calliphora* HSN neuron using our method. Consistent with the previously published data, this receptive field extends laterally well beyond the boundary of our display (Supplementary Figure 2.1). Thus both sexes of *Eristalis* have more frontally located receptive fields than in other flies, particularly so in males.

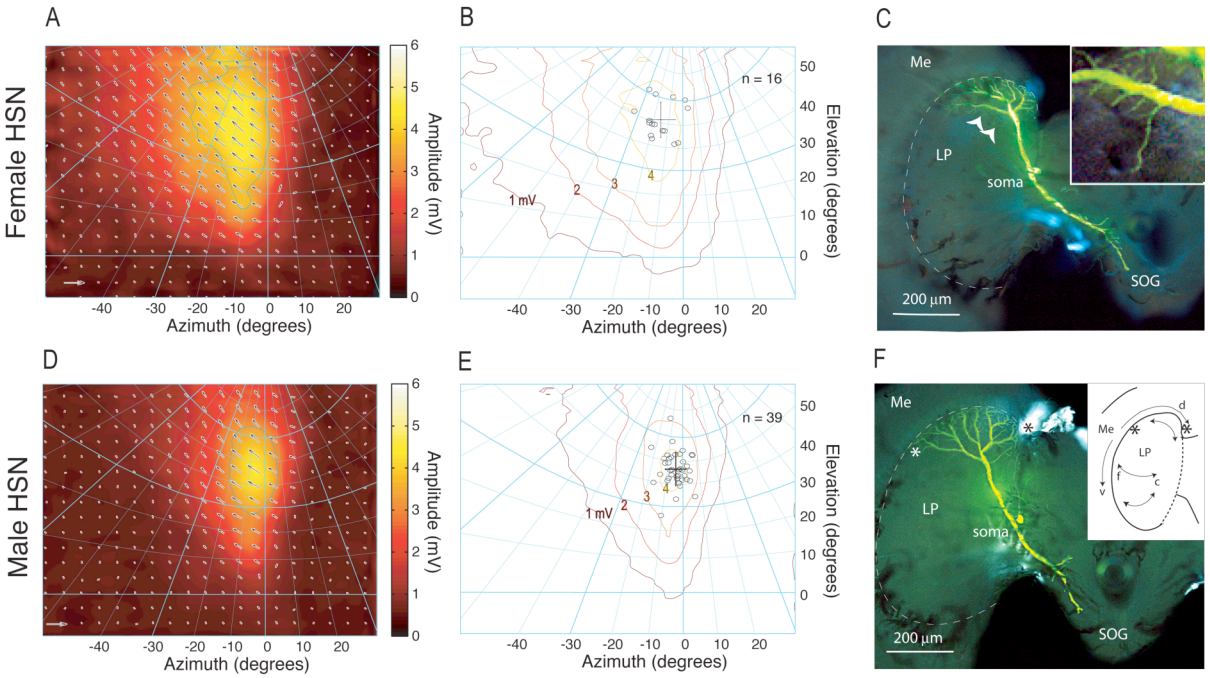

Figure 2.2 Sexual dimorphism of hoverfly HSN.

A) Average LPD and response amplitude of 16 female HSN shows a receptive field extending to the ipsilateral border of the display. The arrows have been normalized to 6 mV (arrow in bottom left hand corner of graph). The average 75% response amplitude is delineated in blue. B) The same data in 1 mV increments. Black circles indicate the centroids of individual receptive fields, with the mean location as a black cross, and the arms representing the standard deviation. C) Z-series maximum intensity projection of an individually Lucifer yellow- filled female HSN. Dendritic input arbors are confined to the dorsal lobula plate (dashed line delineates the lobula plate). Arrowheads indicate input dendrites proximal to the main arbor corresponding to the lateral limits of the receptive field (inset shows a high contrast 10x magnification of this area). D) Average LPD and response amplitude of 39 male HSN with a receptive field contained within the fronto-dorsal visual field. The arrows have been normalized to 6 mV. The average 75% response amplitude is delineated in blue. E) The same data in 1 mV increments. Black circles show individual centroids. F) Lucifer yellow fill of an individual male HSN shows dendritic arbors confined to the dorsal lobula plate (dashed). Inset shows a schematic representation of the retinotopic organization of the lobula plate, with asterisks in the same areas as in the photo. Me = medulla; LP = lobula plate; SOG = sub-esophageal ganglion; v = ventral; d = dorsal; f = frontal; c = caudal.

2.3.3 Sexual isomorphism in HSNE

The additional HS neuron previously identified anatomically in hoverflies [7] has been classified as HSNE, based primarily on its intermediate location between blowfly HSE and HSN [13]. We recorded complete HSNE receptive fields in 11 female and 34 male HSNE *Eristalis*. While HSN neurons display striking sexual dimorphism, HSNE is similar in the two sexes (Figure 2.3). By subtracting the average male from the average female receptive field across the entire visual display we find no significant difference between the two ($p = 0.45$, Figure 2.3B, E).

Although maximal sensitivity is nearly frontal as in HSN, the centroids of female and male (Supplementary Figure 2.2) HSNE receptive fields are more equatorial (females 13 ± 6.0º, males 12 ± 5.3º) and extend further into the ipsilateral visual field (females at an azimuth of -14 ± 7.7º, males at -17 ± 7.6º), but again there is no significant difference between the sexes. This more dorsal receptive field differs from blowfly HSE that straddles the equator symmetrically [6, 8], justifying our morphological label HSNE [13].

The sensitivity of male and female HSNE extends laterally beyond the limits of our display. In some recordings we mapped lateral sensitivity by rotating the monitor 45º around the center of the fly's head. Small differences in apparent sensitivity at the same receptive field locations in these laterally mapped fields (Figure 2.3A, D) result from this being a subset of the neurons for which we mapped frontal sensitivity. Nevertheless, these maps underscore the physiological similarity of HSNE in the two sexes.

Unsurprisingly (given the physiological similarity) the morphology of HSNE in females (Figure 2.3C, and see [13]) and males (Figure 2.3F, filled 5 times) shows little sexual dimorphism. Individual variation in branching pattern is apparent between different fills (not shown), just as Hausen found in blowfly HS neurons [12], but the gross morphology of major branches (Supplementary Movies 3 & 4), and the area of dendritic spread is conserved between individuals and sexes. In particular, the input dendrites in both sexes extend from the frontal (distal) lobula plate more caudally (proximal) and ventrally compared to HSN, consistent with their physiologically recorded receptive fields being closer to the equator and laterally extended.

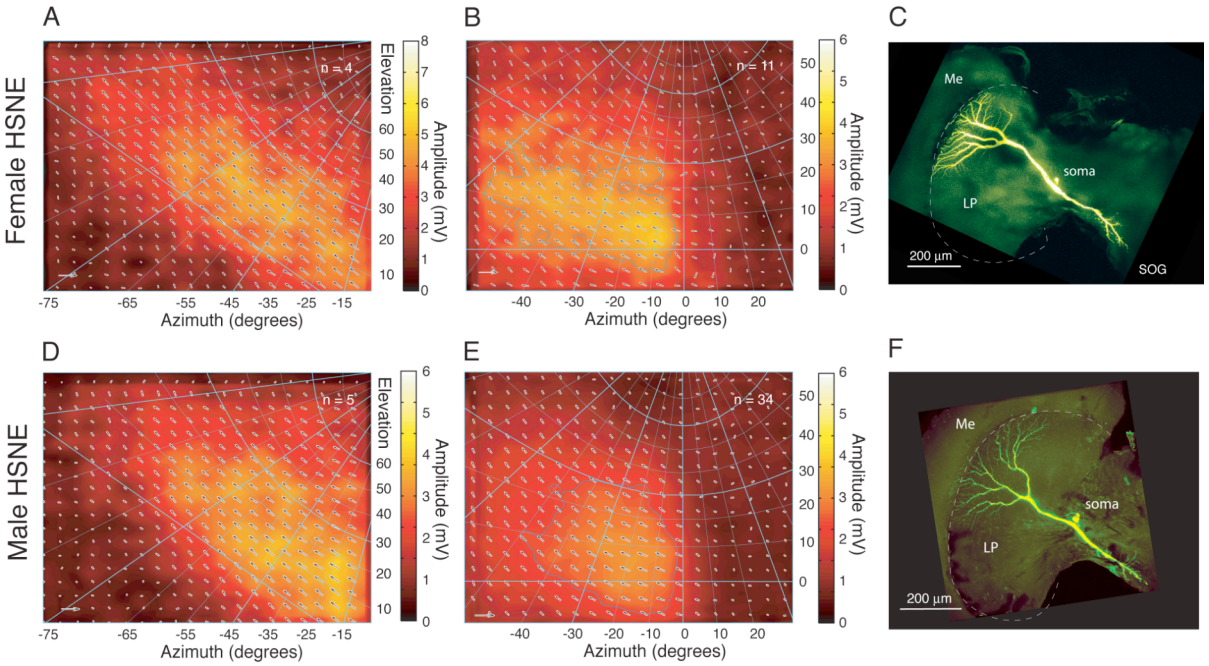

Figure 2.3 Sexually isomorphic HSNE

A) Average LPD and response amplitude of 4 female HSNE with the monitor rotated 45º around the center of the fly's head. This is a subset of HSNE neurons with high sensitivity. The arrows have been normalized to 6 mV (arrow in bottom left hand corner of graph). The skew in the gnomonic azimuthal projection results from the angle of the fly's head (35º). B) Average LPD and response amplitude for the frontal visual field of 11 female HSNE. The arrows have been normalized to 6 mV. The average 75% response amplitude is delineated in blue. C) Lucifer yellow fill of a female HSNE shows dendritic input arbors in the medio-dorsal lobula plate (dashed line delineates the lobula plate). D) Average LPD and response amplitude of 5 male HSNE with the monitor rotated 45º. The arrows have been normalized to 6 mV. E) Average LPD and response amplitude for the frontal visual field of 34 male HSNE. The arrows have been normalized to 6 mV, and the average 75% response amplitude is delineated in blue. F) Lucifer yellow fill of a male HSNE shows dendritic input arbors located in a similar area of the lobula plate (dashed) as in the female neuron (panel C). Me = medulla; LP = lobula plate; SOG = sub-esophageal ganglion.

2.3.4 HSN as a fronto-dorsal yaw detector

We conclude that the differences observed in HSN both between sexes and compared with other diptera are unique to this neuron, and are not due to the different methods we have employed, and thus are likely to be associated with differences in the role of this neuron in behavior. Most dipteran LPTCs have receptive fields with sensitivity extending over a large part of the visual field with properties suggesting tuning to particular patterns of ego-motion, with blowfly HSE and HSN proposed to be 'matched filters' for yaw rotation [15-18]. Large receptive fields have been interpreted as a pre-requisite for reliable signals to particular patterns of ego-motion, as signals from small parts of the visual field can be ambiguous [6]. Small receptive fields could also be more affected by local high-contrast features than neurons that spatially pool across larger number of local motion detectors (i.e. 'pattern noise', see [19]). Considering this, the receptive field of the hoverfly HSN is not only remarkably small, but additionally, local direction tuning is not as clearly aligned with elevation lines on the gnomonic projection (in either sex) as one would expect from a neuron tuned to pure yaw rotation (Figure 2.2A, D).

To test whether the smaller HSN receptive field can code for yaw velocity in complex optic flow, we designed a broadband stimulus containing yaw rotation and forward translation. We moved a camera platform through a park environment with the forward component (2.7 ± 1.1 m/s) interspersed with turns (yaw rotation) towards new trajectories (Figure 2.4A-C). While we have no control over the 3D structure in a natural environment, an analysis of the resulting image sequence shows resulting optic flow within the coding range of these neurons [10] with yaw at 96 ± 107º/s, and off-axis retinal velocity caused by forward translation at 48 ± 38º/s (Supplemental Figure 2.3D-H). This is an artificial stimulus as the highly sexually dimorphic behavior of hoverflies makes it impossible to compare responses between the sexes to behaviorally generated optic flow. Furthermore, saccadic head movements [5] make it extremely difficult to determine the exact gaze of flies (particularly during high-speed pursuit) and complete reconstruction of 'real' optic flow has only been possible in restricted environments [20]. Nevertheless, using this stimulus we find a high correlation between yaw velocity and the response of both HS neurons in either sex, but no difference between neurons (Figure 2.4D, H).

The small HSN receptive field is confined to the fronto-dorsal visual field (Figure 2.2), in the region of the visual world associated with male specializations for conspecific pursuit

[1, 10, 21-23], which could suggest a role in such behavior. In blowflies the male-specific lobula giant MLG1 was described as a key neuron for visualizing conspecifics [24, 25]. However, a recent study found that blowfly HS neurons responded to targets against naturalistic background motion with a higher signal-to-noise ratio than MLG1 [26]. To test whether the smaller hoverfly HSN enables robust target signaling in complex backgrounds, we inserted a target in the fronto-dorsal visual field of the movie, so target motion preceded orienting turns of the camera as in pursuits (Figure 2.4F). Correlation of responses to background motion with and without target motion show 97% similarity in male and female HSN and HSNE (Figure 2.4E). It is thus unlikely that the male HSN is used as a fronto-dorsal target detector when targets are moving against high contrast clutter.

However, hoverflies often chose habitats where they can track targets against the bright background of the sky [21]. Our receptive field scanning technique shows that small targets moving over blank backgrounds induce large membrane potential changes in both neurons of either sex (Figures 2.1-3). When we display the target sequence from the complex optic flow scenario with the target moving over a mean luminance background, we also find a strong correlation with target velocity in both neurons of either sex (Figure 2.4F-H). This suggests that HS neurons could encode target velocity under uncluttered sky conditions. In this context, the smaller, fronto-dorsally located receptive field of the male HSN would be clearly advantageous (Supplementary Figure 2.4).

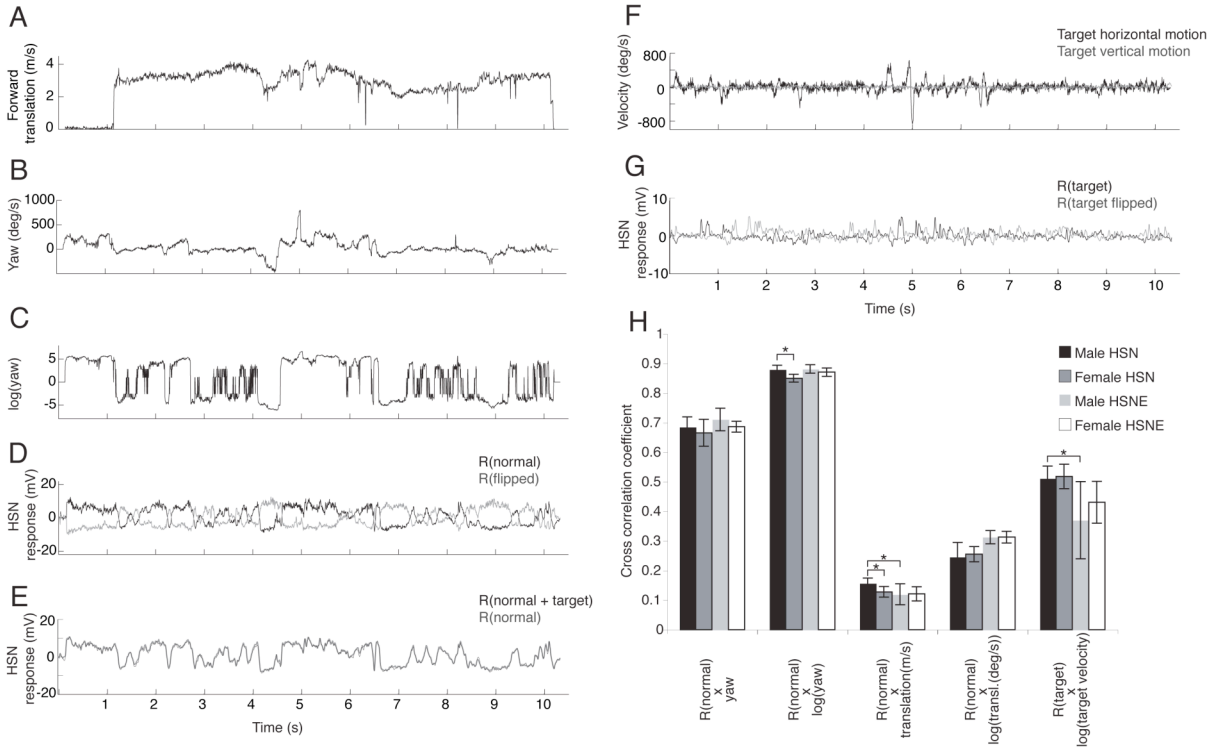

Figure 2.4 Responses to complex optic flow

A) Forward translation velocity (m/s) of the camera platform as a function of time. B) Yaw velocity (deg/s) of the platform. C) Log of the yaw velocity. D) Average of 5 intracellularly recorded responses from a single male HSN to the movie (black), and the movie sequence mirror imaged (grey). E) Intracellularly recorded response to the movie sequence (grey), and the response to the movie with target motion superimposed (black). F) Horizontal and vertical velocity (deg/s) of the target. G) Average of 5 intracellularly recorded responses to the target moving over the mean luminance background (black), and to the target sequence mirror imaged (grey). H) Cross correlation between responses of hoverfly HS neurons and yaw velocity (column 1), log yaw velocity (column 2), and forward translation velocity of the platform (in m/s, column 3). Cross correlation between responses and off-axis retinal velocity caused by forward translation (deg/s, column 4). Cross correlation between responses and target velocity (column 5). Stars (*) indicate significant difference, $p < 0.05$.

2.3.5 Conclusion

We have shown here sexual dimorphism in receptive field properties of a hoverfly tangential neuron, previously described as sexually isomorphic (at least in blowflies [11]). While hoverfly HS neurons are clearly able to code for yaw velocity (Figure 2.4), the question arises as to why the male HSN receptive field is smaller and limited to the frontal visual field (Figure 2.2D). This area is close to the pole of the expansion generated by forward translation, and yaw signals generated by high-contrast features seen against the sky could easily 'swamp' any forward translational optic flow. By shrinking the receptive field to a region where yaw is least ambiguous, this neuron may simplify the otherwise daunting task of disambiguating yaw from forward translation during pursuit. This, however, happens at the expense of a decreased area of sampling, which may explain why this strategy is limited to the HSN neuron, and why it is not observed in some other flies.

2.4 Experimental procedures

Animals: Hoverflies (*Eristalis tenax)* and blowflies *(Calliphora stygia)* were collected under permit from the wild (the Botanic Gardens of Adelaide) and kept in the dark at 4ºC until experimental time.

Electrophysiology: The animal was waxed down with the head tilted forward. A small hole was cut over the left lobula complex leaving the neural sheath intact. Neurons were recorded intracellularly using aluminium silicate micropipettes pulled on a Sutter Instruments P-97 puller and filled with 2 M KCl. Electrodes had a typical tip resistance of 120 MΩ and were inserted with a Piezo micromanipulator. The flies were mounted in front of a RGB CRT display at a distance of 14 cm. They were aligned with the monitor using the planar back surface of the head as a morphological landmark and the eye's equator was assumed to be 90º perpendicular to this. The animal's midline was used to determine the vertical axis. This was used in later analyses to correct for angular distortion introduced by the flat screen. Visual were generated using VisionEgg (www.visionegg.org). The monitor subtended 100 x 75º at the fly's central visual field, with a resolution of 640 x 480 pixels, and a refresh rate of 200 Hz. The monitor could be rotated around the center of the fly's head to retrieve responses to lateral visual input. Data were digitized at 5 kHz using a 16 bit A/D converter (National Instruments) and analyzed off-line with Matlab (a few early recordings were digitized using a 12 bit A/D converter).

Receptive field acquisition: To determine receptive fields we scanned the bright monitor with a black 1.6 x 3.9º bar oriented perpendicular to the direction of motion. Scans were performed with a 2 s horizontal rightward scan, followed by a 1 – 3 s rest, and a 2 s leftward scan back over the same path (50º/s, given for the fly's central visual field). Following a 1 – 3 s rest, a new semi-randomly chosen elevation was scanned, until the entire monitor had been covered 21 times. Vertical scans were performed at the same velocity, with upward drifts followed by downward presentations at 21 azimuths. We recorded complete receptive fields for a total of 27 HS neurons in the left lobula plate of 24 female and 73 neurons in 69 male hoverflies (*Eristalis tenax)*. For each scan direction, we analysed the membrane potential averaged across 21 bins expressed relative to the resting potential. This permitted a 2-dimensional matrix of membrane potentials to be produced,

representing the area of the stimulus display. The data for each bin was transformed into azimuth and elevation coordinates, using the calibrated position of the fly and the angle of its head to correct for distortions introduced by the flat display, before averaging data across animals. Following convention, azimuths are negative left (ipsilateral) of the midline, and elevations are positive dorsal to the equator.

Data analysis: We further analyzed the local preferred direction (LPD) of motion using a method analogous to that of Krapp & Hengstenberg [9] and Frye & Olberg [27]. The response to the 4 directions of motion at each point in the receptive field was fitted in a least squares manner with a sinusoid with variable phase, response amplitude and offset but the frequency fixed at 360º. We used the phase of the fitted function to find the LPD and response amplitude, which we then used to plot the orientation and length of local motion vectors in receptive field maps. To average receptive fields we interpolated the LPD and response amplitude across the visual field using a delaunay-based triangulation method. We also delineated the 75% response amplitude, which we used to measure the widest and tallest part of each receptive field in angular terms. In finding the tallest and widest part we simultaneously identified the centroid, which we express in terms of azimuth and elevation, thereby taking the distortion of the dorsal visual field into account.

We display all data as mean ± SD unless otherwise stated. We performed statistical analyses of width and height at 75% response amplitude, and of centroid location, with un-paired, 2-tailed Student's t-tests. To compare complete receptive field maps across the entire visual display, we subtracted average male from average female receptive fields and determined the difference from 0 (LPD and response amplitude difference of 0 represent identical receptive fields).

Morphology: To identify recorded neurons we backfilled micropipettes with 4% Lucifer Yellow in 0.1 M LiCl. The dye was injected by passing a hyperpolarizing current (0.2 to 2 nA, depending on the amount of current individual electrodes would pass without blockage) for 10-30 minutes. The brain was dissected out of the head capsule, fixed in 4% paraformaldehyde (in 0.1 M phosphate buffer), dehydrated through an ethanol series and cleared in methyl salicylate. A series of digital photographs were taken at different depths of the tissue (Olympus BX-50 epifluorescence microscope), and the morphology of the neuron was reconstructed using Adobe Photoshop. The position of the neuron within the

lobula plate was confirmed by constructing a 3-dimensional image from a Z-series in a scanning confocal microscope (Leica Spectral Confocal SP5).

For 3-dimensional reconstruction we imported the confocal stack into the open-source software package OsiriX (http://www.osirix-viewer.com/). We then utilized OsiriX to generate a movie by giving the appropriate 3-dimensional coordinates in the lobula plate. The movies were saved in Quicktime format for viewing as supplementary information.

Display and analysis of movie: We designed a broadband stimulus by moving a camera platform through a visually rich natural surround. The movie sequence was captured by a 14-bit camera (XCD-V50, Sony™) with a 90º wide-angle lens (TF2.8DA-8, Fujinon™) mounted on a customized robotic platform fitted with a damped, inertial stabilization system (Brinkworth et al, *under review*). Data from wheel-mounted optical encoders gave the trajectory. A green filter (N52-534, Edmund™) was used to match input to the spectral sensitivity of the fly motion pathway [28]. The nonlinear (gamma) characteristics of the camera were quantified by comparing images of the same scene taken at different shutter speeds. The camera was programmed to alter the shutter speed for several samples of each frame (5 different shutter speeds used), which were then combined, thus increasing the dynamic range of the images to 90 dB, providing detail in both the dark and light parts of the scene and reducing noise in any one pixel. The platform was moved slowly so the 5 Hz image acquisition rate could be scaled to the 200 Hz display frame rate used during electrophysiology.

We moved the robot in bright sunlight along a curving path through a visually rich outdoor scene and directed in a 'saccadic' manner, with forward motion (2.7 ± 1.1 m/s) interspersed by rapid turns towards a new trajectory. While optic flow caused by yaw rotation is homogenous across the visual field, forward translation causes different retinal velocities in different parts of the visual field, and also depends on the structure of the environment. To get an estimate of retinal velocities we measured the movement of a feature in the most peripheral part of the movie by comparing frames separated by 50 ms. We repeated this procedure with the selection of frames shifted by 25 ms. To get the retinal velocity caused by forward translation we finally subtracted the yaw rotation.

A small black target (1.4 x 2.8º) was inserted into the reconstructed movie and animated with random jitter (maximum 0.7º/frame) and 'turns' that preceded the actual platform

motion by 0.1 s to simulate 'chasing' of the target. The target elevation was varied slowly and randomly in the dorsal part of the visual field associated with pursuit flight [1].

We recorded responses of HS neurons (8 male HSN, 3 female HSN, 3 male HSNE and 4 female HSNE) to the movie with the background scene alone, combined background and target, or the target only against a mean luminance background. We then repeated all conditions with the movie displayed in a mirror-symmetrical fashion. We performed correlation analysis of visual input signals and recorded responses, with the optimal lag determined for each cell (25 – 40 ms, i.e. 5 – 8 frame delay). Statistical analysis of correlation in different neurons was performed with un-paired, 2-tailed Student's t-tests.

2.5 Acknowledgements

We thank the Manager of the Botanic Gardens of Adelaide for allowing insect collection and two reviewers whose input greatly improved this paper. The research was funded by the Swedish Research Council (2004-3515), the Australian Research Council (LP0667744), and the US Air Force Office of Scientific Research (FA 9550-04-1-0294). We are grateful to Meredith Wallwork and staff of Adelaide Microscopy for assistance with confocal imaging. We also thank past and present members of the Visual Physiology Group who contributed to this paper.

2.6 References

1. Collett, T.S., and Land, M.F. (1978). How hoverflies compute interception courses. J Comp Physiol A *125*, 191-204.

2. Borst, A., and Haag, J. (2002). Neural networks in the cockpit of the fly. J Comp Physiol A *188*, 419-437.

3. Kern, R., van Hateren, J.H., Michaelis, C., Lindemann, J.P., and Egelhaaf, M. (2005). Function of a fly motion-sensitive neuron matches eye movements during free flight. PLoS Biol *3*, e171.

4. Hengstenberg, R. (1991). Gaze control in the blowfly *Calliphora*: a multisensory, two-stage integration process. Sem Neurosci *3*, 19-29.

5. Land, M.F. (1973). Head movements of flies during visually guided flight. Nature *243*, 299-300.

6. Krapp, H.G., Hengstenberg, B., and Hengstenberg, R. (1998). Dendritic structure and receptive-field organization of optic flow processing interneurons in the fly. J Neurophysiol *79*, 1902-1917.

7. Buschbeck, E.K., and Strausfeld, N.J. (1997). The relevance of neural architecture to visual performance: phylogenetic conservation and variation in dipteran visual systems. J Comp Neurol *383*, 282-304.

8. Hausen, K. (1982). Motion sensitive interneurons in the optomotor system of the fly. II. The horizontal cells: receptive field organization and response characteristics. Biol Cybern *46*, 67-79.

9. Krapp, H.G., and Hengstenberg, R. (1997). A fast stimulus procedure to determine local receptive field properties of motion-sensitive visual interneurons. Vision Res *37*, 225-234.

10. Straw, A.D., Warrant, E.J., and O'Carroll, D.C. (2006). A 'bright zone' in male hoverfly (*Eristalis tenax*) eyes and associated faster motion detection and increased contrast sensitivity. J Exp Biol *209*, 4339-4354.

11. Hausen, K., and Egelhaaf, M. (1989). Neural mechanisms of visual course control in insects. In Facets of Vision, D.G. Stavenga and R.C. Hardie, eds. (Berlin Heidelberg: Springer Verlag), pp. 391-424.

12. Hausen, K. (1982). Motion sensitive interneurons in the optomotor system of the fly. I. The horizontal cells: structure and signals. Biol Cybern *45*, 143-156.

13. O'Carroll, D.C., Laughlin, S.B., Bidwell, N.J., and Harris, R.A. (1997). Spatio-temporal properties of motion detectors matched to low image velocities in hovering insects. Vision Res *37*, 3427-3439.

14. Hengstenberg, R., Bülthof, H., and Hengstenberg, B. (1983). Three-dimensional reconstruction and stereoscopic display of neurons in the fly visual system. In Functional Neuroanatomy, N.J. Strausfeld, ed. (Berlin: Springer), pp. 183-205.

15. Krapp, H.G., Hengstenberg, R., and Egelhaaf, M. (2001). Binocular contributions to optic flow processing in the fly visual system. J Neurophysiol *85*, 724-734.

16. Franz, M.O., and Krapp, H.G. (2000). Wide-field, motion-sensitive neurons and matched filters for optic flow fields. Biol Cybern *83*, 185-197.

17. Hausen, K. (1984). The lobula-complex of the fly: structure, function and significance in visual behavior. In Photoreception and vision in invertebrates, M. Ali, ed. (New York: Plenum), pp. 523-559.

18. Krapp, H.G., and Hengstenberg, R. (1996). Estimation of self-motion by optic flow processing in single visual interneurons. Nature *384*, 463-466.

19. Rajesh, S., Rainsford, T., Brinkworth, R.S.A., Abbott, D., and O'Carroll, D.C. (2007). Implementation of saturation for modelling pattern noise using naturalistic stimuli. In Smart Structures, Devices, and Systems III, Volume 6414, S.F. Al-Sarawi, ed., pp. 641421-641415.

20. van Hateren, J.H., and Schilstra, C. (1999). Blowfly flight and optic flow. II. Head movements during flight. J Exp Biol *202*, 1491-1500.

21. Fitzpatrick, S., and Wellington, W. (1983). Contrasts in the territorial behavior of 3 species of hoverflies (Diptera, Syrphidae). Can Entomol *115*, 559-566.

22. Land, M.F., and Eckert, H. (1985). Maps of the acute zones of fly eyes. J Comp Physiol A *156*, 525-538.

23. Barnett, P.D., Nordström, K., and O'Carroll, D.C. (2007). Retinotopic organization of small-field-target-detecting neurons in the insect visual system. Curr Biol *17*, 569-578.

24. Gilbert, C., and Strausfeld, N.J. (1991). The functional organization of male-specific visual neurons in flies. J Comp Physiol A *169*, 395-411.

25. Hausen, K., and Strausfeld, N.J. (1980). Sexually dimorphic interneuron arrangement in the fly visual system. Proc R Soc Lond B *208*, 57-71.

26. Trischler, C., Boeddeker, N., and Egelhaaf, M. (2007). Characterisation of a blowfly male-specific neuron using behaviourally generated visual stimuli. J Comp Physiol A *193*, 559-572.

27. Frye, M.A., and Olberg, R.M. (1995). Visual receptive field properties of feature detecting neurons in the dragonfly. J Comp Physiol A *177*, 569-576.

28. Smakman, J.G., and Stavenga, D.G. (1986). Spectral sensitivity of blowfly photoreceptors: dependence on waveguide effects and pigment concentration. Vision Research *26*, 1019-1025.

2.7 Supplemental Results and Discussion

2.7.1 Male *Calliphora* HSN

Previous work on blowfly HSN neurons [1-3] suggests that their receptive fields are more extended laterally than those described here (Figure 2.2), although the methods used differ and data are for female flies (however, sexual isomorphism has been mentioned [4]). To allow for more direct comparison with our technique, we also characterized a male *Calliphora* HSN neuron, which reveals a receptive field extending laterally well beyond the boundary of our display (Supplementary Figure 2.1A), and corresponding neuronal morphology with much greater ventral-caudal extent of input dendrites (Supplementary Figure 2.1B, Supplementary Movie 2).

2.7.2 Lateral sensitivity of HSNE

Despite the hoverfly HSN (Figure 2.2) showing substantial sexual dimorphism we found no difference between sexes in the hoverfly specific HSNE (Figure 2.3). In addition to similar centroid location in the two sexes (Supplementary Figure 2.2), we found no difference in width or height at 75% maximum amplitude (Figure 2.3B, E). In Supplementary Figure 2.2, it appears that the sensitivity of HSNE drops off towards the lateral edge of the display in its frontal position. However, the receptive fields of a smaller range of neurons with the monitor rotated 45º around the center of the fly's head, show that sensitivity in fact extends far out in the lateral visual field to an azimuth of -90º (Figure 2.3A, D). The apparent drop-off in sensitivity is therefore probably caused by the distortion induced by using a flat screen which reduces the apparent size of the stimulus towards the edges.

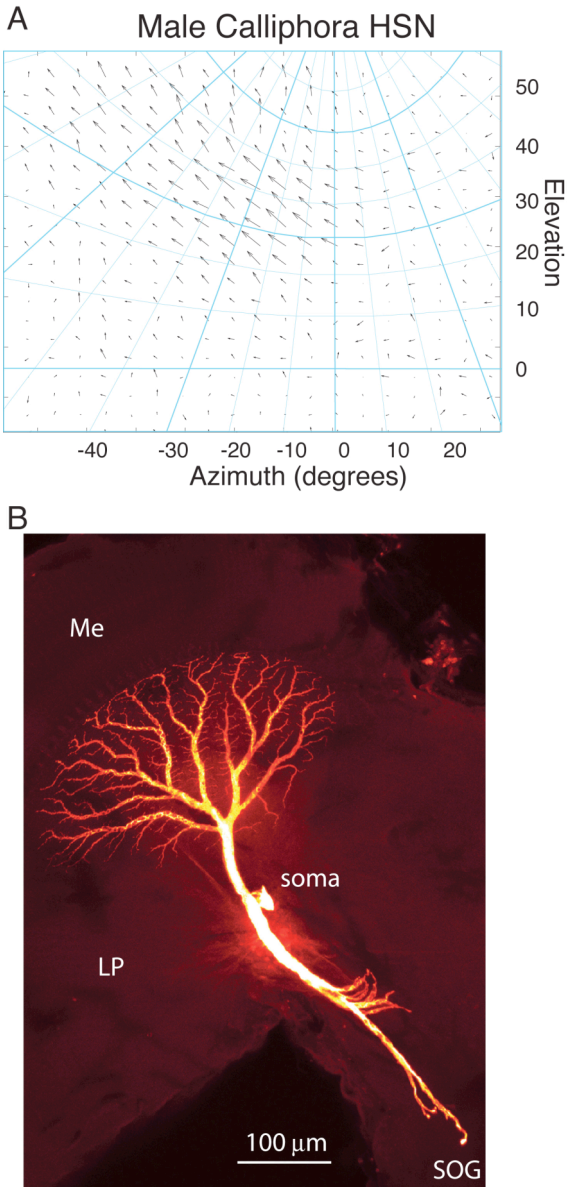

Supplemental Figure 2.1 Male *Calliphora* HSN

A) LPD and amplitude of a male *Calliphora* HSN. B) Lucifer yellow fill of the same HSN shows dendritic arbors to be confined to the dorsal lobula plate, with a large spread of input dendrites. Me = medulla; LP = lobula plate; SOG = sub-esophageal ganglion.

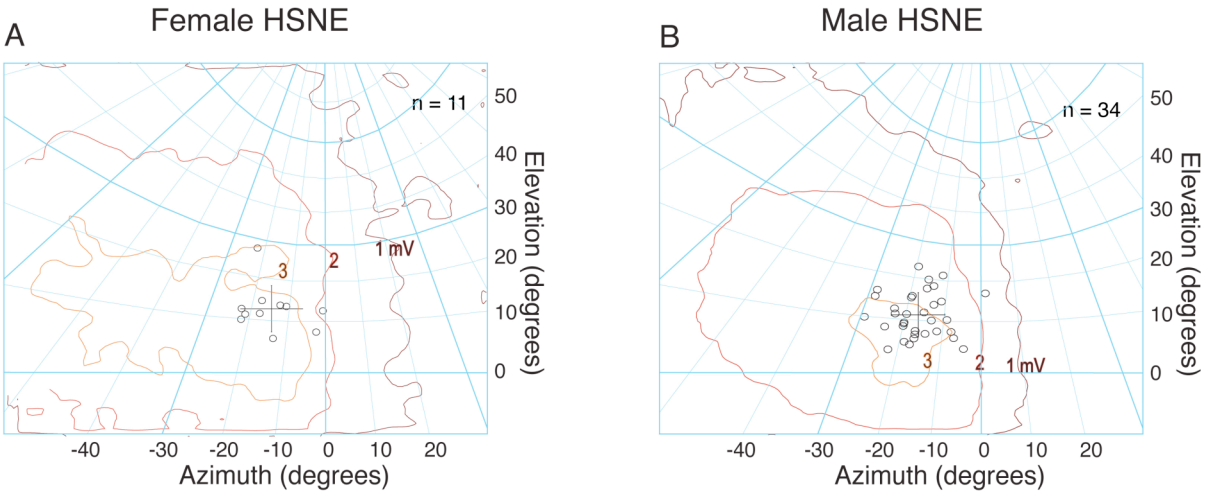

Supplemental Figure 2.2 Frontal sensitivity and centroids of hoverfly HSNE

A) The frontal sensitivity for 11 female HSNE depicted in 1 mV increments shows. Black circles indicate the centroids of individual receptive fields, with the mean location indicated with a black cross, where the arms represent the standard deviation. B) The frontal sensitivity for 34 male HSNE depicted in 1 mV increments. Black circles indicate the centroids of individual receptive fields, with the mean location indicated with a black cross, where the arms represent the standard deviation.

2.7.3 Role of a small HSN

While the optic flow caused by yaw rotation is homogenous across the visual field, forward translation causes different retinal velocities in different parts of the visual field, and also depends on the structure of the environment. For example, near objects will cause higher retinal velocities than distant objects, and objects near the pole of expansion will move little across the retina compared to those further out in the periphery. To get an estimate of the retinal velocity caused by forward translation of the platform (Figure 2.4A) we measured the movement of a feature in the most peripheral part of the movie by comparing frames separated by 50 ms (Supplementary Figure 2.3D, E). We repeated this procedure with the selection of frames shifted by 25 ms. To get the off-axis retinal velocity caused by forward translation we finally subtracted the yaw rotation from the measured value (Supplementary Figure 2.3F-H). The resulting retinal velocity correlates qualitatively well with the forward velocity of the platform (Supplementary Figure 2.3G, H).

Due to input differences it was originally hypothesized that blowfly HSE and HSN were matched filters for the detection of yaw rotation, and that HSS was used for detecting translational optic flow across the ventral visual field [3, 5, 6]. Our data show that hoverfly HSN and HSNE respond primarily to yaw even during complex flight scenarios (Figure 2.4H), and thus lend further support to the matched filter hypothesis [3, 5, 7]. Despite a strong 'progressive' component of our image sequence (forward translation 2.7 ± 1.1 m/s, generating an off-axis retinal velocity of 48 ± 38º/s, Supplementary Figure 2.3G, H), the neurons frequently signal complete hyperpolarizing reversal of responses during turns (Figure 2.4D, black trace). Furthermore, there is little correlation between the responses of the neurons and either the forward velocity of the platform, or the off-axis retinal velocity this movement generates (Figure 2.4H).

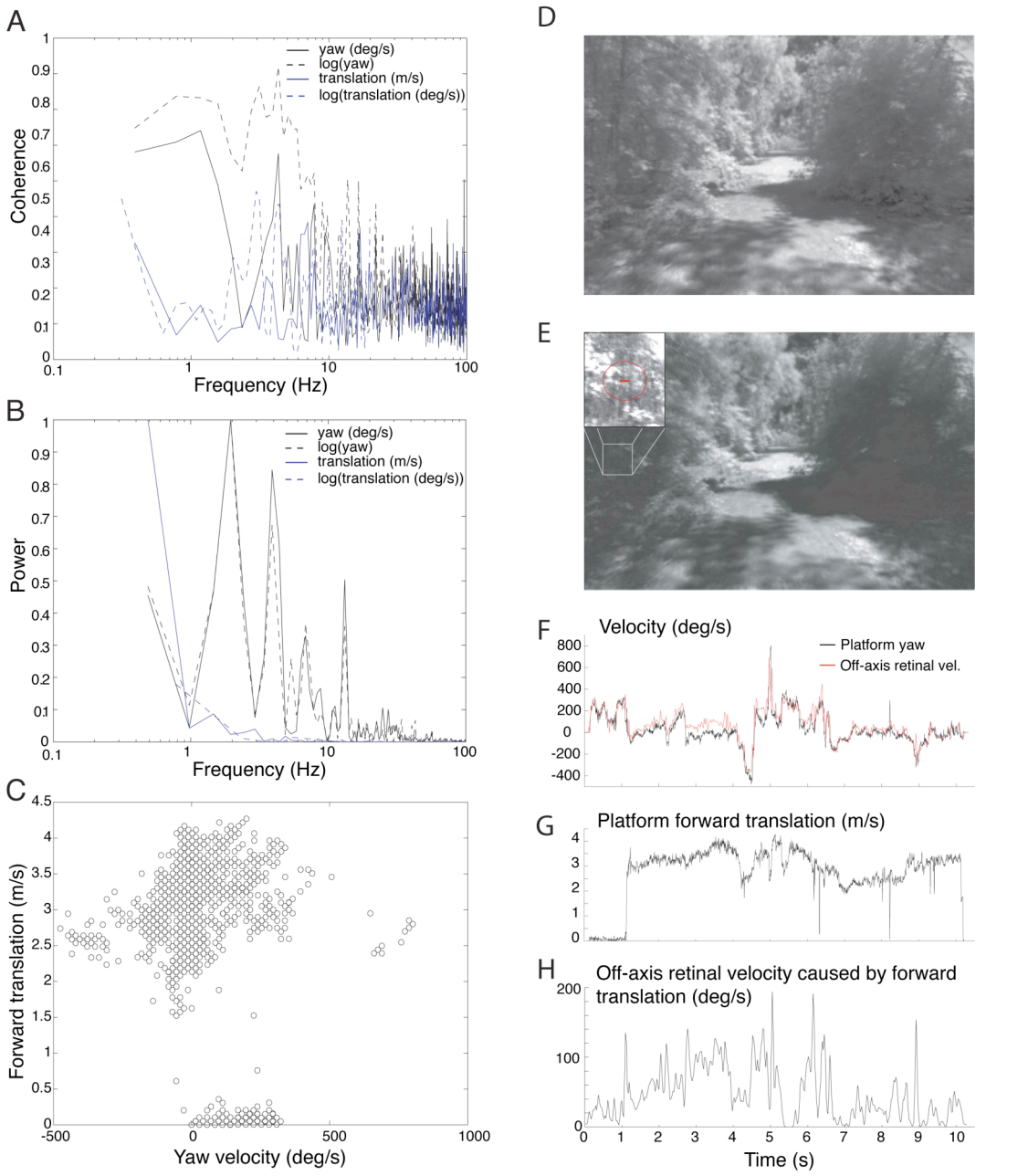
A
yaw (deg/s)
log(yaw)
translation (m/s)
log(translation (deg/s))
Coherence
Frequency (Hz)
B
Power
Frequency (Hz)
C
Forward translation (m/s)
Yaw velocity (deg/s)
D
E
F
Velocity (deg/s)
Platform yaw
Off-axis retinal vel.
G
Platform forward translation (m/s)
H
Off-axis retinal velocity caused by forward translation (deg/s)
Time (s)

Supplemental Figure 2.3 A complex optic flow sequence containing yaw rotation and forward translation

A) Coherence of the response of male HSN neurons to yaw and forward translation of the optic flow. We calculated the coherence for each individual response and show the mean coherence across neurons (n = 8, N = 50). Translation in m/s refers to the forward velocity of the platform, while translation in deg/s refers to the off-axis retinal velocity caused by this forward translation. B) The power spectrum of the yaw and translation of the optic flow. C) The forward velocity of the platform as a function of its yaw velocity. D) A single frame from the movie. E) The same frame superimposed on the frame shown 50 ms earlier. The inset shows an example of how off-axis retinal velocity was measured by measuring the distance a tree (in this case) had moved across the visual field between 2 frames separated by 50 ms. The red circled bar shows how we measured the distance the tree trunk moved. F) Yaw velocity of the platform (black) and the measured off-axis retinal velocity as a function of time. G) The forward translation of the platform (m/s). H) The remaining off-axis retinal velocity after subtracting the yaw rotation.

Our finding is thus contrary to the recent suggestion that blowfly HS neurons are not primarily matched filters for yaw as originally proposed, but instead serve a role in detection of translation [8, 9]. This recent work was based on coherence analysis of responses to reconstructed flight paths that represent the best attempt yet to fully account for both head and body movements [10, 11]. Relative head motion is, however, extremely difficult to estimate in free flight, so this data set was based on flight data from blowflies moving within a limited space (0.4 x 0.4 x 0.4 m^3). This could have promoted a collision avoidance low-speed flight mode in which objects are fixated followed by regular saccades to a new path. The blowflies never reached forward speeds above 0.4 m/s in this scenario [10, 11] compared with those observed in more natural habitats (up to 2 m/s, see [12]), let alone during hoverfly conspecific pursuit (up to 10 m/s, see [13]). Our visual input differs from this scenario in displaying yaw throughout the stimulus (Figure 2.4B). Yaw rotation velocities are also lower, as we aimed at keeping these within the coding range of HS neurons [14], which could potentially explain our different result.

Rapid saccadic turns are, however, well outside the operating range of many LPTCs and it has previously been argued that LPTC responses are deliberately tuned to lower speeds to avoid control-loop instability during high speed turns [15]. It is thus not surprising to find little coherence [8, 9] between the yaw signal in a scenario where there is little or no non-saccadic yaw experienced and the response of HS cells. When more naturalistic conditions were used, with optic flow regenerated from outdoor flight paths, the rotational velocity was found to dominate the HS response for most of the flight [12], despite higher forward translation velocity, although this analysis could not account for the effect of head movements.

To confirm that our analysis method of using overall correlation did not bias our conclusion we also performed coherence analysis of the response of male HSNs to the movie. Again, we found high coherence between the yaw signal and the response over a large range of frequencies, but low coherence between the forward translation velocity and the response (Supplementary Figure 2.3A).

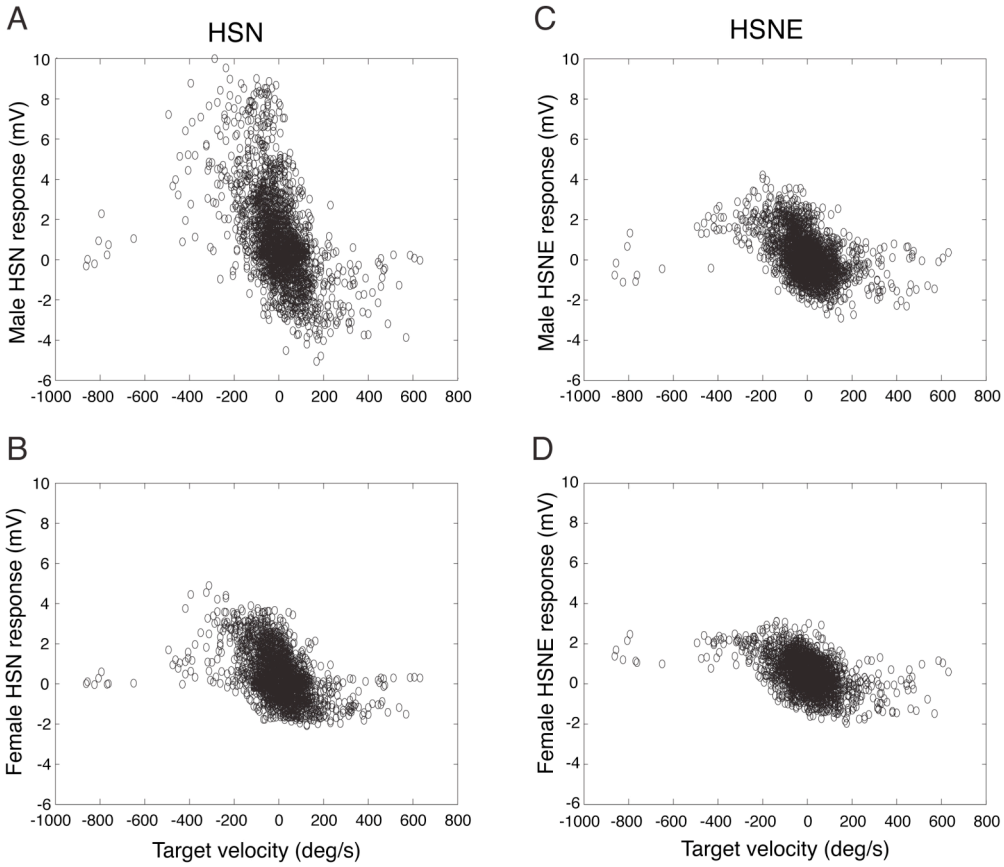

Supplemental figure 2.4 Response of HS neurons to target motion

A) The response of a single male HSN as a function of target velocity. The target was moving across a mean luminance background in the fronto-dorsal visual field in a 'saccadic' manner (Figure 2.4F). The data is plotted assuming a delay of 15 ms (i.e. 3 frames) at a sample rate of 200 Hz (the refresh rate of our monitor). B) The response of a female HSN as a function of target velocity. C) The response of a male HSNE. D) The response of a female HSNE. For each panel we show the response of the single neuron with the highest correlation to target velocity (Figure 2.4H).

An additional sex-specific behavior in hoverflies (as implied by their common name) is the near-stationary hovering flight of males whilst awaiting the approach of conspecifics and the subsequent initiation of pursuit flights and courtship [16]. Stationary hovering has the advantage of facilitating detection of moving features against complex backgrounds, whilst still permitting very rapid responses to incoming targets without the need to become airborne [17]. During stationary hovering in front of textured foliage, all of the HS neurons could generate useful responses to any (undesired) yaw, aiding this 'gaze' stabilization. The frontal receptive field of HSN, however, is also directed towards the part of the world where sideward slip would be best detected. With the higher resolution and very high contrast sensitivity provided by the optics of this visual region [14], this neuron is particularly well suited to detection of the very low angular side-slip velocities that would be generated by more distant image features.

During conspecific pursuits both the pursuer and its target frequently make sharp turns [13] and during these one might expect the optomotor response to be suppressed, perhaps by a re-afferent motor command generated by the target detection pathways [18]. An interesting possibility suggested by the unique male HSN, whose small receptive field would allow for less target position ambiguity, is that such suppression may not be required when targets are pursued against the sky. In this respect it is interesting to note the strong correlation between target velocity and the response seen in a single male HSN, compared to the responses of the other cells (Supplementary Figure 2.4). Our data certainly support the possibility that the signal from the same control system that normally generates syn-directional torque responses to yaw would contribute to centring of the target on the frontal fields when tracked against a uniform background. This remarkable receptive field could thus be an adaptation appropriate for optic flow analysis under several different flight modes of the hoverfly.

2.8 Supplemental References

1. Hausen, K. (1982). Motion sensitive interneurons in the optomotor system of the fly. I. The horizontal cells: structure and signals. Biol Cybern *45*, 143-156.

2. Hausen, K. (1982). Motion sensitive interneurons in the optomotor system of the fly. II. The horizontal cells: receptive field organization and response characteristics. Biol Cybern *46*, 67-79.

3. Krapp, H.G., Hengstenberg, R., and Egelhaaf, M. (2001). Binocular contributions to optic flow processing in the fly visual system. J Neurophysiol *85*, 724-734.

4. Hausen, K., and Egelhaaf, M. (1989). Neural mechanisms of visual course control in insects. In Facets of Vision, D.G. Stavenga and R.C. Hardie, eds. (Berlin Heidelberg: Springer Verlag), pp. 391-424.

5. Franz, M.O., and Krapp, H.G. (2000). Wide-field, motion-sensitive neurons and matched filters for optic flow fields. Biol Cybern *83*, 185-197.

6. Hausen, K. (1984). The lobula-complex of the fly: structure, function and significance in visual behavior. In Photoreception and vision in invertebrates, M. Ali, ed. (New York: Plenum), pp. 523-559.

7. Krapp, H.G., and Hengstenberg, R. (1996). Estimation of self-motion by optic flow processing in single visual interneurons. Nature *384*, 463-466.

8. Kern, R., van Hateren, J.H., Michaelis, C., Lindemann, J.P., and Egelhaaf, M. (2005). Function of a fly motion-sensitive neuron matches eye movements during free flight. PLoS Biol *3*, e171.

9. Karmeier, K., van Hateren, J.H., Kern, R., and Egelhaaf, M. (2006). Encoding of naturalistic optic flow by a population of blowfly motion-sensitive neurons. J Neurophysiol *96*, 1602-1614.

10. Schilstra, C., and van Hateren, J.H. (1999). Blowfly flight and optic flow. I. Thorax kinematics and flight dynamics. J Exp Biol *202*, 1481-1490.

11. van Hateren, J.H., and Schilstra, C. (1999). Blowfly flight and optic flow. II. Head movements during flight. J Exp Biol *202*, 1491-1500.

12. Boeddeker, N., Lindemann, J.P., Egelhaaf, M., and Zeil, J. (2005). Responses of blowfly motion-sensitive neurons to reconstructed optic flow along outdoor flight paths. J Comp Physiol A *191*, 1143-1155.

13. Collett, T.S., and Land, M.F. (1978). How hoverflies compute interception courses. J Comp Physiol A *125*, 191-204.

14. Straw, A.D., Warrant, E.J., and O'Carroll, D.C. (2006). A 'bright zone' in male hoverfly (*Eristalis tenax*) eyes and associated faster motion detection and increased contrast sensitivity. J Exp Biol *209*, 4339-4354.

15. Warzecha, A.-K., and Egelhaaf, M. (1996). Intrinsic properties of biological motion detectors prevent the optomotor control system from getting unstable. Phil Trans Roy Soc Lond B *351*, 1579-1591.

16. Fitzpatrick, S., and Wellington, W. (1983). Contrasts in the territorial behavior of 3 species of hoverflies (Diptera, Syrphidae). Can Entomol *115*, 559-566.

17. Wells, D.J., and Ellington, C.P. (1994). Beyond the vertebrates: achieving maximum power during flight in insects and hummingbirds. Adv Vet Sci Comp Med *38B*, 219-232.

18. Collett, T.S. (1980). Angular tracking and the optomotor response. An analysis of visual reflex interaction in a hoverfly. J Comp Physiol A *140*, 145-158.

Chapter 3:
Motion adaptation and the velocity coding of natural scenes

3.1 Context

In this paper, we investigate the response properties of HS neurons to a large range of natural scenes. We show that these neurons are able to provide robust estimates of image velocity across an enormous range of natural images. Using image manipulation techniques, we explore the likely mechanisms underlying the robust encoding of natural images.

Motion adaptation and the velocity coding of natural scenes

Paul Barnett, Karin Nordström and David C. O'Carroll*

Discipline of Physiology,

School of Molecular and Biomedical Science,

The University of Adelaide, SA 5005, Australia

** To whom correspondence should be addressed Email:*
paul.barnett@adelaide.edu.au

Keywords: Velocity estimation; natural images; motion adaptation; insect vision; lobula plate

Abbreviations: HS: Horizontal System; HSN: Horizontal system north; HSNE: Horizontal system north-equatorial EMD: Elementary Motion Detector; CSF: Contrast Scale Factor; C_{HS}: Neural contrast.

3.2 Summary

Background: It is generally assumed that many animals adopt visually guided behavior for which the accurate estimation of relative image velocity is required. Yet, despite decades of research into the neuronal mechanisms underlying motion detection, the most widely accepted motion-models, classical motion-energy or correlation based schemes, are still unable to account for the apparent ease with which animals are able to estimate image velocity. However, previous investigations of fly visual neurons using natural images revealed robust responses that deviate substantially from the predictions of classical motion-models and encode image velocity independent of other parameters, such as contrast. Recent investigations have revealed mechanisms that are likely to make, at the global scale, the estimation of behaviourally relevant parameters much easier.

Results: Using *in vivo* recordings, we reveal several activity dependent features of the neural response that reconcile the ability to accurately encode the velocity of natural images with the mechanisms underlying motion processing. Images that were initially weak neural drivers have long latencies, with responses continuing to increase in magnitude over several hundred milliseconds. Images that were initially strong neural drivers, reached peak responses more rapidly followed by significant reductions in response over longer time scales. Despite being different in sign and time course, these two activity dependent changes in response act as near-ideal normalisers for images that would otherwise produce highly variable response magnitudes. We further show that a subset of scenes, which contained man-made features, recruits these mechanisms differently despite having similar low-order statistics and hence producing similar responses from correlation-based motion detectors. Hence, the mechanisms underlying this response normalization appear to be matched to the higher order statistics of natural scenes.

3.3 Introduction

It is widely accepted that the Hassenstein-Reichardt Correlator [1] and mathematically equivalent motion energy models [e.g. 2] provide a robust explanation for motion detection in many animal species [for review see 3]. In essence, these models compute motion by correlation of luminance at two neighboring points in space, one delayed with respect to the other [1, 4]. Motion detectors of this type are inherently ambiguous estimators of velocity because they are sensitive to additional stimulus parameters, such as contrast and spatial frequency [5]. Alternative motion processing schemes have been proposed that redress this deficiency [3, 6], but to date the primary evidence and motivation for the implementation of these schemes has been some insects behavioral evidence for velocity estimation [7, 8 , 9, 10]. Specific tests of the predictions of alternative models are not supported by neurobiological evidence [11, 12]. Recent experiments, however, showed that insect tangential neurons involved in optic flow analysis code image velocity reliably when stimulated with natural images, but largely independent of the global contrast and spatial structure of the specific scene [13, 14]. This property, termed 'velocity constancy', enables these neurons to act as accurate velocity estimators to vastly different natural scenes over several decades of image velocity.

The fly tangential neurons used in these recent experiments are the same class that has been used for many years to provide evidence for the Hassentein-Reichardt model using simple stimuli [e.g. sinusoidal gratings, 3, 12]. Located in the third optic ganglion of the fly visual system, the tangential neurons respond to the direction of image motion [15, 16] and synapse with descending neurons that control flight responses [17, 18]. They receive input from arrays of retinotopically arranged elementary motion detectors (EMDs) of the Hassenstein-Reichardt correlator type [5, 19, 20]. Their responses have been shown to be sensitive to the spatial and temporal structure of a moving stimulus as well as its contrast [21]. Behavioral testing with sinusoidal stimuli are consistent with the physiological data and show that the visual system generates ambiguous estimates of velocity in both insects [11, 22] and humans [23, 24].

What additional neural processes might enable these neurons to encode velocity accurately when presented with natural images but not with simple stimuli? Natural images contain a rich blend of spatial structures and contrasts, with some second-order statistical predictability from one scene to the next [25-28]. In a modeling study, Dror et al. [29] showed that this predictability, combined with inclusion of additional non-linear filtering stages such as spatial bandpass filtering and static non-linear saturation, both inspired by observations from basic neurophysiology, reduced the variance in response of correlation-based EMDs when stimulated by natural scenes. Subsequent work [14] elaborated this approach further to include a form of dynamic motion gain reduction in motion detector inputs and non-linear spatial gain control on motion detector outputs, both inspired directly from experiments on fly horizontal system (HS) neurons [30-32]. Although these elaborated models for motion detection provide a certain degree of contrast invariance for natural scenes, none have been shown to match the invariance observed for the HS neurons in a recent experiment [13]. Furthermore, if the contrast of natural images is re-scaled artificially, HS neuron responses rescale in a manner more consistent with the predictions of the Hassenstein-Reichardt correlator, an observation not well captured by the above-mentioned model elaborations [13].

Here, we investigate the neural representation of 26 natural images, which contain an enormous range of natural contrasts and spatial structures. While this image set produces vastly variable responses from the elaborated Hassenstein-Reichardt models tested in earlier studies [14, 29], we reveal several activity dependent non-linear adaptive properties of HS neuron responses that can account for their ability to robustly encode image velocity.

3.4 Results

3.4.1 Accurate encoding of image velocity by HS neurons

In order to quantify image velocity tuning, we displayed natural images moving at a large range of velocities, whilst recording intracellularly from HS neurons in the lobula plate of the hoverfly. We used a protocol, which holds the neuron in a steady motion-adapted state with near-optimal velocity stimulation (100°/s) interleaved with short test pulses of a range of velocities. This protocol allowed us to obtain full velocity tuning curves for many images in a reasonable time frame. Figure 3.1A and 3.1B show the velocity tuning of two different HS neurons from a male and female fly to 16 images from a larger set of 26 panoramas, which includes 6 images from the set used in the earlier study of Straw et al. [13] (Supplemental Figure 3.1A, 3.1K, 3.1M, 3.1N, 3.1U, and 3.1X). To test the limits of the contrast invariant 'velocity constancy' mechanism, we deliberately included images that spanned a wide range of contrasts and textures (Supplementary Figure 3.1).

As observed by Straw et al. [13], HS neurons give responses that increase with image speed to an optimum of 249°/s in the male HSN, and 88°/s for the female HSNE before falling away at higher velocities, with a tightly clustered magnitude of response for the majority of images (Figure 3.1A and 3.1B). Although our image set clearly spans a range of contrasts by any measure, quantifying contrast in natural scenes is not trivial ([33]; Supplemental Data). As in other previous studies [13, 14] we therefore used an elaborated correlation model for motion detection in *Eristalis* HS neurons as a biologically relevant measure of image contrast, C_{HS} (Supplemental Data).

Considering that a 'perfect' correlation EMD ought to give a response that scales quadratically with contrast [29], the response variation we observe between images at any particular image speed is relatively small, e.g. 10.2±1.8 mV (mean ± S.D.) at optimum velocity of 249°/s for males (Figure 3.1A) and 9.9±1.2 mV (mean ± S.D.) at 88°/s for females (Figure 3.1B). Sparse images such as 'Rubble' and 'Field' with lower contrast (C_{HS} 0.14 and 0.12 respectively) than the lowest used in the study by Straw et al. [13] reveal the limits of the invariance mechanism, however. On every occasion we tested (n=5), the 'Field' image produced responses well below the other images, peaking at 6±0.3 mV (mean ± SEM) compared with peak responses of 10.3±0.3 mV (mean ± SEM) for the high contrast image 'Botanic' during the same recordings.

This result is consistent with a relatively simple explanation for the observation of invariance for 'typical' natural scenes by Straw et al. [13], that the contrast is generally high enough to recruit saturation mechanisms within the motion pathway, leading to a similarity in overall response. A key feature of our data argues against this simple explanation, however. Even if saturation limits responses at high contrasts it will not change the order of image responses thus, we should still see a clear correlation between the rank order of responses and image contrast. In Figure 3.1A and 3.1B we have used line-styles with dash length symbolizing the rank order of image contrasts, C_{HS} (shorter dashes = lower contrast; see Supplemental data). With the exception of the 'outlier' sparse images, however, there is little obvious relationship between contrast and neuron response. This is confirmed by data pooled from a larger set of recordings (n=5) for 25 images at a constant velocity of 45°/s (Figure 3.1C). Despite these stimuli producing a greater than 34-fold variation in our elaborated EMD model output (Supplemental data), HS neuron response remains relatively robust, with less than two-fold of variation and little dependence on C_{HS} ($r=0.35$, $p=0.084$, Pearson correlation). On three occasions we were able to record responses in the anti-preferred direction also, where we observed a much better correlation (data not shown, $r=-0.42$, $p=0.038$). However, the response range was still less than two-fold.

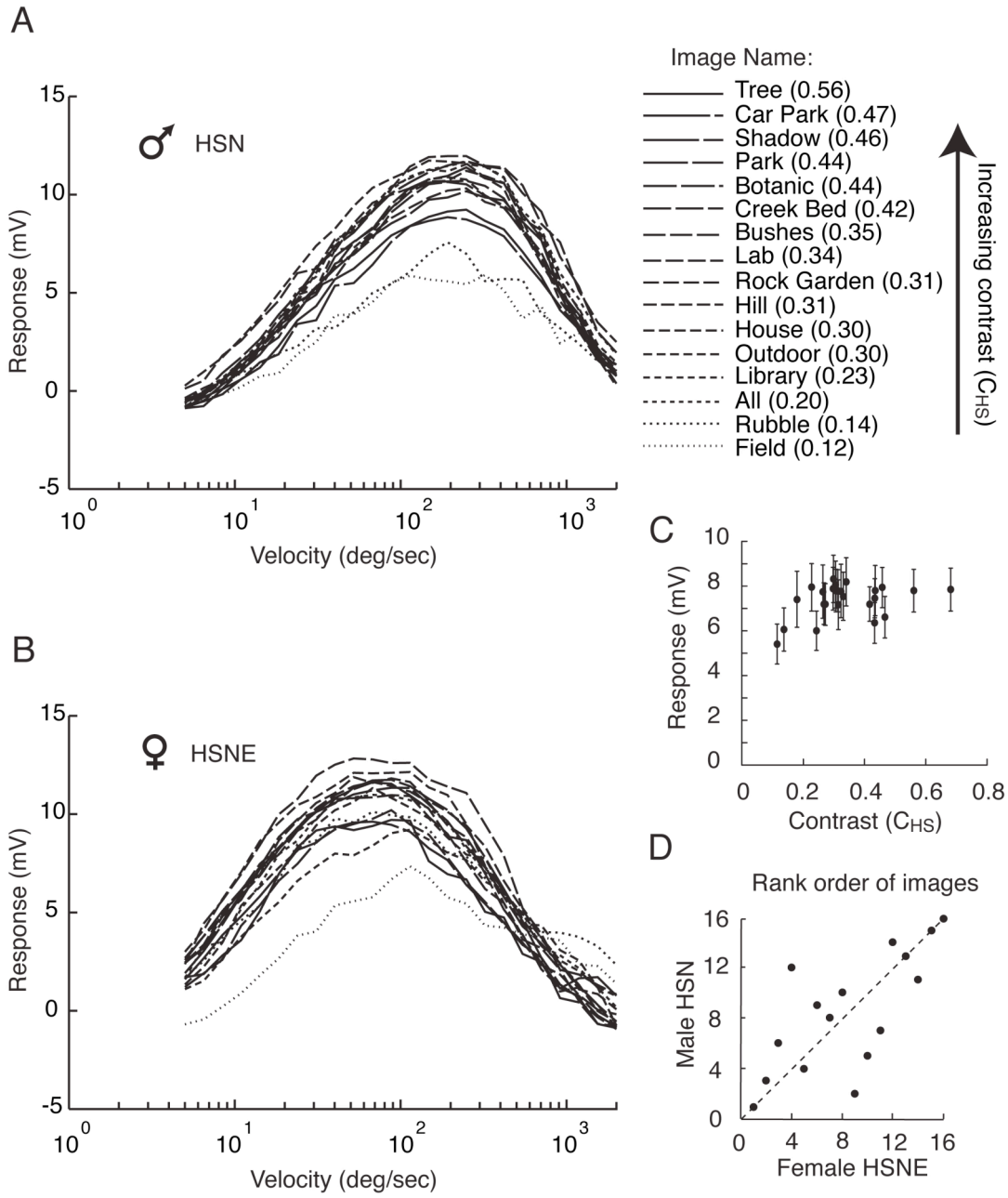
A
HSN
Response (mV)
Velocity (deg/sec)
Image Name:
Tree (0.56)
Car Park (0.47)
Shadow (0.46)
Park (0.44)
Botanic (0.44)
Creek Bed (0.42)
Bushes (0.35)
Lab (0.34)
Rock Garden (0.31)
Hill (0.31)
House (0.30)
Outdoor (0.30)
Library (0.23)
All (0.20)
Rubble (0.14)
Field (0.12)
Increasing contrast (CHS)
B
HSNE
Response (mV)
Velocity (deg/sec)
C
Response (mV)
Contrast (CHS)
D
Rank order of images
Male HSN
Female HSNE

Figure 3.1 Contrast insensitivity to natural images

A. Velocity response function of a male HSN (north) neuron to 16 panoramic images, including 1 image 'All', which is synthesized by averaging the amplitude and phase of all the images in the set. Data are the average of 8 trials with image start position offset by 45° on each occasion, thereby averaging the response over the whole 360° panorama. Neurons were held in the adapted state with 100°/s adapting velocity interleaved with 200ms test velocities pulses. The legend (top right) shows the image name followed by its corresponding contrast (C_{HS}). Line types are organized so that line density is determined by the rank order of C_{HS} (i.e. solid line type is the highest contrast and sparse dotted line is the lowest contrast). B. Similar data for a female HSNE (north-equatorial) neuron to the same set of images. C. Responses to 25 natural images plotted against contrast (C_{HS}). For each image, responses are averaged over one second after constant velocity stimulation (45°/s) for 3 seconds. Data shown are the mean ± SEM (N=5). D. Rank order comparisons of response amplitudes to individual images averaged across all velocities for the data shown in part A (ordinate) and B (abscissa) of this figure. Dashed line represents the line of unity (i.e. where points would lie if the two rank orders were identical).

The weak correlation between neuron response to most images and low order image statistics such as C_{HS} is unlikely to result from experimental variability, as our data reveal consistent trends in responses for specific images between the recordings. For example, Figure 3.1D shows a strong correlation in the rank order of image responses for the two recordings in Figure 3.1A and 3.1B (ρ=0.72, $p<0.01$, Spearman's rank correlation). Such a strong correlation is even more surprising given the substantial differences in receptive fields between HSN and HSNE neurons [34] and spatiotemporal tuning between sexes (as evident from Figure 3.1A and 3.1B) [35]. While individual images depart substantially from unity by several rank values (dotted line in Figure 3.1D), these are mostly from within the intermediate range of response levels, where the curves are tightly clustered and thus, small differences in response could equate to large changes in rank. Hence, while response magnitude is not easily explained by simple statistics (e.g. contrast), we can nevertheless conclude that there are specific features of the scenes that recruit consistent response levels in different neurons.

3.4.2 Saturation and artificial manipulation of contrast

Is the weaker response for the 'Field' image simply a result of it having unusually low global contrast (C_{HS} 0.17), bringing it out of the compliance range for whatever mechanisms may be responsible for apparent contrast invariance for the other images? If so, artificially increasing the contrast of this image ought to boost the response. To test this, we recorded responses for the 'Field' image and two other higher contrast images before and after artificially doubling image contrast. Figure 3.2A-C shows the full response tuning for a single male HSN neuron. Response clearly does not increase following the contrast manipulation and if anything is reduced for two of the images, a conclusion supported by recordings averaged for six neurons over the full range of velocities (Figure 3.2D-F).

While our manipulation had little effect on neuron response, it boosted model response by as much as 200% for the already high contrast 'Botanic' image (Figure 3.2D), showing that our images were not already dominated by saturated and under-saturated pixels. Although the contrast manipulation for the sparse 'Field' image, which contains a large amount of bright sky was slightly less effective, it still boosted model responses by more than 100% (Figure 3.2F) and yet the HS neuron was unaffected as for the other images. We therefore, cannot attribute the invariance in response to a simple mechanism of global response saturation for a system with high response gain.

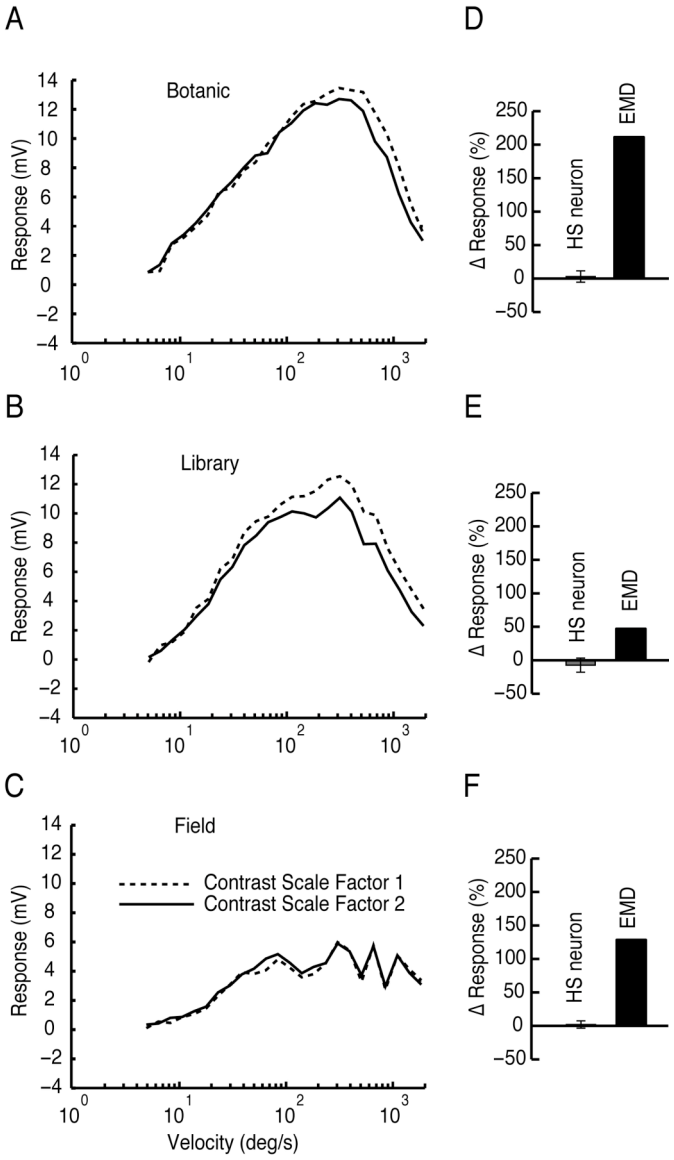

Figure 3.2 Increasing the global contrast does not increase the response

A-C. Velocity tuning curves of a male HSN (north) neuron to the 'Botanic', 'Library', and 'Field' images before (dashed line) and after (solid line) the image contrasts were artificially increased. Data are the average of 8 trials each with image start position offset by 45° on each occasion, thereby averaging the response over the whole 360° panorama. The neuron was held in the adapted state with a 100°/s adapting velocity interleaved with 200 ms test velocities. D-F. Bar graphs showing the percentage change in response averaged across all velocities for several HS neurons (mean ± SEM; N=6) and the elaborated EMD model, after artificially increasing the contrast of the 'Botanic' (D), 'Library' (E), and 'Field' (F) image.

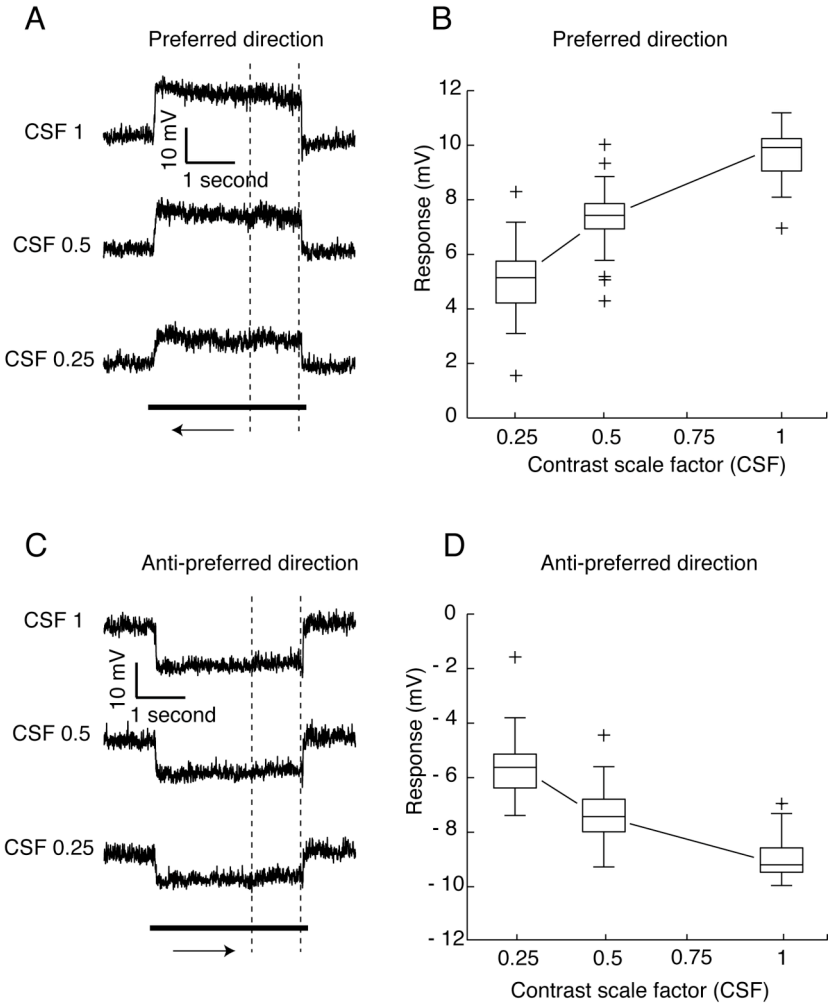

Figure 3.3 Artificial reductions in image contrast reduce overall response and increase variance.

A. Averaged raw responses from a male HSN neuron to the 'Botanic' image in the preferred direction at three contrast scale factors, CSF 1 (unscaled), CSF 0.5 (50% original contrast), CSF 0.25 (25% original image contrast). Vertical dashed lines show the 1 second analysis time window, after velocity stimulation at 45°/s for 2 seconds. B. Box plots show the spread of responses generated by 26 natural images for the three contrast scale factors mentioned above. For each image, responses are averaged over a minimum of 4 start trials with the image start position offset by 90° on each occasion, thereby averaging the response over the whole 360° panorama (N=1). C-D. Show identical data for the same neuron in the anti-preferred direction. Crosses (+) indicate outlier images (see Experimental procedures).

While the experiments in Figure 3.1 and Figure 3.2 seem to preclude an obvious role for global response saturation, local non-linearity, e.g. saturation at an earlier stage in visual processing, remains a possible contributing factor to the observed image contrast invariant responses. To test this, we artificially *reduced* image contrast to 50% or 25% of the original level in order to release the system from any saturating influences. Figure 3.3 shows results for a male HSN (horizontal system north) neuron to which we displayed 26 different images at 45°/s for 3 seconds, averaged across four initial start presentations of the image. We chose the relatively low speed of 45°/s as this produces responses approximately 50% of the maximal value for male HSN neurons (see Figure 3.1A) and so is less likely to recruit strong global saturating non-linearities (i.e. in the HS neuron itself). Consistent with the results of similar rescaling by [13], reducing image contrast produced a significant but non-linear reduction in response (Figure 3.3).

Importantly, as contrast was reduced, image-to-image variance increased in absolute terms by more than 40% for either direction of motion, despite the weaker responses (Figure 3.3B and 3.3D and Table 3.1). Does the increase in response variability for re-scaled images reflect a gradual release of response from saturation? If this were the case, we would expect an improvement in the correlation between the HS neuron response and underlying image contrast for contrast-reduced images. Yet, rank orders of contrast (C_{HS}) and neuron response were never well correlated for preferred direction motion stimuli even when we include the 'outlier' sparse images described (Table 3.1). Interestingly, in the anti-preferred direction, we observe a correlation for unscaled images ($p<0.02$) but as we rescale the image contrast, this correlation becomes weaker (Table 3.1). When we compared the rank order of neuron responses *between* the preferred and anti-preferred direction at each contrast there was a very strong correlation on every occasion ($\rho>0.52$; $p<0.01$). Hence, variability within our data cannot explain the lack of correlation between contrast and neuron response at any individual contrast scale factor.

Direction of motion	Contrast scale factor	Spearman's rank correlation ρ	Standard deviation
Preferred	1	0.04	0.98
	0.5	0.05	1.31
	0.25	0.07	1.44
Anti-preferred	1	0.51 ($p<0.02$)	0.84
	0.5	0.25	1.02
	0.25	0.17	1.20

Table 3.1 Contrast rescaling of natural images.

Rank correlation (ρ) between neuron response and image contrast (C_{HS}) for 26 natural images at three contrast scale factors, 1 (unscaled), 0.5 (50% original contrast), 0.25 (25% original image contrast) for the data shown in Figure 3.3. Standard deviation shows the image-to-image variance for each scale factor.

3.4.3 Motion adaptation reduces response variance across the image set

So far, our analysis considers HS neuron responses under strongly motion-adapted conditions. Might motion adaptation itself contribute to the consistency in velocity coding by HS neurons? Figure 3.4 shows responses to the same three images as used in Figure 3.2 ('Botanic', 'Library' and 'Field', Supplementary Figure 3.2F, 3.1W, and 3.1Z) representing the upper, middle and lower ranges of image contrast (C_{HS}). The time-course of HS response to these three images differs substantially. The higher contrast images give responses that reach a peak value within the first 200 ms but then decline steadily over time, presumably reflecting the influence of motion adaptation. Very low contrast images roll-on much more slowly though, reaching a peak after 400 ms followed by little or no subsequent decrease (Figure 3.4C and 3.4D). Similar effects are observed for both directions of motion, except that at the cessation of motion, preferred direction responses are followed by an antagonistic after-potential. This motion after-effect has a magnitude that is response dependent, as observed in previous work [31, 36] and so is more evident for the higher contrast images (Figure 3.4A and 3.4B).

Our stimulus avoids neural after-image effects [37, 38] by adapting the neurons to a blank screen before presenting motion of the natural images. Unfortunately, this sudden stimulus onset and offset evokes a direction-independent depolarizing transient similar to those previously observed for sinusoidal grating stimuli [39], complicating the analysis of very early response windows and making it difficult to evaluate truly unadapted responses. Because response transients have the same sign and similar magnitude independent of the direction of image motion, subtracting the anti-preferred direction responses from the preferred effectively removes their influence [see 39]. Figure 3.4C shows the result of such an analysis of the first 500 ms of our data, confirming the substantive difference in initial response time course for different natural images. Comparison of the initial and final response levels reveals a significant increase for the 'Field' image, but a significant decrease for the 'Library' and 'Botanic' images (Figure 3.4D).

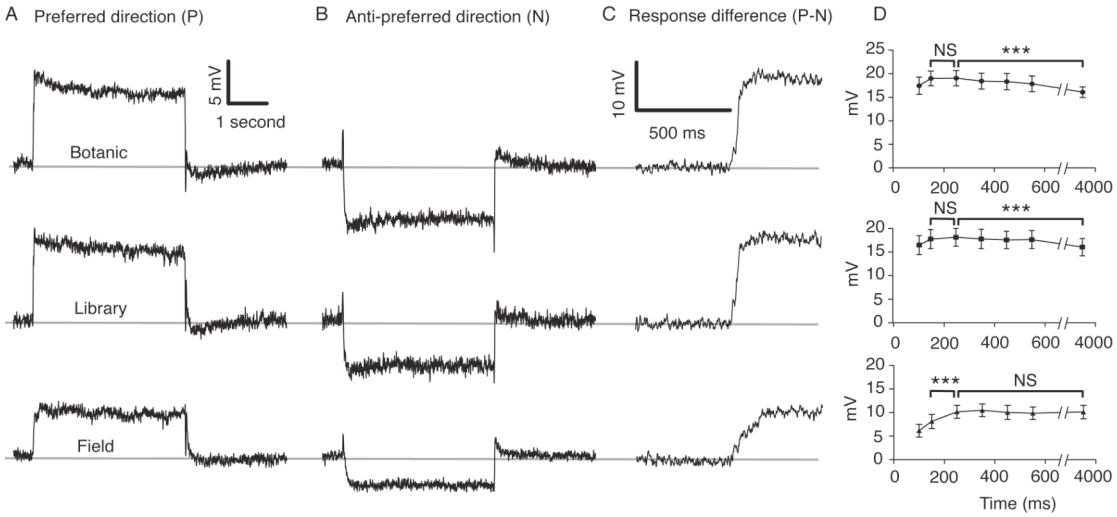

Figure 3.4 Response time course varies for different images

A. Averaged response for 'Botanic', 'Library', and 'Field' image (from top to bottom) rotated in the preferred direction at 45°/s for 4 seconds (N=3). Images were averaged over a minimum of four trials each with image start position offset by 90°, thereby averaging the response over the whole 360° panorama. B. As for A, but in the anti-preferred direction. C. First 1 second of the response after subtracting the anti-preferred direction from the preferred direction data, and thus eliminating the influence of non-directional (flicker) response components. D. Data from part C averaged over 100 ms time windows (x-axis shows the centre of each time window) commencing 50 ms after the onset of stimulus motion. Significance of differences was determined by repeated measures ANOVA and Bonferroni post hoc test for selected pairs, with *** denoting $p<0.001$ and NS: not significant.

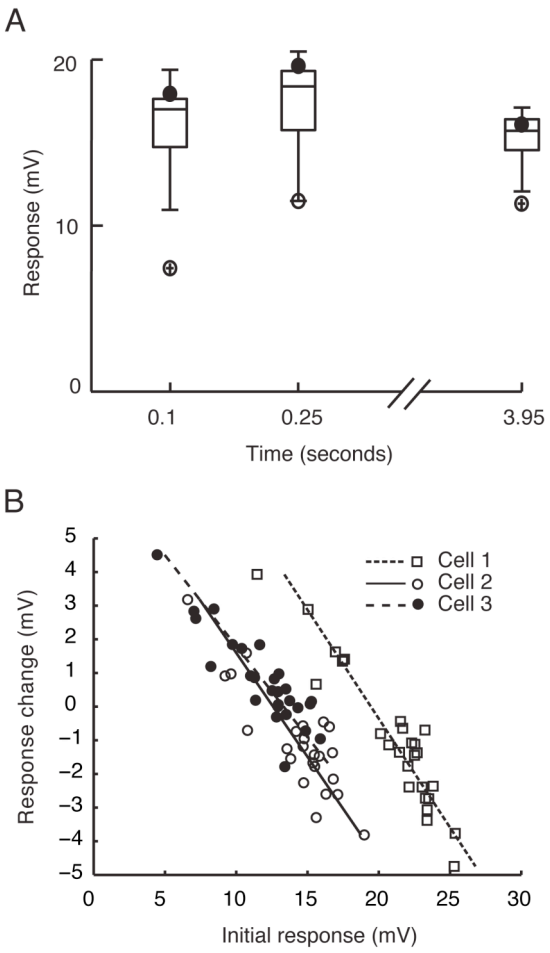
A
20
10
0
Response (mV)
0.1
0.25
3.95
Time (seconds)
B
5
4
3
2
1
0
−1
−2
−3
−4
−5
Response change (mV)
0
5
10
15
20
25
30
Initial response (mV)
Cell 1
Cell 2
Cell 3

Figure 3.5 Adaptation is dependent upon initial response and reduces variability across the image set.

A. Box plots show the spread of responses generated by 25 natural images at three time points after the onset of image motion: an early (unadapted) time window, 50-150 ms, an intermediate time window, 200-300 ms, and a late (adapted) time window, last 100 ms of stimulus. Responses were averaged across 100 ms time windows (centered on the abscissa). Data shown are for the preferred (see Supplementary Figure 3.5A) minus anti-preferred direction (see Supplementary Figure 3.5B) responses (N=3). Crosses (+) show outlier responses. Superimposed open circles show the position of the low contrast 'Field' image and closed circles show the position of the high contrast 'Botanic' image. B. Response change (ordinate), determined by subtracting the averaged response from 50-150 ms after the onset of image motion (initial response) from the averaged response to the last 100 ms of image motion (adapted response), plotted against the initial response (50-150 ms after the onset of image motion). The data for three neurons is indicated with different symbols. Lines show linear regression through data for each individual neuron. Cell 1 and Cell 3 include data for all 26 images; Cell 2 includes data for 25 images. Data shown are for anti-preferred direction (see Supplementary Figure 3.6B) subtracted from preferred direction (see Supplementary Figure 3.6A) to eliminate the influence of non-directional response transients. Data for each image was averaged over a minimum of 4 trials each with image start position offset by 90°, thereby averaging the response over the entire 360° panorama.

Figure 3.5A shows box and whisker plots summarizing the distributions of responses to 25 images at different time points. In the earliest parts of the response these distributions are very broad. Overall spread of image responses is substantially compressed following adaptation, however. The inter-quartile range is 51% smaller for preferred, 37% smaller for anti-preferred (Supplementary Figure 3.4A and 3.4B respectively), and 64% smaller following adaptation for the condition in which the anti-preferred direction was subtracted away from the preferred direction (Figure 3.5A).

Our analysis of an intermediate time-point (50-150ms) shows that the median response actually increases over the first 300 ms, and is associated with some reduction in overall response spread (Figure 3.5A, Supplementary Figure 3.4). Images that produced the weakest responses in the early time window showed the most prominent increases, such as the 'Field' image (open circles in Figures 3.5A). Could this effect be associated with an early onset *increase* in the contrast gain of the system? To investigate this we used a test-adapt-test protocol to measure the contrast gain before and after a brief adapting presentation (200 ms) with the 'Field' image (Supplementary Figure 3.6). Our data revealed that even after such a brief adaptation stimulus, contrast gain was slightly reduced; not increased (Supplementary Figure 3.6). Figure 3.5B shows a comparison between the initial response level and the magnitude of the response change over the 4-second stimulus duration for three neurons. This confirms the trends described above where initially weak responses are subsequently boosted and initially strong responses tend to decline over time Figure 3.5B. When we subtract preferred and anti-preferred responses to minimize response transients, we get a clear linear relationship for each neuron (r^2=0.78, 0.88, 0.74, for cells 1, 2, and 3 respectively; Figure 3.5B). Although the relationship between these parameters appears linear for individual recordings, the operating range differs substantially between recordings, most likely due to differences in the quality of neuronal recordings between experiments that influence absolute response magnitude, and subtle differences in response onset transients. Interestingly, the slope of the relationship between initial response and response change is relatively steep (-0.42, -0.57, and -0.46, for cells 1, 2, and 3 respectively; see Figure 3.5B) so

these opposite direction effects could potentially contribute to strong normalization of the response for different images.

We conclude that the changes observed over the response time-course contribute substantially to contrast invariance, at least at the velocity used for this analysis. These effects appear to be due to two separable components: 1. A slow initial roll-on or build-up in response within the first 500 ms for initially weak stimuli, which is not attributable to a change in contrast gain. 2. And a progressive response reduction for initially stronger stimuli, similar to that characterized for sinusoidal stimuli.

3.4.4 Natural scenes and urban scenes rescale differently

Although none of our images are truly natural in the sense that they are not from completely unspoiled natural fly habitats, our image set nevertheless contained a diverse range of scenes from bushland and park settings to urban, man-made, habitats such as car parks and indoor scenes. While similar in terms of second-order statistics [25, 26, 40], a fractal-based analysis of the same set of images used in the present study suggests higher order statistical differences between images composed primarily of foliage and those that contain man-made structures such as buildings or walls [41]. To investigate the effects of feature distribution we therefore separated a group of 'urban' scenes, which contained at least one major man-made structure, such as a building or a wall, from the remaining group of predominantly 'natural' scenes. These two image subsets do not differ in global contrast (C_{HS} of 0.517 ± 0.053 for the natural group, n=16, versus 0.461 ± 0.040 for the urban group, n=10, p=0.46, unpaired t-test).

When displayed at their normal contrast (i.e. have a contrast scale factor of 1), the two image categories produced similar responses (Figure 3.6A and 3.6B). However, when rescaled to lower contrasts, responses to the two image categories clearly separate, with natural images decreasing in response more than the urban images for either direction of motion (Figure 3.6A and 3.6B). Figures 3.6A and 3.6B show that after contrast rescaling to 25% of the original level, response to the urban images increased relative to the mean for all images, while the response to natural images decreased. Similarly, when we plot the change in rank order of response amplitudes

(i.e. the change in rank for individual images across the whole set) we see a similar shift, with urban images tending to be more highly ranked after contrast reduction (insets in Figure 3.6A and 3.6B). These average trends were not observed for every image in each category, but nevertheless suggest that the hard edges and other structural features typical of man-made scenes are inherently more potent drivers for motion detector responses in a manner not predicted by energy-based motion detector models and hence our C_{HS} values. Consequently, at low contrasts such images produce stronger responses than the natural group. This cannot be easily explained by simple spatial high-pass filtering (e.g. lateral inhibition) on the inputs, however, as responses converge at higher contrasts. Unless, as contrast increases, these images become more effective in recruiting the mechanisms (e.g. adaptation) that drive response invariance for 'normal' contrast images.

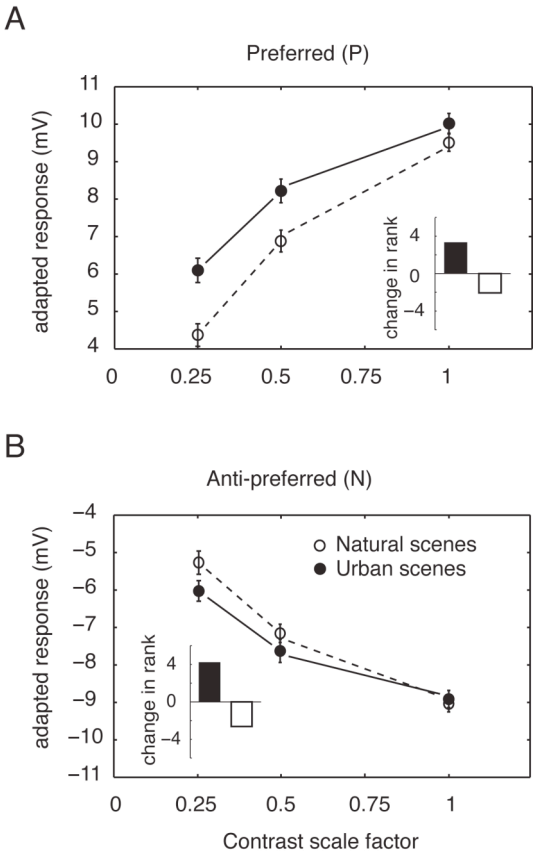

Figure 3.6 Natural and Urban scenes rescale differently with artificial reductions in image contrast

A. The effect of artificially reducing image contrasts on the response of an individual neuron to 'natural' (dashed line, open symbol) and 'urban' images (solid line, closed symbol) in the preferred direction. B. As for A, but in the anti-preferred direction. Insets show the change in average response rank for natural and urban images after contrast rescaling to 25% their original contrast (contrast scale factor 0.25), where responses to all the images are ranked 1-26 with 26 being the largest response.

3.5 Discussion

3.5.1 Velocity constancy and natural image coding

In this study, we use panoramic natural images rotated about the yaw axis to investigate velocity encoding. This type of stimuli is unlikely to represent the kind of flow fields, which a fly might experience during free flight in the natural environment, though. While recording neural activity under truly natural conditions is an ideal goal, to date many technical limitations have prevented this from happening for the fly visual system. Not only does the capture of truly natural optic flow from freely flying flies present a hurdle but, reproducing this optic flow accurately, i.e. with high spatio-temporal resolution at full luminance/color on a panoramic display, is not possible with current technology.

Nevertheless, many recent studies have revealed the importance of the dynamical properties of behaviourally generated optic flow on neuronal responses [42-46]. Some studies have sought to investigate how neurons encode naturalistic stimuli by reconstructing optic flow fields based on the body position of freely flying animals [46]. Although for technical reasons, the head movements of these animals were not resolvable, and thus the real optic flow experienced was not able to be reconstructed. Other studies have used optic flow reconstructed from flight paths of flies flying in confined spaces in order to resolve such head movements. These reconstructed flow fields implicated a role for HS neurons in the encoding of translational optic flow [43, 44], although the flight arena was very small 40 x 40 x 40 cm, and thus altered the animals natural flight behavior.

3.5.2 Saturation and the coding of natural images

Dror et al. [29] showed that the inclusion of saturation in basic correlation type motion detection models mitigated some of the contrast dependence and hence variance produced for different natural images. Other studies, confirmed that the inclusion of saturation to both early visual processing and the motion correlator, on the output of individual EMDs, could reduce the contrast dependence of such a model [14, 30]. However, while there is substantive evidence for non-linear spatial

summation within the HS neuron [i.e. on local motion detector outputs 32, 47], heavy response compression at this stage is inherently in conflict with the requirements of velocity sensitivity – excessive saturation 'flattens' the velocity/response function. Rivera-Alvidrez and Higgins [48] showed that in order to match HS neuron contrast response functions accurately, more moderate saturation is likely on the inputs to the motion processing pathway. Regardless of the location and magnitude, moderate saturation and other compressive non-linearities should still lead to a predictable rank order in responses with respect to global image contrast. We have shown that responses to natural images are poorly predicted by measures of global contrast to which such detectors should be sensitive (Figure 3.1, Table 3.1). Furthermore, our artificial contrast manipulation reveals effects poorly explained by obvious elaborations to basic correlator mechanisms, such as response saturation. We conclude that even the elaborated EMD models accounting for compressive non-linearities are poor predictors of the response magnitudes to different natural images.

3.5.3 Adaptation and its role in natural image coding

Motion adaptation is a prominent feature of the response properties of fly motion sensitive neurons. A great deal of research has focused on quantifying the effect of experimenter-designed stimuli on motion adaptation, e.g. enhanced detection and coding of direction and speed changes [49, 50], relief from saturation due to inherently high contrast gain [31], or adaptive rescaling match stimulus statistics [51, 52]. We show that activity-dependent adaptive components contribute to response invariance in the velocity tuning for natural images, by causing a greater reduction in response for images that recruit initially strong responses and boosting responses that are initially weak (Figures 3.4, 3.5, S3.4, and S3.5). These changes lead to substantially decreased variance in response once images have been in motion for several seconds.

Decreases in the response to initially potent images are consistent with the gain reduction mechanism observed for fly motion sensitive neurons obtained using high contrast sinusoidal patterns [31, 53-55]. The adaptation to images that produce a weak initial response is more problematic to explain, however. We observe a small increase in response to such stimuli over the first 500 ms of stimulation (Figure 3.4).

Yet we show that the initial stimulus period (200 ms) actually leads to a small decrease in contrast gain (Figure S3.6). Hence, this response increase cannot be attributed to increased contrast gain. A slow 'roll-on' for images of low contrast has previously been reported using sinusoidal images [55, 56]. In this earlier work, it was interpreted as a stimulus-dependent effect on response latency. However, response time course ought to depend primarily on the delay mechanism inherent to the motion correlation mechanism [57, 58]. Since the underlying optimum of fly tangential neurons is at relatively high temporal frequencies even in the unadapted state [55, 58, 59], latencies of more than a few tens of milliseconds are difficult to account for by the underlying properties of motion detection. Interestingly, many of the conditions under which Warzecha et al. [56] observed slow response onsets to sinusoidal patterns were for stimuli which were weak initial drivers of neuron responses (e.g. low contrast). Similar results were obtained for monkey cortical neurons [60], in which response latency has been shown to reflect stimulus strength. Hence, previous work is consistent with our observation that 'sparse' natural scenes such as the 'Field' image produced slow initial response onsets, whilst scenes that are more detailed produce rapid onsets.

One mechanism that Warzecha et al. [56] proposed to explain slow response onset was increased dendritic resistance at multiple levels in the motion pathway when input synaptic activation was weak, leading to a cascade of activity-dependent membrane time constants, but primarily operating at peripheral levels. While our data do not refute such a mechanism, they reveal a surprising consequence of it: the magnitude of response roll-on to the 'steady state' level after a few hundred milliseconds scales linearly with initial response level (Figure 3.5, and S3.5). Moreover, the same linear trend is observed, but with opposite sign, once motion adaptation takes effect for images that produce initially stronger responses. Such a bi-directional and linear dependence of final response level on initial level is very strongly suggestive of an active normalization strategy. While the slope that we observe is less than 1, as might be expected for a 'perfect' activity-dependent normalization, this might simply reflect the difficulty inherent in assessing 'initial' response level of a motion sensitive neuron. To avoid after-image phenomena our stimuli were presented following adaptation to a blank screen and thus evoke a

direction-independent (i.e. flicker) response transient (e.g. Figure 3.4). To avoid these transients, our 'initial' response is evaluated between 50 and 150 ms after stimulus onset, so that response normalization may already have commenced by the time we are able to evaluate 'initial' response.

Although our data suggest that several components contribute to response normalization in a manner that depends on activity, we also show (Figure 3.1 and 3.2) that responses still reliably encode the velocity of the stimulus. Because intracellular recording durations are of limited duration, we focused our more detailed analyses (Figures 3.5, S3.4, and S3.5) on a single velocity, 45°/s, selected as it produces half-maximal responses. Individual tuning curves for different images appear consistent across the full velocity range, however (Figure 3.1), arguing against the normalization mechanism being as simple as an antagonistic activity-dependent adaptation. Further work is required to investigate the degree to which the normalization strategy revealed by our analysis extends to other parts of the velocity tuning range.

3.5.4 Higher order scene statistics – urban and natural scenes

Also arguing against a simple activity-dependent phenomenon as an explanation for 'velocity constancy', we found that scenes containing man-made features are stronger drivers for motion detector responses when re-scaled to low contrast (Figure 3.6). There are two possible explanations for this divergence. Despite their similarity in global contrast, the urban scenes could contain structures that are inherently more potent stimuli for the motion detectors, but recruit normalization, including motion adaptation, more strongly at high contrasts. The fact that the two image groups have similar contrast (C_{HS}) suggests that the insect motion-processing pathway must be sensitive to higher order scene statistics in a manner not predicted by our EMD model. An alternative explanation is that the similarity in response at higher contrast reflects the global similarity in contrast for the two image groups, but that the natural scenes may contain features that are distributed in a manner that more effectively recruit adaptation and other normalization mechanisms, persisting to lower rescaled contrasts. The features we used to classify scenes as 'urban' include walls, window frames, buildings and other dominant man-made structures that are generally

characterized by sharp, vertically orientated edges followed by areas of little contrast. It is possible that the upwards shift in rank order for responses to contrast-rescaled urban images (Figure 3.6) results from the local manner in which motion adaptation is recruited [39, 49]. Local adaptation at the 'sparse' edges of large features, which may dominate the global contrast of such scenes, would have little effect on subsequent responses to the low contrast inner texture of many larger features that subsequently stimulate the same receptive field locations. Conversely, natural scenes dominated by foliage may have similar first order statistics, yet have features that are irregularly distributed so that local adaptation exerts a more potent influence on responses to subsequent features even when contrast of the images is reduced.

Regardless of which of these two alternatives turns out to explain our data, we have clearly shown evidence for additional properties poorly predicted by even elaborated models that have dominated our understanding of insect motion detection for more than 50 years. These mechanisms appear to normalize responses to an enormous variety of natural scenes and yet allow those responses to continue to reliably encode velocity via response magnitude. As such, our data have the potential to reconcile the longstanding problems with the correlation EMD model as an explanation for the remarkable abilities of many insects to exploit relevant velocity information for a variety of tasks, from landing on a stationary surface to visual odometry [10]. Since the case for a correlation-based operation lying at the core of these motion detectors is not in dispute [see 12] our findings highlight the need for further work to understand exactly how additional neural mechanisms such as motion adaptation operate both locally and globally, to bring about velocity constancy.

3.6 Experimental Procedures

3.6.1 Experiments

Wild caught drone flies, *Eristalis tenax,* were immobilized with wax. We performed sharp electrode intra-cellular recordings on Horizontal System (HS) neurons in the left lobula plate using aluminosilicate electrodes pulled on a Sutter Instruments P97 electrode puller with a 3 x 3 mm box filament. Electrodes filled with 2M KCl typically had tip resistances of 80-250 MΩ. Upon successful penetration, we identified each neuron on-line based on its receptive field properties, as recently described in detail by Nordström et al. [34].

3.6.2 Data acquisition and analysis

Data were digitized at 5 kHz using a 16-bit A/D converter (National Instruments, Austin Texas, United States) and analyzed off-line with Matlab (http://www.mathworks.com). In all experiments, membrane potential was normalized by subtracting the average resting membrane potential recorded for 1 second immediately prior to each trial. While HS neurons predominantly respond with graded shifts in membrane potential, which makes them ideal models to investigate the nature of the signal arriving at their synaptic inputs, the response is influenced by activity induced spikelets [61]. To reduce the influence of response non-linearities generated in the HS neuron itself from our analysis, such as these spikelets, we 'spike filtered' our data by removing spike-like events and replacing them with the local mean membrane potential [39].

We used Spearman's rank correlation (ρ) to determine the degree two sets of responses correlated. Linear regression fits and r^2 values were computed in Matlab. Two-way repeated-measures analysis of variance and Pearson correlation coefficient (r) were computed in Prism (Graphpad Software Inc. www.graphpad.com). All box plots were generated using the MatLab boxplot function, which identifies outliers as those data that lie beyond 1.5 times the inter-quartile range and are displayed as crosses (+). All data are presented as mean ± standard error of the mean (SEM) unless otherwise mentioned.

3.6.3 Image collection and display

We collected a large range of panoramic natural images from various field sites around South Australia. Scenes ranged from densely forested creek beds, to vast open hillsides, and to entirely man-made environments. Supplementary Figure 3.1 shows the full complement of 26 panoramic images used in this paper, including the six images also used in previous studies done by Shoemaker et al. and Straw et al. [13, 14]. Limitations in recording duration meant that not every image was displayed in all recordings, but where means are shown legends give the number of images presented. We collected images using a Nikon D-70 digital camera and panoramic tripod head. These images are available from Russell Brinkworth upon request (russell.brinkworth@adelaide.edu.au).

We displayed stimuli on a linearized, 8-bit, RGB CRT at 200 Hz refresh rate with mean luminance of 100 cd/m^2 using VisionEgg software (www.visionegg.org). The stimulus monitor was placed 14-15 cm in front of the animal and was centred approximately 20° degrees to the left of the flies mid-line at an elevation of 35°. It subtended approximately 100° x 75° of the fly's visual field. In Figures 3.1 and 3.2 full velocity tuning curves were collected using a rapid motion-adapted protocol developed by Straw et al. [13] whereby the neuron is held in a strongly motion adapted state with optimal velocity (100°/s) stimulation, which after 4 seconds is interleaved with 25 short test pulses (200 ms in duration) of monotonically increasing then decreasing velocities. This protocol produces qualitatively similar responses to displaying each velocity individually but is much quicker and thus allowed us to collect full velocity tuning curves for up to 16 images in individual recordings. For all other experiments (Figures 3.3-3.6 and S3.4-S3.6), images were rotated at 45°/s for a minimum of three seconds in both anti- and preferred directions.

Because natural images are non-homogenous in their distribution of features and contrasts, and because HS neurons have receptive fields of limited width, their responses are strongly influenced by local image properties. To ensure our recordings reflected the average image characteristics across the entire panorama, we

averaged responses over a minimum of 4 different image start phases. Data in Figure S3.6 was averaged over a minimum of 16 different start phases, as images were shown for only short periods.

3.6.4 Image manipulation

In several experiments, we used artificial manipulation of image contrast to probe the HS neurons' responses. We artificially reduced the contrasts of natural images by scaling the value for each pixel (I_{final}) about the mid-grey level of our display such that to $I_{final} = C(I_{image} - 0.5) + 0.5$, I_{image}, is a floating-point number from 0 to 1 representing luminance intensity in the original image and C is the contrast scaling factor [13]. In Figure 2 we increased image contrast in a similar fashion, but scaled luminance around mean image luminance, such that $I_{final} = C(I_{image} - mean(I_{image})) + mean(I_{image})$.

Acknowledgments

We would like to thank the management of the Adelaide, Mt Lofty, and Wittunga Botanic Gardens for allowing us to collect healthy experimental animals all year round and Dr Russell Brinkworth for useful discussions with interpreting the results and for providing us with most of the images used in this study. This work was funded by ARC (LP 0667744 and DP0880983).

3.7 References

1. Hassenstein, B., and Reichardt, W. (1956). Systemtheoretische Analyse Der Zeit, Reihenfolgen Und Vorzeichenauswertung Bei Der Bewegungsperzeption Des Russelkafers Chlorophanus. Naturforsch. *11*, 513-524.

2. Adelson, E.H., and Bergen, J.R. (1985). Spatiotemporal energy models for the perception of motion. J. Opt. Soc. Am. A *2*, 284-299.

3. Clifford, C.W.G., and Ibbotson, M.R. (2002). Fundamental mechanisms of visual motion detection: models, cells and functions. Prog. Neurobiol. *68*, 409-437.

4. Borst, A., and Egelhaaf, M. (1989). Principles of visual-motion detection. Trends Neurosci. *12*, 297-306.

5. Egelhaaf, M., Borst, A., and Reichardt, W. (1989). Computational structure of a biological motion-detecting system as revealed by local detector analysis in the fly's nervous-system. J. Opt. Soc. Am. A *6*, 1070-1087.

6. Srinivasan, M.V. (1990). Generalized gradient shemes for the measurement of 2-dimensional image motion. Biol. Cybern. *63*, 421-431.

7. David, C.T. (1982). Compensation for height in the control of ground speed by *Drosophila* in a new, barbers pole wind-tunnel. J. Comp. Physiol. A *147*, 485-493.

8. Esch, H.E., and Burns, J.E. (1996). Distance estimation by foraging honeybees. J. Exp. Biol. *199*, 155-162.

9. Ronacher, B., and Wehner, R. (1995). Desert ants *Cataglyphis-fortis* use self-induced optic flow to measure distances travelled. J. Comp. Physiol. A *177*, 21-27.

10. Srinivasan, M.V., Zhang, S.W., Lehrer, M., and Collett, T.S. (1996). Honeybee navigation en route to the goal: Visual flight control and odometry. J. Exp. Biol. *199*, 237-244.

11. Buchner, E. (1984). Behavioral analysis of spatial vision in insects. In Photoreception and vision in invertebrates, M.A. Ali, ed. (New York: Plenum), pp. 561-621.

12. Haag, J., Denk, W., and Borst, A. (2004). Fly motion vision is based on Reichardt detectors regardless of the signal-to-noise ratio. Proc. Natl. Acad. Sci. U. S. A. *101*, 16333-16338.

13. Straw, A.D., Rainsford, T., and O'Carroll, D.C. (2008). Contrast sensitivity of insect motion detectors to natural images. J. Vis. *8(3):32*, 1-9.

14. Shoemaker, P.A., O'Carroll, D.C., and Straw, A.D. (2005). Velocity constancy and models for wide-field visual motion detection in insects. Biol Cybern *93*, 275-287.

15. Hausen, K. (1982). Motion Sensitive Interneurons in the Optomotor System of the Fly .2. The Horizontal Cells - Receptive-Field Organization and Response Characteristics. Biol Cybern *46*, 67-79.

16. Hengstenberg, R. (1982). Common visual response properties of giant vertical cells in the lobula plate of the blowfly, *calliphora*. J. Comp Physiol. *149*, 179-193.

17. Strausfeld, N.J., and Bassemir, U.K. (1985a). Lobula plate and ocellar interneruons converge onto a cluster of decending neurons leading to the neck and leg motor neuropil in *Calliphora-erythrocephala.* Cell and Tissue Res. *240*, 617-640.

18. Strausfeld, N.J., and Bassemir, U.K. (1985b). The organization of giant horizontal-motion-sensitive neurons and their synaptic relationships in the lateral deutocerebrum of *Calliphora-erythrocephala* and *Musca-domestica*. Cell and Tissue Res. *242*, 531-550.

19. Franceschini, N., Riehle, A., and Le Nestour, A. (1989). Directionally selective motion detection by insect neurons. In Facets of vision, D.G. Stavenga and R.C. Hardie, eds. (Berlin Heidelberg New York: Springer), pp. 360-390.

20. Krapp, H.G., Hengstenberg, B., and Hengstenberg, R. (1998). Dendritic structure and receptive-field organization of optic flow processing interneurons in the fly. J. Neurophysiol. *79*, 1902-1917.

21. Dvorak, D., Srinivasan, M., and French, A. (1980). The contrast sensitivity of fly movement-detecting neurons. Vision Res. *20*, 397-407.

22. Duistermars, B.J., Chow, D.M., Condro, M., and Frye, M.A. (2007). The spatial, temporal and contrast properties of expansion and rotation flight optomotor responses in *Drosophila*. J. Exp. Biol. *219*, 3218-3227.

23. Boulton, J.C., and Baker, C.L. (1991). Motion detection is dependent on spatial-frequency not size. Vision Res. *31*, 77-&.

24. Stone, L.S., and Thompson, P. (1992). Human speed perception is contrast dependent. Vision Res. *32*, 1535-1549.

25. Tadmor, Y., and Tolhurst, D.J. (1993). Both the phase and amplitude spectrum may determine the appearance of natural images. Vision Res *33*, 141-145.

26. Tolhurst, D.J., Tadmor, Y., and Chao, T. (1992). Amplitude spectra of natural images. Ophthalmic Physiol. Opt. *12*, 229-232.

27. Dong, D.W., and Atick, J.J. (1995). Statistics of natural time-varying images. Network-Computation in Neural Systems *6*, 345-358.

28. Ruderman, D.L., and Bialek, W. (1994). Statistics of natural images - scaling in the woods. Physical Review Letters *73*, 814-817.

29. Dror, R.O., O'Carroll, D.C., and Laughlin, S.B. (2001). Accuracy of velocity estimation by Reichardt correlators. J. Opt. Soc. Am. A *18*, 241-252.

30. Borst, A., Egelhaaf, M., and Haag, J. (1995). Mechanisms of Dendritic Integration Underlying Gain-Control in Fly Motion-Sensitive Interneurons. J Compl Neurosci *2*, 5-18.

31. Harris, R.A., O'Carroll, D.C., and Laughlin, S.B. (2000). Contrast gain reduction in fly motion adaptation. Neuron *28*, 595-606.

32. Single, S., and Borst, A. (1998). Dendritic integration and its role in computing image velocity. Science *281*, 1848-1850.

33. Tadmor, Y., and Tolhurst, D.J. (2000). Calculating the contrasts that retinal ganglion cells and LGN neurones encounter in natural scenes. Vision Res *40*, 3145-3157.

34. Nordström, N., Barnett, P.D., Moyer de Miguel, I.M., Brinkworth, R.S.A., and O'Carroll, D.C. (2008). Sexual dimorphism in the hoverfly motion vision pathway. Curr Bio *18*, 661-667.

35. Straw, A.D., Warrant, E.J., and O'Carroll, D.C. (2006). A 'bright zone' in male hoverfly (*Eristalis tenax*) eyes and associated faster motion detection and increased contrast sensitivity. J. Exp. Biol. *209*, 4339-4354.

36. Kurtz, R., Durr, V., and Egelhaaf, M. (2000). Dendritic calcium accumulation associated with direction-selective adaptation in visual motion-sensitive neurons *in vivo*. J. Neurophysiol. *84*, 1914-1923.

37. Harris, R.A., and O'Carroll, D.C. (2002). Afterimages in fly motion vision. Vision Res. *42*, 1701-1714.

38. Maddess, T. (1986). Afterimage-like effects in the motion-sensitive neuron H1. Proc. R. Soc. Lond. B Biol. Sci. *228*, 433-459.

39. Nordstrom, K., and O'Carroll, D.C. (2009). The motion after-effect: local and global contributions to contrast sensitivity Proc. R. Soc. Lond. B Biol. Sci. *276*, 1545-1554.

40. Torralba, A., and Oliva, A. (2003). Statistics of natural image categories. Network-Comp. Neural *14*, 391-412.

41. Deng, J.D., Brinkworth, R.S.A., and O'Carroll, D.C. (2008). Assessing the naturalness of scenes: An approach using statistics of local features. Image

and Vision Computing New Zealand, 2008. 23rd International Conference 1-6.

42. van Hateren, J.H., Kern, R., Schwerdtfeger, G., and Egelhaaf, M. (2005). Function and coding in the blowfly H1 neuron during naturalistic optic flow. J Neurosci *25*, 4343-4352.

43. Kern, R., van Hateren, J.H., Michaelis, C., Lindemann, J.P., and Egelhaaf, M. (2005). Function of a fly motion-sensitive neuron matches eye movements during free flight. Plos Biol *3*, 1130-1138.

44. Kern, R., Petereit, C., and Egelhaaf, M. (2001). Neural processing of naturalistic optic flow. J Neurosci *21*, art. no.-RC139.

45. Egelhaaf, M., Grewe, J., Kern, R., and Warzecha, A.K. (2001). Outdoor performance of a motion-sensitive neuron in the blowfly. Vision Res *41*, 3627-3637.

46. Boeddeker, N., Lindemann, J.P., Egelhaaf, M., and Zeil, J. (2005). Responses of blowfly motion-sensitive neurons to reconstructed optic flow along outdoor flight paths. J. Comp. Physiol. A *191*, 1143-1155.

47. Haag, J., Egelhaaf, M., and Borst, A. (1992). Dendritic Integration of Motion Information in Visual Interneurons of the Blowfly. Neurosci Letters *140*, 173-176.

48. Rivera-Alvidrez, Z., and Higgins, C.M. (2005). Contrast saturation in a neuronally-based model of elementary motion detection. Neurocomputing *65*, 173-179.

49. Maddess, T., and Laughlin, S.B. (1985). Adaptation of the Motion-Sensitive Neuron H-1 Is Generated Locally and Governed by Contrast Frequency. Proc. R. Soc. Lond. B Biol. Sci. *225*, 251-275.

50. Neri, P., and Laughlin, S.B. (2005). Global versus local adaptation in fly motion-sensitive neurons. Proc. R. Soc. Lond. B Biol. Sci. *272*, 2243-2249.

51. Brenner, N., Bialek, W., and van Steveninck, R.D. (2000). Adaptive rescaling maximizes information transmission. Neuron *26*, 695-702.

52. Fairhall, A.L., Lewen, G.D., Bialek, W., and van Steveninck, R.R.D. (2001). Efficiency and ambiguity in an adaptive neural code. Nature *412*, 787-792.

53. Borst, A., Flanagin, V.L., and Sompolinsky, H. (2005). Adaptation without parameter change: Dynamic gain control in motion detection. Proc. Natl. Acad. Sci. U. S. A. *102*, 6172-6176.

54. Kurtz, R. (2007). Direction-selective adaptation in fly visual motion-sensitive neurons is generated by an intrinsic conductanc based mechanism. Neurosci *146*, 573-583.

55. Reisenman, C., Haag, J., and Borst, A. (2003). Adaptation of response transients in fly motion vision. I: Experiments. Vision Res *43*, 1293-1309.

56. Warzecha, A.K., and Egelhaaf, M. (2000). Response latency of a motion-sensitive neuron in the fly visual system: dependence on stimulus parameters and physiological conditions. Vision Res *40*, 2973-2983.

57. Borst, A., and Bahde, S. (1986). What kind of movement detector is triggering the landing response of the housefly. Biol Cybern *55*, 59-69.

58. Harris, R.A., O'Carroll, D.C., and Laughlin, S.B. (1999). Adaptation and the temporal delay filter of fly motion detectors. Vision Res *39*, 2603-2613.

59. O'Carroll, D.C., Laughlin, S.B., Bidwell, N.J., and Harris, R.A. (1997). Spatio-temporal properties of motion detectors matched to low image velocities in hovering insects. Vision Res *37*, 3427-3439.

60. Raiguel, S.E., Xiao, D.K., Marcar, V.L., and Orban, G.A. (1999). Response latency of macaque area MT/V5 neurons and its relationship to stimulus parameters. J Neurophysiol *82*, 1944-1956.

61. Hengstenberg, R. (1977). Spike response of "non-spiking" visual interneurone. Nature *270*, 338-340.

3.8 Supplemental Data

3.8.1 Measuring image contrast

Although our image set spans a large range of contrasts by any measure, quantifying contrast in natural scenes is not trivial. Tadmor and Tolhurst [1] argued that an appropriate contrast measure should account for the receptive field properties of the neurons, since many features may be outside the range encoded. As in other recent studies [2, 3] we adopted an elaborated correlation model for motion detection in *Eristalis* HS neurons to generate a biologically relevant measure of image contrast (Supplementary Figure 3.1A). Because models of this type inherently produce outputs, which are the square of image contrast, we take the square root of model output to get a measure of image contrast, C_{HS} (Supplementary Figure 3.1B). Spatial and temporal filtering matched to *Eristalis tenax* optics, early visual processing, and motion correlation ensures that C_{HS} reflects the spatio-temporal pass-band of the insect motion-sensitive neurons we record from (Supplementary Figure 3.1A).

The elaborated correlation model (Supplementary Figure 3.1A) had an interreceptor angle of $\Delta\phi$=1.1°, which is a physiologically realistic value for the separation of frontally orientated elementary motion detectors (EMDs) in *Eristalis*. Spatial pre-filtering was implemented as a two dimensional gaussian blur $\Delta\rho$=1.4°, which approximates the acceptance function of typical fly photoreceptors [4, 5]. Temporal pre-filtering was based on the work of James [6] who characterized the response of *Eristalis* large monopolar cells (LMCs) to continuously varying white noise stimuli. James showed that the response could be modelled as the difference of two log normals with different time constants. At high light levels he found typical values of t_p=10.3ms and σ=0.236 for the positive log normal and t_p=15.6ms and σ=0.269 for the negative log normal, where t_p represents the time to peak of the curve and σ is a dimensionless parameter that determines the curves width [5, 7]. The delay was implemented as a first-order low-pass filter with a time constant, τ, of 31ms. Model output was taken as the mean steady state response to horizontal image motion at 45°/s to a panoramic array of EMDs.

We normalized model output by the response to a maximum contrast sine wave grating of optimal spatial and temporal frequency (Supplementary Figure 3.1B). As C_{HS} is the square root of model output, our analysis revealed that the image set used herein had a maximum C_{HS} of 0.68 and minimum C_{HS} of 0.12 ('Hamlin' and 'Field', Supplementary Figure 3.2A and 3.1Z respectively), which is a near six-fold range of contrast (Supplemental Figure 3.1B). Supplemental Figure 3.2 shows the full image set used in this study, with respective C_{HS} values.

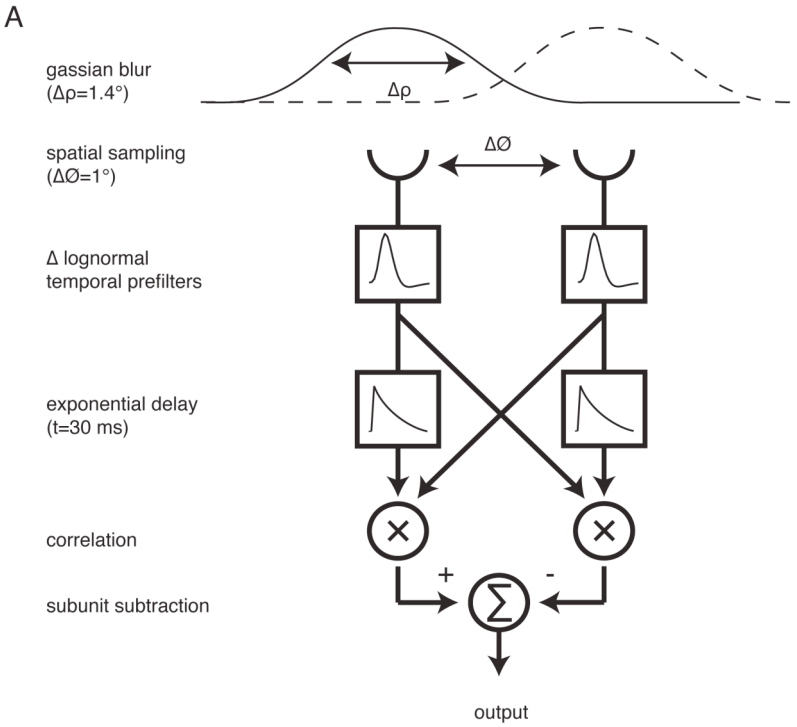
A
gassian blur
(Δρ=1.4°)
Δρ
spatial sampling
(ΔØ=1°)
ΔØ
Δ lognormal
temporal prefilters
exponential delay
(t=30 ms)
correlation
subunit subtraction
+
-
output

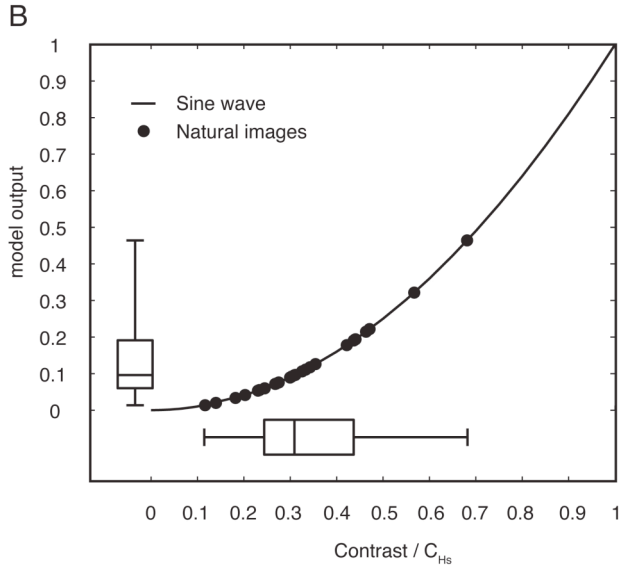
B
Sine wave
Natural images
model output
Contrast / C_Hs
0
0.1
0.2
0.3
0.4
0.5
0.6
0.7
0.8
0.9
1

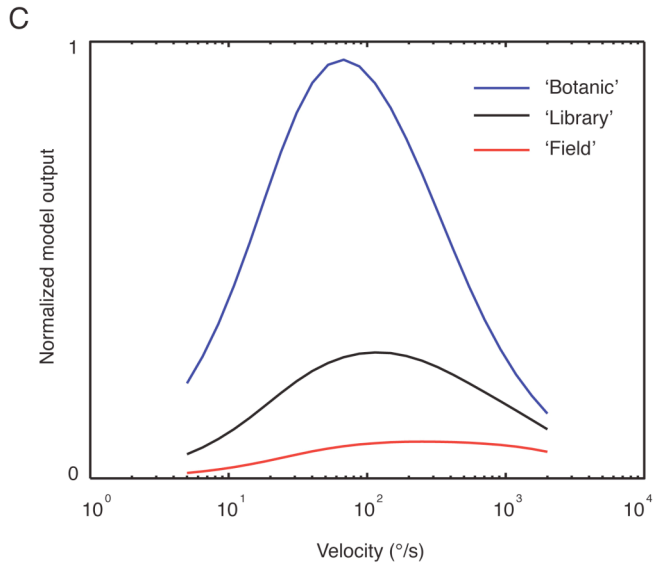
C
'Botanic'
'Library'
'Field'
Normalized model output
Velocity (°/s)
10^0
10^1
10^2
10^3
10^4

Supplementary Figure 3.1 Calculating natural image contrast

A. Shows a schematic of the elaborated Hassenstein – Reichardt correlator used to calculate image contrast. All model simulations were run on an array of EMDs. spanning the size of the panorama. S, spatial low-pass filters on the luminance input. T, temporal band-pass filtering. D, delay implemented as a first-order low-pass filter. As the correlator output represents the square of luminance contrast, we take the square root of the mean output across an entire image as a physiologically relevant measure of image contrast (C_{HS}). B. C_{HS} is normalized by output to maximum contrast sine wave grating of optimal spatial and temporal frequency. Superimposed red circles show C_{HS} and equivalent sine wave contrast of the 26 natural images used in the present study. Box plot inset reveals the spread of natural image C_{HS} relative to the sine wave contrast.

3.8.2 Image contrast manipulation

In Figure 3.2, we increase the contrast of three images to investigate the contribution of a simple mechanism of global saturation on neural response. Note that a nominal doubling of image contrast is not trivial given the limited dynamic range of our display, since some parts of the original image are likely to be already rendered at the maximum and minimum luminance that the display can produce *before* the contrast is increased. The artefacts introduced by this type of image manipulation will vary between images. For example, an image with large amounts of bright sky, close to maximal luminance, and deep shadow, close to minimum, may be barely altered by a nominal doubling of contrast once this 'clipping' by the display is accounted for, whilst a scene with many values close to mid luminance will be more strongly altered (Supplemental Figure S3.3). To ensure that our contrast manipulation was providing an effective boost to contrast after clipping, we therefore compared neural response with the output of the elaborated EMD model using the same re-scaled 8-bit images as in the experiment (Figure 3.2D-F).

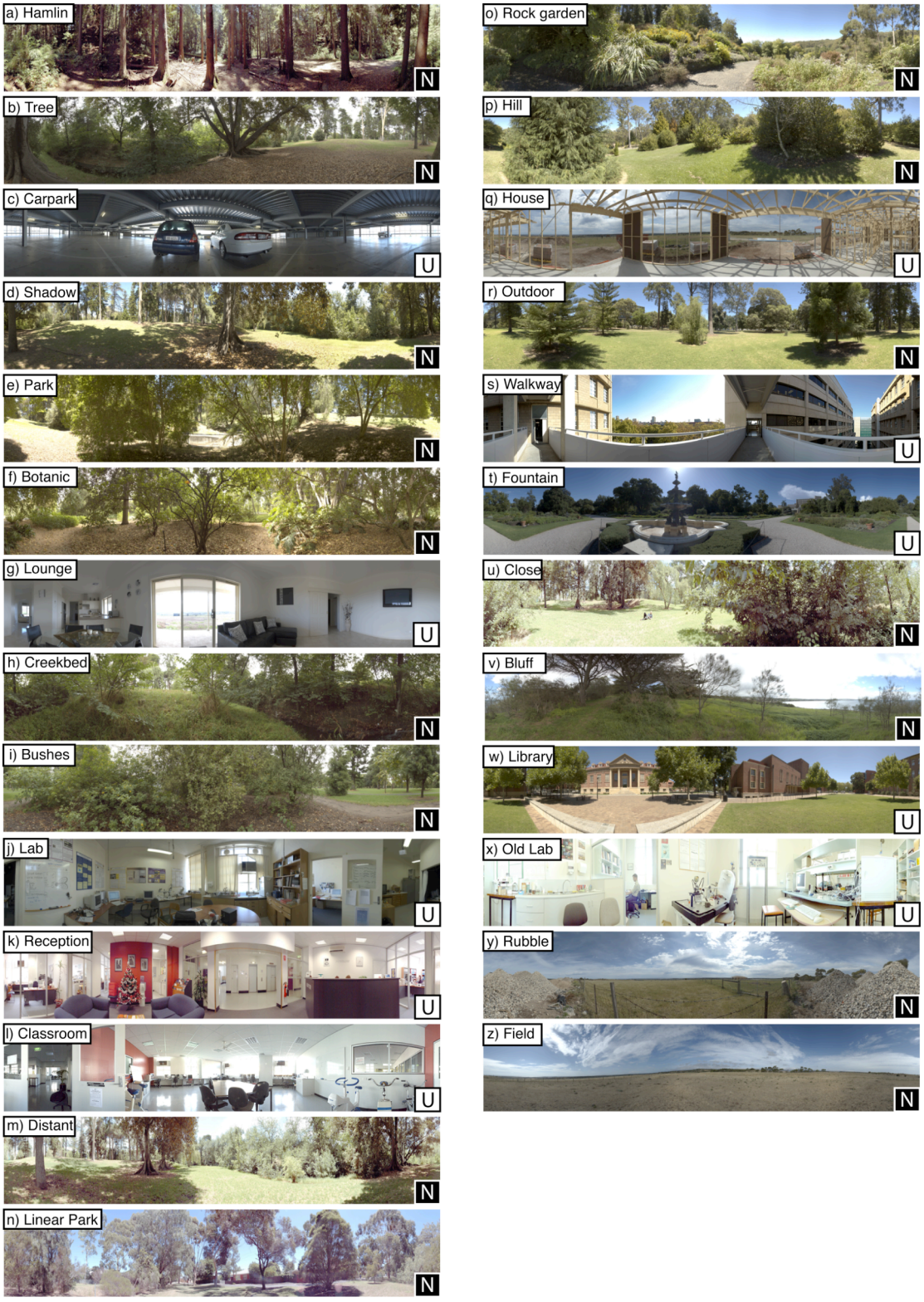
a) Hamlin
N
b) Tree
N
c) Carpark
U
d) Shadow
N
e) Park
N
f) Botanic
N
g) Lounge
U
h) Creekbed
N
i) Bushes
N
j) Lab
U
k) Reception
U
l) Classroom
U
m) Distant
N
n) Linear Park
N
o) Rock garden
N
p) Hill
N
q) House
U
r) Outdoor
N
s) Walkway
U
t) Fountain
U
u) Close
N
v) Bluff
N
w) Library
U
x) Old Lab
U
y) Rubble
N
z) Field
N

Supplementary Figure 3.2 Panoramic natural images

A-Z show the complement of panoramic images used in this study ordered from A, highest contrast, to Z, lowest contrast. This image set also includes six images (A, K, M, N, U, and X) used in an earlier study done by Straw et al. [14].

3.8.3 Motion adaptation and response normalization

Supplemental Figure 3.4 shows box and whisker plots summarizing the distribution of responses to 25 images at different time points for both the preferred and anti-preferred direction. In the earliest parts of the response these distributions are very broad, however, following adaptation the overall spread of responses is substantially compressed. The inter-quartile range is 51% smaller for preferred, 37% smaller for anti-preferred direction (Supplemental Figure 3.4), and 64% smaller for the condition in which the anti-preferred direction was subtracted away from the preferred direction following adaptation (Figure 3.5A).

While the initial response to a high contrast image in our set ('Botanic') is at the upper end of this distribution, after 4 seconds of preferred direction adaptation it actually lies below the median (filled circles in Supplemental Figure 3.4A). In the anti-preferred direction, responses to this same image are somewhat different, with a weaker initial response and less obvious response decrease (Supplemental Figure 3.4B). When the anti-preferred direction is subtracted away from the preferred direction though, this image occupies a similar response strength compared to the population across the analysis period (Figure 3.5C). Our analysis of an intermediate time-point (50-150ms) shows that the median response actually increases over the first 300 ms, and is associated with some reduction in overall response spread (Supplemental Figure 3.4; Figure 3.5). Images that produced the weakest responses in the early time window showed the most prominent increases, such as the 'Field' image (open circles in Supplemental Figure 3.4; and Figure 3.5A). Interestingly, despite the initially strong increase in response this image remains an outlier in

preferred direction but is boosted in response enough in the anti-preferred direction to join the group.

Supplemental Figure 3.5 and Figure 3.5B show a comparison between the initial response level and the magnitude of the response change over the 4-second stimulus duration for three neurons. This confirms the trends described above where initially weak responses are subsequently boosted for either preferred direction (Supplemental Figure 3.5A) or anti-preferred direction stimuli (Supplemental Figure 3.5B), while initially strong responses tend to decline over time. The relationship between these parameters appears linear for individual recordings, although the operating range differs, likely due to differences in the quality of neuronal recordings between experiments that influence absolute magnitude, and subtle differences in response onset transients. If we subtract preferred and anti-preferred responses to minimize the transients, we get a clear linear relationship for all the neurons (r^2=0.78, 0.88, 0.74, for cells 1, 2, and 3 respectively; Figure 3.5B).

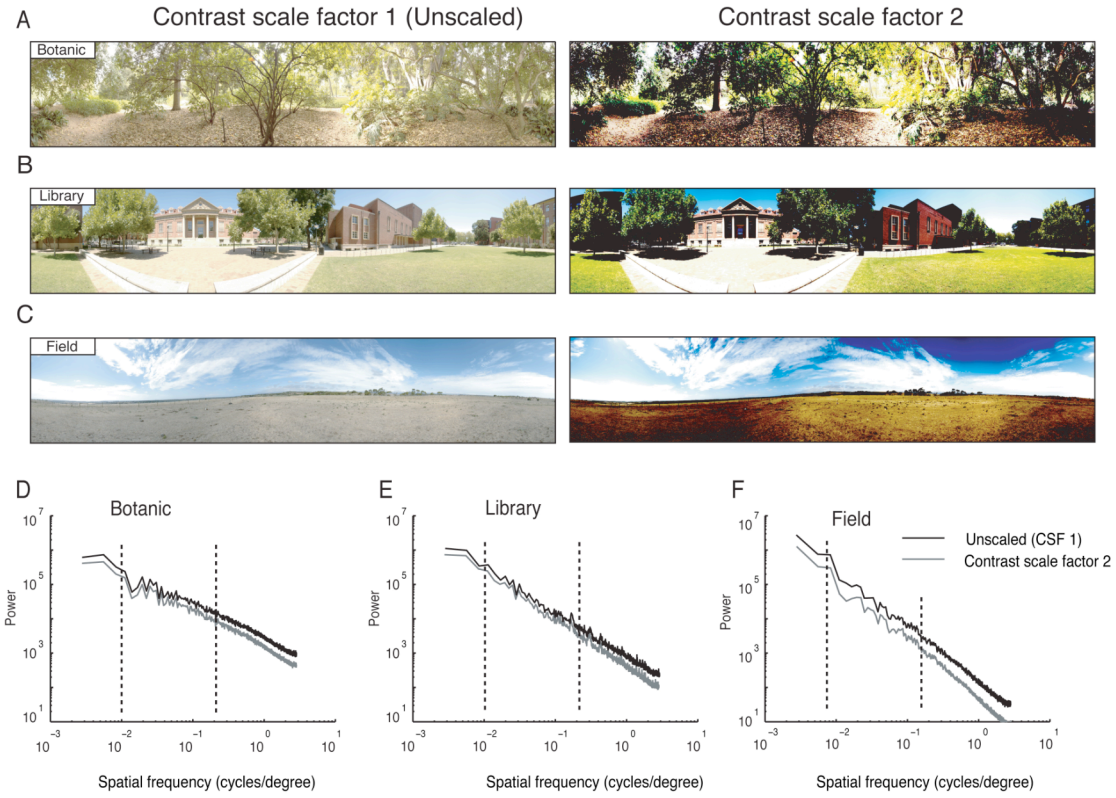

Supplementary Figure 3.3 Image power is increased across all relevant spatial frequencies after increasing image contrast.

A-C shows the three images used in Figure 2 before and after a nominal doubling of image contrast. A. The 'Botanic' image before (left; Contrast scale factor 1) and after artificially increasing image contrast (right; Contrast scale factor 2). B. As for A, but for the 'Library' image. C. As for A, but for the 'Field' image. D. Horizontal spatial frequency power spectrum for the 'Botanic' image before and after artificially increasing image contrast. Dashed lines outline the range of spatial frequencies relevant for fly motion detectors. E. As for D, but for the 'Library' image. F. As for D, but for the 'Field' image.

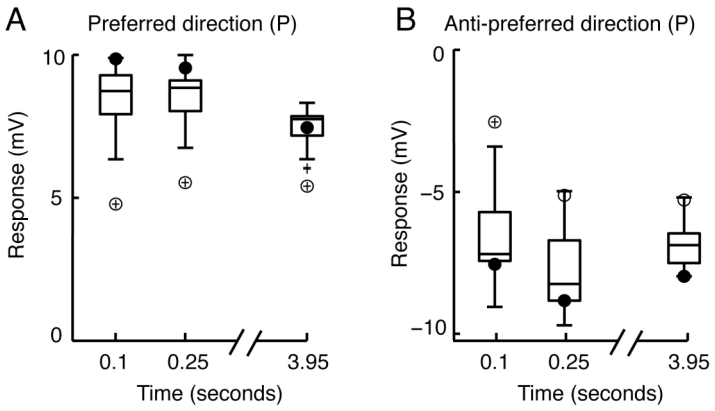

Supplementary Figure 3.4 Adaptation reduces response variability across the image set.

Box plots show the spread of responses generated by 25 natural images at three time points after the onset of image motion: an early (unadapted) time window, 50-150 ms, an intermediate time window, 200-300 ms, and a late (adapted) time window, last 100 ms of stimulus. Responses were averaged across 100 ms time windows (centered on the abscissa) for a minimum of four trials within each neuron. Image start position was offset by 90° for each trial, thereby averaging the response over the whole 360° panorama. A. Preferred direction (N=6). B. Anti-preferred direction (N=3). Crosses (+) show outlier responses. Superimposed open circles show the position of the low contrast 'Field' image and closed circles show the position of the high contrast 'Botanic' image. Data for the anti-preferred direction (B) subtracted from preferred direction (A) to eliminate non-directional response transients, is shown in the paper (Figure 3.5A).

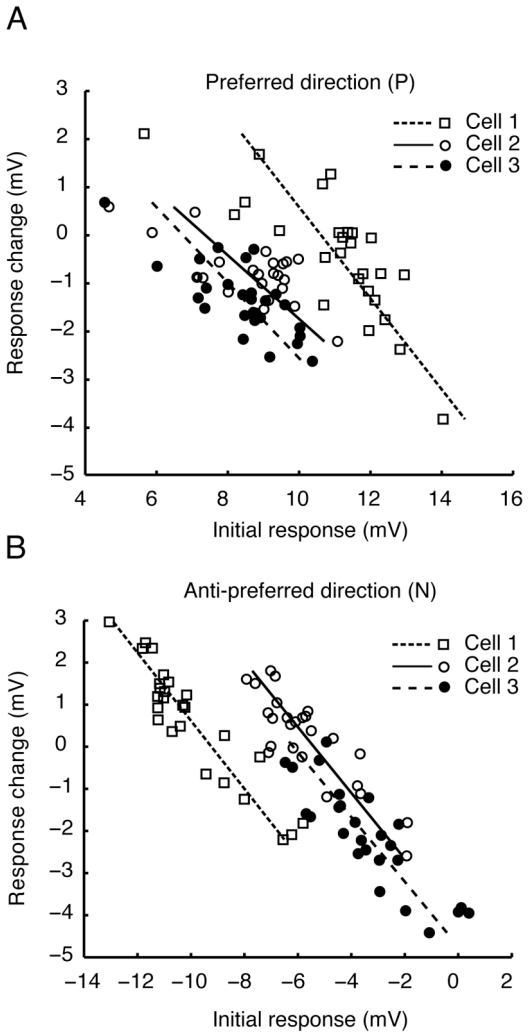

Supplementary Figure 3.5 Adaptation is dependent upon initial response

A. Response change (ordinate), determined by subtracting the averaged response from 50-150 ms after the onset of image motion (initial response) from the averaged response to the last 100 ms of image motion (adapted response), plotted against the initial response (50-150 ms after the onset of image motion). Each image was averaged over a minimum of 4 trials each with image start position offset by 90°, thereby averaging the response over the entire 360° panorama. The data for three neurons is indicated with different symbols. Lines show linear regression through data for each individual neuron. Cell 1 and Cell 3 include data for all 26 images; Cell 2 includes data for 25 images. B. Same as part A but for anti-preferred direction. Data for the anti-preferred direction (B) subtracted from preferred direction (A) to eliminate non-directional response transients, is shown in the paper (Figure 3.5B).

3.8.4 Contrast gain

Although the progressive reduction in response magnitude, seen for some images in Figures 3.4-3.6 and Supplemental Figures 3.4 and 3.5 is consistent with an adaptive reduction in contrast gain, as extensively described for artificial stimuli such as sinusoidal gratings [8], the increase in response to images that initially produced weak responses are less easily explained. Could this effect be associated with an early onset *increase* in the contrast gain of the system? To investigate this we used a test-adapt-test protocol to measure the contrast gain before and after a brief adapting presentation (200 ms) with the 'Field' image (Supplemental Figure 3.6). Supplemental Figure 3.6A shows that the contrast gain, determined using a sinusoidal test image with a near optimal spatial and temporal frequency, is slightly reduced (i.e. shifted to the right). Supplemental Figure 3.6B shows the contrast gain of the system assessed using the same image ('Field') used as the adaptor. Because this is an inherently low contrast image, the unadapted contrast threshold is much higher and responses never reached the magnitude seen for the sinusoidal gratings (Supplemental Figure 3.6). At lower contrasts, contrast sensitivity again seems slightly reduced. However, when the test pattern reaches maximum contrast (i.e. the same as the unscaled test image) responses are significantly increased compared with the unadapted response (see inset in Supplemental Figure 3.6B). Hence, we conclude that the facilitation in response seen for some images is an image-specific effect and is not due to an increase in contrast sensitivity. As in all previous work, we only observe decreased contrast gain in the adapted state (albeit subtle for this particular image).

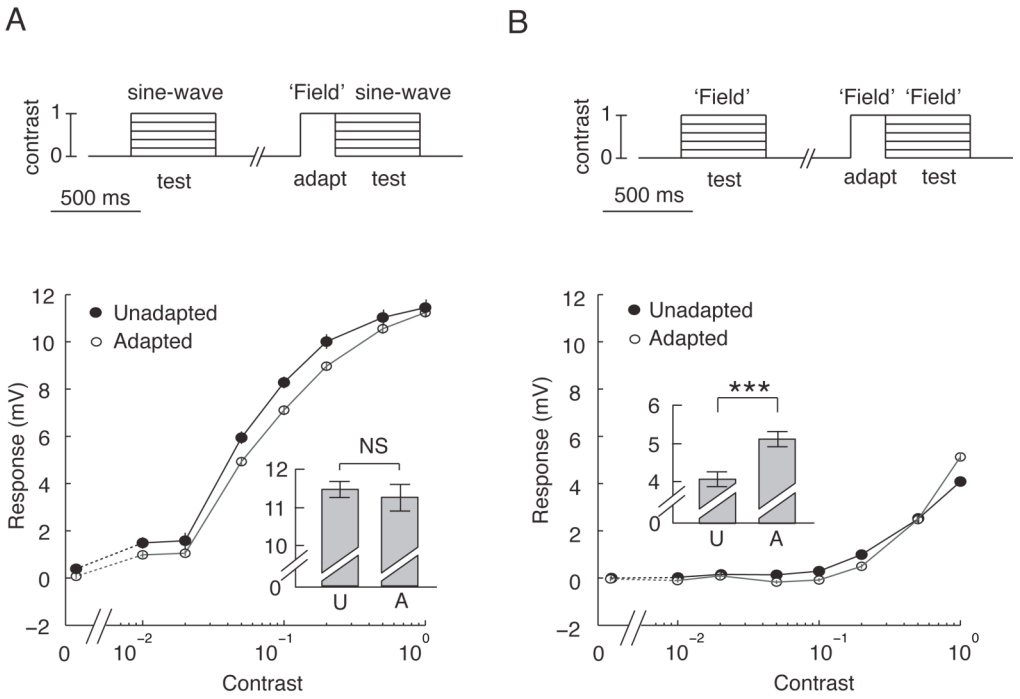

Supplementary Figure 3.6 Contrast response functions before and after adaptation with the 'Field' image

A. Average contrast response functions before and after 200 ms adaptation with the low contrast 'Field' image using a sine wave of near optimal spatial frequency (0.1 cycles/degree). Both adapting and test patterns were moved at 45°/s, which is equal to 4.5 Hz temporal frequency for the sinusoid (N=3). Closed symbols show the unadapted response and open symbols show the response after adaptation. Data shown are the mean ± SEM for 63 trials in the unadapted condition and 142 trials in adapted condition (N=3). Inset shows a bar graph of the responses before (U) and after (A) adaptation at a contrast of 1. B. As for part A, except that in this example the test stimulus is the same image as the adaptor, 'Field'. Data shown are the mean ± SEM for 140 trials in the unadapted condition and 151 trials in adapted condition (N=3). *** denotes $p<0.001$ determined with paired t-test. Insets above the figure show the test-adapt-test protocol used to acquire the contrast response functions.

3.9 Supplemental References

1. Tadmor, Y., and Tolhurst, D.J. (2000). Calculating the contrasts that retinal ganglion cells and LGN neurones encounter in natural scenes. Vision Res *40*, 3145-3157.

2. Shoemaker, P.A., O'Carroll, D.C., and Straw, A.D. (2005). Velocity constancy and models for wide-field visual motion detection in insects. Biol Cybern *93*, 275-287.

3. Straw, A.D., Rainsford, T., and O'Carroll, D.C. (2008). Contrast sensitivity of insect motion detectors to natural images. J. Vis. *8(3):32*, 1-9.

4. Hardie, R.C., (1985) Functional organization of the fly retina, in Progress *in sensory physiology*, D. Ottoson, Editor. Springer-Verlag: Berlin. p. 1-80.

5. Dror, R.O., O'Carroll, D.C., and Laughlin, S.B. (2001). Accuracy of velocity estimation by Reichardt correlators. J. Opt. Soc. Am. A *18*, 241-252.

6. James, A.C., (1990) White-noise studies in the fly Lamina. PhD thesis, Australian National University: Canberra.

7. Payne, R. and J. (1981) Howard, Response of an insect photoreceptor: a simple log-normal model. Nature. 290, 415-416.

8. Harris, R.A., O'Carroll, D.C., and Laughlin, S.B. (2000). Contrast gain reduction in fly motion adaptation. Neuron *28*, 595-606.

Chapter 4:
Receptive fields of fly motion detecting neurons integrate local features within natural scenes unpredictably.

4.1 Context

In the previous chapter, we investigated HS neuron responses to a range of natural images. We show that these neurons have a remarkable ability to encode velocity accurately across an enormous range of image. Their robust responses appear to be mediated by powerful static and dynamic non-linearities that are recruited differently from one image to the next. However, in order to get reliable velocity responses, we carried out the analysis on time-averaged data, in effect averaging out any transient response fluctuations recruited by structure within the scenes.

In this paper, we investigate the transient response properties of these neurons to a subset of the images used in the previous chapter. Our aim was to investigate these transient response characteristics both globally and locally, down to the level of individual motion sensitive elements.

Receptive fields of fly motion detecting neurons integrate local features within natural scenes unpredictably

Paul Barnett and David O'Carroll

Discipline of Physiology,

School of Molecular and Biomedical Science,

The University of Adelaide, SA 5005, Australia

**To whom correspondence should be addressed: paul.barnett@adelaide.edu.au, +61-8-8303 6216.*

Key words: pattern noise; motion detection; natural images; velocity encoding; receptive field; insect vision; transient responses

Abbreviations: lobula plate tangential cells (LPTC); horizontal system (HS); horizontal system north (HSN); horizontal system noth-east (HSNE); elementary motion detector (EMD); large monopolar cell (LMC).

4.2 Summary

As an animal moves through its environment, the visual panorama projects onto the retina as a sequence of locally variable light intensities from which the visual system computes motion. A consequence of the nonlinear correlation underlying motion estimation in animals is that the variability in pattern structure and contrast inherent within natural scenes profoundly influences local motion responses. To accurately interpret optic-flow induced by self-motion, neurons in the fly's visual system average locally variable responses by integrating visual inputs across wide regions of space. This does not occur in a single stage however, but rather hierarchically, such that many neurons have small receptive fields poorly optimised for averaging ambiguous local responses. Using motion sensitive neurons in the hoverfly, we investigated the integration local motion responses to natural scenes. We used a correlation-type model for motion detection that takes into account the receptive field properties of the neurons as a predictor for pattern dependence. Our results reveal that receptive field alone is a poor predictor of the spatial integration properties of these neurons. Specialized optic-flow detecting neurons sensitive to horizontal motion with vertically elongated but narrow receptive fields respond unpredictably to natural scenes, suggesting an additional role in the extraction of image features.

4.3 Introduction

Accurately interpreting motion in the natural world presents a major challenge for biological visual systems. Natural scenes vary enormously in structure, luminance and contrast (Ruderman, 1994, Simoncelli & Olshausen, 2001). These are all parameters known to modulate the responses of biological motion detectors, which use nonlinear correlation of local changes in light intensity across space and time to estimate motion (for review see Clifford & Ibbotson, 2002). Consequently, even when presented with relatively simple stimuli, local motion responses show pronounced dependence on pattern structure and contrast (Egelhaaf, Borst & Reichardt, 1989, Reichardt, 1987, Reichardt & Egelhaaf, 1988).

The visual system of the fly overcomes this, in part, through the spatial integration of retinotopically arranged local motion-sensitive elements by the so-called lobula plate tangential neurons (LPTCs) (Borst & Egelhaaf, 1992). In the third optic ganglion, there are approximately 60 individually identifiable LPTCs (Strausfeld, 1976) collectively thought to act as a neural centre for course control and visual stabilization (Borst & Haag, 2002, Egelhaaf & Borst, 1993). LPTCs have local preferred directions which vary across their receptive fields matched to optic-flow fields generated by the animal's self-rotation about different body axis (Franz & Krapp, 2000, Krapp, Hengstenberg & Hengstenberg, 1998, Krapp & Hengstenberg, 1996).

The large receptive fields of these LPTCs have been interpreted as a prerequisite for parsing optic-flow fields generated from self-rotations about different body axes (Krapp et al., 1998, Krapp & Hengstenberg, 1996, Lappe, Bremmer & van den Berg, 1999); however, they may also play an important role in the reduction of local pattern-dependence to image motion (Reichardt, 1987). Additional to their already large receptive fields, recent studies revealed that many LPTCs share axo-axonal gap junctions with neighbours (Elyada, Haag & Borst, 2009, Farrow, Borst & Haag, 2005, Haag & Borst, 2004, Haag & Borst, 2005), resulting in receptive fields exceeding the size predicted from their dendritic arbours (Elyada et al., 2009, Franz

& Krapp, 2000, Hausen, 1982a, Krapp & Hengstenberg, 1996). This cross-communication of retinotopic inputs has been suggested to lead to more robust representation of specific optic-flow fields (Cuntz, Haag, Forstner, Segev & Borst, 2007).

Further spatial pooling of local motion signals takes place in motor and pre-motor neurons. For example the descending neurons of the ocellar and vertical system (DNOVS) integrate across different combinations of LPTC, most likely via direct electrical connections, in such a way as to further improve their selectivity for specific rotational optic-flow fields (Haag & Borst, 2005, Haag, Wertz & Borst, 2007, Wertz, Borst & Haag, 2008). In a hierarchical manner the neck motor neurons (NMNs), which synapse directly on muscles that control head rotations, further collate their inputs both directly from various LPTCs and via descending interneurons, such as those just mentioned (Gronenberg, Milde & Strausfeld, 1995, Huston & Krapp, 2008, Strausfeld & Bassemir, 1985, Strausfeld & Seyan, 1985). Many neck motor neurons have receptive fields that extend substantially into each visual hemisphere, far beyond the extent of any individual LPTCs or DNOVS (Huston & Krapp, 2008).

Although integration over large regions of visual space is an important means for overcoming ambiguity in local motion responses, this does not occur in a single stage but rather hierarchically. The existence of intermediate stages of optic-flow processing, such as the LPTCs, suggesting that for many tasks, more local representations of visual motion remain important. Recently, for example, Nordström et al., (2008) described an intriguing sexually dimorphic adaptation in the horizontal system (HS) neurons of the hoverfly, where the receptive field of the dorsal most HS neuron, HSN, in males is far narrower than in females. The HS neurons are a subset of the LPTCs whose receptive field organizations resemble self-motion about vertical meridian, yaw rotation (Krapp, Hengstenberg & Egelhaaf, 2001, Nordström et al., 2008). The two most dorsal HS neurons in the hoverfly, HSN and HSNE, have receptive fields that overlap substantially and spatio-temporal tuning, which is similar when stimulated frontally (Straw, Warrant & O'Carroll, 2006); yet, their receptive fields vary in size and shape dramatically (Nordström et al., 2008). For the

detection yaw rotation, a receptive field such as the male HSN in hoverflies, which is substantially limited in spatial extent along its preferred directional axis, is more likely to provide ambiguous signals about image motion.

Spatial integration is not the only means for overcoming local pattern dependence, however. HS neurons rapidly adapt to prior motion stimuli with strong local changes in contrast gain (Harris, O'Carroll & Laughlin, 2000, Nordström & O'Carroll, 2009) and increased sensitivity to changes in stimulus velocity (Maddess & Laughlin, 1985). Recently, time-averaged responses from HS neurons were shown to provide robust estimates of image velocity when stimulated with natural images, which varied enormously in spatial structure and contrast (Straw, Rainsford & O'Carroll, 2008). This consistency in the velocity coding of natural scenes has been attributed to an active normalization strategy that minimizes the response variability from one image to the next (Barnett et al., 2009, submitted). However, these studies only analysed the 'time-averaged' responses of HS neurons and thus, didn't consider their time dependent response characteristics to the motion of the natural images.

In this paper, we have investigated the consequences of receptive field size and shape in the processing of natural-image motion by comparing the time dependent responses of the unique male HSN and HSNE optic-flow processing neurons. We have implemented an elaborated correlation type motion detection model, which incorporates the receptive field properties of the neurons we recorded from as a linearly weighted sum, to generate a prediction of pattern dependence in response. Our results reveal that the receptive fields of these neurons are poor predictors of the integration of local motion signals. Furthermore, the integration of local motion signals within the receptive field of HSN appears to result in an enhanced sensitivity to structure within natural scenes. Unpredictable responses to natural scenes combined with the unusual shape of the HSN receptive field, suggests that it may play an important role in the encoding of local optic-flow and the detection of image features.

4.4 Results

4.4.1 Natural images induce large response fluctuations in HS neurons to constant velocity stimuli

We employ two basic stimulus classes to investigate pattern dependence in the response of HS neurons to the motion of panoramic natural images. The first occupies the entire stimulus monitor to investigate pattern dependence at the global level, e.g. allowing the neuron to integrate local motion signals across large regions of the receptive field ('whole-screen' stimulus; Figure 4.1-4.5). The second isolates the stimulus to a small region within the receptive field to investigate pattern dependence in responses at the resolution of only a couple of local motion sensitive elements ('slit stimulus'; Figure 4.6-4.8).

Figure 4.1 shows an example of the whole screen stimulus and the panoramic natural image, 'Field', which was centred on the stimulus monitor and rotated at 45 °/s in the preferred direction for nine seconds (Figure 4.1A). To avoid confounding pattern dependence with adaptation of the HS neurons response, we pseudo-randomly varied the stimulus over eight initial start phases each separated by 45° (Figure 4.1C). For subsequent analysis we took the 'phase aligned' average of the response recorded at the eight different start phases, but excluded the first second of image motion to avoid the influence of the transient phases of adaptation.

As different parts of the scene move across the stimulus monitor, they generate local response fluctuations that are repeatable across the start phases and from one recording to the next (Figure 4.1). For example, the group of vertically aligned clouds, shown on the left hand edge of the monitor (Figure 4.1A), appears to produce a large increase in response at around 3.5 seconds (Figure 4.1B). The region immediately preceding it, on the other hand, has few vertically aligned features and produces a negligible response from the neuron (obvious at around 2-2.5 seconds; Figure 4.1A and 4.1B). Over the course of a full image rotation, eight seconds, average neural response varied by 85% from maximum to minimum for this image, even though image velocity remained constant at 45°/s. Undoubtedly, such large fluctuations in response would make it impossible for a neuron of this kind to provide accurate instantaneous velocity information to the animal.

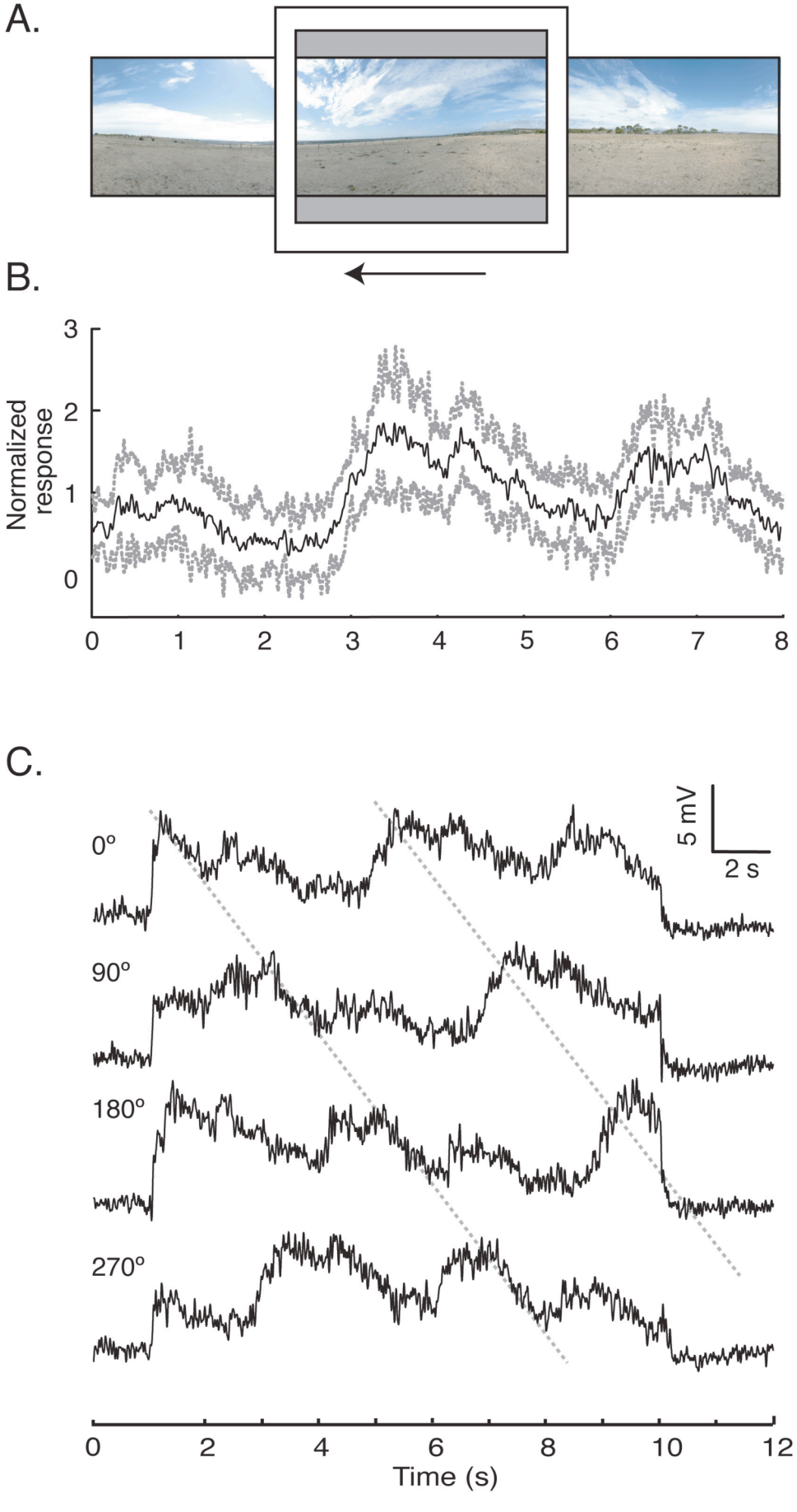
A.
B.
Normalized response
3
2
1
0
0
1
2
3
4
5
6
7
8
C.
0°
90°
180°
270°
5 mV
2 s
0
2
4
6
8
10
12
Time (s)

Figure 4.1 Natural image pattern dependence

A. The 'Field' image, one of six natural panoramic images used in this study as stimuli. Images rotated at 45°/s for nine seconds along the preferred directional axis of the HS neurons. B. 'Phase aligned' normalized response (mean±standard deviation; black solid line±grey dashed lines) for male HSN neurons to stimulation with the field image shows remarkable dependence upon structure when stimulated with natural images. The response of each neuron was normalized by its mean, therefore reducing the variance of absolute magnitude differences from one recording to the next. To avoid the influence of onset transients and the early adaptation period, we omitted the first second of the stimulus period. The data and the image are space-time aligned so that features of the image correspond to the neural responses immediately below it. C. Because the time course of HS neuron responses adapts to the stimuli presented, we started each trial at one of eight pseudorandom image start phases for each recording, with a minimum of four for each recording (0°, 90°, 180°, and 270° offset). The 'phase aligned' data (B) is the average of the response recorded adjusted for the image start phase and thus, aligned for space rather than time (see Experimental Procedures). Diagonal dotted lines connect time points where the same image segment is present on the stimulus monitor. Note the different time axis shown for parts B and C. Image start phase of 0° (C) is the same alignment as that shown for the average data (B). Responses are the average of N=4 neurons with n=32 repeats.

4.4.2 Receptive field size and shape influences neuron pattern dependence

How does receptive field size and shape influence pattern dependence? The male HSN and HSNE neurons have largely overlapping receptive fields with similar centres along the azimuth and spatio-temporal frequency tuning, which is well matched when stimulated frontally (Straw et al., 2006). However, these two neurons have demonstrable differences in receptive field shape and size (Figure 4.2A and 4.2B). The male HSN neuron has a compact fronto-dorsally located receptive field, which prefers motion from bottom right to top left across the stimulus monitor, although local preferred directions vary across the receptive field (Nordström et al., 2008). The receptive field stretches vertically from the equator beyond the upper limit of our stimulus display, yet has limited spread along the azimuth (11° at 75% maximum response) (Figure 4.2A). The HSNE neuron on the other hand, has a more ventrally located receptive field centre but also prefers motion from bottom right to top left across the monitor. The HSNE receptive field however, spreads laterally along its preferred directional axis well into the ipsilateral visual field beyond the limits of our stimulus display (Figure 4.2B) (Nordström et al., 2008).

Figure 4.2C-2E shows the average responses from HSN (red) and HSNE (blue) neurons to six different natural images using the whole screen paradigm as described in Figure 4.1 (see Figure S4.1 for images). Despite producing time-averaged responses of similar magnitude from one image to the next (HSN: 7.8±1.5 mV; HSNE: 6.5±0.9 mV; mean±standard deviation), structures within some images clearly induces more response fluctuations than other images (compare Figure 4.2C with 4.2H, for example). Although HSN and HSNE have receptive fields centred at similar locations, using correlation analysis that assumes a 0 time lag between their responses there is a poor correlation between HSN (red) and HSNE neurons (blue), r=0.23±0.13 (mean cross-covariance coefficient±SEM; see insets on Figures). Given that the maximum sensitivity region of the HSNE receptive field is shifted along the azimuth by 10.5° compared to that of HSN, we might expect to see a small temporal delay (0.233 seconds at 45°/s) in the HSNE neuron's response. When we accounted for such a delay, there was a slight improvement in the correlation between the two neuron classes. However, this was still relatively weak, r=0.47±0.1 Interestingly,

despite the substantial overlap of HSN and HSNE receptive fields, the differences in structure and integration within the receptive fields lead to very clear differences in the phase and magnitude of the residual pattern dependencies in the response (Figure 4.2).

When we compared the pattern dependence of HSN with HSNE, as measured by the response deviation for each image averaged across the set, HSN revealed a significantly larger mean standard deviation: SD=1.29±0.15 (mean±SEM) compared to SD=0.98±0.0.11 (mean±SEM) for the HSNE, $p<0.05$ (paired, t-test). The variance-to-mean ration (VMR), however, was not significantly different. The large lateral extent of the HSNE neuron's receptive field extends far beyond the limit of the stimulus monitor thus, we are only able to stimulate the frontal part of the receptive field (Nordström et al., 2008) (Figure 4.2A and 4.2B). Consequently, we expect that these results significantly overestimate the amount of response fluctuation for HSNE, thus this difference may have been more profound if we were able to stimulate the neurons panoramically.

Close inspection of the data reveals substantial variation between responses to different images (arrows inset on Figure 4.2). For some images (e.g. 'Hamlin', Figure 4.2D), the difference in response fluctuation between the two neural classes is profound, with a time lag-corrected correlation coefficient r=0.17. Whereas, for other images (e.g. 'Field', Figure 4.2G), the responses of the two neural classes is very similar, r=0.81. The arrows inset on Figure 4.2 highlight some response regions where the two neural classes differ substantially.

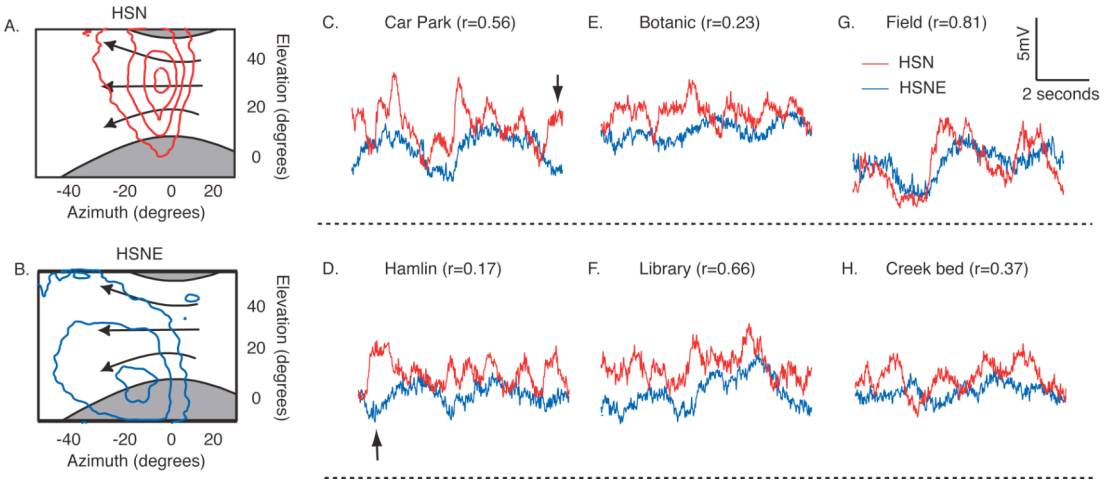

Figure 4.2 Effect of receptive field on pattern dependence

A. The average receptive field of male HSN neurons, the arrows show the direction of image motion. The images were perspective distorted to simulate pure yaw rotation about the fly's head on our stimulus monitor, which is flat, whited-out areas shown within monitor outline. The receptive fields were mapped using a small black bar scanned across the screen left to right and vice versa then up to down and vice versa at 50°/s. The receptive field contour lines (red) connect points of equal response in 1 mV increments. Outermost contour line is 1 mV response level inner most 4 mV. The receptive field data is from Nordström et al., (2008). B. The same as A but for male HSNE neurons. C-H. Average 'phase aligned' response of male HSN (red) and HSNE (blue) to rotation of the 'Car Park' image (C), 'Hamlin' image (D), 'Botanic' image (E), 'Library' image (F), 'Field' image (G), and 'Creekbed' image (H). The dashed line shows resting membrane potential. Cross-covariance coefficient (r), shown in brackets after the image name, is for the correlation between HSN and HSNE for each image. HSN: N=4 neurons, with a minimum of 26 repeats for each image; HSNE: N=5 neurons, with a minimum of 21 repeats. Despite having largely overlapping receptive fields, the responses of HSN and HSNE are often obviously out of phase arrows inset (C and D).

4.4.3 Differences in response are not merely a consequence of different neuronal receptive fields

We compared neuron responses with the output of an elaborated model for motion detection, which included filters matched to many of the processing stages known to occur up to the level of the HS neurons in *Eristalis* (Dror, O'Carroll & Laughlin, 2001, Straw et al., 2008). However, on this occasion we weighted the outputs of an array of local motion detectors with the average receptive fields recorded from the neurons, to get a prediction of the pattern dependence generated by each image (for full description of the models implementation and simulation see Supplementary data; Figure S4.2). For the six images used in this study, mean model output varied more than 45-fold from one image to the next though (HSN: 0.29±0.22; HSNE: 0.39±0.35; mean±standard deviation from image to image). To overcome this for display purposes, in Figures 4.3 and 4.5 we have normalized model output to the maximum neural response for each image. Figure 4.3 shows the neural responses, as plotted in Figure 4.2, in grey with the model response for each image overlaid. There is a poor correlation between the observed pattern dependence (grey; data from Figure 4.2) and that predicted by our model for either of the neural classes (HSN: red; HSNE: blue), with average covariance coefficients of r=0.36±0.04 for the HSN and r=0.39±0.11 for the HSNE (Figure 4.3). Though once again, there was substantial variation from one image to the next. Some images for example, 'Library' and 'Field', Figure 4.3D and 4.3E, were poorly predicted by our model; whereas, other images were well predicted, for example, 'Creek bed' (Figure 4.3F).

In contrast to the neural recordings, despite taking into account the large differences between receptive fields, the model HSN and model HSNE responses are well correlated (r=0.78±0.02, mean±SEM; Figure 4.3). The correlation was even better when we added a delay to account for the small lateral shift in the receptive field centre of the HSNE (0.23 s at 45°/s; r=0.86±0.02, mean±SEM). Thus, we conclude that the observed differences in pattern dependencies in HSN and HSNE (as seen in Figure 4.2), and differences between the model and the neurons (Figure 4.3) are not only the result of the receptive field size and shape but are also modulated by additional non-linear processes acting either locally, globally or both.

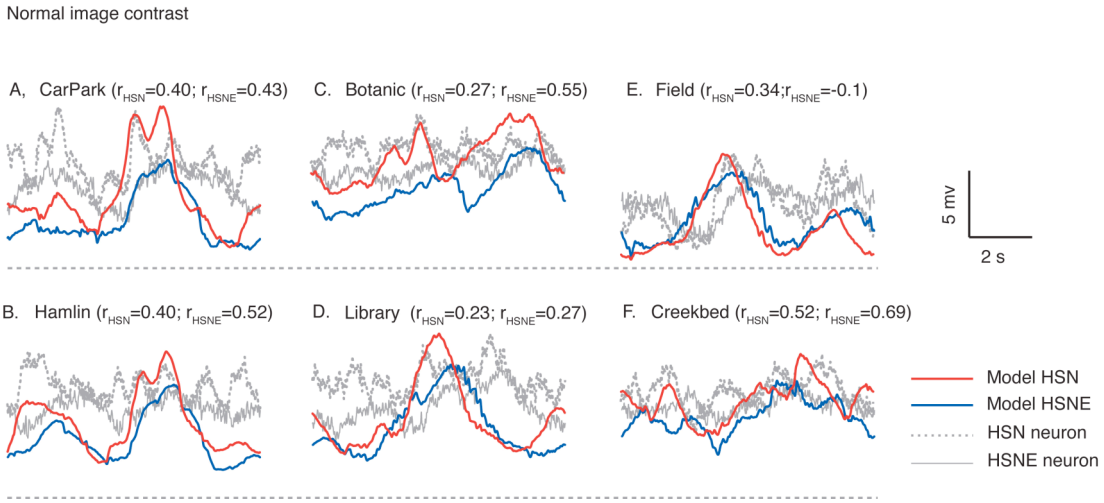

Figure 4.3 Model pattern dependence

A-F shows the output of a motion detector array with receptive field weightings taken from HSN (red) and HSNE (blue) for the same six images used in Figure 2. 'Car Park' image (A), 'Hamlin' image (B), 'Botanic' image (C), 'Library' image (D), 'Field' image (E), and 'Creekbed' image (F). Average neuron data taken from Figure 2 is shown in grey (HSN: dashed grey lines; HSNE: solid grey lines). Cross-covariance coefficients (r) are shown at the top of each panel. r_{HSN} compares the model HSN response (red) with the neuron HSN response (dashed grey lines); r_{HSNE} compares the model HSNE response (blue) with the neuron HSNE response (solid grey lines). The straight dashed line running across the bottom of the panels shows zero model output and the resting membrane potential of the neuronal data. We normalized maximum model responses to equal the maximum neuronal response for each image. Non-normalized model responses show a 45-fold variation in average response across the six images.

4.4.4 Artificially lowering image contrast produces unpredictable changes in pattern dependence

Compressive nonlinearities such as response saturation (Dvorak, Srinivasan & French, 1980) and nonlinear spatial summation (Haag & Borst, 2004) are well established as mechanisms that influence the responses of LPTCs. Recent studies showed that the inclusion of such nonlinearities in correlation-type motion detector models reduced inter-scene variance in response when stimulated with the motion of natural images (Dror et al., 2001, Shoemaker & O'Carroll, 2005). While we cannot remove these nonlinear influences from the response of HS neurons entirely, they are largely activity dependent. Thus, a common approach to reduce the influence of such nonlinearities is to 'linearize' the neural response by reducing the contrast of the stimulus.

A four-fold reduction in image contrast resulted in an increase in the VMR for each image and both neuron classes, consistent with a release from the influence of compressive nonlinearities (Figure 4.4). HSN had a mean VMR of 0.27±0.11 at full image contrast, which increased to 0.70±0.13 at ¼ image contrast ($p<0.05$; Wilcoxon signed rank test; Figure 4.4, red). HSNE showed a similar change in VMR, increasing from 0.17±0.04 at full image contrast, to 0.64±0.12 at ¼ image contrast ($p<0.05$; Figure 4.4, blue). Furthermore, after reducing image contrast, the model did a much better job at predicting neural responses (Figure 4.5). Mean correlation coefficients significantly improved from r=0.36±0.04 to r=0.62±0.06 in HSN ($p<0.05$) and r=0.39±0.11 to r=0.65±0.08 in HSNE ($p<0.05$) after reducing image contrast. However, again there was a great deal of variation from one image to the next. For example, for 'Hamlin' the model accurately predicted the neural response (r=0.84 for HSN, and r=0.88 for HSNE; Figure 4.5B), whereas for 'Field' the model remained a poor predictor (r=0.41 for HSN, and r=0.35 for HSNE; Figure 4.5E).

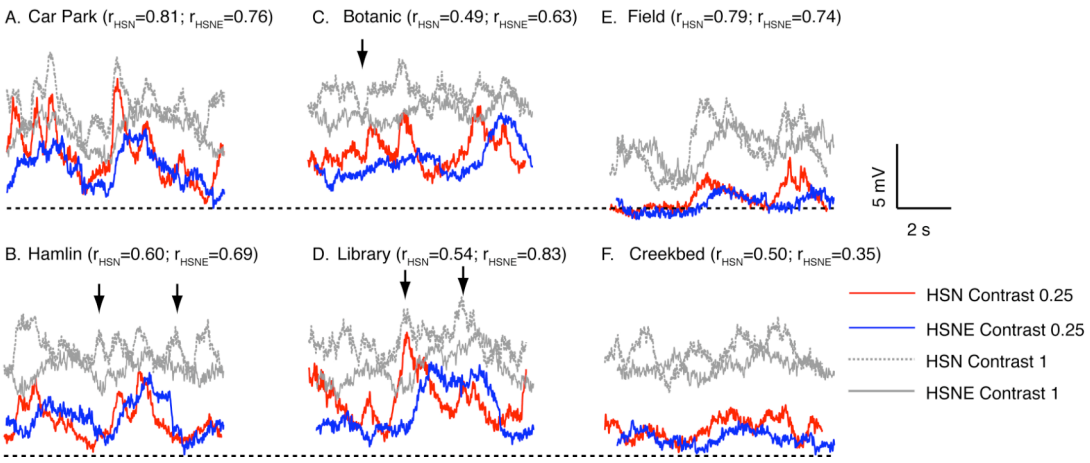

Figure 4.4 Affect of reducing image contrast on pattern dependence

We artificially reduced the contrast of all six images in the set and recorded HSN (red) and HSNE (blue) neuronal responses. 'Car Park' image (A), 'Hamlin' image (B), 'Botanic' image (C), 'Library' image (D), 'Field' image (E), and 'Creekbed' image (F). Responses to the full contrast images taken from Figure 2 are shown in grey (HSN, dashed grey line; HSNE, solid grey line). The straight dashed line running across the bottom of the panels shows the resting membrane potential. Cross-covariance coefficients (r) are shown at the top of each panel. r_{HSN} compares the low contrast HSN response (red) with the normal contrast HSN response (dashed grey lines); r_{HSNE} compares the low contrast HSNE response (blue) with the normal contrast HSNE response (solid grey lines).

After reducing image contrast, the model matched the relative shape and magnitude of the residual pattern dependence relatively well (Figure 4.5). However, remember that the response of the model in these examples has been normalised to the maximum neural response for each image. The absolute model response actually varied more than 45 fold across these six images. Thus, although our elaborated model in combination with the receptive field provides a reasonable prediction of the pattern dependence once image contrast is reduced, it fails dismally at capturing the absolute magnitude of responses produced.

The inclusion of simple compressive nonlinearities in a further elaborated version of the model would, without doubt, reduce some of the spread of absolute response magnitudes (as shown by Dror et al, 2001) However, it would also severely 'flatten' the local response fluctuations far more than that evident in the physiological data. Although there is some evidence of a release from response saturation in the data (Figure 4.4 and Figure 4.5), the neural responses did not merely rescale after we lowered image contrast. In fact, for several images the shape of the response after reducing the image contrast shared little resemblance to the response produced at the full image contrast, despite the structure within the scenes remaining the same. The emergence of residual effects, such as the appearance or disappearance of new peaks and troughs in the data, are difficult to account for solely with an explanation based on a release from the influence of compressive nonlinearities (for example see solid arrows inset in Figure 4.4). Consequently, on average in both neuron classes there was only a mediocre mean correlation between the two contrast conditions (HSN, r=0.62±0.06; HSNE, r=0.67±0.07). Once again, this varied greatly from image to image. For example, in both neuron classes 'Car park' and 'Field' showed strong correlations (HSN: r=0.81, and r=0.79 respectively; HSNE: r=0.76, and r=0.74 respectively; see Figure 4.4A and 4.4E) whereas, 'Creek bed' showed a much poorer correlation (HSN, r=0.5; HSNE, r=0.35; see Figure 4.4F). In addition, there were differences between the two neuron classes, for example 'Library' produced a very strong correlation in HSNE (r=0.83) and yet only a mediocre correlation for HSN (r=0.54; Figure 4.4D).

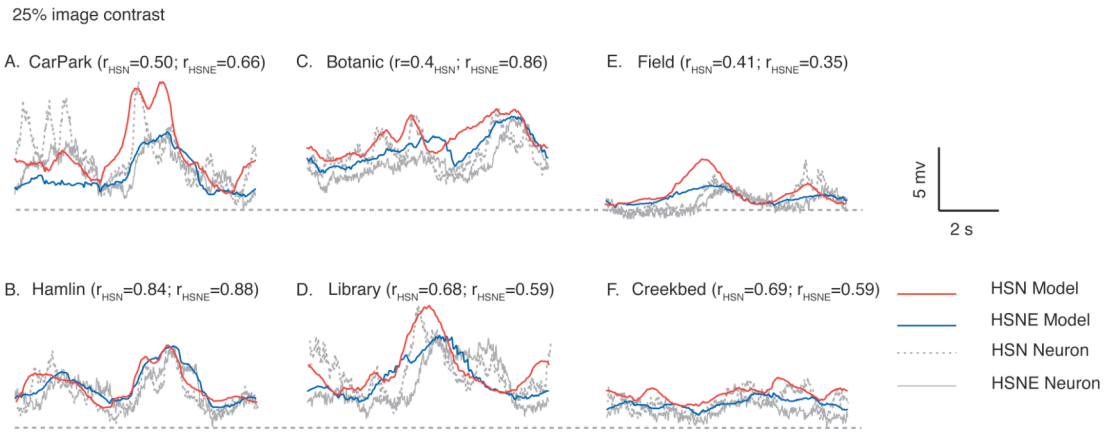

Figure 4.5 Model pattern dependence and reducing image contrast

A-F shows a comparison of the model HSN (red) and HSNE (blue) responses with the neuronal data (taken from Figure 4) for HSN (grey dashed lines) and HSNE (grey solid lines) for the contrast-reduced images. 'Car Park' image (A), 'Hamlin' image (B), 'Botanic' image (C), 'Library' image (D), 'Field' image (E), and 'Creekbed' image (F). Cross-covariance coefficients (r) are shown at the top of each panel. r_{HSN} compares the model HSN response (red) with the neuron HSN response (dashed grey lines); r_{HSNE} compares the model HSNE response (blue) with the neuron HSNE response (solid grey lines). The straight dashed line running across the bottom of the panels shows zero model output and the resting membrane potential of the neuronal data. We normalized maximum model responses to equal the maximum neuronal response for each image. Non-normalized model responses show a 45-fold variation in average response across the six images.

4.4.5 Local motion responses to natural scenes show pronounced pattern dependence

Up until now, we have only analysed pattern dependence to natural images on a global level, with our stimulus largely filling the receptive field. To investigate local response properties, we used a window to mask the stimulus, limiting its spatial extent to the size of only one or two local motion-sensitive subunits (Figure 4.6A) (Egelhaaf et al., 1989, Reichardt & Egelhaaf, 1988). Figure 4.6B and 4.6C show the strip of the 'Close' image (Figure S4.1G) visible through the window (stretched vertically for display purposes) and the membrane fluctuations recorded axonally from a HS neuron. Areas in the image strip that contain few contrast boundaries generate almost no response, i.e. in the grass from 1-3.5 seconds and in the dark bushy area from 5-7.5 seconds (Figure 4.6C). Conversely, obvious contrast boundaries in the image produce sizeable membrane potential depolarisations (Figure 4.6C). Figure 4.6D shows the output of the model to the same image strip. Although the model captures the general phase and relative magnitude of the neural pattern dependence, its local response profile is quite different from that of the neuronal recording (see arrows in Figure 4.6D).

Experiments using the window stimulus evoke only weak responses and thus require averaging over many identical trials to isolate neural response from noise (see Figure 4.6C). To allow us to collect the equivalent of local responses in fewer trials, we adapted a method originally developed to study local motion detector responses to grating patterns (Egelhaaf et al., 1989, Reichardt & Egelhaaf, 1988). We extended the height of single image rows to stretch across many vertically aligned local motion sensitive elements. The stimulus image was vertically blurred to account for the optics of *Eristalis tenax* (Straw et al., 2006). The resultant neural response is much larger and effectively equivalent to the sum of many individual local motion sensitive elements viewing the same image row (Egelhaaf et al., 1989, Reichardt & Egelhaaf, 1988). This allowed us to obtain full response maps for six cells and two images in recordings that were greater than an hour in duration.

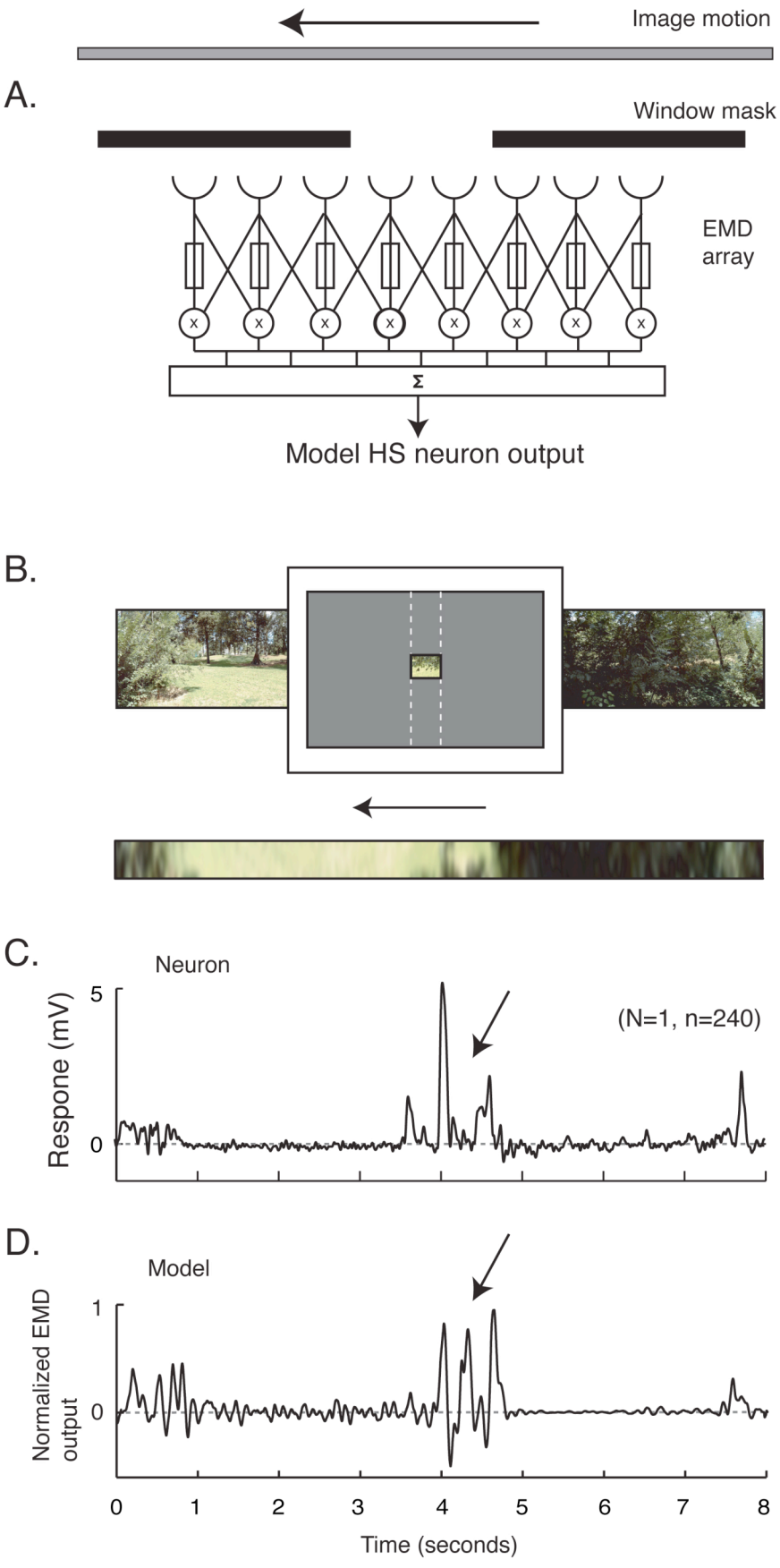
A.
Image motion
Window mask
EMD
array
Σ
Model HS neuron output
B.
C.
Neuron
(N=1, n=240)
Respone (mV)
5
0
D.
Model
Normalized EMD
output
1
0
0
1
2
3
4
5
6
7
8
Time (seconds)

Figure 4.6 The slit-window stimulus

A. Pictogram of the slit, or window, paradigm used to limit the size of the stimulus down to the size of only a couple of elementary motion sensitive elements. The natural image panorama is rotated about the fly's head, as in the previous experiments in this paper, but on this occasion, the stimulus monitor is windowed ('window mask') such that only a small portion of the stimulus is visible to the animal. Thus, as represented in the pictogram, which represents the couple elementary motion sensitive elements as basic Hassenstein-Reichardt correlator schemes, the signal recorded from the HS neuron is only that produced from one or two elementary motion sensitive elements. B. Shows the 'Close' image, only used in this Figure due to the clear distinction between cluttered and uncluttered regions within the scene, as it appeared through the 'window paradigm'. The window paradigm limited the stimulus to a 5°x5° window. The image strip below shows the strip of image visible to the animal through the widow, for display purposes the image strip has been stretched vertically so its structure is clearly visible. C. Average response of 240 repeats in one HSN neuron to the 'Close' image rotating at 45°/s with the 'window paradigm' as shown immediately above (N=1, n=240). The image strip shown in part B and the data are space-time aligned such that response fluctuations in the data correspond to image feature directly above in the image slit. D. Model response to the same strip of image as that viewed by the neuron above. The arrows inset on the neuronal and model data traces highlight one major difference between the two data traces, which, in this case, maybe the result of adaptation. Because the stimulus in the 'widow paradigm' was small responses were frequently tiny and thus required large numbers of averages to obtain reliable data. In the experiments shown in Figure 7, however, the window mask was extended vertically to represent a slit, the dashed white lines in B show this diagrammatically. In these 'slit paradigm' conditions the image strip was also vertically stretched such the stimulus was effectively the same as the 'window paradigm' but rather stimulated many vertically aligned elementary motion elements simultaneously thus, significantly reducing the number of repeats required to obtain useful data.

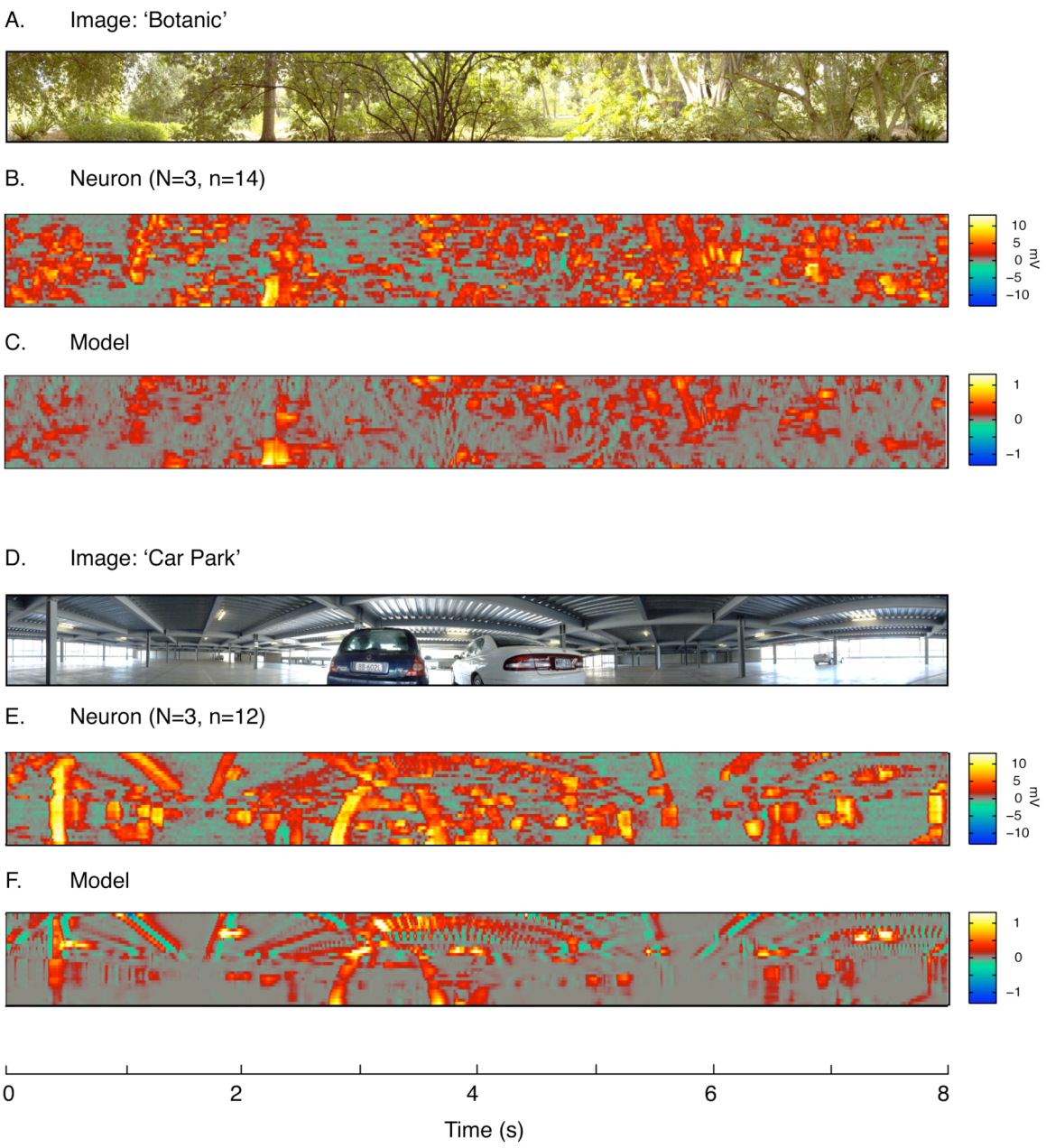
A. Image: 'Botanic'
B. Neuron (N=3, n=14)
10
5
0
−5
−10
mV
C. Model
1
0
−1
D. Image: 'Car Park'
E. Neuron (N=3, n=12)
10
5
0
−5
−10
mV
F. Model
1
0
−1
0
2
4
6
8
Time (s)

Figure 4.7 Local pattern dependence

A. A central strip taken from the 'Botanic' image. Individual rows were stretched vertically and then played back to the animal using the 'slit window stimulus' as described in Experimental Procedures. B. Average neuronal responses recorded from stimulation with the section of the 'Botanic' image shown directly above (N=3, n=~12). The neural response is spatially mapped to the equivalent vertical location of the image rows and has the response time course matched to horizontal locations in the image. Membrane potential is represented in colour as indicated by the colour bar, such that red through to yellow colours reflect membrane depolarisations of increasing magnitude; grey shows membrane potentials proximal to the resting membrane potential; and green through to blue colours reflect membrane hyperpolarizations of increasing magnitude. C. Model output to the same stimulus. The model response is the average of three neighbouring elementary motion detectors to match the width of the stimulus window used (see Methods and Materials). D-E show the same configuration as A-C but for the 'Car Park' image.

Figure 4.7 shows two images, ‘Botanic’ and ‘Car Par’ (Figure 4.7A and 4.7D, respectively), and the recorded local motion responses using the ‘slit windowed stimulus’ (Figure 4.7B and 4.7D). Large transient depolarisations associated with obvious image features (e.g. the edge of the car or columns in the ‘Car park’ image) dominate the neural response for both images (Figure 4.7B and 4.7E). Between these transients, the membrane potential tends to remain slightly hyperpolarized, despite the image moving continually in the preferred direction (Figure 4.7B and 4.7E). The slight hyperpolarization of the membrane potential between depolarising events likely reflects the antagonistic motion after-effect previously reported (Harris et al., 2000, Nordström & O'Carroll, 2009, Srinivasan & Dvorak, 1979).

While the local response of the elaborated model to the same scenes predicts the location of the gross features of the response, it only results in a mediocre correlation with that of the neuronal data (average row coefficients: r=0.58±0.05 for ‘Botanic’, and r=0.53±0.15 for ‘Car Park’; Figure 4.7C and 4.7D). In the model data, many features that produced responses are associated with subsequent hyperpolarizations, a prediction of basic Hassenstein/Reichardt correlator response to discrete contrasting objects (Geurten, Nordstrom, Sprayberry, Bolzon & O'Carroll, 2007), however such transient hyperpolarizations are not apparent in the neuronal response (Figure 4.7B and 4.7E)

4.4.6 Local motion responses are a poor predictor of neural pattern dependence produced when the entire receptive field is stimulated

If we take into account the neurons receptive fields, how well do the locally measured neuronal motion responses predict the global pattern dependence? To test this we weighted the local motion responses with the neurons receptive fields and then linearly summed them to generate a prediction of the pattern dependence under the 'whole screen stimulus' (Figure 4.8). Interestingly, once again we see poor correlations between recorded pattern noise and that predicted by the local motion detector responses (r=0.29 for the HSN and r=0.41 for the HSNE; Figure 4.8A). Moreover, if we compare this same prediction with the response to pattern dependence recorded under reduced image contrast conditions the correlations improved but remained relatively weak (r=0.52 for the HSN and r=0.62 for the HSNE; Figure 4.8B). Surprisingly, the predictions of this neuronal response derived 'model' for spatial integration are, if anything, worse than those of our Hassenstein/Reichardt correlator derived model (Figures 4.3 and 4.5). Part of this discrepancy may be due to recording noise that persists in our locally measured responses. Unfortunately though, the technically demanding nature of this technique means that it is very time consuming to collect repetitions of locally generated neuronal responses or, for that matter, explore this effect across a wider range of images.

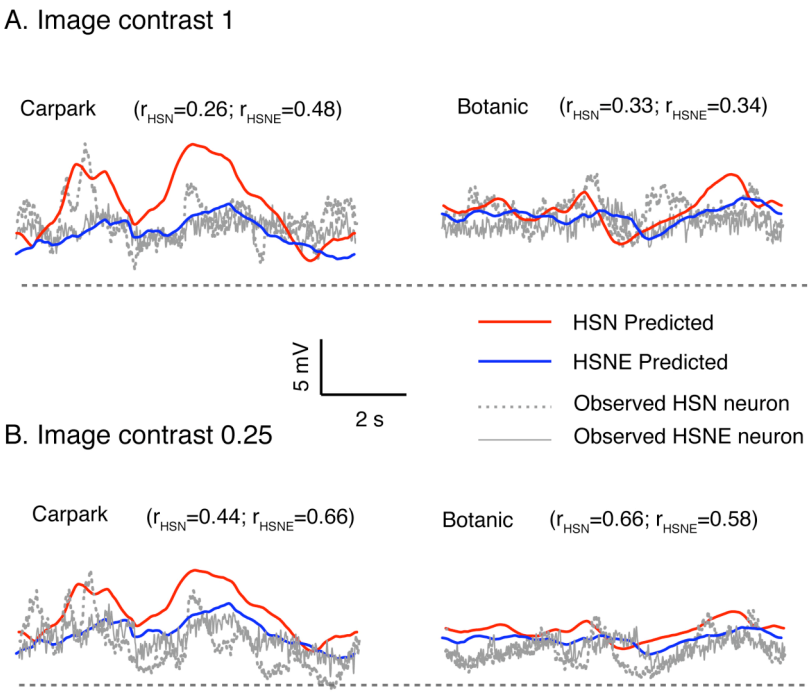

Figure 4.8 Predict pattern dependence

We used local motion responses (shown in figure 4.7) to generate a prediction of pattern dependence based on the receptive fields of the HSN (red) and HSNE (blue) neurons. A. Shows predicted pattern dependence overlaid on the observed pattern dependence recorded with the 'whole screen' stimulus (HSN, dashed grey line; HSNE solid grey line) for the Botanic and Car park images. B. Shows the same as (A) except that the observed pattern dependence on this occasion was recorded at ¼ image contrast. Insets show the covariance coefficients computed at zero time lag for the observed versus predicted pattern dependence for each neuron and image. Local response predicted pattern dependence is normalized to the maximum of the observed pattern dependence for each image. Arrow inset show response feature poorly accounted for by the prediction.

4.5 Discussion

We never intended to implement a model that was going to fully account for all the processes occurring in the biological motion vision pathway. For simpler models, such as the one used here, it is often not the features of the data that the model captures, but rather the features of the data that it fails to capture, which lead to useful interpretations of the processes occurring within the system. The model we implemented, however, does incorporate spatial and temporal pre-filtering matched to *Eristalis* yet, it frequently fails to provide accurate predictions of the biological data, despite wide spread support for its predictive powers under conditions where simple experimenter defined stimuli are used (Clifford & Ibbotson, 2002, Egelhaaf & Borst, 1993).

4.5.1 Absolute magnitude of responses

Despite the time-averaged neuronal responses showing little variation in absolute terms from image to image (HSN: 7.8±1.5 mV; HSNE: 6.5±0.9 mV; mean±standard deviation; Figure 4.2), the model had time-averaged responses that varied more than 45-fold from one image to the next. Nonlinearity inherent within basic correlation based models means that model output varies with the square of image contrast, thus the massive differences in absolute model response reflects the highly variable contrasts of the natural scenes (Dror et al., 2001) (see also Chapter 3). Dror et al. (2001) showed that the inclusion of saturation as an elaboration on the inputs of correlation based models for motion detection greatly reduced the spread in absolute time-averaged response to different natural scenes. However, recent results from HS neurons under natural image conditions suggest that simple saturating processes are unlikely to be playing a prominent role in limiting the spread of time-averaged responses (Straw et al., 2008) (see also Chapter 3).

When we reduce image contrast, there was some evidence for a release from the influence of compressive nonlinearites for some features of the response (Figure 4.4). However, a clear prediction of compressive nonlinearites, is that images which are strong drivers of response, will show a ‘flattening’ of residual pattern

dependence; whereas, images, which are weak neural drivers, will show more pronounced residual pattern dependence. Despite these images producing a greater than 45-fold spread in time-averaged model response, when we reduced image contrast, there was little evidence for the influence of prominent compressive effects in the neuronal data. Furthermore, once normalized to the maximum neuronal response for each image, our model, which does not contain compressive nonlinearities, shows an impressive match for the overall shape and magnitude of many of the residual pattern dependencies in response (Figure 4.5). This observation lends further support to the notion that static compressive nonlinearities are unlikely to be reducing image-to-image variance in the neuronal recordings.

Shoemaker et al. (2005) showed that the inclusion of dynamic adaptive nonlinearities, in the form of motion adaptation in correlation-based motion detection models, also reduced the image-to-image spread in time-averaged responses to natural scenes. Although, Shoemaker et al. (2005) noted that none of the combination of saturating and adaptive elaborations to basic correlation-based schemes they tried could match the image-to-image response consistency observed in the biological recordings (Shoemaker, O'Carroll & Straw, 2005). Furthermore, Brinkworth and O'Carroll (2009, in press) show that, by carefully cascading many of the features known to exist on the motion processing pathway with some of those processes that are reasonably expected to exist, they were able to match the consistency in response from image to image observed in the biological data. However, in recent work, Barnett et al. (2009, submitted; Chapter 3) showed that a combination of dynamic adaptive properties of motion detectors, likely arising from different stages along the motion processing pathway, act as a powerful response normaliser, minimizing variance between images.

4.5.2 The existence of local hyperpolarizing transients in the model data

The non-linear interactions underlying correlation-based models can lead to complex interactions between leading and trailing edges of features. Discreet features can generate complex triphasic responses, which transiently inhibit response even with preferred direction motion (Figure 4.6D; Geurten et al., 2007). The model's response to the natural scenes often revealed such interactions, responding to image features with a brief depolarisation-hyperpolarization-depolarisation triplet (Figure 4.7F). The neuronal recordings however, showed little evidence for the existence of such interactions responding to the same image features with tonic depolarisations (Figure 4.7E).

A means for overcoming the transient hyperpolarizations in the model responses is to include temporal high-pass filtering on the inputs to the correlator. However, the model used in this paper already has high-pass filtering implemented on its inputs, based on observations from recordings from the lamina monopolar cells (LMCs) in *Eristalis tenax* (James, 1990). The response properties of the LMCs have been extensively studied and can be approximated by high-pass filtering in space and time (James, 1990; Laughlin, 1981; Srinivasan, Laughlin & Dubbs, 1982). This has been shown to be effective for removing redundant information in the visual input and enhancing edge-like boundaries (Srinivasan et al., 1982; Srinivasan, Pinter & Osorio, 1990). The observation that the hyperpolarizing transients persist despite the implementation of temporal filtering to the level of the LMCs, suggests that the biological motion-processing pathway may also have additional temporal high-pass characteristics at least one serial stage of processing after LMCs. Alternatively, it is also possible that the filtering characteristics of early visual processing in flies are adapting to match the spatial and temporal structure of the prevailing stimulus, such that the observations based on white noise stimuli no longer reflect LMC response properties in more natural conditions (Kim & Rieke, 2001).

4.5.3 Nonlinear spatial integration across the receptive field

The spatial integration properties of LPTCs have been studied thoroughly (Borst, Egelhaaf & Haag, 1995, Gauck & Borst, 1999, Haag, Egelhaaf & Borst, 1992, Hausen, 1982b, Single, Haag & Borst, 1997). As the size of a stimulus increases, the response of the LPTCs saturate significantly. Single et al. (1997) showed that this could be predicted by a compartment model of the LPTC if the opponent operation from a Reichardt correlator-type local-motion element occurs on its dendrites, because motion in one direction jointly activates both excitatory and inhibitory conductance's.

Nonlinearity in spatial integration, such as that mentioned above, has a compressive effect on the spatial integration of local motion responses (Borst et al., 1995, Haag et al., 1992, Elyada et al., 2009). Yet, when we varied the area of a natural image across the receptive field of HSNE, we saw that the neurons response increased relatively linearly up to an image height of about 50° (Figure S4.3). Interestingly, our model, which linearly summed local motion responses across the receptive field, began to saturate at smaller image sizes than the neuronal recording. The sub-linear response of the model results from spatial sensitivity profile of the receptive fields of these neurons, because as a stimulus gets larger it first spreads into areas of the receptive field that have weaker sensitivity and then beyond the bound of the receptive field. The observation that the neuron shows a more linear increase in response with image height than our model suggests that under these conditions the neuron may be integrating local motion signals supra-linearly.

The HSN neuron shows observed pattern dependence that is far more erratic than that predicted from the local motion responses we recorded and the neurons receptive field (Figure 4.8). In these examples it would appear as if integration across the receptive field is having the effect of sharpening the response to local pattern features within the image. This is most apparent for the 'Car Park' image (Figure 4.8B), where although the prediction captures the two main depolarising 'bumps', the whole receptive field response includes many sharp de- and hyperpolarizations

within these (Figure 4.8). This observation does not appear to hold true for the HSNE, which much better matched with the prediction (Figure 4.8).

4.5.4 Function of the narrow male HSN in feature detection

Despite having a putative role in the processing of rotatory optic-flow, the male HSN has an extremely narrow receptive field (Nordström et al., 2008). Such a narrow receptive field is poorly optimised for averaging out residual pattern dependent response fluctuations. What role, then, might the male HSN serve in optic flow processing? Nordström et al. argued that the small frontally oriented receptive of HSN was ideally positioned, at the pole of expansion for forward translation, to disambiguate rotatory and translatory optic-flow fields.

Male hoverflies have very distinctive behaviour, often hovering in a stationary position for many minutes before switching flight modes and shooting off to chase conspecifics that encroach into their territory. Hovering perfectly stationarily is a challenging task and hoverflies will often place themselves in small openings in the foliage or on the edges of bushes. In windy conditions, these animals can often be observed continually adjusting their hovering position, staying in sink with the swaying foliage immediately adjacent to them. The vertically elongated, narrow receptive field shape of the male HSN neuron along with its increased sensitivity to structural features within natural scenes is well adapted to respond strongly to prominent vertically aligned edges and thus, may be an important adaptation to aid in controlled hovering.

4.6 Experimental Procedures

4.6.1 Experiments and neuron identification

We used wild caught drone flies, *Eristalis tenax,* immobilized with wax and mounted 14-15 cm in front of the stimulus display. We performed sharp electrode intracellular recordings on Horizontal System (HS) neurons in the left lobula plate using aluminosilicate electrodes pulled on a Sutter Instruments P97 electrode puller with a 3 x 3 mm box filament. Electrodes were filled with 2 M KCl and typically had tip resistances of 80-250 MΩ. Upon successful penetration, we identified each neuron on-line based on its receptive field properties, as recently described in detail by Nordström et al. (2008).

4.6.2 Data acquisition and analysis

Data were digitised at 5 kHz using a 16-bit A/D converter (National Instruments, Austin Texas, United States) and analysed off-line with Matlab (http://www.mathworks.com). In all experiments, we normalized the response to the resting membrane potential. HS neurons are ideal models to investigate the nature of signals arriving at their synaptic inputs because they predominantly respond with graded shifts in membrane potential. However, activity-induced spikelets often influenced the response adding an additional nonlinearity to the axonally recorded membrane potential (Hengstenberg, 1977). To reduce the influence of such spikelets in our analysis, we 'spike filtered' our data by removing spike-like events and replacing them with the local mean membrane potential (Nordström & O'Carroll, 2009). Where we have shown neural pattern dependence, we have attempted to minimize the effects of adaptation on our results by presenting each image several times (minimum of 4) with each subsequent presentation at a different start phase (see Figure 4.1).

4.6.3 Statistics

We performed cross-covariance analysis (r) in Matlab (http://www.mathworks.com) to compare pattern dependence between conditions and with model predictions. Where we have quoted cross-covariance coefficients, they have been taken at zero lag between the two data, i.e. when the data are time aligned with each other, unless otherwise mentioned. Wilcoxon signed rank tests and t-tests were performed to determine significance using GraphPad Prism software (http://www.graphpad.com). All data are presented as mean ± standard deviation unless otherwise mentioned.

4.6.4 Image collection and display

The panoramic natural images used in the present paper were chosen from the image set used in Barnett et al, (2009) and represent various field sites around South Australia. Scenes ranged from densely forested areas (e.g. 'Botanic', 'Creek bed', 'Hamlin'; Figure S4.1), to vast open hillsides (e.g. 'Field'), and to entirely man-made environments ('Car park'; Figure S4.1). Figure S4.1 shows the full complement of the seven panoramic images used in this paper. We collected images using a Nikon D-70 digital camera and panoramic tripod head. These images are available from Russell Brinkworth upon request (russell.brinkworth@adelaide.edu.au). We displayed images on a linearized, 8-bit, RGB CRT at 200 Hz refresh rate with mean luminance of 100 cd/m^2 using VisionEgg software (www.visionegg.org). The display subtended approximately 100° x 75° of the fly's visual field. In several experiments, we used artificial manipulation of image contrast to probe the HS neurons' responses. We artificially reduced the contrasts of natural images by scaling the value for each pixel (I_{final}) about the mid-grey level of our display such that to $I_{final} = C(I_{image} - 0.5) + 0.5$, I_{image}, is a floating-point number from 0 to 1 representing luminance intensity in the original image and C is the contrast scaling factor (Straw et al., 2008).

4.6.5 Local motion detector analysis

To investigate local motion responses, we windowed our stimulus to the size of only a couple of local motion sensitive elements (Figure 4.6). The stimulus window was a 5°x 5° square window located at -10 of azimuth on the equator in the frontal visual

field of the fly, such that the central rows of the image were visible through it (Figure 4.6). Experiments using the window stimulus evoke only weak responses and thus require averaging over many identical trials to isolate neural response from noise (see Figure 4.6C). To allow us to collect the equivalent of local responses in fewer trials, we adapted a method originally developed to study local motion detector responses to grating patterns (Egelhaaf et al., 1989, Reichardt & Egelhaaf, 1988). We extended the height of single image rows and the stimulus window to stretch across many vertically aligned local motion sensitive elements, such that the widow was now a slit 5° wide by 50° high. The stimulus image was vertically blurred to account for the optics of *Eristalis tenax* (Straw et al., 2006). The resultant neural response is much larger and effectively equivalent to the sum of many individual local motion sensitive elements viewing the same image row (Egelhaaf et al., 1989, Reichardt & Egelhaaf, 1988). This allowed us to obtain full response maps for six cells and two images in recordings that were greater than an hour in duration.

4.6.6 Model predictions

We used an elaborated Hassenstein – Reichardt correlator model for motion detection to get a prediction of pattern dependence in the response of HSN and HSNE neurons. This model incorporated many of the spatial and temporal filtering processes known to occur on the motion-processing pathway of *Eristalis.* A full description of the model used to generate predicted responses has been included as Supplemental data. Briefly, the model was the sum of an array of local motion detectors of the Reichardt correlator type that were weighted by average receptive fields for these neurons as published in Nordtröm et al, (2008). For obtain local motion detector predicted pattern dependence (Figure 4.8), we combined the responses recorded to natural images using the slit window stimulus and then weighted them with the average local motion sensitivity of the neurons' receptive fields.

Acknowledgements:

We are greatly indebted to the Adelaide, Mt Lofty, and Wittunga Botanical gardens for allowing us to collect healthy wild hoverflies within their grounds all year round. We would also like to thank Dr Russell Brinkworth and Dr Karin Nordström for comments and help with the manuscript and with the development of experiments. This work was funded by ARC (LP 0667744).

4.7 References

1. Borst, A., & Egelhaaf, M. (1992). Invivo imaging of calcium accumulation in fly interneurons as elicited by visual-motion stimulation. *Proceedings of the National Academy of Sciences of the United States of America, 89* (9), 4139-4143.

2. Borst, A., Egelhaaf, M., & Haag, J. (1995). Mechanisms of Dendritic Integration Underlying Gain-Control in Fly Motion-Sensitive Interneurons. *Journal of Computational Neuroscience, 2* (1), 5-18.

3. Borst, A., & Haag, J. (2002). Neural networks in the cockpit of the fly. *Journal of Comparative Physiology a-Neuroethology Sensory Neural and Behavioral Physiology, 188* (#), 419-437.

4. Clifford, C.W.G., & Ibbotson, M.R. (2002). Fundamental mechanisms of visual motion detection: models, cells and functions. *Progress in Neurobiology, 68* (6), 409-437.

5. Cuntz, H., Haag, J., Forstner, F., Segev, I., & Borst, A. (2007). Robust coding of flow-field parameters by axo-axonal gap junctions between fly visual interneurons. *Proceedings of the National Academy of Sciences of the United States of America, 104* (24), 10229-10233.

6. Dror, R.O., O'Carroll, D.C., & Laughlin, S.B. (2001). Accuracy of velocity estimation by Reichardt correlators. *Journal of the Optical Society of America a-Optics Image Science and Vision, 18* (2), 241-252.

7. Dvorak, D., Srinivasan, M., & French, A. (1980). The contrast sensitivity of fly movement-detecting neurons. *Vision Research, 20*, 397-407.

8. Egelhaaf, M., & Borst, A. (1993). A Look into the Cockpit of the Fly - Visual Orientation, Algorithms, and Identified Neurons. *Journal of Neuroscience, 13* (11), 4563-4574.

9. Egelhaaf, M., Borst, A., & Reichardt, W. (1989). Computational structure of a biological motion-detecting system as revealed by local detector analysis in the flys nervous-system. *Journal of the Optical Society of America a-Optics Image Science and Vision, 6* (7), 1070-1087.

10. Elyada, Y.M., Haag, J., & Borst, A. (2009). Different receptive fields in axons and dendrites underlie robust coding in motion-sensitive neurons. *Nature Neuroscience, 12* (3), 327-332.

11. Farrow, K., Borst, A., & Haag, J. (2005). Sharing receptive fields with your neighbors: Tuning the vertical system cells to wide field motion. *Journal of Neuroscience, 25* (15), 3985-3993.

12. Franz, M.O., & Krapp, H.G. (2000). Wide-field, motion-sensitive neurons and matched filters for optic flow fields. *Biological Cybernetics, 83* (3), 185-197.

13. Gauck, V., & Borst, A. (1999). Spatial response properties of contralateral inhibited lobula plate tangential cells in the fly visual system. *Journal of Comparative Neurology, 406* (1), 51-71.

14. Geurten, B.R.H., Nordstrom, K., Sprayberry, J.D.H., Bolzon, D.M., & O'Carroll, D.C. (2007). Neural mechanisms underlying target detection in a dragonfly centrifugal neuron. *Journal of Experimental Biology, 210* (18), 3277-3284.

15. Gronenberg, W., Milde, J.J., & Strausfeld, N.J. (1995). Oculomotor control in calliphorid flies - organization of descending neurons to the neck motor - responding to visual stimuli. *Journal of Comparative Neurology, 361* (2), 267-284.

16. Haag, J., & Borst, A. (2004). Neural mechanism underlying complex receptive field properties of motion-sensitive interneurons. *Nature Neuroscience, 7* (6), 628-634.

17. Haag, J., & Borst, A. (2005). Dye-coupling visualizes networks of large-field motion-sensitive neurons in the fly. *Journal of Comparative Physiology a-Neuroethology Sensory Neural and Behavioral Physiology, 191* (5), 445-454.

18. Haag, J., Egelhaaf, M., & Borst, A. (1992). Dendritic Integration of Motion Information in Visual Interneurons of the Blowfly. *Neuroscience Letters, 140* (2), 173-176.

19. Haag, J., Wertz, A., & Borst, A. (2007). Integration of lobula plate output signals by DNOVS1, an identified premotor descending neuron. *Journal of Neuroscience, 27* (8), 1992-2000.

20. Harris, R.A., O'Carroll, D.C., & Laughlin, S.B. (2000). Contrast gain reduction in fly motion adaptation. *Neuron, 28* (1,22), 595-606.

21. Hausen, K. (1982a). Motion Sensitive Interneurons in the Optomotor System of the Fly .1. The Horizontal Cells - Structure and Signals. *Biological Cybernetics, 45* (2), 143-156.

22. Hausen, K. (1982b). Motion Sensitive Interneurons in the Optomotor System of the Fly .2. The Horizontal Cells - Receptive-Field Organization and Response Characteristics. *Biological Cybernetics, 46* (1), 67-79.

23. Hengstenberg, R. (1977). Spike response of "non-spiking" visual interneurone. *Nature, 270*, 338-340.

24. Huston, S.J., & Krapp, H.G. (2008). Visuomotor transformation in the fly gaze stabilization system. *Plos Biology, 6* (7), 1468-1478.

25. James, A.C. (1990). White-noise studies in the fly Lamina. PhD (Canberra: Australian National University.

26. Kim, K.J., & Rieke, F. (2001). Temporal contrast adaptation in the input and output signals of salamander retinal ganglion cells. *Journal of Neuroscience, 21* (1), 287-299.

27. Krapp, H.G., Hengstenberg, B., & Hengstenberg, R. (1998). Dendritic structure and receptive-field organization of optic flow processing interneurons in the fly. *Journal of Neurophysiology, 79* (4), 1902-1917.

28. Krapp, H.G., & Hengstenberg, R. (1996). Estimation of self-motion by optic flow processing in single visual interneurons. *Nature, 384* (6608), 463-466.

29. Krapp, H.G., Hengstenberg, R., & Egelhaaf, M. (2001). Binocular contributions to optic flow processing in the fly visual system. *Journal of Neurophysiology, 85* (2), 724-734.

30. Lappe, M., Bremmer, F., & van den Berg, A.V. (1999). Perception of self-motion from visual flow. *Trends in Cognitive Sciences, 3* (9), 329-336.

31. Laughlin, S.B. (1981). Neural principles in the peripheral visual system of invertebrates. In: H. Autrum (Ed.) *Handbook of Sensory Physiology* (Berlin: Springer.

32. Maddess, T., & Laughlin, S.B. (1985). Adaptation of the Motion-Sensitive Neuron H-1 Is Generated Locally and Governed by Contrast Frequency. *Proceedings of the Royal Society of London Series B-Biological Sciences, 225* (1239), 251-275.

33. Nordström, K., & O'Carroll, D.C. (2009). The motion after-effect: local and global contributions to contrast sensitivity. *Proceedings of the Royal Society B-Biological Sciences, 276* (1662), 1545-1554.

34. Nordström, N., Barnett, P.D., Moyer de Miguel, I.M., Brinkworth, R.S.A., & O'Carroll, D.C. (2008). Sexual dimorphism in the hoverfly motion vision pathway. *Current Biology, 18*, 661-667.

35. Reichardt, W. (1987). Evaluation of optical motion information by movement detectors. *Journal of Comparative Physiology a-Sensory Neural and Behavioral Physiology, 161* (4), 533-547.

36. Reichardt, W., & Egelhaaf, M. (1988). Properties of individual movement detectors as derived from behavioral experiments on the visual system of the fly. *Biological Cybernetics, 58* (5), 287-294.

37. Ruderman, D.L. (1994). The statistics of natural images. *Network-Computation in Neural Systems, 5*, 517-548.

38. Shoemaker, P.A., & O'Carroll, D.C. (2005). Insect-based visual motion detection with contrast adaptation. *Infrared Technology and Applications XXXI,* 5783 (pp. 292-303): SPIE.

39. Shoemaker, P.A., O'Carroll, D.C., & Straw, A.D. (2005). Velocity constancy and models for wide-field visual motion detection in insects. *Biological Cybernetics, 93* (1,24), 275-287.

40. Simoncelli, E.P., & Olshausen, B.A. (2001). Natural image statistics and neural representation. *Annual Review of Neuroscience, 24*, 1193-1216.

41. Single, S., Haag, J., & Borst, A. (1997). Dendritic computation of direction selectivity and gain control in visual interneurons. *Journal of Neuroscience, 17* (16), 6023-6030.

42. Srinivasan, M.V., Laughlin, S.B., & Dubs, A. (1982). Predictive coding - a fresh view of inhibition in the retina. *Proceedings of the Royal Society of London Series B-Biological Sciences, 216* (1205), 427-459.

43. Srinivasan, M.V., & Dvorak, D.R. (1979). Waterfall illusion in an insect visual-system. *Vision Research, 19* (12), 1435-1437.

44. Srinivasan, M.V., Pinter, R.B., & Osorio, D. (1990). Matched filtering in the visual system of the fly - large monopolar cells of the lamina are optomized to detect moving edges and blobs. *Proceedings of the Royal Society of London Series B-Biological Sciences, 240* (1298), 279-293.

45. Strausfeld, N.J. (1976). Atlas of an Insect brain. (Berlin: Springer.

46. Strausfeld, N.J., & Bassemir, U.K. (1985). Lobula plate and ocellar interneruons converge onto a cluster of decending neurons leading to the neck and leg motor neuropil in Calliphora-erythrocephala *Cell and Tissue Research, 240* (3), 617-640.

47. Strausfeld, N.J., & Seyan, H.S. (1985). Convergence of visual, haltere, and prosternal inputs at the neck motor neurons of calliphora-erythrocephala. *Cell and Tissue Research, 240* (3), 601-615.

48. Straw, A.D., Rainsford, T., & O'Carroll, D.C. (2008). Contrast sensitivity of insect motion detectors to natural images. *Journal of Vision, 8(3):32*, 1-9.

49. Straw, A.D., Warrant, E.J., & O'Carroll, D.C. (2006). A 'bright zone' in male hoverfly (*Eristalis tenax*) eyes and associated faster motion detection and increased contrast sensitivity. *Journal of Experimental Biology, 209*, 4339-4354.

50. Wertz, A., Borst, A., & Haag, J. (2008). Nonlinear integration of binocular optic flow by DNOVS2, a descending neuron of the fly. *Journal of Neuroscience, 28* (12), 3131-3140.

Supplemental data

4.7.1 Natural scenes

We chose a set of panoramic natural images taken from the study done by Barnett et al. (2009, submitted; Chapter 3) as a representation of the natural scenes that flying insects might encounter (Figure S4.1). The scenes were chosen to represent a large spread of different environments ranging from highly cluttered bush and woodland scenes to barren field scenes. We also included a couple of images with prominent man made objects, e.g. 'Library' and 'Car park' (Figure S4.1).

Figure S4.1 Natural image panoramas

The seven natural panoramic images used in this study taken from Barnett et al., (2009, submitted; Chapter 3). The panoramic natural images were chosen to represent a wide range of natural and urban environments. Note that some of the images have many prominent vertical edges (A), whereas others have few prominent vertical features (D). A. 'Car park' image; B. 'Hamlin' image; C. 'Botanic' image; D. 'Library' image; E. 'Field' image; F. 'Creek bed' image; and G. 'Close' image.

4.7.2 Model predictions of pattern dependence

As a predictor of neural response, we used an elaborated correlation based model for motion detection (Figure S4.2). The model includes spatial and temporal filtering matched to *Eristalis tenax* optics, early visual processing, and motion correlation, to ensure that model output reflects the spatio-temporal pass-band of the insect motion-sensitive neurons we recorded from (Figure S4.2A). The elaborated correlation model (Figure S4.2A) had an interreceptor angle of $\Delta\phi$=1.1°, which is a physiologically realistic value for the separation of frontally orientated elementary motion detectors (EMDs) in *Eristalis* (Straw, Warrant & O'Carroll, 2006). Spatial pre-filtering was implemented as a two dimensional gaussian blur $\Delta\rho$=1.4°, which approximates the acceptance function of typical fly photoreceptors (Dror, O'Carroll & Laughlin, 2001, Hardie, 1985). Temporal pre-filtering was based on the work of James (1990) who characterized the response of *Eristalis* large monopolar cells (LMCs) to white noise stimuli. James showed that LMC responses could be modelled as the difference of two log normals with different time constants. At high light levels he found typical values of t_p=10.3ms and σ=0.236 for the positive log normal and t_p=15.6ms and σ=0.269 for the negative log normal, where t_p represents the time to peak of the curve and σ is a dimensionless parameter that determines the curves width (Dror et al., 2001, Payne & Howard, 1981). The delay was implemented as a first-order low-pass filter with a time constant, τ, of 31ms.

In order to predict pattern noise, we needed to incorporate the receptive fields of the neurons we recorded from. Recently, we published (Chapter 2) detailed results on the receptive field properties of HS neurons in the hoverfly, *Eristalis tenax* (Nordström, Barnett, Moyer de Miguel, Brinkworth & O'Carroll, 2008). To model the receptive field, we weighted the outputs of an array of elaborated EMDs with the average receptive fields shown in Chapter 3 (Nordström, Barnett, Moyer de Miguel, Brinkworth & O'Carroll, 2008). Model output was taken as the sum of these weighted local responses (Figure S4.2B). However, the absolute time-averaged model responses varied by more than 45-fold across the image set, so for Figure 4.3 and 4.5 we normalized model output by the maximum neural response for each image to allow us to display model and neuron responses on the same vertical axis.

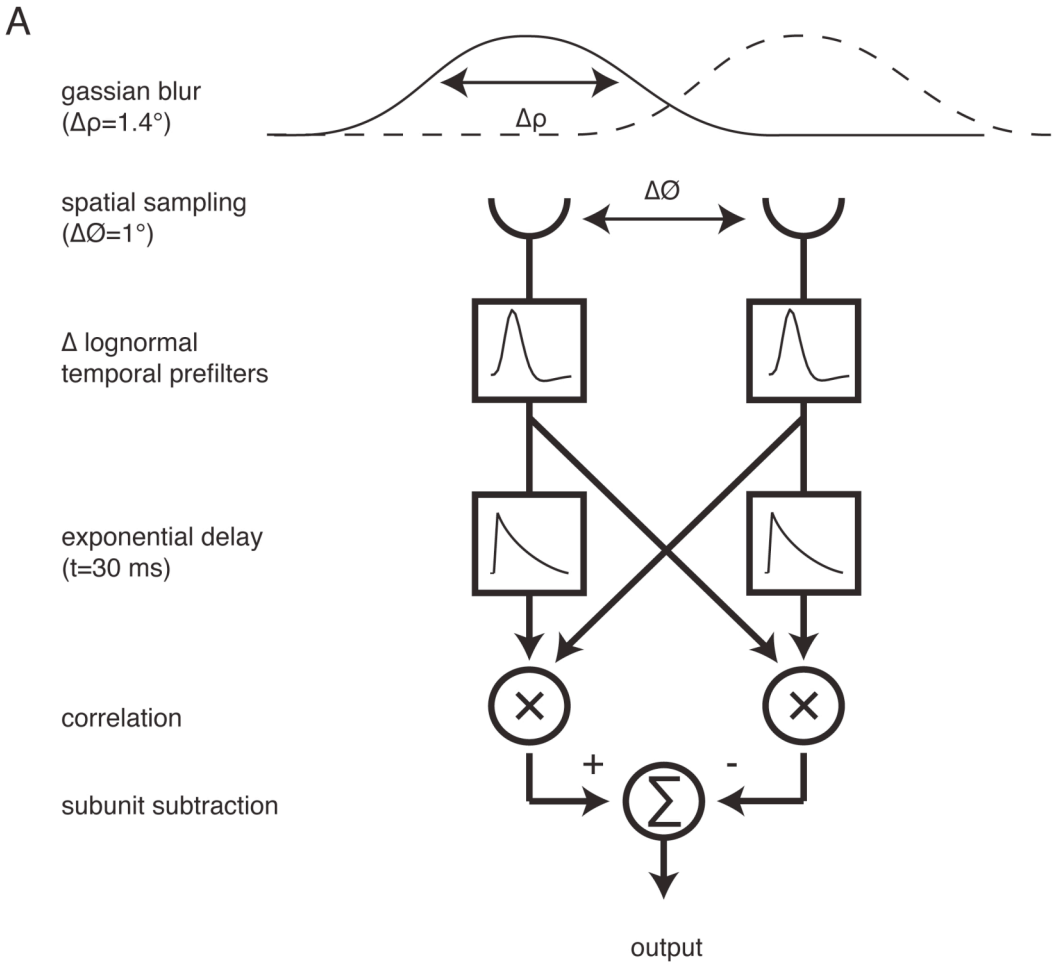
A
gassian blur
(Δρ=1.4°)
Δρ
spatial sampling
(ΔØ=1°)
ΔØ
Δ lognormal
temporal prefilters
exponential delay
(t=30 ms)
correlation
subunit subtraction
+
-
output

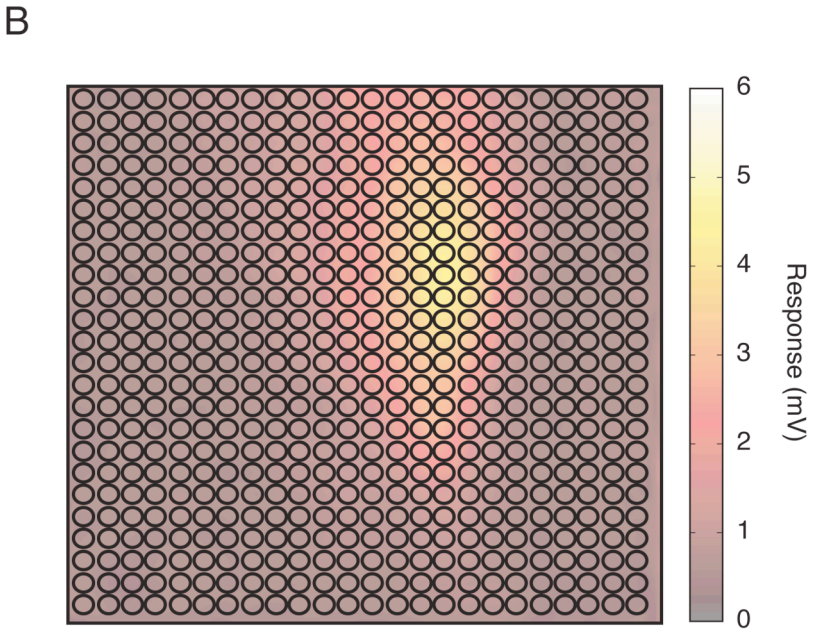
B
6
5
4
3
2
1
0
Response (mV)

Figure S4.2 Reichardt correlator

A. Shows a schematic of the elaborated Hassenstein–Reichardt correlator (EMD) model used. S, spatial low-pass filters on the luminance input. T, temporal band-pass filtering. D, delay implemented as a first-order low-pass filter. B. Shows the average receptive field strength of male HSN neuons in hoverflies, *Eristalis tenax*, taken from Nordström et al. (2008; Chapter 2). Response strengths are indicated in mV by the colour bar. Superimposed is a representative array of EMDs shown as black circles, note that for display purposes these are not scaled to their actual size relative to the receptive field. We weighted local EMD responses by the average local motion sensitivities from within the neurons receptive and then linearly summed the weighted outputs.

4.7.3 Justification for using weighted linear spatial integration of local motion responses

To integrate local motion responses across the receptive field we took a receptive field weighted linear sum of EMD outputs. However, there is a large base of literature established which indicates significant nonlinearity in the spatial integration properties of LPTCs (Borst, Egelhaaf & Haag, 1995, Gauck & Borst, 1999, Haag, Egelhaaf & Borst, 1992, Hausen, 1982, Single, Haag & Borst, 1997). As the size of a stimulus increases, the response of the LPTCs saturate significantly. Single et al. (1997) showed that this could be predicted by a compartment model of the LPTC if the subtraction operation of a Reichardt correlator type local motion element (Figure S4.2) occurs on its dendrites, because motion in one direction jointly activates both excitatory and inhibitory conductances with a ratio that depends upon pattern velocity.

None of the previous studies investigating the spatial integration properties of LPTCs had considered the integration of natural images though. Thus to test how local motion responses are integrated when natural images are used as stimuli, we recorded the response of an HSNE to images with varying vertical extent. We compared the response of the neuron with that of the EMD model, where integration across the receptive field was simulated as weighted linear sum (Figure S4.3). The implemented receptive field properties of these neurons already mean that the model response shows a sub-linear relationship with increasing image height (Figure S4.3). As image height increases, more of the image extends beyond the 'hot spot' of the receptive field into less responsive regions. Consequently, increases in image height greater than 50° yield a negligible increase in model response (Figure S4.3). Although the neuron shows a similar plateau for image heights above 50°, for image heights below this, response appears to increase approximately linearly with increasing stimulus height (Figure S4.3). Thus, once the limited receptive field size and variability in local motion sensitivity across it are considered, these neurons appear to spatial integrate local responses to natural images in a supra-linear way.

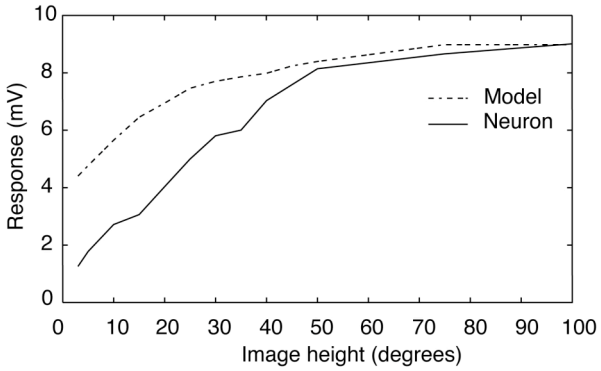

Figure S4.3 Spatial integration

We varied the extent of the visible region of the 'Botanic' image by windowing the stimulus about the central row of the image whilst rotating the panorama at a constant velocity of 45°/s as per the other experiments. The Figure shows neuron response (dotted line) and model response (dashed line) to different stimulus heights in degrees. Model response is normalized to the maximum neural response.

4.8 Supplemental References

1. Borst, A., Egelhaaf, M., & Haag, J. (1995). Mechanisms of Dendritic Integration Underlying Gain-Control in Fly Motion-Sensitive Interneurons. Journal of Computational Neuroscience, 2 (1), 5-18.

2. Dror, R.O., O'Carroll, D.C., & Laughlin, S.B. (2001). Accuracy of velocity estimation by Reichardt correlators. Journal of the Optical Society of America a-Optics Image Science and Vision, 18 (2), 241-252.

3. Gauck, V., & Borst, A. (1999). Spatial response properties of contralateral inhibited lobula plate tangential cells in the fly visual system. Journal of Comparative Neurology, 406 (1), 51-71.

4. Haag, J., Egelhaaf, M., & Borst, A. (1992). Dendritic Integration of Motion Information in Visual Interneurons of the Blowfly. Neuroscience Letters, 140 (2), 173-176.

5. Hardie, R.C. (1985). Functional organization of the fly retina. In: D. Ottoson (Ed.) Progress in sensory physiology, 5 (pp. 1-80). Berlin: Springer-Verlag.

6. Hausen, K. (1982). Motion Sensitive Interneurons in the Optomotor System of the Fly .2. The Horizontal Cells - Receptive-Field Organization and Response Characteristics. Biological Cybernetics, 46 (1), 67-79.

7. James, A.C. (1990). White-noise studies in the fly Lamina. PhD (Canberra: Australian National University.

8. Nordström, N., Barnett, P.D., Moyer de Miguel, I.M., Brinkworth, R.S.A., & O'Carroll, D.C. (2008). Sexual dimorphism in the hoverfly motion vision pathway. Current Biology, 18, 661-667.

9. Payne, R., & Howard, J. (1981). Response of an insect photoreceptor: a simple log-normal model. Nature, 290, 415-416.

10. Single, S., & Borst, A. (1998). Dendritic integration and its role in computing image velocity. Science, 281 (5384), 1848-1850.

11. Single, S., Haag, J., & Borst, A. (1997). Dendritic computation of direction selectivity and gain control in visual interneurons. Journal of Neuroscience, 17 (16), 6023-6030.

12. Straw, A.D., Warrant, E.J., & O'Carroll, D.C. (2006). A 'bright zone' in male hoverfly (Eristalis tenax) eyes and associated faster motion detection and increased contrast sensitivity. Journal of Experimental Biology, 209, 4339-4354.

Chapter 5:
Local motion detection: temporal and spatial modulation of gain and transient responses to features

5.1 Context

In the previous two chapters, we explored HS neurons responses to natural images at both the local and global level. We show that the reliable encoding of natural images, likely results from a combination of static and dynamic nonlinearities that act as powerful response normalisers to images that would otherwise produce highly variable responses. These active normalization strategies appear to operating on both a local and global scale.

In this paper, we investigate the transient response properties of the HS neurons to discreet features. The aim of the chapter is to investigate transient feature-feature interactions that might be locally modulating the neurons gain, and thus response to natural image. We use variants of local stimulus method, the *slit-windowed stimulus*, used in the previous chapter to investigate local transient responses to image features and their influence on local response gain.

Local motion detection: temporal and spatial modulation of gain and transient responses to features

Paul D. Barnett[1,], Karin Nordström[1,2], and David C. O'Carroll[1]*

[1]School of Molecular and Biomedical Science, The University of Adelaide, SA 5005, Australia

[2]Department of Neuroscience, Uppsala University Biomedical Centre, Box 593, 75124 Uppsala, Sweden

*To whom correspondence should be addressed. Email paul.barnett@adelaide.edu.au. Phone +61 8 8303 6216.

Key words: Motion adaptation; Reichardt correlator; Motion detection; Insect vision; Spatial integration; Contrast sensitivity

Abbreviations: alternating current (AC); direct current (DC); elementary motion detector EMD; horizontal system (HS); lobula plate tangential cell (LPTC); motion after effect (MAE).

5.2 Summary

Background: Interpreting motion of the natural environment is a challenging visual task. Natural scenes have enormous variance in brightness, contrast and spatial structure. Several recent studies have shown that neurons on the motion-processing pathway in flies are able to make robust estimates of image velocity when shown natural images, an observation poorly predicted by models that otherwise predict their response properties to simple experimenter defined stimuli. We investigated how local features within scenes influence local transient responses to subsequent features and thus contribute to the normalization of global responses to motion of complex patterns.

Method: We recording intracellular local-motion responses of identified motion-sensitive neurons in the third optic ganglion of the hoverfly, *Eristalis tenax*. We adapted a method originally developed to study local motion responses to sine wave gratings, which limits the stimulus to a small vertically elongated strip, to investigate local and global neural responses to stimuli that are designed to interact with each other in the temporal and spatial domain.

Results: Correlation-based models for motion detection predict local motion responses well for relatively simple stimuli. However, when image features are combined, neural responses show additional response characteristics. We show that after the passing of a high contrast feature local motion detectors transiently show reduced gain. However, this gain reduction appears to be recruited only when features stretch across several neighbouring ommatidia and are aligned perpendicular to their direction of feature motion.

Conclusion: Local gain reduction is gated by the simultaneous activation of local motion sensitive elements. Features in natural scenes with vertically aligned edges, such as tree, which would be most likely drive motion detectors strongly would also be expected to recruit the greatest amount of response suppression. Mechanisms such as this may facilitate more robust neural encoding of otherwise highly variable natural scenes.

5.3 Introduction

The Reichardt correlator is generally accepted to underlie local motion computation in insects (Borst & Egelhaaf, 1989, Borst & Haag, 2002, Clifford & Ibbotson, 2002, Haag, Denk & Borst, 2004, Hassenstein & Reichardt, 1956). However, it generates ambiguous estimates of image velocities because it is sensitive to additional parameters, such as image contrast and spatial structure. Although many behavioral and neurophysiological response properties corroborate with the predictions of the correlator (Borst & Egelhaaf, 1989, Borst & Haag, 2002, Clifford & Ibbotson, 2002, Hassenstein & Reichardt, 1956, Reichardt, 1961), substantial evidence suggests that insects use apparent retinal velocities to control navigation (Baird, Srinivasan, Zhang & Cowling, 2005, Esch & Burns, 1996, Ronacher & Wehner, 1995, Srinivasan, Lehrer, Kirchner & Zhang, 1991, Srinivasan, Zhang, Lehrer & Collett, 1996).

The lobula plate tangential cells (LPTCs) pool inputs from large arrays of elementary motion detectors (EMDs) with Reichardt correlator-like response properties (Borst & Egelhaaf, 1989, Borst & Haag, 2002, Egelhaaf, Borst & Reichardt, 1989, Reichardt & Egelhaaf, 1988, Single, Haag & Borst, 1997). They have been show to be involved in behavioral responses to moving patterns (Borst & Bahde, 1988, Geiger & Nässel, 1981, Hausen & Wehrhahn, 1983, Heisenberg, Wonneberger & Wolf, 1978) and have complex receptive fields suggesting an important role in visually guided navigation (Franz & Krapp, 2000, Krapp, Hengstenberg & Hengstenberg, 1998, Krapp & Hengstenberg, 1996, Krapp, Hengstenberg & Egelhaaf, 2001). When stimulated with sinusoidal grating, LPTCs show a dependence on pattern contrast and spatial frequency as predicted by the Reichardt correlator (Eckert, 1980, Harris, O'Carroll & Laughlin, 2000, Srinivasan & Dvorak, 1980, Straw, Warrant & O'Carroll, 2006).

However, in the natural environment, the visual system encounters scenes that vary enormously in these very parameters (Ruderman & Bialek, 1994, Tolhurst, Tadmor & Chao, 1992). When natural images are used as stimuli, the LPTCs respond independent of such parameters and encode images velocity robustly (Straw, Rainsford & O'Carroll, 2008, Barnett et al., 2009, submitted; Chapter 3). HS neuron

responses to natural images are hard to reconcile with both their response characteristics to experimenter-defined stimuli, such as sine gratings, and the outputs of correlation-based schemes for motion detection (Dror, O'Carroll & Laughlin, 2001, Shoemaker, O'Carroll & Straw, 2005, Straw et al., 2008).

What additional neural processing might enable LPTCs to encode the velocity of natural images accurately? Although non-linear spatial integration might mitigate much global variability (Haag et al, 1992, Borst et al., 1995, Elyada et al., 2009), our recent work suggests that it is unlikely that static compressive non-linearities such as response saturation alone can explain the robust encoding of image velocity (Barnett et al., 2009, submitted; Chapters 3 and 4). However, dynamic changes to global motion encoding could contribute to the normalisation of neural responses (Chapter 3). Furthermore, it is difficult to predict the *global* neural response based on the integration of responses to *local* features (Chapter 4).

Could adaptive mechanisms such as local gain control be contributing to the observed velocity constancy? Harris et al. (2000) showed that fly LPTCs adapt to visual motion with a powerful reduction in contrast gain (Harris et al., 2000). Such motion adaptation can be broken down into four main separate components (Harris et al., 2000, Kohn & Movshon, 2003, Nordström & O'Carroll, 2009, Neri & Laughlin, 2005). Two of these, the contrast gain reduction and the output range reduction, are non-directional, local components, which are substantially, or even entirely, reduced when testing and adapting in different parts of a neuron's receptive field. Two additional components, an activity dependent DC after-potential and a post-inhibitory AC component exert a global effect in adapted neurons by transferring to previously unstimulated parts of the receptive field (Nordström & O'Carroll, 2009).

Natural scenes often contain many high-contrasting, local features such as tree trunks, borders between the horizon and the sky, or other sharp boundaries between shaded and well illuminated areas. Although such features would generate locally transient responses from EMDs, it is possible that local adaptation following the passage of such features will alter the neural response to subsequent features, and thus affect the global response to natural scenes. Indeed, recent studies have

suggested that the dynamic nonlinear properties of neurons are likely to be optimised for the statistics of natural signals (Schwartz & Simoncelli, 2001).

To investigate this in more detail we decided to determine how local features within a scene interact with each other to recruit local adaptation. We recorded intracellularly from HS neurons, which respond with graded membrane potential changes making it possible to record changes that would otherwise be below the spike threshold. We have especially investigated how the temporal and spatial distribution of the same features affect local adaptive processes. We show that local high contrasting features recruit powerful local adaptation and suppress the response to subsequently seen features. We show that these interactions are rapid but extend beyond the interactions expected for simple correlation-based models. Finally, we show that this local gain reduction is facilitated by simultaneous activation of neighbouring motion sensitive elements.

5.4 Results:

5.4.1 Local motion detector analysis

To determine how local responses interact to generate the global response of fly LPTCs we developed two stimulus display modes. The *whole-screen* mode (Figure 5.1A) displays the entire stimulus across the width of the monitor allowing us to investigate neural responses following spatial integration (Figure 5.1B). The *slit-windowed* mode, adapted from a method originally developed to study local motion detector responses to grating patterns (Egelhaaf et al., 1989, Reichardt & Egelhaaf, 1988), limits the width of the stimulus to the size of only a couple of local EMDs (2.5º, Figure 5.1E). This enables us to investigate local response properties of just a few EMDs (Figure 5.1F).

The effectiveness of the slit-windowed stimulus in revealing local motion-detector properties is illustrated by figure 5.1. When we display a vertically limited (20° high) sinusoidally modulated luminance grating strip of near optimal spatial frequency (0.06 cycles/°, 90º/s) moving in the preferred direction, using the 'whole-screen' stimulus, the HS neuron responds with a tonic depolarisation of approximately 2.25 mV (Figure 5.1C). However, if we display the same grating strip using the slit-window, the HS neuron responds with pronounced time-dependent membrane potential fluctuations (Figure 5.1G). Despite the image continuously moving in the neuron's preferred direction, local motion responses often feature subtle hyperpolarizations. While the mean membrane potential is similar to the response generated using the whole-screen approach, hyperpolarizations reflect motion in the anti-preferred direction. Note that although this stimulus is designed to stimulate a single row of vertically aligned EMDs, windowing the stimulus does not necessarily limit exposure to one EMD, as the window is likely to stimulate parts of the neighbouring EMDs.

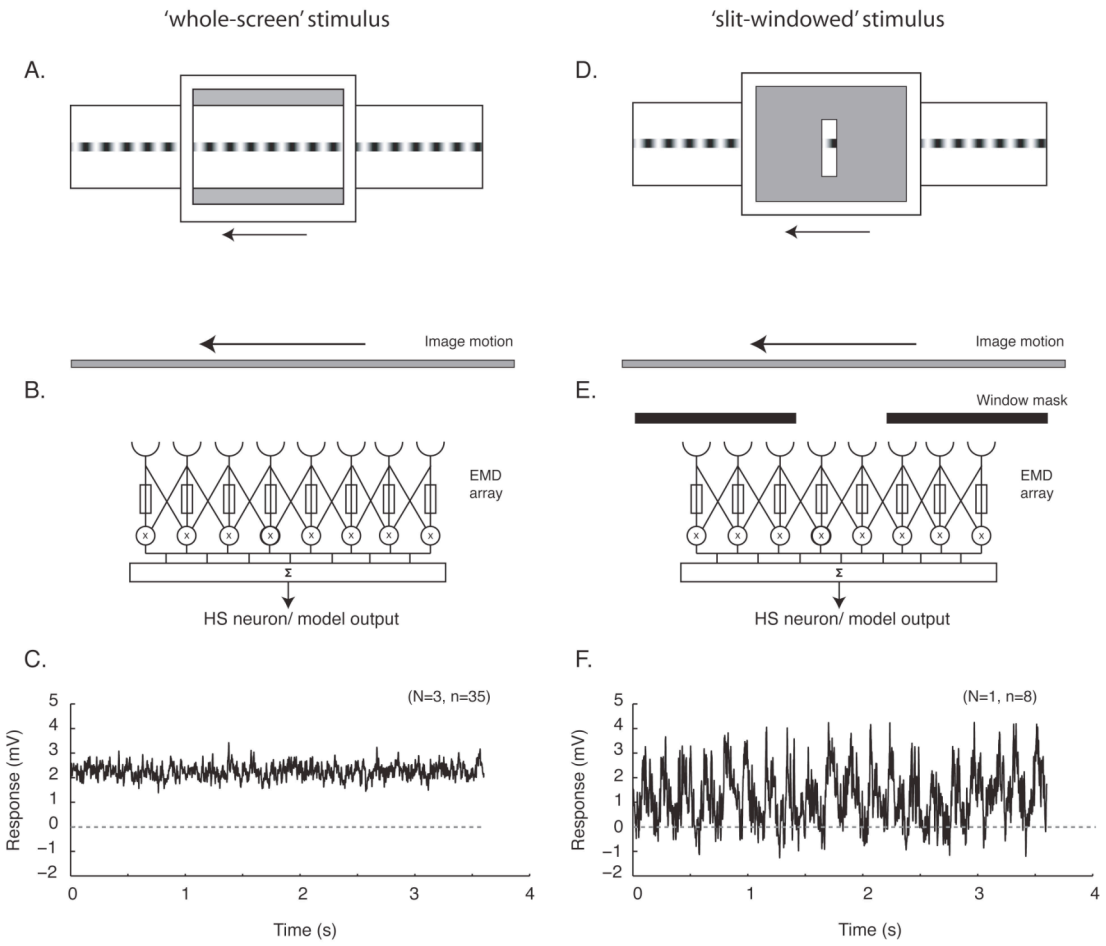

Figure 5.1 Slit window stimulus and local motion responses

A. A strip (20º) of a sinusoidally modulated luminance grating displayed at 90°/s with the whole screen mode. The whole screen mode is designed to stimulate large regions of the neuron's receptive field simultaneously, to investigate global response properties. B. A pictogram of the whole-window mode, showing how spatial integration across an array of EMDs (representing either the model or the neuron's dendritic tree) is un-attenuated using the whole screen mode. C. The neural response represents the spatial average across many EMDs and shows a tonic depolarization by the stimulus. E. The *slit windowed* mode, which horizontally limits the stimulus width horizontally. F. In this case only vertically aligned EMDs are stimulated. G. Using this stimulus regime, the local neural response shows pronounced pattern dependent fluctuations with a frequency doubling in the time domain.

5.4.2 Response characteristics of local motion-sensitive elements supplying the HS neurons

To investigate the influence of transient responses to locally discrete features more typical of those in natural scenes than the continuous grating stimuli in figure 5.1, we designed a simple stimulus comprising a square-wave, white-black luminance step on a mean luminance (grey) background, referred to as a '*doublet'* (Figure 5.2A and 5.2B). The doublet is 14° wide and 84° high (the height of the display). Although this apparently simple stimulus is actually more complex than a continuous sinusoid in terms of spatial frequency content, it has a fundamental row frequency of 0.053 cycles/°, just below optimum for *Eristalis* (Straw et al., 2006). Using the slit-window mode, we displayed the doublet at full and 10% contrast, in both the preferred and anti-preferred direction (Figure 5.2A and 5.2B). We flipped the doublet order before displaying in the anti-preferred direction, so that the temporal order of luminance change at a single point in space was the same in both directions, as is evident from the time-luminance traces (Figure 5.2C and 5.2D).

To investigate our stimulus from a motion detection theory perspective, we first consider the local response of an elaborated EMD model. We elaborated a Hassenstein-Reichardt correlation-based model with spatial and temporal filtering matched to the optics, early vision, and motion computation of *Eristalis tenax* (Dror et al., 2001, Straw et al., 2008) Barnett et al, 2009, submitted). For full details of the local model implementation and simulation see Chapter 4, Figure S4.2 and for slit windowing see Figure 5.1B and 5.1E in this chapter. We stimulated an array of such EMDs with the same stimuli as those used in neural recordings, i.e. taking full account of the slit window, if applied.

The slit window is 2.5° wide and thus just wide enough to stimulate a few neighbouring EMDs. When the doublet moves across the slit window the EMD model produces a complex triphasic response (Figure 5.2E). The stimulus is characterized by three contrast boundaries: grey-to-white, white-to-black, and black-to-grey (Figure 5.2A and 5.2B). The three peaks in the model output (arrowheads in Figure 5.2E) correlate well with the timing of each of these contrast boundaries,

albeit with a slight delay due to the low-pass filtering stages of the EMD. As expected from an EMD type model, where we implement the opponent stage as an equally weighted subtraction (Figure S4.2, Chapter 4), the output following motion in the anti-preferred direction is identical but inverted (Figure 5.2F). The arrowheads highlight the timing of the three peaks in these, and subsequent figures (Figure 5.2F).

Although our model incorporates several elaborations designed to match motion processing in the hoverfly, it is obviously far simpler than the biological system. Nevertheless, when we measure the neural response to doublet motion at full contrast in the preferred direction it is remarkably similar to the model output (compare Figure 5.2E and 5.2G). Like the model output, the neural response is characterised by three dominant peaks, which correspond well in relative magnitude and timing to the peaks produced by the model (see arrowheads in Figure 5.2G which indicate the timing of the model output peaks). The membrane potential remains well depolarised relative to the resting potential, with a mean of 2.93±0.18 mV (mean±SEM; mean is taken as the average response in a window that coincides with the stimulus).

Unlike the model, however, which gives a symmetrical output to the two directions of motion, the response to anti-preferred direction motion shows some notable differences to that produced by preferred direction (compare Figure 5.2G and 5.2H). First, the three hyperpolarization peaks are much more similar in magnitude. The second response peak is only twice the magnitude of the first, while the third peak is similar in magnitude to the second (Figure 5.2H). Second, between the second and third hyperpolarization peak there is a brief and small depolarisation of the membrane potential (see * in Figure 5.2H). This small depolarisation could reflect the recruitment of voltage-gated sodium conductances within the HS neuron itself which may boost large depolarising transients (Haag, Theunissen & Borst, 1997), a feature not implemented in our model. Despite the brief depolarisation, the neuron produces a net mean hyperpolarized response of -1.41±0.16 mV (Figure 5.2H), which corresponds to 48% of the mean response magnitude to preferred direction motion (Figure 5.2G).

A reduction in contrast of the stimulus might be expected to induce locally weaker activation of the inputs and be less likely to recruit non-linearities such as amplification or rectification due to voltage gated conductances and thus to yield responses more similar in shape to the predictions of our simple model. Surprisingly, however if we display the doublet at 10% contrast, the neural response no longer retains an obvious triphasic shape. Instead, we see a single dominant depolarisation in the preferred direction (Figure 5.2I) and two smaller hyperpolarizations in the anti-preferred direction (Figure 5.2J). In both these cases, the peaks to low contrast motion correspond in time with the largest peaks observed to high contrast motion (compare Figure 5.2I, J with Figure 5.2G, H). However, despite the 10-fold reduction in stimulus contrast, the net neural responses only rescaled by approximately 1/3 and display the same asymmetry in response magnitude for the two directions. The mean response was 0.99±0.19 mV to preferred direction motion and -0.67±0.23 to anti-preferred direction motion. The EMD model, on the other hand, is sensitive to the square of image contrast and thus simply rescales to 1% of its original response magnitude, but retains the same shape (not shown).

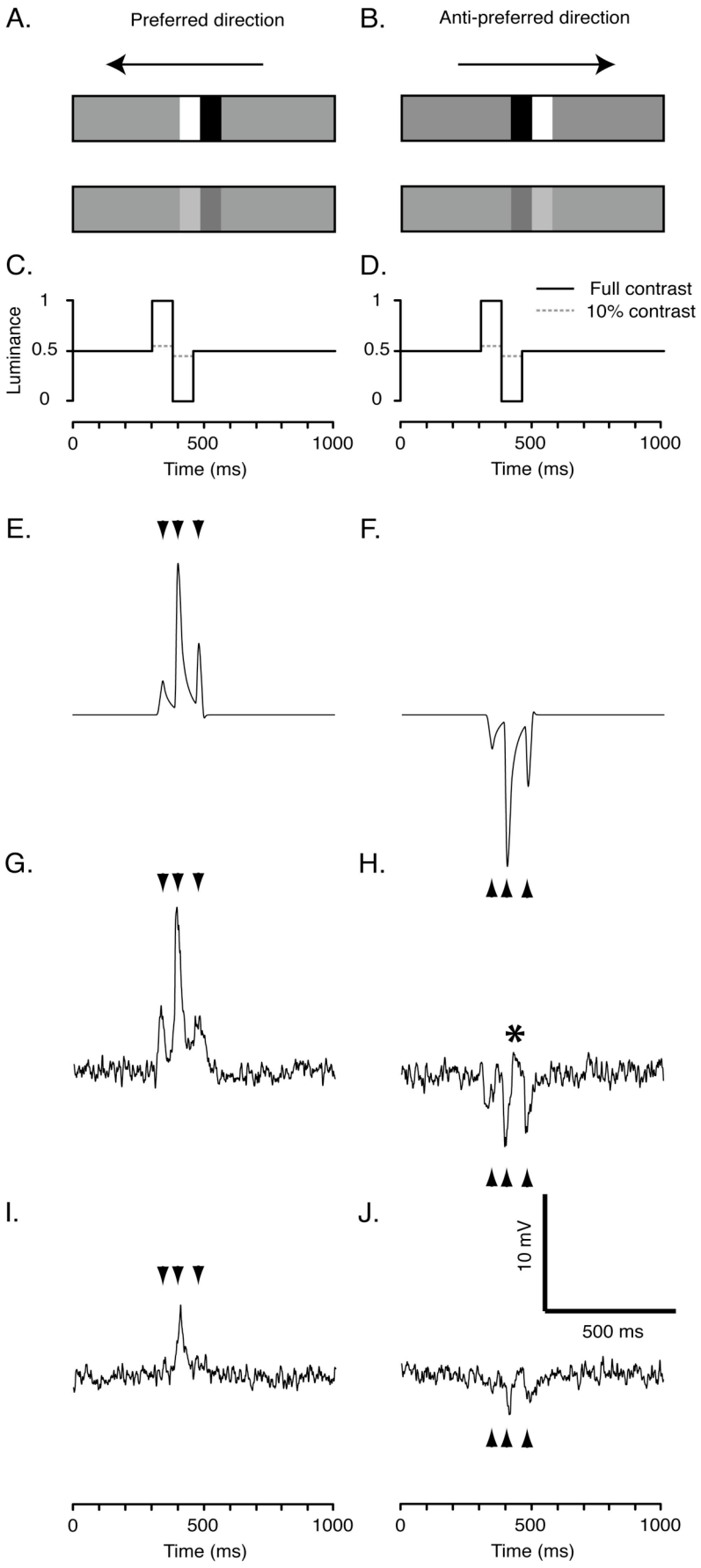
A.
Preferred direction
B.
Anti-preferred direction
C.
D.
Full contrast
10% contrast
Luminance
1
0.5
0
0
500
1000
Time (ms)
E.
F.
G.
H.
I.
J.
10 mV
500 ms

Figure 5.2 Blocklet response

A, B. A combination of two square-wave, white-black luminance steps on mean luminance (grey) background, referred to as a doublet. The doublet is 14° wide and 75° high and has a fundamental row frequency of 0.053 cycles/°, near optimal for HS neurons in the hoverfly. We simulated doublet motion at 90°/s with the doublet at either full or 10% contrast in both the preferred (A) and anti-preferred direction (B). For display purposes the doublets are not shown at their true contrasts but adjusted for print. C, D. Normalized stimulus luminance plots as seen at the first edge of the slit-window, i.e. the right hand edge for preferred, right-left motion, and the left hand edge for anti-preferred left-right motion, e.g. time-luminance graphs. Solid black lines represent the full contrast condition, dashed grey lines show the 10% original contrast condition. E. The doublet stimulus produces a characteristic triphasic response from the model in the preferred direction. F. The output is similar in the anti-preferred direction. G. The neuron response is also characterized by a triphasic response profile that closely resembles the model in the preferred direction. H. The neuron response to anti-preferred direction motion. I, J. The neural responses to the low contrast doublet. Arrowheads indicate the timing of response peaks produced by the model to the doublet stimuli. Although responses are qualitatively indistinguishable from one recording to the next, absolute response magnitude can vary. To enable accurate comparison of the responses across the six stimulus conditions in Figures 5.2-5.4, we show the response to one neuron in which all six conditions were performed, n=20.

5.4.3 Feature-feature interactions to transient stimuli depend on the temporal order of contrasts within a stimulus ensemble

To investigate the adaptation recruited by high and low-contrast temporal changes respectively, we combined the high and low contrast doublets (from Figure 5.2A and 5.2B). Initially we displayed the two doublets as an increasing contrast ensemble with the low contrast doublet followed by the high contrast doublet, but separated by a 1.2° gap (corresponding to a 14 ms delay at a velocity of 90°/s; Figure 5.3A-D).

Figure 5.3E and 5.3F show the model output to the increasing contrast ensemble. Due to the sensitivity of the model to stimulus contrast, the high-contrast doublet completely dominates the output on the scale shown here (Figure 5.3E and 5.3F). To investigate how the separate doublets interact with each other, we compared the model with the linear sum of the outputs from the individual doublets (see Figure 5.2E, F) with an appropriate delay to account for the timing (dashed grey lines, Figure 5.3E, F). The model output to the increasing contrast ensemble lies perfectly over the top of the linear sum of the independently modelled doublet responses (compare dashed and solid lines in Figure 5.3E and 5.3F). When we zoom in on the model's response it is clear that the response to the second doublet slightly precedes that predicted by the linear sum (compare grey and black lines in Figure 5.3G and 5.3H), revealing a weak predicted interaction between them.

Again, the model output to the different contrasts is a poor predictor of the neural response. The neuron's response to the increasing contrast ensemble shows four major peaks (Figure 5.3I, J) corresponding to the same contrast edges that generated responses to the single stimuli (compare figure 5.2G, I and 5.2H, J with Figure 5.3I and 5.3J, solid black lines). The arrowheads in Figure 5.3 indicate the timing of the three peaks from the model output to a single high contrast doublet (see Figure 5.2E, F). Much like the model output, the neural response can be largely predicted by the linear sum of the independently-recorded doublet responses, as seen in Figure 5.2G-J (compare grey and black lines, Figure 5.3I and 5.3J). The same observations holds for the anti-preferred direction.

We now consider a *decreasing* contrast ensemble, which presents the doublets in the opposite order, i.e. with the high contrast doublet followed by the low contrast doublet (Figure 5.4A-D). It is important to note that this ensemble is statistically identical to the one if Figure 5.3 with respect to global spatial frequency power spectrum, luminance, and contrast. It only differs in the temporal order that the different contrasts are seen by local motion elements.

When we run the decreasing contrast ensemble past the model, the output to the high contrast feature dominates the output (Figure 5.4E and 5.4F). However, if we zoom in on the model's response to the low contrast doublet it is clear that it differs from that predicted by the responses to the two doublets on their own (compare grey prediction and black output, Figure 5.4G and 5.4H). When we linearly sum the independently modelled doublet responses (dashed grey line Figure 5.4G), a small hyperpolarizing transient that follows the 3rd peak overshadows the initial response to the second (low contrast) doublet - i.e. the first of the 3 predicted response peaks(Figure 5.4G, first arrowhead). However, when the two doublets are combined in the model, we actually see an amplification of the output (Figure 5.4G, solid black line). On the other hand, the second response peak to the low contrast doublet is suppressed to about 50% of its original magnitude (Figure 5.4G, second arrowhead). Importantly however, by the time the final contrasting edge falls within the field of the model, there are no remaining interactive effects - the model output perfectly overlies the linear sum of the independently modelled responses (Figure 5.4G, third arrowhead).

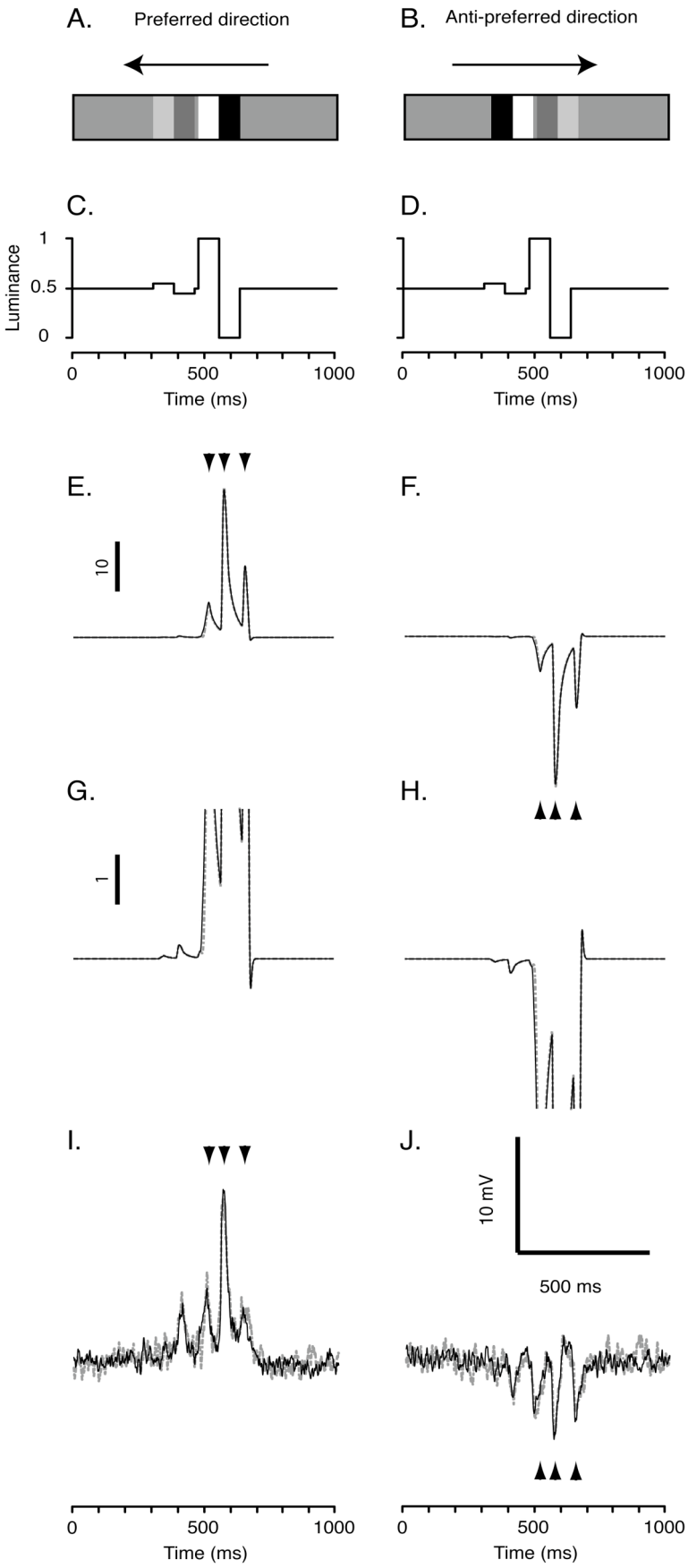
A.
Preferred direction
B.
Anti-preferred direction
C.
D.
Luminance
1
0.5
0
0
500
1000
Time (ms)
E.
F.
10
G.
H.
1
I.
J.
10 mV
500 ms

Figure 5.3 The increasing contrast ensemble

A. We combined the high and low contrast doublets to produce an ensemble where the low contrast (10%) doublet is followed by the high contrast doublet, referred to as the increasing contrast doublet ensemble. B. The spatial arrangement is flipped for stimulation in the anti-preferred direction so that the temporal order of doublet contrasts remains the same. C. The time-luminance trace for motion in the preferred direction. D. The time-luminance trace for motion in the anti-preferred direction is identical. E. Model output to the ensemble moving in the preferred direction. The dashed grey line indicates the predicted output based on the linear sum of the response to each doublet individually (see Figure 5.2). The arrowheads highlight the timing of the three peaks in the output. F. Model output to the ensemble moving in the anti-preferred direction. The dashed grey line shows the linear sum of the individual responses. G. Magnified model output (x10 vertically) reveals the response to the low contrast doublet in the preferred direction. H. Magnified model out reveals the response to low contrast doublet in the anti-preferred direction. I. Intracellular response of an HS neuron to the increasing contrast ensemble moving in the preferred direction. The dashed grey line indicates the predicted response based on the linear sum of the response to each individual doublet (see Figure 5.2). The arrowheads highlight the timing of the three peaks in the model output. J. Intracellular response of an HS neuron to the ensemble moving in the anti-preferred direction. The dashed grey line indicates the linear sum of the response to the individual doublets (see Figure 5.2). The arrowheads highlight the timing of the three peaks in the model output. n=20 from the same neuron as shown in Figure 5.2 and 5.4, see Figure 5.2 legend for justification.

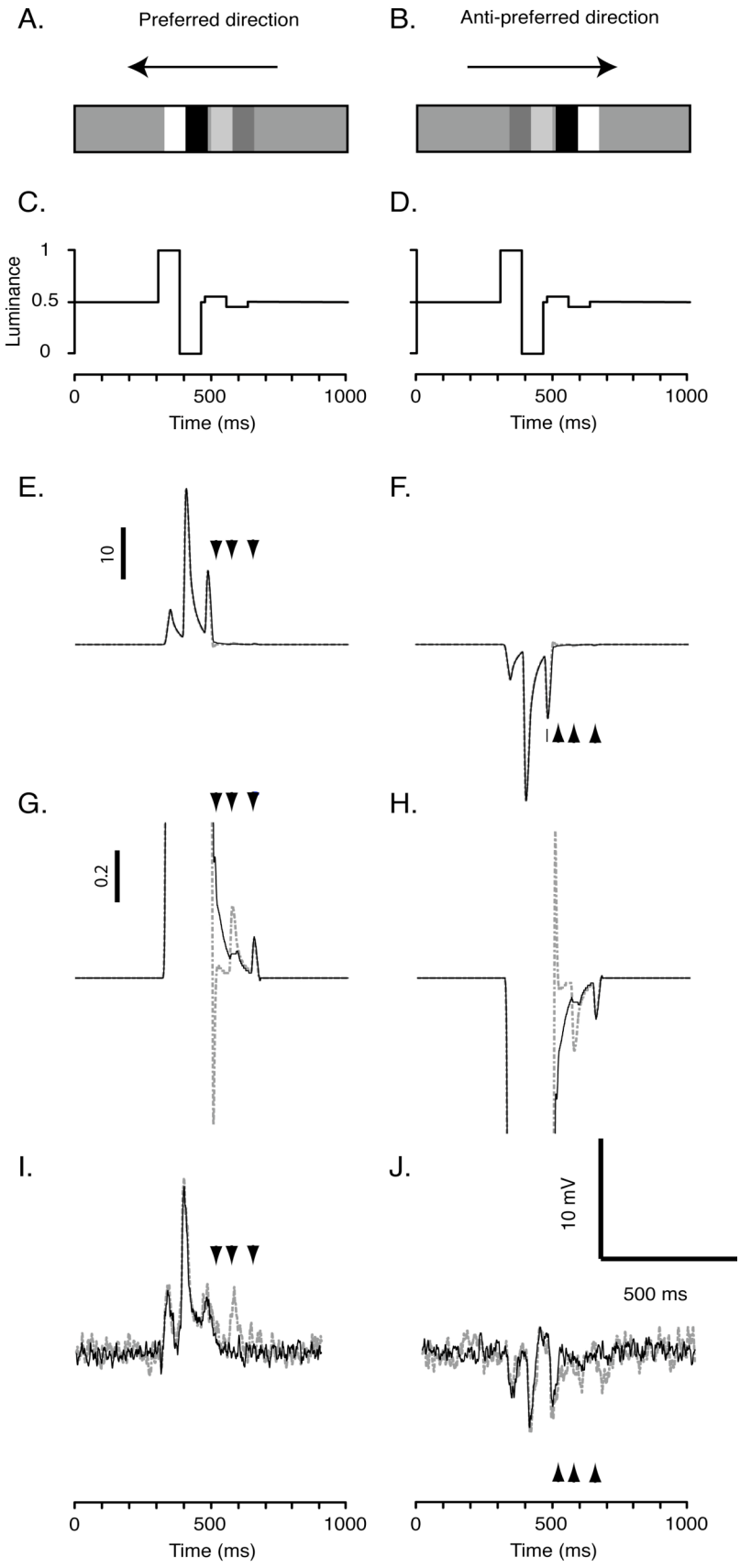
A.
Preferred direction
B.
Anti-preferred direction
C.
D.
Luminance
1
0.5
0
0
500
1000
Time (ms)
E.
F.
10
G.
H.
0.2
I.
J.
10 mV
500 ms

Figure 5.4 The decreasing contrast ensemble.

A. We combined the high and low contrast doublets to produce an ensemble with the high-contrast doublet preceding the low contrast doublet. B. The spatial arrangement is flipped for stimulation in the anti-preferred direction so that the temporal order of doublet contrasts remains the same. C. The time-luminance trace for motion in the preferred direction. D. The time-luminance trace for motion in the anti-preferred direction is identical. E. Model output to the ensemble moving in the preferred direction. The dashed grey line indicates the predicted output based on the linear sum of the response to each doublet individually (see Figure 5.2). The arrowheads highlight the timing of the three peaks in the output to the low-contrast doublet. F. Model output to the ensemble moving in the anti-preferred direction. The dashed grey line shows the linear sum of the individual responses. G. Magnified model output (x10 vertically) reveals the response to the low contrast doublet in the preferred direction. The dashed grey line shows the linear sum of the individual responses. H. Magnified model output reveals the response to the low contrast doublet in the anti-preferred direction. The dashed grey line shows the linear sum of the individual responses. I. Intracellular response of an HS neuron to the decreasing contrast ensemble moving in the preferred direction. The dashed grey line indicates the predicted response based on the linear sum of the response to each individual doublet (see Figure 5.2). The arrowheads highlight the timing of the three peaks in the model output. J. Intracellular response of an HS neuron to the ensemble moving in the anti-preferred direction. The dashed grey line indicates the linear sum of the response to the individual doublets (see Figure 5.2). The arrowheads highlight the timing of the three peaks in the model output. n=20 from the same neuron as shown in Figure 5.2 and 5.3, see Figure 5.2 legend for justification.

If we now look at the neural response, again it differs quite substantially from the prediction by the model, and also by the prediction based on summing the independently measured doublet responses (Figure 5.4I). The neuron's response to the first low contrast doublet (solid line, first arrowhead, Figure 5.4I) is suppressed compared to the prediction (grey dashed line, first arrowhead, Figure 5.4I), whereas the model response was substantially facilitated (Figure 5.4G, first arrowhead). This is particularly evident in the anti-preferred direction (compare grey and black lines, Figure 5.4J, first arrowhead). Furthermore, the neuron's response to the second (predicted to be largest) peak is entirely suppressed (solid black line, second arrowhead, Figure 5.4I, J), whereas the model only showed a partial suppression (second arrowhead, Figure 5.4G, H). The third major difference between the model and neural response occurs in the vicinity of the third predicted response peak to the second doublet. Whereas the model predicted no residual interactions between the two doublets (Figure 5.4G, H), the neural response is clearly still strongly suppressed, particularly evident in the anti-preferred direction (third arrowhead, solid lines, Figure 5.4I and 5.4J). Indeed, the overall impression of the physiologically recorded response is that the response to all three peaks predicted for the second doublet is completely suppressed by the prior passage of the first.

The change in presentation order of these features leads to a 30% net decrease in the mean response in the preferred direction, from 2.1±0.092 mV (N=2, n=40) for the increasing contrast ensemble to 1.5±0.099 mV for the decreasing contrast ensemble ($p<0.001$; two-tailed t-test). It decreased by 15% in the anti-preferred direction, from -1.0±0.12 mV (mean±SEM; N=2, n=40) for the increasing contrast ensemble to -0.85±0.095 mV for the decreasing contrast ensemble. However, this difference was not statistically significant.

Does the EMD model predict the neural responses? Qualitatively the model captures some of the interactions caused by the doublets in decreasing contrast order, but the neural response is still suppressed well after the model predicts that there will be no further interactions (third arrowheads in Figure 5.4G-J). The suppressed responses to the low-contrast features are likely caused by a local dynamic reduction in contrast gain that outlasts the stimulus. This is not recruited when the feature order is

reversed, as might be expected for an adaptation mechanism that is itself sensitive to feature contrast. Additional experiments varying the spatial (and thus temporal) separation of the doublet features (not shown) reveal that the suppression remains substantial for features separated by 60 ms, and is weakly evident when features are separated by 165 ms, however, there is no interaction at larger separations (Data not shown).

5.4.4 Global effects of feature-feature interactions within an image

Up until now, we have considered the interactions between doublets from the perspective of local motion detector responses. How do these feature-feature interactive effects change the neuron's global response? To investigate this, we first displayed the same doublet ensembles as in Figures 5.3 and 5.4 but recorded neural responses using the whole-screen mode (Figure 5.5).

As the doublet ensembles sweep across the relatively narrow HSN receptive field, the neuron response builds to a peak before decaying away more slowly (Figure 5.5B, C). In both the preferred and anti-preferred direction, the decreasing contrast ensemble (blue, Figure 5.5B and 5.5C) generates a peak response faster than the increasing contrast ensemble (red, Figure 5.5B and 5.5C). The peak response to the increasing contrast ensemble (red) is delayed by 131 ms in the preferred direction, on the order of the width of a doublet (156 ms at 90°/s). In the anti-preferred direction this shift is only 66 ms (Figure 5.5C). The slower response to the increasing contrast ensemble most likely reflects the delayed arrival of the high contrast doublet (second in this ensemble) in the receptive field. However, the peak response is reached more rapidly than predicted by this temporal offset in the anti-preferred direction (Figure 5.5C).

The mean neural response was significantly larger for the 'increasing contrast ensemble' 7.4±0.37 (mean±SEM) compared to 6.1±0.4 for the 'decreasing contrast ensemble' ($p<0.0001$, two-tailed t-test) in the preferred direction (Figure 5.5D). A similar change in response was evident for anti-preferred direction, -3.9±0.2 for the increasing contrast ensemble compared to -3.4±0.2 for the decreasing contrast ensemble ($p<0.001$, two-tailed t-test; Figure 5.5D).

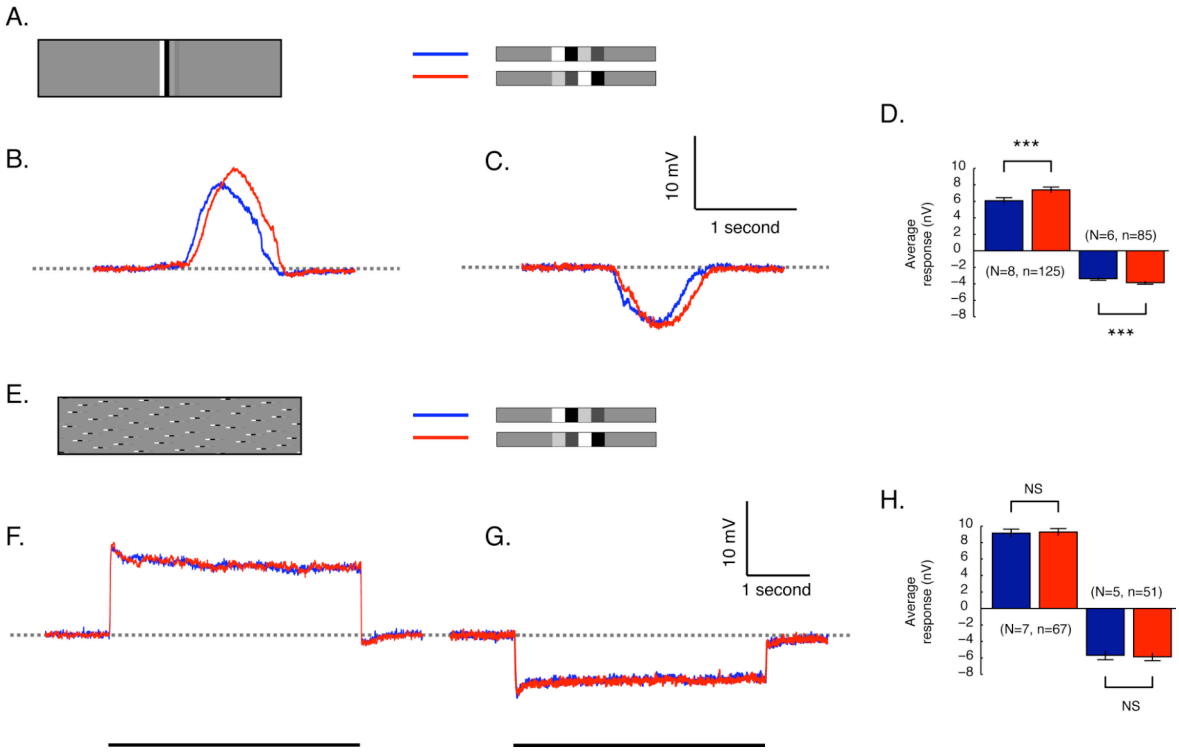

Figure 5.5 The vertical distribution of the stimulus

A. The doublet ensembles as whole-screen stimuli. Blue indicates the decreasing contrast ensemble, and red the increasing ensemble. B. Intracellular HS neuron response to the doublets as they pass through the receptive field in the preferred direction (blue = decreasing contrast, red = increasing contrast). C. Intracellular response to the doublets moving in the anti-preferred direction (blue = decreasing contrast, red = increasing contrast). D. The mean response to the doublets moving in the preferred and anti-preferred direction (blue = decreasing contrast, red = increasing contrast). Stars indicate a significant difference ($p < 0.001$, Student's t-test). E. The doublet ensemble broken up into individual pseudo-randomly distributed 1.8º high segments. The stimulus was displayed using the whole-screen mode. Blue indicates the decreasing contrast ensemble, and red the increasing ensemble. F. Intracellular HS neuron response as the stimulus moves in the preferred direction (blue = decreasing contrast, red = increasing contrast). G. Intracellular HS neuron response as the stimulus moves in the anti-preferred direction (blue = decreasing contrast, red = increasing contrast). H. The mean response to motion in the preferred and anti-preferred direction (blue = decreasing contrast, red = increasing contrast). NS = no significant difference.

However, in most scenes there will be many features simultaneously interacting with local EMDs across the receptive field. We therefore altered the stimulus by separating the doublets into 1.8° high segments (i.e. just larger than the predicted vertical extent of a single EMD), and redistributed these segments pseudo-randomly across the panoramic cylinder. The resultant image (Figure 5.5E) is identical along individual rows to the image used above (Figure 5.5A), but differs only in the alignment of the doublets between rows.

When we display this image (Figure 5.5E) using the whole-screen mode (Figure 5.1A), the neuron responds with a rapid onset transient, which then decays exponentially to a steady-state within a couple of seconds (Figure 5.5F and 5.5G). The grossly different response profile compared to Figure 5.5B, C highlights an important difference between the stimuli: Because we spread the doublets across the entire panorama, many segments are already present within the receptive field at the commencement of image motion, resulting in the initial response transient (Figure 5.5F and 5.5G).

Surprisingly, there is no evidence of a difference between the two different contrast ensembles (Figure 5.5F-H). For the increasing contrast ensemble in the preferred direction, mean neuron responses was 9.3±0.46 (mean±SEM), compared to 9.1±0.52 for the decreasing contrast ensemble (Figure 5.5F and 5.5H). In the anti-preferred direction mean responses were -5.9±0.53 for the increasing contrast ensemble compared with -5.7±0.59 for the decreasing contrast ensemble (Figure 5G and 5.5H). In fact, in several individual recordings there was actually an opposite change to what might be expected on the basis of the earlier experiments.

Thus, when our stimuli were vertically aligned we saw large response changes between the two doublet ensembles (Figure 5.5A-D). Yet despite the fact that each local EMD viewed the same stimulus, when the features were split up and distributed across the entire panorama, there was no longer any response change between the two doublets. There are a couple of important differences between the two stimuli used in Figure 5.5. First, the spatially confined stimulus (Figure 5.5A) sweeps through the receptive field but commences motion from outside. As a result, the

stimulus ensemble never permits the neuron to reach a steady state response (Figure 5.5B and 5.5C), whereas, the spatially spread ensembles (Figure 5.5E) allow the neuron to rapidly reach a steady state (Figure 5.5F and 5.5G) despite obvious recruitment of global adaptation (evident from the post-depolarization after-potential in Figure 5.5F). Second, the vertically-aligned stimulus (Figure 5.5A) stimulates many local EMDs simultaneously as it enters the vertically aligned HSN receptive field (Nordström, Barnett, Moyer de Miguel, Brinkworth & O'Carroll, 2008) and might thus be expected to be a stronger underlying driver of neural response. The spatially spread out stimulus (Figure 5.5E) on the other hand results in fewer doublets present within the receptive field at any one instance, and it may well be expected to be a weaker underlying driver of neural response. Could the different responses to the two contrast ensembles be a consequence of either of these two factors?

We designed a new set of images to further investigate the mechanisms underlying the difference in response observed between the increasing and decreasing contrast ensembles. The images were similar to those used in Figure 5.5 but they included a continuum between having all the doublet ensembles perfectly aligned (Figure 5.5A, 5.6B) to being spread evenly across the entire panorama (Figure 5.5E, 5.6J). These images are thus expected to generate similar responses from local EMDs but they differ in how coherently the local elements within a receptive field are stimulated. They all commenced motion from outside the receptive field in a similar way to the images shown in Figure 5.5A-C.

When we show the image where we have pseudo-randomly offset vertically neighbouring doublet segments by a maximum of 8° (Figure 5.6B) the neuron response differs quite substantially from that in Figure 5.5B (Figure 5.6A). Although there is still a difference in the peak responses produced by the two contrast ensembles (compare blue and red lines Figure 5.6A), this is substantially less than that observed for the perfectly vertically aligned stimulus (Figure 5.5A). The inset (Figure 5.6A) shows the data from Figure 5.5B as dashed lines. Although the response to the increasing contrast ensemble remains the same (red, Figure 5.6A), despite the stimulus having changed slightly, the response to the decreasing contrast

ensemble is larger than that observed in Figure 5.5B (compare dashed grey line with solid blue lines, inset Figure 5.6A). Quantitative analysis reveals that the mean neural response is different between the two contrast ensembles in the preferred direction, but that no difference was evident in the anti-preferred direction (Figure 5.6B).

As we spread the stimulus out more (with segments varied by up to 20°, Figure 5.6D), the overall neural response increases slightly for both the decreasing and increasing contrast ensembles (Figure 5.6C and 5.6D). However, the difference between the two contrast ensembles is even smaller (Figure 5.6C). Preferred direction motion still generated a small decrease in response for the decreasing contrast ensemble (blue, Figure 5.6C and 5.6D), however, in the anti-preferred direction there is no response change (Figure 5.6D). Dispersing the doublet ensembles further across the panorama (Figure 5.6F and 5.6H) produced even larger neural responses (Figure 5.6E and 5.6G). However, the two different contrast ensembles no longer generated different neural responses in either direction of motion (Figure 5.6E-H).

In the final example, we spread doublet ensembles out over more than half the panorama (Figure 5.6J). While the neural response has become weaker, there is no magnitude difference between the two contrast ensembles (Figure 5.6I and 5.6J). In terms of recruiting a response difference between the two contrast ensembles, it appears that only a slight mis-alignment of doublets drastically alters the influence of local gain reduction recruited by the high-contrast doublet passing each location before the lower contrast feature. We thus conclude that while earlier work suggests that adaptive gain reduction is locally recruited within EMDs, this is somehow dependent on more global structure of the features and is more pronounced for coherent, vertically aligned edges. It is worth noting that in the earlier experiments using the slit-windowed stimulus, the doublet ensembles would have been vertically aligned, as the slit-window was 84° high (see Figure 5.1E).

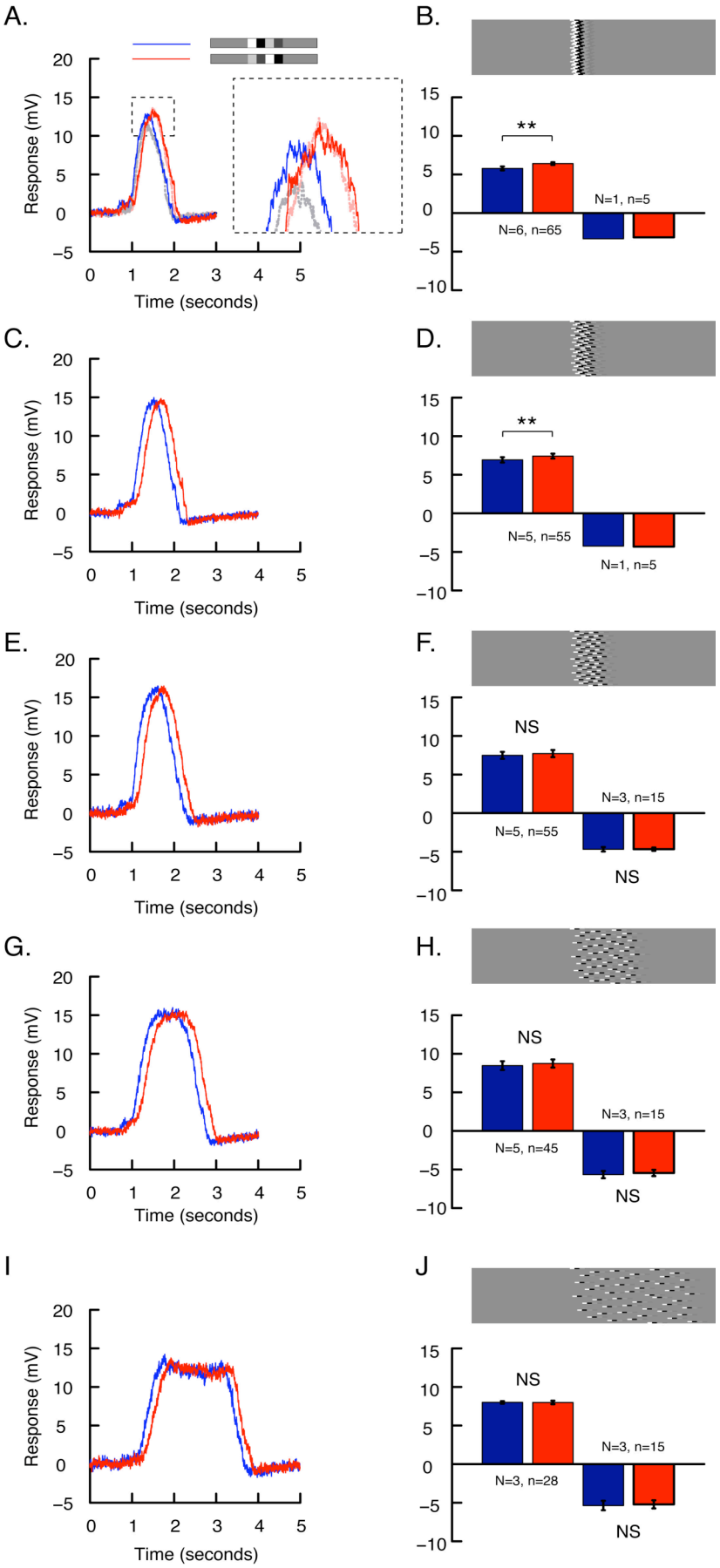
A.
B.
C.
D.
E.
F.
G.
H.
I
J
Response (mV)
Time (seconds)
**
N=1, n=5
N=6, n=65
N=5, n=55
NS
N=3, n=15
N=5, n=45
N=3, n=28

Figure 5.6 The horizontal distribution of the stimulus

A. Intracellular HS neuron response to preferred direction motion for the image shown in part B, using the whole screen stimulus (blue = decreasing contrast, red = increasing contrast). The inset highlights the difference between the responses to this image (B) and that shown in Figure 5.5A (dashed grey = decreasing contrast, dashed light red = increasing contrast). The increasing contrast ensemble (red) produces a similar response to that for the image shown in Figure 5.5A (dashed light red), however, the decreasing contrast ensemble (blue) is significantly larger than that seen for the image shown in Figure 5.5A (dashed grey). B. The doublet ensemble is broken up into individual 1.8º high segments, which are pseudo-randomly shifted horizontally, so that the maximum horizontal offset is 11º (The absolute spread of the ensembles horizontally is thus, 11º+ the doublet ensemble width, 11º+30º). The stimulus was displayed using the whole-screen mode. The bars show the mean response to motion in the preferred and anti-preferred direction. Stars indicate a significant difference (** $p < 0.01$, Student's t-test). C. Response to preferred direction motion of the image shown in D. Once again, the doublet ensemble are broken up into individual 1.8º high segments, which are pseudo-randomly shifted such that the maximum horizontal displacement is 22º. The bars show the mean response to motion in the preferred and anti-preferred direction. Stars indicate a significant difference (** $p < 0.01$, Student's t-test). E. As above but for the image shown in F. The doublet ensembles are now distributed over 45º. The bars show the mean response to motion in the preferred and anti-preferred direction (NS = no significant difference, Student's t-test). G. As above but for the image shown in H. The doublet ensembles are now distributed over 90º. The bars show the net mean response to motion in the preferred and anti-preferred direction (NS = no significant difference, Student's t-test). I. As above but for the image shown in J. The doublet ensembles are now distributed over 180º. The bars show the mean response to motion in the preferred and anti-preferred direction (NS = no significant difference, Student's t-test). In all cases blue = decreasing contrast, red = increasing contrast.

5.4.5 Simultaneous stimulation of neighbouring local motion sensitive elements recruits a powerful reduction of motion detector gain for subsequent features

Could the change in neural response observed when the doublet ensembles are vertically aligned (Figures 5.3, 5.4, and 5.5B-D) result from the interactions of simultaneously activated neighbouring local motion elements? When the doublet ensembles are vertically aligned, a column of local EMDs are activated simultaneously, whereas when the doublet ensembles are separated there is no, or less, simultaneous activation of vertically neighbouring EMDs (Figure 5.5A and 5.5E). If the reduction in response is the result of the simultaneous activation of vertically aligned local EMDs feeding into the HS neuron, we should be able to prevent the reduction in response by limiting the doublet ensembles to just one row of local EMDs.

To test this hypothesis, we first limited the size of our doublet ensembles to 1.8° high (Figure 5.7A), the same height as in the experiments shown in Figure 5.5E and 5.6E-J, where we showed no response magnitude difference between the two doublet ensembles. Interestingly, when we did this, neural response showed a difference between the two doublet ensemble conditions in the preferred direction (Figure 5.7B). For the increasing contrast ensemble, the mean responses were 1.67±0.051 (mean±SEM) compared with 1.52±0.055 for the decreasing contrast ensemble in the preferred direction ($p<0.05$; Figure 5.7C). In the anti-preferred direction, the response change was in the opposite direction, however this was only recorded in one neuron and the variability was large (Figure 5.7C). The response magnitude difference between the two doublet ensembles was smaller than that observed for the full size doublets (compare Figure 5.7B with Figure 5.5B). However, it was still a notable difference of approximately 9%.

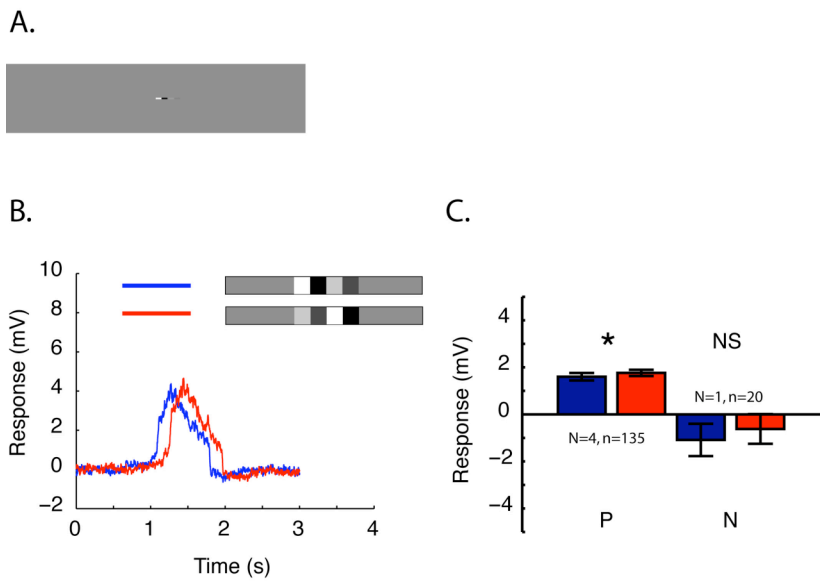

Figure 5.7 The vertical extent of a small stimulus

A. The doublet ensembles as whole-screen stimuli. The doublet has the same width as before, but is now only 1.8º high. B. Intracellular HS neuron response to the doublets as they pass through the receptive field in the preferred direction (blue = decreasing contrast, red = increasing contrast). C. The mean response to the doublets moving in the preferred (P) and anti-preferred (N) direction (blue = decreasing contrast, red = increasing contrast). The star indicates a significant difference ($p < 0.05$, Student's t-test). NS = no significant difference (Student's t-test).

The stimulus in Figure 5.7 is 1.8° high, and is thus almost certainly simultaneously stimulating more than a single EMD as it passes through the receptive field. Therefore, it is still possible that the response reduction to the decreasing contrast ensemble is resulting from interactions between vertically neighbouring EMDs. However, it is still unclear why a similar change in response was not evident for the images that had doublet ensembles of the same size, but distributed around the panorama (Figure 5.5E-H and Figure 5.6E-J). If the response difference to the two doublets shown in Figure 5.7 is the result of marginal interactions between nearest neighbour EMDs, then an additional mechanism is required to account for the absence of such a change when the stimulus segments are more sparsely distributed across the panorama (Figure 5.5E-H and Figure 5.6E-J).

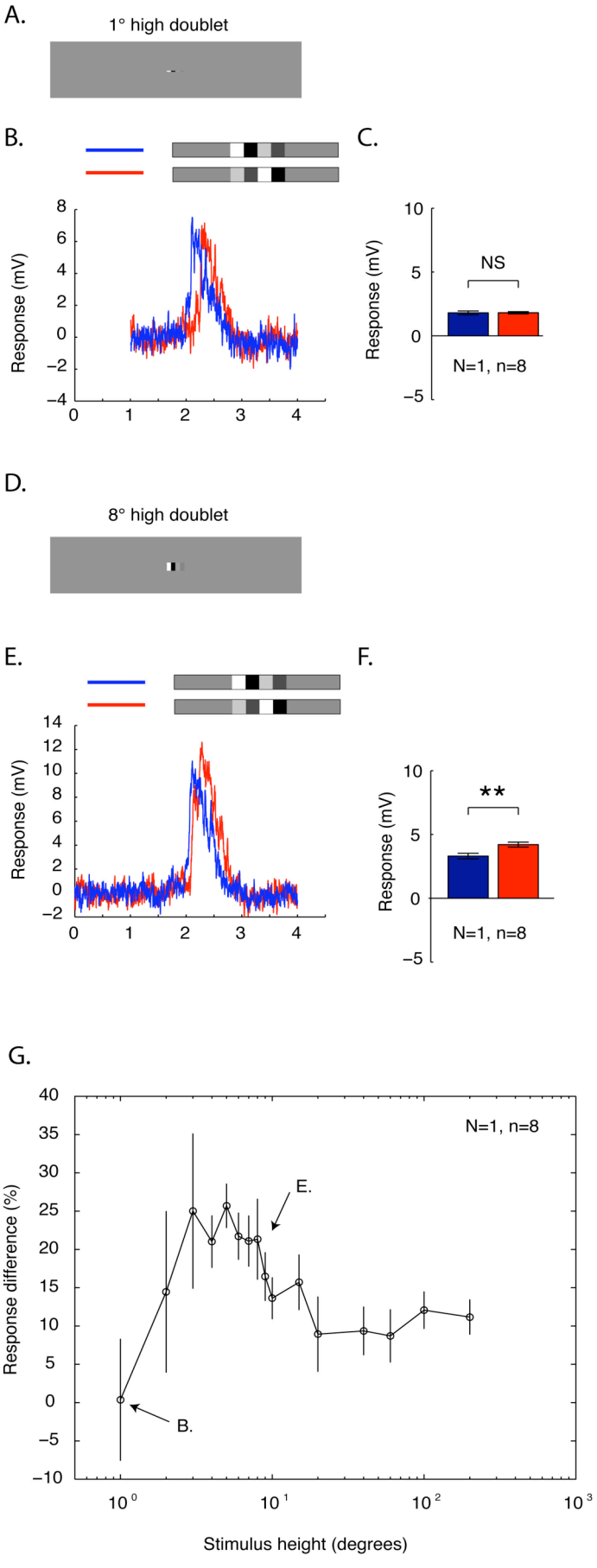
A.
1° high doublet
B.
C.
Response (mV)
NS
N=1, n=8
D.
8° high doublet
E.
F.
Response (mV)
**
N=1, n=8
G.
Response difference (%)
N=1, n=8
E.
B.
Stimulus height (degrees)

Figure 5.8 Varying vertical extent

A. The doublet ensembles as whole-screen stimuli. The doublet has the same width as before, but is now only 1º high, approximately the size of an individual ommatidium. B. Intracellular HS neuron response to the doublet ensemble shown in A, as it passes through the receptive field in the preferred direction (blue = decreasing contrast, red = increasing contrast. C. The mean response to the doublets as shown in part B (blue = decreasing contrast, red = increasing contrast). NS = no significant difference (Student's t-test). Response is averaged over a window while the stimulus is visible on the monitor. D. The doublet ensembles as whole-screen stimuli. The doublet ensembles are now 8º high. E. Intracellular response to the doublet ensembles as they pass through the receptive field in the preferred direction (blue = decreasing contrast, red = increasing contrast. F. The mean response to the doublet ensembles as shown in part E (blue = decreasing contrast, red = increasing contrast). Stars indicate a significant difference (** $p < 0.01$, Student's t-test). G. The average response difference between the increasing and decreasing contrast ensembles as a function of their vertical extent. A positive difference indicates that the response to the increasing contrast ensemble is larger. Data displayed as mean ± sem.

To investigate this further, we varied the vertical extent of the doublet ensembles from below the size of an individual ommatidium up to the maximum height possible on our stimulus monitor (Figure 5.8). We were primarily interested in two questions: 1. If we do not stimulate vertically aligned EMDs, will there still be a response difference to the two contrast ensembles? 2. What stimulus heights are required to effectively recruit a response difference?

Interestingly, when we limited the height of the stimulus to just 1° (Figure 5.8A), approximately the same size as the receptive field of an individual ommatidium in *Eristalis tenax* (Straw et al, 2006), we see no change in mean response between the two doublet scenarios (Figure 5.8B and 5.8C). The mean response was 1.8±0.091 mV for the increasing contrast ensemble and 1.8±0.15 mV for the decreasing contrast ensemble in the preferred direction (mean±SEM; Figure 5.8B and 5.8C). However, when we extend the stimulus height to stretch across more than one ommatidium, the increasing contrast ensemble produces a stronger response than its counterpart, much like that observed in the earlier experiments (Figure 5.8D-F).

Even for relatively small increases in stimulus height, the increasing contrast ensemble produces up to a 25% stronger response than the decreasing contrast ensemble (Figure 5.8G). Data for multiple doublet heights shows that the maximum difference in mean response between the two doublet ensemble scenarios is reached at stimulus heights of around 3-5° (Figure 5.8G). After the stimulus exceeds 10°, the difference between the two stimulus ensembles gets smaller, receding to approximately 10% (Figure 5.8G). This is lower than that observed for the earlier experiments (Figure 5.5) and as this is the average from just one neuron, it might simply reflect recording variability (although the response magnitude in this recording was similar to that for the average responses seen in Figure 5.5). Nevertheless, for this neuron at least, a maximum difference between responses were observed for relatively small stimulus heights, ca. 2-10º (Figure 5.8G), strongly suggesting that local adaptation is facilitated by between-EMD interactions aligned orthogonal to the preferred direction.

5.5 Discussion

5.5.1 Reconciling model response magnitude with neuron response

Motion adaptation and its influence on the coding of image motion by the insect visual system has been extensively investigated at the level of the LPTCs (Fairhall et al, 2001; Harris et al, 2000; Maddess and Laughlin, 1985; Neri and Laughlin, 2005; Safran et al, 2007) Motion adaptation has been shown to enhance LPTC sensitivity to changes in stimulus velocity (Maddess and Laughlin, 1985; Neri and Laughlin, 2005) and to reduce contrast gain to subsequent stimulation (Harris et al, 2000; Nordström and O'Carroll, 2009) as well alter information transmission (Safran et al, 2007)

However, despite progress in this field, the potential role of adaptation as an explanation for our recent observations that hoverfly HS neurons provide robust responses largely independent of global contrast in natural scenes has been largely limited to studying the steady-state behaviour of the system (Chapter 3, Barnett et al submitted). A complete understanding of how dynamic adaptation at a local level is integrated into the global representation of image motion is still some way off. Among the key questions to be addressed are whether the dynamics of local adaptation are fast enough to provide strong normalization of local features within a scene, or whether the gain of the system is adjusted more gradually in response to global structure. Here we made the first steps towards addressing these questions by studying the influence of local transient responses to simple local features on subsequent features that pass the same location. We make 3 key observations:

(1) The magnitude of local transient responses to local feature ensembles is poorly predicted by the total contrast of the feature, yet within a feature the relative magnitude of transient responses is well predicted by simple models.

(2) Local adaptation is contrast dependent and this leads to differences in transient response depending on the order of local contrasts experienced. When low contrast features pass a location within the receptive field, they

exert little influence on subsequent responses, but even transient stimuli with high contrast lead to potent suppression of responses to subsequent features.

(3) The influence of dynamic adaptation in local transient responses is not determined solely by temporal order of stimuli that reach local motion detectors, but is recruited selectively for features that span larger parts of the receptive field of the tangential cell, with an orientation orthogonal to the direction of motion.

5.5.2 Reconciling model response magnitude with neuron response for local transient responses

The largest difference between the model response and the response of the HS neuron is in the *relative* magnitude of responses to the different contrast doublets, whether presented independently, or as an ensemble. While much work suggests that insect motion detection employs an expansive non-linearity, thus leading to a supra-linear dependence on contrast (e.g. a quadratic relationship where the EMD employs multiplication), we found that a 10-fold reduction in contrast produced only a 3-fold reduction in transient response magnitude – i.e. a sub-linear effect of contrast. The simplest explanation for this discrepancy might be the recruitment of a compressive non-linearity such as saturation, as evident from the supra-threshold response-contrast relationship observed in earlier work (Dvorak et al, 1980; Egelhaaf and Borst, 1989; Harris et al, 2000).

Arguing against this, however, each doublet stimulus consists of 3 edge features, the 2nd of which has double the contrast of the 1st and 3rd. These different components enter the visual field of each EMD in quick succession and the temporal delay intrinsic to the EMD leads to some interaction between these components, so our model (which employed pure multiplication as the essential non-linear correlation operation), did not predict a strict 4-fold difference between the middle and flanking contrast boundaries (Figure 2E). Nevertheless, despite these interactions the model predicts that a saturation-free system would still display substantial differences in response to each of these three edges, with the middle (higher contrast) boundary

dominating the response. Suprisingly, this was what we observed even for the higher contrast doublet (Figure 2).

Based on these considerations, either saturation is not playing a dominant role in shaping the dynamics of transient responses to features, or some other mechanism is re-scaling the response gain at high contrast so that it is less subject to saturation. Note that while the edges within our doublet features are locally discrete, they would be blurred in space by the optics, and in time by the dynamics inherent to motion detectors, so while they pass a fixed point in space in an instant, the transient response to them lasts tens of milliseconds. Given that one of the first papers on adaptation by LPTCs suggested both that adaptation acts locally and that it may serve to relieve the system from saturation (Maddess & Laughlin 1985) a potential explanation for our observation is that adaptation to the first of the 3 edge features of the stimulus is fast enough that responses are already adapting as they occur. This is further suggested by our observation that while the model predicts that the 3rd feature would provide a stronger response than the first our data shows the opposite (Figure 2G).

5.5.3 Locally acting response-gain reduction

The small overall magnitude difference that we observed between the low and high contrast doublet features (Figure 2) might thus be explained by local adaptation within the doublet itself leading to strong local gain reduction and thus relief from saturation even as the feature is passing individual EMDs. This is strongly supported by our observations (Figure 3,4) that the specific order of doublet ensembles shapes the overall response. The low contrast doublet feature seems to exert little effect on subsequent stimulation by the higher contrast doublet. Yet even allowing for the likely dynamics of the motion detector itself, we see little evidence of any response at all to the lower contrast feature when it follows the higher.

A critical consideration in understanding the potential influence of this effect in coding natural scenes is its time-course. Our data suggests that the duration of local gain reduction is similar to that of the stimulus itself. Nevertheless, since the adaptive effect outlasts the passage of the individual doublet by more than 100ms, it

is clearly slower than the dynamics of motion detection itself, at least given the delay time constant of 30-40 ms suggested by experiments based on sinusoidal stimulation (Harris et al 1998, Reisenmann et al, 2003). Of course we have investigated only a single type of local feature moving at a single velocity (albeit one close to the global optimum indicated by our earlier experiments). It is highly likely that the dynamics of adaptation depend strongly on the dynamics of the scene itself – as suggested by work from other labs (Fairhall, Lewen, Bialek & van Steveninck, 2001). We clearly need much further work to quantify the dynamics of recruitment of adaptation both locally and globally. Nevertheless, our results at least support the idea that adaptation is both rapid enough in recruitment yet long-lasting enough to influence global responses in a manner that depends strongly on the higher-order relationship between features within a scene. This is an important point when considering natural scenes, since features that generate high local contrasts within some parts of such scenes (e.g. the branches of a tree seen against the bright sky) may 'cluster' within scenes. Hence EMDs viewing a patch of such texture be strongly adapted, while others viewing lower contrast patches may maintain very high contrast gain.

5.5.4 Higher order structure and its influence on local adaptation

Our 3rd key observation is perhaps the most surprising. If we take feature ensembles (high followed by low contrast) that in figure 4 we show produce strong local adaptation and now examine their influence on global responses by removing the slit window, we only observe the expected adaptation if the feature is presented in-phase *orthogonal* to the direction of motion (Figure 5). Splitting the feature into multiple local elements that are distributed horizontally completely abolishes the effect, even though individual EMDs are seeing identical stimuli and are clearly powerfully recruited by the stimulus. Two further observations suggest that this is very likely the result of a higher order interaction within the receptive field. Firstly even small horizontal displacement of the features leads to a dramatic decrease in the amount of local adaptation that is recruited (figure 6). Secondly, as we extend a local doublet feature into a vertical edge (i.e. orthogonal to its direction of motion) the adaptive effect strengthens up to several degrees in height and then declines (although the effect remains pronounced for full-screen stimuli). These data argue strongly for a

role in facilitation or recruitment of local adaptation by a component that is not as local as the EMD itself.

The observation that this is most effectively recruited by a vertical coherent edge of intermediate size, and orthogonal to the preferred-null axis of the EMDs is particularly intriguing, as it raises the possibility of involvement of a separate neuron to facilitate local adaptation. Our data (Figure 5.8) suggest that such facilitation might be mediated on a scale of several ommatidia in the local surround. In mammalian V1 and also auditory neurons local responses have been shown to be scaled by an adaptive processes based on local surround excitation (Schwartz and Simoncelli, 2001). In these examples local adaptation can be modelled by a divisive feedback of surround activity, therefore normalizing local neural response based on its surround. Such adaptive normalization strategies have the advantage over linear filters in that they rescale neural response and maximize coding range for the prevailing stimulus. Such local adaptive rescaling could be particularly advantageous in the encoding of natural image motion, as natural scenes have local structures and contrasts that are highly erratic from one location to the next. This is clearly a question that requires more careful consideration in future work.

Experimental Procedures

5.5.5 Experiments and neuron identification

We used wild caught hoverflies, *Eristalis tenax,* immobilized with wax and mounted 14-15 cm in front of a CRT display, which subtended approximately 100° x 75° of the fly's visual field. We performed sharp electrode intracellular recordings on Horizontal System (HS) neurons in the left lobula plate using aluminosilicate electrodes pulled on a Sutter Instruments P97 electrode puller with a 3 x 3 mm box filament. Electrodes were filled with 2 M KCl and typically had tip resistances of 80-250 MΩ. Upon successful penetration, we identified each neuron on-line based on its receptive field properties, as recently described in detail by Nordström et al. (2008).

5.5.6 Data acquisition and analysis

Data were digitised at 5 kHz using a 16-bit A/D converter (National Instruments, Austin Texas, United States) and analysed off-line with Matlab (http://www.mathworks.com). In all experiments, we normalized membrane potential by subtracting the average resting membrane potential recorded for 1 second immediately prior to each trial. HS neurons are ideal models to investigate the nature of signals arriving at their synaptic inputs because they predominantly respond with graded shifts in membrane potential. However, activity-induced spikelets often influenced the response adding an additional nonlinearity to the axonally recorded membrane potential (Haag et al., 1997, Hengstenberg, 1977, Nordström & O'Carroll, 2009). To reduce the influence of such spikelets in our analysis, we 'spike filtered' our data by removing spike-like events and replacing them with the local mean membrane potential (for details see Nordström & O'Carroll, 2009).

5.5.7 Statistics

All data are presented as mean ± standard error of the mean (SEM) unless otherwise mentioned. All statistics were performed using GraphPad Prism software

(http://www.graphpad.com). Data was analysed off-line in Matlab (http://www.mathworks.com). N refers to the total number of animals, while n refers to the number of trial done.

5.5.8 Images and display

All the images used in this study were developed using Matlab. We displayed stimuli on a linearized, 8-bit, RGB CRT at 200 Hz refresh rate with mean luminance of 100 Cd/m^2 using VisionEgg software (Straw, 2008).

5.5.9 Local motion detector analysis

We use a slit paradigm method for determining local motion detector responses similar to that used in behavioural experiments by Reichardt and Egelhaaf (1988) and in electrophysiological experiments by Egelhaaf et al, (1989). By limiting our stimulus display to the size of only a few ommatidia, 2.5° in the fronto-dorsal visual field, we limited the amount of spatial integration occurring in the HS neuron itself. This means that only a fraction of the image is seen at any one point in time and the axonal response we record in the HS neuron reflects the output of local motion elements in that region of the visual field. Stimulating just one local motion sensitive element is problematic though, because the axonal signal recorded is very small and hard to distinguish from membrane noise without performing very large numbers of repetitions (but see Chapter 4, Figure 4.6). To overcome this issue we vertically elongated our stimulus so that it simultaneously stimulated many local motion elements with the same stimuli. This means that on each individual trial we recorded the summed response of several local motion sensitive elements, which save performing large numbers of repeats.

5.5.10 Model predictions

We used an elaborated Hassenstein – Reichardt correlator model for motion detection to obtain a prediction of local motion response. This model incorporated many of the spatial and temporal filtering processes of the motion-processing pathway of *Eristalis.* A full description of the model is included in Chapter 4 Supplemental data. Briefly, the model was the sum of an array of EMDs that were

limited in space by the size of the slit window used in the neuronal experiments (Figure 5.1).

As the slit window in the neural experiments was 2.5°, it did not limit the stimulus exclusively to just one elementary motion sensitive element, but rather most likely partially stimulated some neighbouring elements also. To emulate this in our model simulations, we mimicked the experimental conditions and windowed the array of model EMDs with the same size window. Each frame of the stimulus simulation was then convolved with a gaussian blur kernel of 1.4° half-width so that the edge effects of the stimulus window were accounted for.

Acknowledgements

We thank the Managers of the Botanic Gardens for allowing insect collection. The research was funded by the Australian Research Council (LP 0667744) and the Swedish Research Council (2008-2933).

5.6 References

1. Borst, A., & Bahde, S. (1988). Visual information-processing in the flys landing system Journal of Comparative Physiology a-Sensory Neural and Behavioral Physiology, 163 (2), 167-173.

2. Borst, A., & Egelhaaf, M. (1989). Principles of Visual-Motion Detection. Trends in Neurosciences, 12 (8), 297-306.

3. Borst, A., Egelhaaf, M., & Haag, J. (1995). Mechanisms of Dendritic Integration Underlying Gain-Control in Fly Motion-Sensitive Interneurons. Journal of Computational Neuroscience, 2 (1), 5-18.

4. Borst, A., & Haag, J. (2002). Neural networks in the cockpit of the fly. Journal of Comparative Physiology a-Neuroethology Sensory Neural and Behavioral Physiology, 188 (6), 419-437.

5. Baird, E., Srinivasan, M.V., Zhang, S.W., & Cowling, A. (2005). Visual control of flight speed in honeybees. Journal of Experimental Biology, 208, 3895-3905.

6. Clifford, C.W.G., & Ibbotson, M.R. (2002). Fundamental mechanisms of visual motion detection: models, cells and functions. Progress in Neurobiology, 68 (6), 409-437.

7. Dror, R.O., O'Carroll, D.C., & Laughlin, S.B. (2001). Accuracy of velocity estimation by Reichardt correlators. Journal of the Optical Society of America a-Optics Image Science and Vision, 18 (2), 241-252.

8. Dvorak, D., Srinivasan, M., & French, A. (1980). The contrast sensitivity of fly movement-detecting neurons. Vision Research, 20, 397-407.

9. Eckert, H. (1980). Functional properties of the H1-neurone in the third optic ganglion of the blowfliy, Phaenicia. Journal of Comparative Physiology A, 135, 29-39.

10. Egelhaaf, M., & Borst, A. (1989). Transient and steady-state response properties of movement detectors Journal of the Optical Society of America a-Optics Image Science and Vision, 6 (1), 116-127.

11. Egelhaaf, M., Borst, A., & Reichardt, W. (1989). Computational structure of a biological motion-detecting system as revealed by local detector analysis in the flys nervous-system. Journal of the Optical Society of America a-Optics Image Science and Vision, 6 (7), 1070-1087.

12. Elyada, Y.M., Haag, J., & Borst, A. (2009). Different receptive fields in axons and dendrites underlie robust coding in motion-sensitive neurons. Nature Neuroscience, 12 (3), 327-332.

13. Esch, H.E., & Burns, J.E. (1996). Distance estimation by foraging honeybees. Journal of Experimental Biology, 199 (1), 155-162.

14. Fairhall, A.L., Lewen, G.D., Bialek, W., & van Steveninck, R.R.D. (2001). Efficiency and ambiguity in an adaptive neural code. Nature, 412 (6849), 787-792.

15. Franz, M.O., & Krapp, H.G. (2000). Wide-field, motion-sensitive neurons and matched filters for optic flow fields. Biological Cybernetics, 83 (3), 185-197.

1) Geiger, G., & Nässel, D.R. (1981). Visual orientation behaviour of flies after selective laser beam ablation of interneurones. . Nature, 293, 398-399.

16. Haag, J., Denk, W., & Borst, A. (2004). Fly motion vision is based on Reichardt detectors regardless of the signal-to-noise ratio. Proceedings of the National Academy of Sciences of the United States of America, 101 (46), 16333-16338.

17. Haag, J., Egelhaaf, M., & Borst, A. (1992). Dendritic Integration of Motion Information in Visual Interneurons of the Blowfly. Neuroscience Letters, 140 (2), 173-176.

18. Haag, J., Theunissen, F., & Borst, A. (1997). The intrinsic electrophysiological characteristics of fly lobula plate tangential cells .2. Active membrane properties. Journal of Computational Neuroscience, 4 (4), 349-369.

19. Harris, R.A., O'Carroll, D.C., & Laughlin, S.B. (2000). Contrast gain reduction in fly motion adaptation. Neuron, 28 (1,22), 595-606.

20. Hassenstein, B., & Reichardt, W. (1956). Systemtheoretische Analyse Der Zeit, Reihenfolgen Und Vorzeichenauswertung Bei Der Bewegungsperzeption Des Russelkafers Chlorophanus. Zeitschrift Fur Naturforschung Part B-Chemie Biochemie Biophysik Biologie Und Verwandten Gebiete, 11 (9-10), 513-524.

21. Hausen, K., & Wehrhahn, C. (1983). Microsurgical Lesion of Horizontal Cells Changes Optomotor Yaw Responses in the Blowfly Calliphora-Erythrocephala. Proceedings of the Royal Society of London Series B-Biological Sciences, 219 (1215), 211-216.

22. Heisenberg, M., Wonneberger, R., & Wolf, R. (1978). Optomotor-blind H31 - a drosophila mutant of the lobula giant neurons. Journal of Comparative Physiology A, 124, 287-296.

23. Hengstenberg, R. (1977). Spike response of "non-spiking" visual interneurone. Nature, 270, 338-340.

24. Kohn, A., & Movshon, J.A. (2003). Neuronal adaptation to visual motion in area MT of the macaque. Neuron, 39 (4), 681-691.

25. Krapp, H.G., Hengstenberg, B., & Hengstenberg, R. (1998). Dendritic structure and receptive-field organization of optic flow processing interneurons in the fly. Journal of Neurophysiology, 79 (4), 1902-1917.

26. Krapp, H.G., & Hengstenberg, R. (1996). Estimation of self-motion by optic flow processing in single visual interneurons. Nature, 384 (6608), 463-466.

27. Krapp, H.G., Hengstenberg, R., & Egelhaaf, M. (2001). Binocular contributions to optic flow processing in the fly visual system. Journal of Neurophysiology, 85 (2), 724-734.

28. Maddess, T., & Laughlin, S.B. (1985). Adaptation of the Motion-Sensitive Neuron H-1 Is Generated Locally and Governed by Contrast Frequency. Proceedings of the Royal Society of London Series B-Biological Sciences, 225 (1239), 251-275.

29. Neri, P., & Laughlin, S.B. (2005). Global versus local adaptation in fly motion-sensitive neurons. Proceedings of the Royal Society B-Biological Sciences, 272 (1578), 2243-2249.

30. Nordström, K., & O'Carroll, D.C. (2009). The motion after-effect: local and global contributions to contrast sensitivity. Proceedings of the Royal Society B-Biological Sciences, 276 (1662), 1545-1554.

31. Nordström, N., Barnett, P.D., Moyer de Miguel, I.M., Brinkworth, R.S.A., & O'Carroll, D.C. (2008). Sexual dimorphism in the hoverfly motion vision pathway. Current Biology, 18, 661-667.

32. Reichardt, W. (1961). Autocorrelation, a principle for the evaluation of sensory information by the central nervous system. In: W.A. Rosenblith (Ed.) Sensory communication (pp. 377-390). New York: MIT Press/Wiley.

33. Reichardt, W., & Egelhaaf, M. (1988). Properties of individual movement detectors as derived from behavioral experiments on the visual system of the fly. Biological Cybernetics, 58 (5), 287-294.

34. Reisenman, C., Haag, J., & Borst, A. (2003). Adaptation of response transients in fly motion vision. I: Experiments. Vision Research, 43 (11), 1293-1309.

35. Ronacher, B., & Wehner, R. (1995). Desert ants Cataglyphis-fortis use self-induced optic flow to measure distances travelled. Journal of Comparative Physiology a-Sensory Neural and Behavioral Physiology, 177 (1), 21-27.

36. Ruderman, D.L., & Bialek, W. (1994). Statistics of natural images - scaling in the woods. Physical Review Letters, 73 (6), 814-817.

37. Safran, M.N., Flanagin, V.L., Borst, A., & Sompolinsky, H. (2007). Adaptation and Information Transmission in Fly Motion Detection. Journal of Neurophysiology, 98 (6), 3309-3320.

38. Schwartz, O., & Simoncelli, E. (2001). Natural signal statistics and sensory gain control. Nature Neuroscience, 4 (8), 819-825.

39. Shoemaker, P.A., O'Carroll, D.C., & Straw, A.D. (2005). Velocity constancy and models for wide-field visual motion detection in insects. Biological Cybernetics, 93 (1,24), 275-287.

40. Single, S., Haag, J., & Borst, A. (1997). Dendritic computation of direction selectivity and gain control in visual interneurons. Journal of Neuroscience, 17 (16), 6023-6030.

41. Srinivasan, M.V., & Dvorak, D.R. (1980). Spatial processing of visual information in the movement-detecting pathway of the fly - characteristics and functional significance. Journal of Comparative Physiology, 140 (1), 1-23.

42. Srinivasan, M.V., Lehrer, M., Kirchner, W.H., & Zhang, S.W. (1991). Range perception through apparent image speed in freely flying honeybees. Visual Neuroscience, 6 (5), 519-535.

43. Srinivasan, M.V., Zhang, S.W., Lehrer, M., & Collett, T.S. (1996). Honeybee navigation en route to the goal: Visual flight control and odometry. Journal of Experimental Biology, 199 (1), 237-244.

44. Straw, A.D., Rainsford, T., & O'Carroll, D.C. (2008). Contrast sensitivity of insect motion detectors to natural images. Journal of Vision, 8(3):32, 1-9.

45. Straw, A.D., Warrant, E.J., & O'Carroll, D.C. (2006). A 'bright zone' in male hoverfly (Eristalis tenax) eyes and associated faster motion detection and increased contrast sensitivity. Journal of Experimental Biology, 209, 4339-4354.

46. Tolhurst, D.J., Tadmor, Y., & Chao, T. (1992). Amplitude spectra of natural images. Ophthalmic and Physiological Optics, 12 (2), 229-232.

Chapter 6:
Discussion

6.1 Summary of findings

This thesis investigates natural image processing by the HS neurons in the lobula plate of the hoverfly. The main finding is that on the one hand, when shown natural images, HS neurons reliably estimate image velocity (Chapter 3). However, on the other hand, when shown experimenter-defined stimuli, such as sinusoidal gratings, these neurons generate ambiguous estimates of velocity. Although this property of their response operates across an enormously range of scenes, it does not hold for all natural images. Some scenes that are particularly barren, containing few notable features, break this consistency and generate weaker responses than the other images (Chapter 3). Thus, although the mechanisms of response normalization are robust, some natural images lie outside the compliance range of response normalization.

By analysing the time course of neural response and manipulating image contrast, we show that this property is likely to emerge from a combination of static and dynamic non-linarities within the motion processing pathway. Notably, we reveal at least two distinct dynamic adaptive non-linearities that act as powerful normalisers to images that would otherwise generate highly variable responses (Chapter 3). Due to the different time courses of these adaptive affects, we conclude that they are likely to arise from different processes occurring along the motion-processing pathway. These characteristics are additional to that typically included in motion-processing models, such as the Reichardt correlator.

In chapter 4, we show that the local responses provide a poor prediction of the global response of HS neurons when natural images are presented at their full contrast, even when we take full account of the receptive field structure of the neuron. However, when we reduce image contrast and thus bring the input signals to local motion detectors closer together (i.e. ‘linearize’ the stimulus) the essential non-linearity of the correlator model provides a better prediction of global responses. This strongly

supports an important role for non-linear mechanisms being recruited by high contrast local features in the production of robust responses to different scenes.

In Chapter 5, we investigate in more detail the mechanisms underlying locally recruited contrast gain control. We use an experimental paradigm that reduces the influence of spatial integration and thus enables the analysis of responses equivalent to the outputs of the local motion sensitive elements presynaptic to the HS neuron (Chapter 5). We show evidence for an adaptive gain reduction that affects the sensitivity of individual motion detector responses to subsequent features. This adaptive effect is driven by the contrast of local image features and operates on very rapid time scales. Interestingly, subsequent experiments show that local gain reduction is likely to be recruited only when neighbouring motion sensitive elements are stimulated simultaneously.

In Chapter 2 we show a comprehensive characterization of the receptive field properties of HS neurons in the hoverfly, *Eristalis tenax*, (Chapter 2). We revealed an interesting sex specific difference in the HSN neuron, such that the receptive field of the male HS was far smaller than that of its female counterpart (Chapter 2, Figure 2.3). This kind of receptive field shape is in contradiction to what one would expect for a neuron tuned to rotational optic flow. Furthermore, in Chapter 4, we reveal that the spatial integration properties of this neuron are unpredictable, showing unexpectedly large response fluctuations to certain image features. These observations suggest that male HSN neurons may be specifically adapted to subserve different behaviours than its female counterparts.

6.2 Mechanisms of natural image contrast invariance

6.2.1 Response saturation

Although HS neuron response increases as a function of the square stimulus contrasts for sinusoids at very low contrast, as the contrast of the stimulus increases further the response becomes saturated, such that high stimulus contrasts are no longer accompanied by increases in response (Dvorak, Srinivasan & French, 1980, Egelhaaf & Borst, 1989). Subsequently, several authors have investigated the effects of including saturating elements in computational models of motion detection as a means for achieving contrast invariance (Rajesh, Rainsford, Brinkworth, Abbott & O'Carroll, 2007, Rajesh, Straw, O'Carroll & Abbott, 2005, Rivera-Alvidrez & Higgins, 2005, Shoemaker, O'Carroll & Straw, 2005).

We show several lines of evidence (Chapters 3-5) suggesting that this normalization is not due to a simple saturation-like mechanism:

1. Rescaling images to 25% of their original contrast reveals little evidence for a release from saturation, in terms of revealing the underlying contrast dependence in the time averaged neural response (Figure 3.3; Chapter 4, Figure 4.4).

2. The time dependent response fluctuations to the natural images are well matched in relative magnitude by a model with no compressive non-linearities once the receptive field of the neurons are considered, despite the models absolute response varying 40-fold from one image to the next.

3. Local responses show little evidence of static saturation mechanisms even when we show stimuli at the highest contrast our monitor can generate (Figure 5.1).

4. Even compressive non-linearities known to influence the response of these neurons when shown experimenter defined stimuli don’t appear to be recruited by natural images (Chapter 4, Supplementary data). Once the receptive field of the neuron is taken into account response appears to increase supra-linearly with increases in image size (Chapter 4, Supplementary data, Figure S4.3).

6.2.2 Response normalization

Chapter 3 reveals evidence for an activity dependent response normalization strategy based on image driving strength (Figure 3.4 and 3.5). This acts by reducing the response to images that generate initially strong responses, whilst boosting the response to images that initially generated weak responses. Such a mechanism is ideally suited to provide powerful response normalization across vastly different natural images. Thus, this mechanism might be able to account for the apparent contrast independence in response to natural images. Our results in Chapter 3 suggest that these two effects have different time courses suggesting they may arise from different mechanisms.

6.2.3 Local gain control

Much recent work highlights several different components of dynamic adaptation in LPTCs (Harris, O'Carroll & Laughlin, 2000, Nordström & O'Carroll, 2009b). Some of these exert their influence globally on the neuron (MAE and AC component; see Introduction), although they may still be locally generated (Nordström & O'Carroll, 2009b). Other components of adaptation, such as contrast gain reduction and output range reduction, are local in their effect and most likely arise from changes in local synaptic weights (Harris et al., 2000, Maddess & Laughlin, 1985, Nordström & O'Carroll, 2009b). In Chapter 5, to investigate the influence of local changes in response gain, we used a stimulus with limited size, to reduce the influence of spatial integration and thus, record responses that reflect the neurons local inputs.

The stimulus produces a transient response from local motion detectors and reveals a rapidly acting reduction of local gain that influences the response to subsequently viewed image features (Chapter 5). The gain reduction is contrast dependent, so is only recruited following the passage of a high contrast feature (Figure 5.4). Lower contrast features, on the other hand, have little obvious influence on subsequent response (Figure 5.3). Correlation-based models of motion detection matched to *Eristalis tenax* do not predict this stimulus history dependent modulation of gain, thus it is not merely an intrinsic property resulting from the nonlinear nature of Reichardt correlators. This observation is, however, consistent with the previously reported contrast gain reduction component of motion adaptation in these neurons. Interestingly, the transient nature of the stimulus reveals little evidence for any of the other components of motion adaptive (see Chapter 5 and Chapter 1.7.2; Harris et al., 2000).

Can local contrast gain reduction, like that describe in Chapter 5, account for the active normalization of HS neuron responses to natural images?

The most obvious effect of the neurons time-averaged response to natural images is a continual decay in response through the time-course of stimulation (Figure 3.4). This likely reflects the combined effect of several of the adaptive components observed for stimulation with artificial images (Chapter 1.7.2; Harris et al., 2000, Maddess & Laughlin, 1985). Indeed, preliminary experiments using the same protocol as used by Harris et al (2000), show that natural images recruit each of the adaptive components shown for the grating experiments, albeit in amounts for different images (data not shown).

Local gain control is likely to be continually altering the response to subsequent features of the image. For example, a local motion unit that just viewed a high contrast image feature, such as a dark tree trunk, will have lower response gain to subsequently viewed image features; whereas, an area that has had little stimulation in the recent past is going to be more sensitive to changes in the stimulus. Such a mechanism could quite possibly account for much of the reduction in response variance for natural images. However, the local contrast gain reduction shown here, occurs on a very short time scale. In Chapter 3, even the strongest driving images do not show any evidence for a decrease in their time-averaged response within the first few hundred milliseconds of stimulus motion (see Figure 3.4A). Furthermore, some images showed continued *increases* in response over this time course (see Figure 3.4B). Although, it is important to distinguish between response level and the underlying gain of the system, as we show that adaptation always reduces gain, even when response goes up (Figure S3.6)

We show that the local gain reduction appears to be facilitated by simultaneous activation of neighbouring motion detectors. Interestingly, Schwartz and Simoncelli (2001) used a divisive normalization mechanism based on weighted local responses to predict the nonlinear response properties of both neurons in the primary visual cortex of monkeys and auditory nerve fibres of cats. Furthermore, they showed that a gain control mechanism mediated by local activity is ideally suited to take advantage of the predictability of natural signals (Schwartz & Simoncelli, 2001).

6.3 Why do insects use Reichardt correlator like computations for motion detection?

Despite all the apparent flaws of Reichardt correlator based mechanisms of motion detection, many animals seem to have adopted similar computations for the detection of local image motion (Clifford & Ibbotson, 2002). Additional non-linear processes on the motion-processing pathway seem to be able to overcome some of the deficiencies associated with motion computation of this kind. Why would a visual system adopt a mechanism for motion detection that is inherently flawed and then attempt to 'fix' it by cascading additional nonlinear processes, rather than simply employing a more desirable mechanism in the beginning?

Firstly, the Reichardt correlator relies on very simple mechanisms at its core, which are highly likely to already exist in one form or another in the early stages of visual processing on an evolutionary time scale. The Reichardt correlator relies on sampling two neighbouring points in space and combining them in a non-linear way (Reichardt, 1961, Reichardt, 1987). Any non-linear lateral interactions between neighbouring photoreceptors will be likely to generate some direction selectivity. If this proves advantageous for behaviour it is likely to be selected for in the further evolution of the visual system. Since lateral interactions between neighbouring receptors are so ubiquitous in visual systems (e.g. lateral inhibition) it is highly likely that correlator-like interactions will evolve.

Secondly, although the Reichardt correlator has several flaws, discussed extensively throughout this thesis, there are some distinct advantages to computing motion in this way. For example, the correlation stage multiplies the inputs, thus producing a response that increases with the square of contrast. A down side is this results in correlator output being highly variable across different natural images. However, this same stage inherently means that the correlator's response amplifies the more reliable features within the scene. This is clearly illustrated in Figure 5.7, where the local motion responses to the natural scenes are dominated by parts of the image that stand out to us as salient features or objects to us.

This built-in 'reliability filter' for the higher contrasting signals explain why a statistical mechanics analysis of the theoretical mechanisms for motion detection

concluded that the Reichardt correlator was an optimal mechanism whenever signal noise was large (Potters & Bialek, 1994). This is a likely scenario for the apposition compound eye, as this eye design is a fundamentally poor scavenger of light, especially given the constraints of the eye (and thus head) size (Land, 1981).

The gradient detector is a popular alternative for producing a reliable estimate of image velocity. However, in order to generate an accurate estimate of image velocity independent of many of the stimulus features that the Reichardt correlator is sensitive to, the gradient detector calculates motion by dividing the temporal luminance gradient taken from one receptor by the spatial luminance gradient measured across at least two different points in space. Consequently, if the spatial derivative is small, noise in the temporal derivate gets amplified and furthermore, if the spatial derivative is equal to zero, then the velocity is undefined (Limb & Murphy, 1975, Srinivasan, 1990). Subsequently, at low light levels the gradient detector has a poor signal to noise ration (Borst, 2007, Srinivasan, 1990). So, in this case the Reichardt correlator maybe a highly advantageous scheme for computing local motion.

Nevertheless, Potters and Bialek (1994) argued that in order to maximize information transmission, a motion detecting system should use gradient-like schemes in high luminance conditions (i.e. high signal to noise conditions) to enable the accurate calculation of image velocity and switch to Reichardt correlator-like mechanisms in lower luminance conditions, where signal to noise ratios are low (Potters & Bialek, 1994). Many insects (including *Eristalis*) are active in very bright light, where signal to noise ratios in photoreceptors are high, even given the constraints of eye design noted above (Lewen, Bialek & de Ruyter van Steveninck, 2001). It is unreasonable to expect the system to 'switch' from Reichardt correlator to a gradient detector as light level, or contrast, rises. The additional adaptive elements described in this thesis might be functioning equivalent to such a switch, make the system more gradient like in bright outdoor environments. This may partially reconcile the discrepancy between Lewen et al's outdoor experiments and those of Haag et al. (2004), which showed that the system remained temporal frequency tuned even at high luminance (Haag, Denk & Borst, 2004).

6.4 Velocity estimation in the insect visual system

The optomotor response of insects is well predicted by Reichardt correlator-like computations (Buchner, 1984, Poggio & Reichardt, 1976, Virsik & Reichardt, 1976). Both the optomotor response and motion detection schemes of this kind generate locally variable responses that don't explicitly signal image velocity, but are rather sensitive to additional image parameters, such as contrast and spatial frequency (Borst & Egelhaaf, 1989, Borst & Haag, 2002, Clifford & Ibbotson, 2002, Srinivasan, Poteser & Kral, 1999). However, in free flight, flying insects seem to be able to engage in exquisitely controlled aerobatic feats that require the estimation of apparent retinal velocity (Baird, Srinivasan, Zhang & Cowling, 2005, Collett & Land, 1975, Collett & Land, 1978, Srinivasan, Zhang, Lehrer & Collett, 1996). This has led to the proposal that the mechanisms subserving velocity estimation must be different from those underlying the optomotor response (Srinivasan et al., 1999).

The HS neurons receive inputs from arrays of local motion sensitive elements with Reichardt correlator-like response properties and been shown to be both necessary and sufficient for optomotor responses (Blondeau & Heisenberg, 1982, Geiger & Nässel, 1981, Hausen & Egelhaaf, 1989, Hausen & Wehrhahn, 1983, Hausen & Wehrhahn, 1990, Heisenberg, Wonneberger & Wolf, 1978, Srinivasan & Dvorak, 1980). However, when presented with natural images, the HS neurons produce robust estimates of image velocity across vastly different scenes (Straw, Rainsford & O'Carroll, 2008; see also Chapter 3, Figure 3.1). Natural images have highly variable contrasts, thus this observation is in stark contradiction to their response properties to experimenter-defined stimuli. We have shown that power normalization mechanisms tuned to the statistics of natural images (Chapters 3-5) enable the HS neurons to globally overcome their inherent sensitivity to image contrast when shown natural scenes (Chapter 2, Figure 2.1).

6.4.1 The HS neurons as velocity estimators

Could the HS neurons be playing a role in estimating forward flight speed? Reconstructions of free-flight trajectories have shown that although the HS neurons generate large responses during saccadic periods of flight, they also produce reliable responses in the inter-saccadic periods when the animal is experiencing almost pure

translation (Karmeier, van Hateren, Kern & Egelhaaf, 2006, Kern, van Hateren & Egelhaaf, 2006, Kern, van Hateren, Michaelis, Lindemann & Egelhaaf, 2005). Forward translation produces optic flow fields with maximum velocity perpendicular to the direction of heading (Chapter 1, Figure 1.1A and 1.1B). The receptive fields of the HSE, in blowflies, and the HSNE, in the hoverfly, spread laterally into the same regions of the visual field that would be maximally stimulated by forward translation (Hausen, 1982, Nordström, Barnett, Moyer de Miguel, Brinkworth & O'Carroll, 2008). As these neurons have responses that provide reliable estimates of velocity for natural images, they may play an important role in the estimation of apparent retinal image velocity.

Translation causes nearer objects to have faster retinal velocities than objects that are father away. Consequently, the HS neurons would encode for faster velocities if objects in the surround were closer to the animal and thus, lead to an over estimation of forward flight speed. Bees show similar behavioural characteristics, slowing their flight speed down when passing through narrow corridors by balancing apparent retinal velocities (Srinivasan et al., 1996).

However, vast amounts of the behavioural evidence for apparent velocity estimation have arisen from freely flying animal experiments using experimenter-defined stimuli, such as gratings (Baird et al., 2005, Srinivasan, Lehrer, Kirchner & Zhang, 1991, Srinivasan et al., 1996). These experiments show that bees use apparent velocity to control their flight independent of spatial frequency or stimulus contrast (Baird et al., 2005, Srinivasan et al., 1991, Srinivasan et al., 1996). Yet, the HS neurons produce ambiguous estimates of image velocity for experimenter-defined stimuli (Borst & Egelhaaf, 1989, Borst & Haag, 2002, Buchner, 1984, Clifford & Ibbotson, 2002), which makes it difficult to reconcile their response properties with the behavioural evidence for velocity estimation.

6.4.2 Behavioural evidence for velocity estimation

In the honeybee behavioural experiments, the bees fly though a narrow corridor. The bees use the patterns on the sidewalls of the corridor, to control their flight speed and centre their trajectory in the corridor. By altering pattern spatial wavelength, contrast, velocity, as well as grating orientation Srinivasan and colleagues have provided conclusive evidence for velocity estimation. More recent experiments have also shown that the same holds true even if the patterns are shown on the floor, i.e. in the ventral visual field as opposed to the lateral visual field (Barron & Srinivasan, 2006).

There are some key difference between the behavioural paradigm and the experiments performed on the LPTCs or the optomotor response though. Firstly, although the walls lateral to the bees heading are flat, she is still in a three dimensional environment. This means that as the bee flies forwards, from the sidewalls alone she experiences a range of temporal and spatial frequencies across the retina. This is because laterally the grating is closer than more frontal regions of the eye that view the corridor walls obliquely. Therefore, in this paradigm the whole visual system is simultaneously experiencing a range of spatial and temporal frequencies accompanied with a range of retinal speeds. This range of spatio-temporal frequencies experienced during forward flight in combination with extra visual cues arising from objects that might reside outside of the tunnel (i.e. the vedeo camera recording the flights from above), might provide the animal with enough additional visual information to extract velocity cues from the scene despite relying on ambiguous local motion information.

Nevertheless, the hypothesis is that bees balance the amount of optic flow in their left and right hemispheres to regulate flight speed and centre their flight trajectory within the tunnel. This is exemplified when the corridor becomes narrow at a point. As the corridor narrows the walls become closer to the bee who is flying down the centre, this generates fast apparent retinal velocities and the bee subsequently slows himself down, holding the apparent velocity of the corridor walls constant on the retina. Recent experiments however, have shown evidence that the behavioural context may influence whether bees attempt to match speed. Serres et al. (2008) showed that when entering a wider tunnel (95 cm) bees tended to follow either one wall or the other when they entered the tunnel on the same side as the feeder.

Furthermore, removing a section of wall completely from the opposite visual hemisphere did not affect the bees wall following behaviour (Serres, Masson, Ruffier & Franceschini, 2008). If the bees were balancing optic flow in either hemisphere this would cause them to veer away from the wall where the retinal velocities are highest. This suggests an alternate optic flow control system whereby the bee doesn't need to rely on optic flow from both hemispheres.

6.4.3 Small-field motion detection

While the additional mechanisms, such as dynamic adaptation, may allow LPTCs to generate responses that are robust in a global sense. As we have shown here, the local variance in response predicted by the correlator mechanism is only mitigated by averaging in either space or time. Furthermore, residual pattern dependence doesn't matter in tasks that integrate responses over time, e.g. path integration by and honeybees using optic flow. However, this presents a fundamental problem for other visual tasks where more local estimates of image speed are important. Small target motion analysis si one such task.

There is substantive evidence suggesting that insects are able to accurately estimate the velocity of small objects. For example both hoverflies and dragonflies have been shown to be able to compute interception courses for moving targets (Collett & Land, 1978, Olberg, Seaman, Coats & Henry, 2007, Olberg, Worthington, Fox, Bessette & Loosemore, 2005, Olberg, Worthington & Venator, 2000). Several neural classes have been identified that are likely to subserve this small-field target detection and tracking system (Nordström & O'Carroll, 2009a). Recent investigation has suggested that these neurons receive inputs from Reichardt correlator-like elements and thus they are inherently poor encoders of image velocity (Geurten, Nordstrom, Sprayberry, Bolzon & O'Carroll, 2007). This line of research is still in its infancy and as yet it is unclear whether similar adaptive mechanisms as described for the HS neurons might influence target selective responses.

6.4.4 Multiple speed tuning channels

An alternate explanation for the robust velocity analysis in behaviour is that animals may not be limited to a single motion detector as the basis for their analysis. In principle, it is not necessary to explicitly compute image velocity on the first iteration, as implemented in both the families of Reichardt correlators and gradient detectors. Rather, velocity sensitivity can be built-up by combining the responses of 'lower-order' neurons with different spatio-temporal receptive fields. In area MT of the primate visual system (Dubner & Zeki, 1971, Maunsell & Newsome, 1987) there is evidence for a large percentage of speed-tuned neurons (Perrone & Thiele, 2001), which are believed to be derived from non-speed neurons with different spatio-temporal tuning in the primary visual cortex (Perrone & Thiele, 2002).

In the insect, there is some evidence in wide-field motion detectors for fast and slow motion processing channels, which could be combined at higher order stages of processing (Douglass & Strausfeld, 2007, Horridge & Marcelja, 1992, O'Carroll, 2001). Furthermore, there is also some evidence for velocity tuned neurons that show little dependence on spatial wavelength (Ibbotson, 2001, Olberg, 1981). However, although these studies show some independence of neural response on spatial frequency, none of them test the influence of other image parameters, such as contrast, for which the behavioural experiments of Srinivasan and colleagues have revealed insensitivity to (Baird et al., 2005). Nevertheless, it is possible that such a mechanism could account for the behavioural evidence for velocity estimation. However, this hypothesis is at odds with the optomotor experiments carried out in flies, suggesting that their behavioural response closely matches that of the physiological recordings from LPTCs or, for that matter, predictions of the simple correlator models (Buchner, 1984).

6.5 Limitations of the current study

6.5.1 Naturalistic conditions

Many animals are known to tightly control their behaviour as to control the visual motion they experience (Schilstra & Van Hateren, 1999, Van Hateren & Schilstra, 1999). For example, flies are known to go to incredible lengths to separate rotatory and translatory optic flow whilst flying freely (Kern et al., 2005, Schilstra & Van Hateren, 1999, Van Hateren & Schilstra, 1999). Saccadic movements act to compress rotational components of optic flow into brief periods of time (Schilstra & Van Hateren, 1999, Van Hateren & Schilstra, 1999). In between saccades the visual system stabilizes its gaze and therefore, enhances its sensitivity to detecting relevant information resulting from translation (Kern et al., 2006, Kern et al., 2005, Schilstra & Van Hateren, 1999, Van Hateren & Schilstra, 1999).

Either way, animals carefully control their behaviour and thus, their visual input. Several resent studies in the reconstructing image motion in flies has revealed the importance of taking into consideration their flight mode and also gaze direction in the spatial temporal structure of the scene generated (Karmeier et al., 2006, Kern, Petereit & Egelhaaf, 2001, Kern et al., 2006, Kern et al., 2005, Schilstra & Van Hateren, 1999, van Hateren, Kern, Schwerdtfeger & Egelhaaf, 2005, Van Hateren & Schilstra, 1999). This has profound repercussions for the response properties of motion sensitive neurons such as the LPTCs (Kern et al., 2006, Kern et al., 2005).

The stimulus paradigms used herein, although collected from natural scenes frequented by flies, aren't moving dynamically in a way that is likely to reflect natural flight behaviour of these flies. However, an important role for the HS neurons might be to stabilize image slip and thus facilitate intersaccadic flight periods where the animal only experiences translation. In fact, a neuron with a frontally localized receptive field, like HSN, might be ideally suited for this job, because its receptive field would be positioned at the pole of expansion for forward translation and thus, would experience little optic-flow. However, it would remain sensitive to subtle yaw rotations or lateral sideslip that might result from wind or imperfections in flight control. If this is the role of the HSN neuron then the stimulus we use might well

reflect the kind of image slip the neuron is adapted to encode. This is indeed what we show in Chapter 2.

The other major limitation of our stimulus is its absolute luminance of our display, which has a mean luminance of ~90 Cdm^{-2}, several orders of magnitude lower than the outdoor environment. When luminance increases over a naturalistic range, LPTCs signal increased information about the motion trajectory (Lewen et al., 2001).

6.6 Future directions

Despite a wealth of knowledge surrounding their response properties, well beyond the basic level, there a few clues to the precise mechanisms underlying accurate velocity estimation. Rather than identifying these mechanisms, this thesis reveals additional processes to those already well characterized, which are likely to be contributors.

What mechanisms drive the apparent normalization strategy (Chapter 3) observed for natural image processing? Adaptation is an interesting potential candidate. Preliminary experiments (data not shown) suggest that different natural scenes recruit different amounts of adaptation. This may well account for part of the response normalization. Adaptation allows neurons to rescale their response range and maximize information transmission. Recent studies have shown that the non-linearities associated with adaptation are not just a consequence of the biophysical processes underlying the neurons signal transmission, but rather have an important functional role in the encoding of natural statistics (Schwartz & Simoncelli, 2001).

The increase in response observed over initial response period is still completely unaccounted for (Chapter 3, Figure 3.4). What are the mechanisms underlying an increase in response? We show that when an independent adapting stimulus is used that this is not the result of a rapidly recruited increase in the gain of the system, but rather seems to be matched to the specific image in question (see Chapter 3, Figure 3.S6). These mechanisms are almost certainly related to the ‘latency’ mechanisms described by Warzecha and Egelhaaf who also stopped short of identifying a mechanism (Warzecha & Egelhaaf, 2000). Further dissection of the adaptive

components and their recruitment in more naturalistic condition will certainly lead to a greater understanding of motion adaptations role in response normalization.

An important consequence of adaptation being a dominant element in response normalization (Schwartz & Simoncelli, 2001), is that it acts to keep the neurons in the more linear part of their response range. This kind of effect has beneficial consequences for reconciling some of our data. For example, Chapters 4 and 5 present data, whereby a model with *no* compressive elements, fits the relative magnitude of response features to certain images or image features (see Figure 4.3-4.5; Figure 5.1). Yet, from one situation to the next the model incorrectly estimates the *absolute* magnitude by an enormous degree. In Chapter 4, for the natural images this is a >40-fold discrepancy and in Chapter 5 this is more like 100-fold (see Chapter 4, Figure 4.5; and Chapter 5, Figure 5.1). Powerful adaptive mechanisms acting to rescale neural response without any compressive effects like that describe to account for adaptation in the V1 and the auditory cortex by Schwartz and Simoncelli (2001), would provide an ideal mechanism to account these observations in our data. Are these linked to additional lack of predictability of spatial integration of the HSN neuron (Chapter 4) to natural images?

Modern genetic tools allow for an advanced approach to understanding key missing links in the motion processing pathway. This thesis looks at the brains processing of visual motion from a 'black-box' point of view. However, there remain many questions surrounding the neural substrates of the observed phenomenon. Up until recently these elements have been relatively unacsessable dure to the small size, but new genetic toolkits available in *Drosophila* are already providing critical information about the elements on the motion processing pathway flies and their role in generating response to motion (for example see Rister, Pauls, Schnell, Ting, Lee, Sinakevitch, Morante, Strausfeld, Ito & Heisenberg, 2007).

6.7 References

1. Baird, E., Srinivasan, M.V., Zhang, S.W., & Cowling, A. (2005). Visual control of flight speed in honeybees. *Journal of Experimental Biology, 208*, 3895-3905.

2. Barron, A., & Srinivasan, M.V. (2006). Visual regulation of ground speed and headwind compensation in freely flying honey bees. *Journal of Experimental Biology, 209*, 978-984.

3. Blondeau, J., & Heisenberg, M. (1982). The 3-dimentional optomotor torque system of Drosophila-melanogaster - studies on wildtype and the mutant optomotor-blind H31. *Journal of Comparative Physiology, 145* (3), 321-329.

4. Borst, A. (2007). Correlation versus gradient type motion detectors: the pros and cons. *Philosophical Transactions of the Royal Society B-Biological Sciences, 362* (1479), 369-374.

5. Borst, A., & Egelhaaf, M. (1989). Principles of Visual-Motion Detection. *Trends in Neurosciences, 12* (8), 297-306.

6. Borst, A., & Haag, J. (2002). Neural networks in the cockpit of the fly. *Journal of Comparative Physiology a-Neuroethology Sensory Neural and Behavioral Physiology, 188* (6), 419-437.

7. Buchner, E. (1984). Behavioral analysis of spatial vision in insects. In: M.A. Ali (Ed.) *Photoreception and vision in invertebrates* (pp. 561-621). New York: Plenum.

8. Clifford, C.W.G., & Ibbotson, M.R. (2002). Fundamental mechanisms of visual motion detection: models, cells and functions. *Progress in Neurobiology, 68* (6), 409-437.

9. Collett, T.S., & Land, M.F. (1975). Visual Control of Flight Behavior in Hoverfly, Syritta-Pipiens L. *Journal of Comparative Physiology, 99* (1), 1-66.

10. Collett, T.S., & Land, M.F. (1978). How Hoverflies Compute Interception Courses. *Journal of Comparative Physiology, 125* (3), 191-204.

11. Douglass, J.K., & Strausfeld, N.J. (2007). Diverse speed response properties of motion sensitive neurons in the fly's optic lobe. *Journal of Comparative*

Physiology a-Neuroethology Sensory Neural and Behavioral Physiology, 193 (2), 233-247.

12. Dubner, R., & Zeki, S.M. (1971). Response properties and receptive fields of cells in an anatomically defined region of the superior temporal sulcus *Brain Research, 35*, 528-532.

13. Dvorak, D., Srinivasan, M., & French, A. (1980). The contrast sensitivity of fly movement-detecting neurons. *Vision Research, 20*, 397-407.

14. Egelhaaf, M., & Borst, A. (1989). Transient and steady-state response properties of movement detectors *Journal of the Optical Society of America a-Optics Image Science and Vision, 6* (1), 116-127.

15. Geiger, G., & Nässel, D.R. (1981). Visual orientation behaviour of flies after selective laser beam ablation of interneurones. . *Nature, 293*, 398-399.

16. Geurten, B.R.H., Nordstrom, K., Sprayberry, J.D.H., Bolzon, D.M., & O'Carroll, D.C. (2007). Neural mechanisms underlying target detection in a dragonfly centrifugal neuron. *Journal of Experimental Biology, 210* (18), 3277-3284.

17. Haag, J., Denk, W., & Borst, A. (2004). Fly motion vision is based on Reichardt detectors regardless of the signal-to-noise ratio. *Proceedings of the National Academy of Sciences of the United States of America, 101* (46), 16333-16338.

18. Harris, R.A., O'Carroll, D.C., & Laughlin, S.B. (2000). Contrast gain reduction in fly motion adaptation. *Neuron, 28* (1,22), 595-606.

19. Hausen, K. (1982). Motion Sensitive Interneurons in the Optomotor System of the Fly .2. The Horizontal Cells - Receptive-Field Organization and Response Characteristics. *Biological Cybernetics, 46* (1), 67-79.

20. Hausen, K., & Egelhaaf, M. (1989). Neural mechanisms of visual course control in insects. In: D.G. Stavenga, & R.C. Hardie (Eds.), *Facets of vision* (pp. 391-424). Berlin Heidelberg New York: Springer.

21. Hausen, K., & Wehrhahn, C. (1983). Microsurgical Lesion of Horizontal Cells Changes Optomotor Yaw Responses in the Blowfly Calliphora-Erythrocephala. *Proceedings of the Royal Society of London Series B-Biological Sciences, 219* (1215), 211-216.

22. Hausen, K., & Wehrhahn, C. (1990). Neural Circuits Mediating Visual Flight Control in Flies .2. Separation of 2 Control-Systems by Microsurgical Brain-Lesions. *Journal of Neuroscience, 10* (1), 351-360.

23. Heisenberg, M., Wonneberger, R., & Wolf, R. (1978). Optomotor-blind H31 - a drosophila mutant of the lobula giant neurons. *Journal of Comparative Physiology A, 124*, 287-296.

24. Horridge, G.A., & Marcelja, L. (1992). On the existence of fast and slow diectionally senstitve motion detector neurons in insects. *Proceedings of the Royal Society of London Series B-Biological Sciences, 248* (1321), 47-54.

25. Ibbotson, M.R. (2001). Evidence for velocity-tuned motion-sensitive descending neurons in the honeybee. *Proceedings of the Royal Society of London Series B-Biological Sciences, 268* (1482), 2195-2201.

26. Karmeier, K., van Hateren, J.H., Kern, R., & Egelhaaf, M. (2006). Encoding of naturalistic optic flow by a population of blowfly motion-sensitive neurons. *Journal of Neurophysiology, 96* (3), 1602-1614.

27. Kern, R., Petereit, C., & Egelhaaf, M. (2001). Neural processing of naturalistic optic flow. *Journal of Neuroscience, 21* (8). art no RC 139

28. Kern, R., van Hateren, J.H., & Egelhaaf, M. (2006). Representation of behaviourally relevant information by blowfly motion-sensitive visual interneurons requires precise compensatory head movements. *Journal of Experimental Biology, 209* (7), 1251-1260.

29. Kern, R., van Hateren, J.H., Michaelis, C., Lindemann, J.P., & Egelhaaf, M. (2005). Function of a fly motion-sensitive neuron matches eye movements during free flight. *Plos Biology, 3* (6), 1130-1138.

30. Land, M.F. (1981). Optics and vision in invertebrates. In: H. Autrum (Ed.) *Handbook of sensory physiology,* VII/6B (pp. 472-592). Berlin: Springer.

31. Lewen, G.D., Bialek, W., & de Ruyter van Steveninck, R.R. (2001). Neural coding of naturalistic motion stimuli. *Network, 12*, 317-329.

32. Limb, J.O., & Murphy, J.A. (1975). Estimating the velocity of moving objects in television signals. *Computer graphics and image processing, 4*, 311-327.

33. Maddess, T., & Laughlin, S.B. (1985). Adaptation of the Motion-Sensitive Neuron H-1 Is Generated Locally and Governed by Contrast Frequency. *Proceedings of the Royal Society of London Series B-Biological Sciences, 225* (1239), 251-275.

34. Maunsell, J.H.R., & Newsome, W.T. (1987). Visual processing in monkey extrastriate cortex. *Annual Review of Neuoscience, 10*, 363-402.

35. Nordström, K., & O'Carroll, D.C. (2009a). Feature detection and the hypercomplex property in insects. *Trends in Neurosciences, 32* (7), 383-391.

36. Nordström, K., & O'Carroll, D.C. (2009b). The motion after-effect: local and global contributions to contrast sensitivity. *Proceedings of the Royal Society B-Biological Sciences, 276* (1662), 1545-1554.

37. Nordström, N., Barnett, P.D., Moyer de Miguel, I.M., Brinkworth, R.S.A., & O'Carroll, D.C. (2008). Sexual dimorphism in the hoverfly motion vision pathway. *Current Biology, 18*, 661-667.

38. O'Carroll, D.C. (2001). Motion adaptation and evidence for parallel processing in the lobula plate of the bee-fly Bombylius major. In: J.M. Zanker, & J. Zeil (Eds.), *Motion Vision, Computational, Neural, and Ecological Constraints* (pp. 381-394). Berlin Heidelberg New York: Springer Verlag.

39. Olberg, R.M. (1981). Object-movement and self-movement detectors in the ventral nerve cord of the dragonfly. *Journal of Comparative Physiology, 141* (3), 327-334.

40. Olberg, R.M., Seaman, R.C., Coats, M.I., & Henry, A.F. (2007). Eye movements and target fixation during dragonfly prey-interception flights. *Journal of Comparative Physiology a-Neuroethology Sensory Neural and Behavioral Physiology, 193* (7), 685-693.

41. Olberg, R.M., Worthington, A.H., Fox, J.L., Bessette, C.E., & Loosemore, M.P. (2005). Prey size selection and distance estimation in foraging adult dragonflies. *Journal of Comparative Physiology a-Neuroethology Sensory Neural and Behavioral Physiology, 191* (9), 791-797.

42. Olberg, R.M., Worthington, A.H., & Venator, K.R. (2000). Prey pursuit and interception in dragonflies. *Journal of Comparative Physiology a-Sensory Neural and Behavioral Physiology, 186* (2), 155-162.

43. Perrone, J.A., & Thiele, A. (2001). Speed skills: measuring the visual speed analyzing properties of primate MT neurons. *Nature Neuroscience, 4* (5), 526-532.

44. Perrone, J.A., & Thiele, A. (2002). A model of speed tuning in MT neurons. *Vision Research, 42* (8), 1035-1051.

45. Poggio, T., & Reichardt, W. (1976). Visual control of orientation behaviour in the fly II. Towards the underlying

46. neural interactions. *Quart Rev Biophys, 9*, 377-438.

47. Potters, M., & Bialek, W. (1994). Statistical-mechanics and visual signal-processing. *Journal De Physique I, 4* (11), 1755-1775.

48. Rajesh, S., Rainsford, T., Brinkworth, R.S.A., Abbott, D., & O'Carroll, D. (2007). Implementation of saturation for a modelling pattern noise using naturalistic stimuli. *Smart structures, devises, and systems III,* 6414 (pp. 24-39).

49. Rajesh, S., Straw, A., O'Carroll, D.C., & Abbott, D. (2005). Effects of compressive nonlinearity on insect-based motion detection. *Smart Structures, Devices, and Systems II,* 5649 (pp. 798-810): SPIE.

50. Reichardt, W. (1961). Autocorrelation, a principle for the evaluation of sensory information by the central nervous system. In: W.A. Rosenblith (Ed.) *Sensory communication* (pp. 377-390). New York: MIT Press/Wiley.

51. Reichardt, W. (1987). Evaluation of optical motion information by movement detectors. *Journal of Comparative Physiology a-Sensory Neural and Behavioral Physiology, 161* (4), 533-547.

52. Rister, J., Pauls, D., Schnell, B., Ting, C.Y., Lee, C.H., Sinakevitch, I., Morante, J., Strausfeld, N.J., Ito, K., & Heisenberg, M. (2007). Dissection of the peripheral motion channel in the visual system of Drosophila melanogaster. *Neuron, 56* (1), 155-170.

53. Rivera-Alvidrez, Z., & Higgins, C.M. (2005). Contrast saturation in a neuronally-based model of elementary motion detection. *Neurocomputing, 65*, 173-179.

54. Schilstra, C., & Van Hateren, J.H. (1999). Blowfly flight and optic flow I. Thorax kinematics and flight dynamics. *Journal of Experimental Biology, 202* (11), 1481-1490.

55. Schwartz, O., & Simoncelli, E. (2001). Natural signal statistics and sensory gain control. *Nature Neuroscience, 4* (8), 819-825.

56. Serres, J.R., Masson, G.P., Ruffier, F., & Franceschini, N. (2008). A bee in a corridor: centering and wall following. *Naturwissenschaften, 95*, 1181-1187.

57. Shoemaker, P.A., O'Carroll, D.C., & Straw, A.D. (2005). Velocity constancy and models for wide-field visual motion detection in insects. *Biological Cybernetics, 93* (1,24), 275-287.

58. Srinivasan, M.V. (1990). Generalized gradient shemes for the measurement of 2-dimentional image motion. *Biological Cybernetics, 63* (6), 421-431.

59. Srinivasan, M.V., & Dvorak, D.R. (1980). Spatial processing of visual information in the movement-detecting pathway of the fly - characteristics and functional significance. *Journal of Comparative Physiology, 140* (1), 1-23.

60. Srinivasan, M.V., Lehrer, M., Kirchner, W.H., & Zhang, S.W. (1991). Range perception through apparent image speed in freely flying honeybees. *Visual Neuroscience, 6* (5), 519-535.

61. Srinivasan, M.V., Poteser, M., & Kral, K. (1999). Motion detection in insect orientation and navigation. *Vision Research, 39* (16), 2749-2766.

62. Srinivasan, M.V., Zhang, S.W., Lehrer, M., & Collett, T.S. (1996). Honeybee navigation en route to the goal: Visual flight control and odometry. *Journal of Experimental Biology, 199* (1), 237-244.

63. Straw, A.D., Rainsford, T., & O'Carroll, D.C. (2008). Contrast sensitivity of insect motion detectors to natural images. *Journal of Vision, 8(3):32*, 1-9.

64. van Hateren, J.H., Kern, R., Schwerdtfeger, G., & Egelhaaf, M. (2005). Function and coding in the blowfly H1 neuron during naturalistic optic flow. *Journal of Neuroscience, 25* (17), 4343-4352.

65. Van Hateren, J.H., & Schilstra, C. (1999). Blowfly flight and optic flow II. Head movements during flight. *Journal of Experimental Biology, 202* (11), 1491-1500.

66. Virsik, R.P., & Reichardt, W. (1976). Detection and Tracking of Moving-Objects by Fly Musca-Domestica. *Biological Cybernetics, 23* (2), 83-98.

67. Warzecha, A.K., & Egelhaaf, M. (2000). Response latency of a motion-sensitive neuron in the fly visual system: dependence on stimulus parameters and physiological conditions. *Vision Research, 40* (21), 2973-2983.